UNIVERSITÀ
DEGLI STUDI
DI BRESCIA

DOTTORATO DI RICERCA IN INGEGNERIA CIVILE, AMBIENTALE, DELLA COOPERAZIONE INTERNAZIONALE E DI MATEMATICA
Curriculum: Analisi e gestione dei rischi naturali

Settore Scientifico Disciplinare: ICAR/01 Idraulica

CICLO
XXXV

EXPLORING THE ROLE OF CONNECTIVITY IN A SHALLOW LAKE: FIELD STUDIES AND HYDRODYNAMIC MODELLING OF TORBIERE DEL SEBINO

Tesi di dottorato di:
STELLA VOLPINI

Relatore:
MARCO PILOTTI

Correlatore:
GIULIA VALERIO

Abstract

This Thesis summarizes the research and monitoring activities accomplished at Riserva Naturale Torbiere del Sebino within the framework of my PhD activities. Torbiere del Sebino belongs to the Natura 2000 Network and is listed in the Ramsar Convention since 1984. As many other wetlands in the world, Torbiere are an extremely productive system and used to be a chest of biodiversity. They are of great socio-economic as well as ecological importance and they drain an urbanized watershed delivering water to the receiving body of lake Iseo.

In a rapidly changing environment, with land use changes and climate change impacts, monitoring such a vulnerable ecosystem is key to protecting it. In the past, very little studies, if any at all, were carried out for the understanding of the hydrological balance and the hydrodynamics of this system. There are many biological and zoological studies about Torbiere, but to our knowledge there are no studies regarding the water circulation and residence time distribution, that would provide the overall picture of an already complex subject.

In the first part of this Thesis, the monitoring project is presented. A fixed meteorological and water monitoring station was installed, allowing a real-time consultation of the measured data, which are publicly available. Several surveys were carried out to characterize the different ponds that made up Torbiere. So far, a 2/3 year long time series was provided for Torbiere for parameters like water level, temperature and specific conductivity. This will provide future studies with a basic knowledge of the basin, and it will allow to detect any trend in those parameters. Moreover, the measurements of wind will provide the primary forcing for any hydrodynamic modeling of this area.

The observation of the measured data, along with the study of the sewer overflow weir of Provaglio and with the water quality data measured at the main tributary creek, arose concerns about the water quality of Torbiere, which has been worsening over the last decades. In addition to a clear change in land use of its watershed, which decreased the filtering potential against pollutants and nutrients, a change in the internal separation in ponds was observed. The hypothesis that the enhancement of internal

circulation, that followed the bank collapse and demolition, has contributed to the worsening of water quality begun to emerge. Actually, joining the different ponds originally present within the Torbiere di Iseo, led to a strongly interconnected environment where the polluted inflow can propagate everywhere. The best tool suited for the investigation of this idea was found in hydrodynamic modeling (and in particular 3D modelling), as it can help understanding inner circulation patterns of a basin, as well as its residence time distribution.

In order to assess the role of connectivity and the trade-off with the worsening of water quality, the 3D model needed to be calibrated. Being a shallow wetland, whose circulation is triggered by winds, its flow field and transport patterns are highly sensitive, in addition to Manning's roughness coefficient, to eddy viscosity and diffusivity.

For the turbulence parameters, a plume of specific conductivity caused by the tributary creek during a high-flow period in April 2021, was used: point measurements of specific conductivity were compared against modelled results, obtained by changing the parameters to be calibrated. The final values were chosen between the ones that minimized the RMSE between measured and modeled results.

For the Manning's roughness coefficient, which parameterizes the resistance law at the bottom of the basin, measurements of flow velocities are needed. Unfortunately, in a system like Torbiere, traditional measuring devices like current meters could not be used due to very low velocities and the absence of a clearly detectable principal direction of the flow. We eventually decided to use a drifter, as already done in other wetlands, but the shallow nature of these ponds required a specific design for a device that was suitable for waters of depth lower than 2 m and that actually measured flow velocities (and was not influenced by wind). A drifter was designed specifically for Torbiere, equipped with a GPS and GSM modules programmed using the potential of Arduino. The design was modelled in Fluent ANSYS to ensure that the drag force acting on the submerged portion of the device was predominant with respect to the air drag force. The device was deployed ten times and the data acquired were processed to obtain a balanced flow velocity along its depth. The Manning's coefficient

value in the 3D model was calibrated on the basis of the comparative analysis provided by the model with respect to the ones measured during the deployments. The final value was chosen as the one that minimizes the RMSE between the measured and the modeled velocities in terms of a linear correlation coefficient.

Once a satisfying calibration for the above-mentioned parameters was obtained, the link between connectivity and worsening of water quality was explored. Model simulations were carried out, considering two different geometries: one corresponding to the 1950s layout of Torbiere del Sebino, where all the ponds were separated by banks; the other, considering the present one, obtained after the collapse and the demolition of some banks and where practically all the ponds are interconnected. The two systems were forced in the same way, in order to isolate the sole effect of the geometry. The systems were filled with unitary concentrations at the beginning of the simulation and were flushed by the average discharge of the main affluent, characterized by a null concentration. The decrease over time in the average tracer concentration in the basin was computed for the two configurations. This analysis showed that the 1950s configuration resembles the behavior of a plug flow reactor, with the flow entering from the tributary stream and the water being driven towards the outflow along a tortuous path. Considering the polluted nature of the entering waters, this means that they can be cleared up by removal processes more efficiently than in the present configuration. A simplified set of 1D models was also specifically implemented to test the possibility of modeling this system with a simpler approach.

Starting from these findings, an idea for a remediation strategy for Torbiere was eventually proposed, consisting in building a constructed wetland for the treatment of the pollutant loading coming from the two affluents. After planting cattails on its bottom and guaranteeing a tortuous path, much less volume would be required for the same removal efficiency that is reached now. This would allow the rest of the ponds to be isolated, creating the premise for their recovery over time.

Keywords: Torbiere del Sebino, wetland, residence time, circulation, drifter

Sommario

Questa tesi riassume i lavori di monitoraggio e modellazione svolti presso la Riserva Naturale Torbiere del Sebino durante la mia attività di dottorato. Le Torbiere appartengono alla rete Natura 2000 e alla Convenzione Ramsar dal 1984. In quanto zona umida, sono un sistema altamente produttivo e tra gli habitat più ricchi di biodiversità. La loro collocazione all'interno di un bacino fortemente urbanizzato, unita al fatto che il loro effluente termina direttamente nel vicino lago di Iseo le rende estremamente importanti sia da un punto di vista socioeconomico, che ecologico.

Si tratta di un ecosistema vulnerabile, sottoposto a variazioni di uso del suolo e cambiamenti climatici, i cui effetti dovrebbero essere sistematicamente monitorati. Tuttavia, negli anni precedenti non sono stati fatti studi volti alla comprensione del bilancio idrologico o dell'idrodinamica di questo sistema, mentre numerose sono state le analisi legate ad aspetti biologici e zoologici.

Concentrarsi sugli aspetti specifici di un ecosistema, prescindendo dallo studio dell'habitat naturale rischia di non fornire un'adeguata visione di insieme di un sistema già così complesso.

Nella prima parte di questa tesi, viene presentato il progetto di monitoraggio per le Torbiere del Sebino. Una stazione fissa di monitoraggio è stata installata e consente una consultazione in tempo reale dei dati misurati, disponibile pubblicamente per chiunque fosse interessato. Numerosi sopralluoghi e campagne di misurazione svolte in questi anni hanno consentito la caratterizzazione delle diverse vasche delle Torbiere. Ad oggi, un dataset di 2/3 anni è disponibile per parametri come livelli, temperatura dell'acqua e conducibilità specifica. Costituirà una conoscenza di base per studi futuri e consentirà di individuare eventuali trend nei parametri sopra citati.

Dall'osservazione dei dati misurati sono sorte diverse preoccupazioni riguardo la qualità delle acque delle Torbiere, che è peggiorata negli ultimi decenni. Oltre alle drastiche variazioni nell'uso del suolo, che hanno portato ad una diminuzione delle capacità di filtraggio del bacino stesso da inquinanti e nutrienti, è stato osservato anche un cambiamento per quanto

riguarda la separazione interna delle vasche. È così emersa l'ipotesi secondo cui l'aumento della circolazione interna, conseguentemente al collasso dei setti di separazione e ad una loro parziale demolizione, abbia contribuito al peggioramento della qualità dell'acqua.

La modellazione idrodinamica 3D è stata scelta come strumento per investigare questa ipotesi, in quanto può essere utile a comprendere pattern di circolazione interni di uno specchio d'acqua, nonché la distribuzione dei tempi di residenza. Per valutare il ruolo della connettività e il suo legame con il peggioramento della qualità dell'acqua, è stato necessario calibrare il modello 3D.

Essendo una zona umida poco profonda, la cui circolazione è governata dal vento, il suo campo di moto e il trasporto di sostanze sono sensibili a parametri come viscosità e diffusività turbolente, nonché al coefficiente di scabrezza del fondo (coefficiente di Manning).

La calibrazione dei primi due è stata fatta a partire dall'osservazione di un pennacchio di conducibilità avvenuta nell'aprile 2021: le misure puntuali di conducibilità specifica sono state confrontate con i risultati ottenuti dalla modellazione dell'evento stesso. Variando i parametri, è stato scelto il valore che minimizzasse il RMSE tra il misurato e il modellato.

Per quanto riguarda il coefficiente di Manning, da cui dipende la legge di resistenza del flusso al fondo, la sua calibrazione necessita di misure della velocità di flusso. In un sistema come le Torbiere, non è possibile utilizzare metodi di misurazione tradizionali come mulinelli, in quanto le velocità sono estremamente basse e non è chiaramente individuabile una direzione principale di flusso. In casi come questo, è diffuso l'utilizzo di drifter; tuttavia, essendo le profondità molto basse, è necessario progettare uno strumento specifico, adatto a profondità inferiori ai 2 m e che effettivamente misuri le velocità dell'acqua (e non sia influenzato da quelle del vento).

Un drifter è stato quindi progettato specificatamente per le Torbiere, contenente moduli GPS e GSM per la sua localizzazione e programmato tramite Arduino. Il design è stato quindi modellato in Fluent ANSYS per confermare che la forza di trascinamento agente sulla parte sommersa fosse preponderante rispetto a quella esercitata dal vento. Il drifter è stato rilasciato dieci volte all'interno di diverse vasche delle Torbiere e i dati

ottenuti sono stati processati per ottenere la velocità del flusso integrata sulla sua profondità. I rilasci sono stati riprodotti all'interno del modello 3D, variando il valore di coefficiente di Manning. Il valore finale è stato scelto tra quelli che minimizzavano il RMSE e massimizzavano il coefficiente di correlazione lineare tra misurato e modellato.

Una volta ottenuti soddisfacenti risultati di calibrazione per i parametri sopra citati, si è proceduto con la valutazione del legame tra connettività e peggioramento della qualità dell'acqua. Sono state svolte due simulazioni, considerando due geometrie differenti: una, corrispondente a quella del 1950, con le vasche ben separate dai setti; una, corrispondente alla configurazione attuale, ottenuta dopo il collasso e la parziale demolizione di alcuni setti.

I due sistemi sono stati sottoposti alle medesime forzanti, al fine di isolare l'effetto della geometria. Come condizione iniziale è stata assegnata una concentrazione unitaria in tutto il dominio, mentre gli affluenti entrano con concentrazione nulla. È stata quindi osservata la diminuzione nella concentrazione media di tracciante nel tempo per le due configurazioni, che equivale allo studio della percentuale di "acqua vecchia" rimanente nel sistema.

Questa analisi ha mostrato che la geometria del 1950 si avvicina al comportamento di un reattore del tipo a pistone, con il flusso che entra dall'affluente e viene guidato verso l'uscita attraverso un percorso tortuoso. Essendo l'affluente delle Torbiere inquinato, ciò significa che può essere depurato attraverso i processi di rimozione più efficacemente rispetto che nella configurazione attuale. In aggiunta alla modellazione tridimensionale, un modello 1D è stato creato con l'intento di esplorare le possibilità di modellazione di questo sistema anche con un approccio semplificato.

Grazie a queste analisi, è nata l'idea di proporre una strategia di rimedio per le Torbiere, consistente nella creazione di una zona umida artificiale per il trattamento del carico inquinante proveniente dai due affluenti. Dopo aver piantato delle tife sul fondo di questa delimitata zona umida, e garantendo un percorso tortuoso, l'attuale efficienza di rimozione potrebbe essere raggiunta con molto meno volume. Ciò consentirebbe di isolare le

vasche rimanenti, che potrebbero quindi migliorare la loro qualità nel tempo.

Parole-chiave: Torbiere del Sebino, zona umida, tempo di residenza, circolazione, drifter

Acknowledgements

First of all, I would like to thank the whole hydraulic team of University of Brescia. In particular, my supervisor Marco Pilotti and my co-supervisor Giulia Valerio, who directed me and supported me both creatively and in practice. I thank my colleague Riccardo Bonomelli, who has taken to heart and strongly participated in the realization of some of the projects of Torbiere; and Gabriele Farina who is always ready to help.

This research project would not have been possible without the collaboration with Ente Gestore della Riserva Torbiere del Sebino and in particular the director Nicola della Torre and its willingness to help and share his knowledge with me.

I would like to thank Consorzio dell'Oglio, that allowed me to browse its archive and gave me some precious information about the management of Torbiere.

I here list the people and the associations who helped me during my research: Steve Chapra, Laura Barone (Acque Bresciane), Aldo Lazzaroni, all the ecological guards of Torbiere, the Carp Team, La Schiribilla, Associazione Monte Alto, Alessandro Nastro.

Then I would like to thank ARPA Lombardia and Consorzio per la tutela del Franciacorta for the important meteorological data they shared with me.

Contents

1. **Introduction** …… **p.1**
   - 1.1 Motivation and Objectives …….. p.1
   - 1.2 Thesis outline …….. p.3
   - 1.3 Hydrodynamics of shallow lakes: the role of the wind…….. p.4
   - 1.4 Ecology of shallow lake ……. p.5
   - 1.5 Ecological services of wetlands: Torbiere as a Carbon sink and a pretreatment pond …… p.7
   - 1.6 Wetland conservation …….. p.9
     - 1.6.1 Wetland restoration …… p.10
   - 1.7 Research questions ……. p.11
   - 1.8 References ……... p.14
2. **Field site** ……. **p.18**
   - 2.1 Geographical and geomorphological setting ……. p.18
   - 2.2 Land use within the watershed …… p.25
   - 2.3 History of Torbiere del Sebino ……. p.27
   - 2.4 Overview of the meteorological, hydrological and water quality data already available …….. p.28
     - 2.4.1 Meteorological station data in Iseo ……. p.29
     - 2.4.2 Rain gauge in Provaglio managed by Consorzio per la Tutela del Franciacorta ……... p.29
     - 2.4.3 Hydrobiological studies by Barbato …… p.29
     - 2.4.4 ARPA's final report on Lake Iseo's basin …….. p.31
     - 2.4.5 Consorzio dell'Oglio's water gauges' measurements of the water level of Torbiere and pump ON/OFF intervals ……..... p.32
     - 2.4.6 Unibs, Unipr and Acque Bresciane: preliminary study of a natural wetland and evaluation of the nutrient loading …….. p.33
     - 2.4.7 Cozzaglio's report about Torbiere's hydrological balance …… p.34
     - 2.4.8 Others ……..... p.35
   - 2.5 Some conclusions on data availability …… p.35
   - 2.6 References ……... p.38

3. **Monitoring activities accomplished in this study** …… **p.39**
3.1 Lame …… p.42
3.1.1 Water levels …… p.42
3.1.2 Water temperatures ……... p.44
3.1.3 Transparency ……..... p.47
3.1.4 Wind stations …….. p.49
3.2 Sparse sampling ……. p.56
3.2.1 2D-interpolated maps …… p.60
3.2.2 Vertical profiles ……..... p.62
3.3 Clay tanks: water temperatures …….. p.73
3.3.1 Estimation of diffusion coefficient ……. p.74
3.4 Inflow stations …… p.75
3.4.1 Rì: discharge, conductivity, and plume dynamics ……. p.75
3.4.2 Combined sewer overflow: discharge …… p.83
3.5 Water balance of Lame …….. p.83
3.6 References ……. p.87
4. **Numerical simulations** …….. **p.89**
4.1 Water levels and setup ……..... p.98
4.2 Temperatures ……. p.100
4.3 Clay tank temperature simulation ……..... p.102
4.4 Plume dynamics ……. p.106
4.5 References ……... p.110
5. **Drifter design and experiment** …… **p.113**
5.1 Drifter design ……. p.114
5.1.1 Hardware …… p.115
5.1.2 Software …….. p.119
5.1.3 Verification ……. p.120
5.2 Deployment analysis ……. p.125
5.2.1 An example of application: deployment of Feb 28th, 2022……. p.128
5.3 Model calibration ……... p.130
5.4 Discussions …….. p.133
5.5 References …… p.134

6. **Residence time simulation** ……..... **p.138**
6.1 Reactor analogy …….. p.139
6.2 The models …… p.143
6.2.1 Box model setup …… p.143
6.2.2 3D model setup ……. p.149
6.3 Results …. …….. p.151
6.4 A proposal for a remediation strategy …… p.157
6.5 References ……... p.164
7. **Conclusions** …….. **p.167**

Appendix A. Maps and Images p.174
Appendix B. Summary of the interviews p.188
Appendix C: Drogue deployments p.191
Appendix D: Additional material p.202

1. Introduction

1.1 Motivation & objectives

This Thesis summarizes the monitoring and modelling activities accomplished within my PhD on the hydrodynamics of a shallow lake in Northern Italy, Torbiere del Sebino, which belongs to the Natura 2000 network. This is the first extensive research published about this system and therefore, it is relevant for future attempts at deepening and improving the environmental aspects of this area. Given the absence of any specific work on the hydrology of Torbiere (see ch. 2.4 for existing previous studies), this topic has been addressed with an interdisciplinary approach, in the attempt to create a foundation for any future studies. If, on one side, this research has been challenging due to the lack of previous monitoring data, on the other it offered the possibility to set a monitoring program from scratch.

Being a complex aquatic ecosystem, beginning its study in terms of hydrology and hydraulic as a foundation of further analysis on water quality assessment and biological investigation, should be taken for granted, as also shown in Figure 1.1. However, historically, much more interest has been given to biological issues, neglecting or underestimating the role of the physics of the aquatic environment. This Thesis is a contribution to fill this knowledge gap.

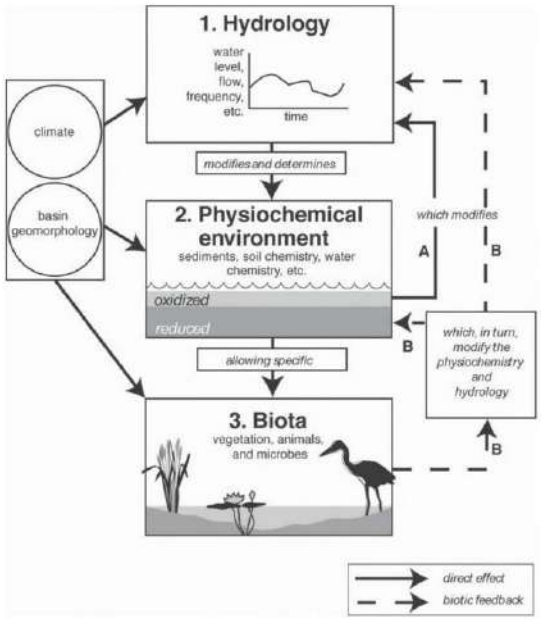

Figure 1.1 (Mitsch and Gosselink, 2007) Conceptual diagram illustrating the effects of hydrology on wetland function and the biotic feedbacks that affect wetland hydrology.

The ecosystem of Torbiere proved to be an emblematic case study for many environmental issues. It consists of a set of shallow lakes, differently interconnected, whose water quality depends also on their residence time distribution; within its borders, both polymictic and monomictic ponds are found, according to the different morphology and inflow conditions; wind plays a major role in the inner circulation, offering a great opportunity for its modelling; two major inflows, differently polluted, enter the system providing an excessive nutrient loading that negatively affects the trophic state of the basin; some ponds receive a considerable volumetric contribution from groundwater: the different nature of this inflow and its quality create a different ecosystem. All these peculiarities were not clear at the beginning of this research, but they have emerged as the Thesis progressed. What results is the picture of a very complex system, that will offer fertile ground for many different studies and that will require an interdisciplinary approach to be understood and improved.

The need of understanding the hydrodynamics of Torbiere del Sebino arises from the observation of its historical evolution and from environmental issues. This set of shallow lakes evolved during the past 70 years, passing from being a man-made ensemble of separated ponds to the actual

situation, where it is a unique wetland. Originated from the excavation of peat, it is now reduced both in extension and depth due to the progressive deposition of organic matter and advancement of the coastline under the pressure of growing vegetation. Most of the ponds are now in a hypereutrophic state, in striking contrast with the historical record of people that used to drink its, once clear, waters. All these changes occurred in a few decades together with a progressive loss in biodiversity, both aquatic and terrestrial, as a clear sign of anthropogenic influence.

There is no unique entity responsible for the deterioration of this system. The causes are many, mostly led by a poor understanding of the system that caused unfortunate managing choices and the increase of nutrient loading coming from the two inflows and climate change.

Torbiere del Sebino provides a set of important ecological services for its territory and its contribution is certainly underrated. This research aims to provide a deeper understanding of this system, disentangle some major environmental questions about its waters and provide insights and ideas for future studies in the fields of hydraulics, hydrology, and biology.

1.2 Thesis outline

The structure of this Thesis follows the course of the research itself. The first part of the study consisted of a literature review on shallow lakes hydrodynamics and ecology [ch.1.3 and 1.4] and of the acquisition of the past knowledge about this case in order to collect any available data [ch.2]. This phase confirmed that very few data had been collected about Torbiere, making it necessary to set up a monitoring activity and organize surveys and monitoring campaigns [ch.3] that highlighted the evidence of heterogeneity in the water quality of Torbiere [ch.3.2]. The experimental data that was obtained was used to support numerical simulations of water level and temperature [ch.4] and allowed for the calibration of turbulent diffusion coefficient [ch.4.4].

To address the one-of-a-kind topic of wind-induced circulation, a drifter was built and deployed in the system and the results of its recordings were used to calibrate the hydrodynamic model [ch.5].

Residence time distribution was evaluated by means of a box model and a 3D model and results were compared in order to understand how the system hydrodynamically responded to the change in geometry and pond separation that occurred during the years [ch.6]. Based on the findings of these simulations, a possible remediation strategy was proposed for Torbiere, following the idea that a nature-based solution is desirable for this wetland [ch.6.4].

1.3 Hydrodynamics of shallow lakes: the role of the wind

In shallow water bodies, especially in enclosed or semi-enclosed ones, wind is the critical meteorological factor that drives hydrodynamic processes and therefore influences water quality. Actually, being only a few meters deep, shallow lakes are much more influenced by bottom and nearshore processes compared to deep lakes.

The wind momentum transferred into the water at the lake surface results in waves, turbulent mixing, drift currents, Langmuir circulations, as well as large scale circulations and seiches. This momentum flux then drives the exchange processes at the lake bottom, the mixing in the water body, and influences the interaction between the littoral and the pelagic zones (Józsa J. 2006), resulting in a modification of the biogeochemical processes. By moving the surface waters, the wind can induce a shear stress at the bottom and stir up the uppermost sediment layer of the lakebed (Sheng and Lick, 1979; Dyer, 1986; Luettich et al. 1990; Rakoezi and Jozsa, 1999). They also can easily destroy diurnal temperature stratification making the water column homogeneous during the night.

Spatial changes in temperature, salinity, dissolved and particulate material depend on hydrodynamics and therefore, on wind conditions. Wind can impact suspended solids concentration, total phosphorus and chlorophyll-a (Tammeorg O. et al, 2013). The re-distribution of suspended substance may have significant influence on water transparency and light attenuation (Bubinas and Repeeka, 2003; Hawley, 2000, Havens et al., 2012). The alteration of the thermal stratification can influence the ammonium/ammonia concentration (Kann and Welch, 2005). Wind can also trigger nutrient release from the sediments causing an increase in the ammonium concentration of the water column (Wu et al. 2010) and other

nutrients (Cozar et al 2005, Hampel et al. 2018, Kann and Welch, 2005). Wind alters the distribution of phytoplankton in shallow lakes (Bresciani et al 2013, Wang et al. 2016), can enhance phytoplankton blooms (Carrick et al. 1993, Cyr 2017, Jiang and Xia 2017) and might cause a shift in phytoplankton species abundance (Huisman et al. 2004).

1.4 Ecology of shallow lakes

Eutrophication is a worldwide environmental issue in lakes. Shallow systems in particular are vulnerable to this process and to algal blooms due to the strong lake-land, air-water and water-sediment interactions (Boquiang Q., 2007).

Shallow lakes are found in nature in two alternative stable state: the clear and transparent ponds with submerged rooted plants and the turbid ponds with suspended sediments and blooming algae (Scheffer M., 2004). The reason for many lakes to become turbid is often eutrophication and the best way to address this issue appears to be the control of external sources of nutrients, without which a lake would continue to receive supply for its primary production. However, a sole reduction of nutrients in the attempt to restore the clear state of a shallow lake is often unsuccessful. Scheffer (2004) showed the tendency of systems with alternative stable states to stay in the same state despite changes in external conditions (Figure 1.2).

This phenomenon is referred to as “hysteresis” and indicates that to restore a phytoplankton-dominated lake to a previous macrophyte-dominated state, it is necessary to reduce external nutrient loads to levels that are lower than the ones present when the lake originally shifted state. The reason for this inertia lies in the role of the sediment-water interaction: the internal nutrient loads might exceed external loads on an annual basis; wind induces sediment resuspension; Phosphorus might be released from the sediment in anoxia conditions; animals rework the sediment (Abell et al, 2020).

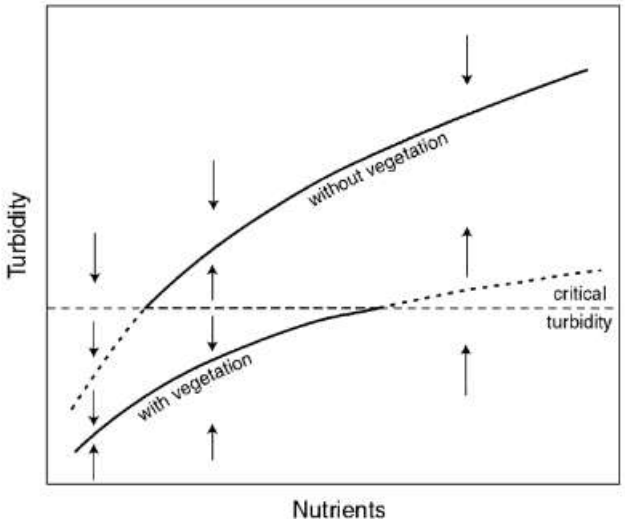

Figure 1.2 Alternative equilibrium turbidities caused by an abrupt disappearance of submerged vegetation when a critical turbidity is exceeded. When conditions are reversed, the system can change back to the original state at a different nutrient threshold. The arrows indicate the direction of change when the system is not in one of the two alternative stable states. (from Scheffer et al. 1993).

The reasons for a shallow lake to be eutrophic are multiple and include its location, its connectivity, the aquatic ecosystem, the amount and features of pollutants and nutrients coming both from external sources and from bottom deposits. In general, eutrophication is a natural process that leads waters to become more fertile and shallower. However, anthropogenic pressures can speed up this process (cultural eutrophication) as human activity accelerates land runoff, causing more nutrients to reach lakes and rivers and increase the supply by the use of fertilizers, the creation of treatment plants and the presence of untreated sewage.

In the context of climate change lakes and shallow lakes are some of the most threatened ecosystems. Greater mean temperatures are predicted to increase phytoplankton biomass, planktivorous fish, internal loading, nutrient mineralization, and nutrient loads during more intense precipitation events (Moss et al, 2011).

The Riserva Naturale Torbiere del Sebino shows clear signs of eutrophication (see ch.3.1.3) and is currently in a turbid phytoplankton-dominated state. Several algal blooms were recorded during this three year - study, with some occurring during winter months as well. Macrophyte

growth is currently limited to few areas, while there is evidence that some years ago was extended to more ponds. According to several people who are acquainted with this area for technical reasons, the last decades have also witnessed a worrying loss in biodiversity, that has been documented as far as birds and fishes are concerned (Gentili G., 2020). All these information make up an intricate puzzle whose dynamics are impossible to reconstruct based on sporadic observations only. Although there are some fundamental choices that go in the direction of hindering a further worsening of the quality of this ecosystem, we believe that what is needed is a long-term and interdisciplinary scientific study of this area, oriented to a wide and comprehensive knowledge of the eutrophication phenomenon and of its interconnections. We also strongly believe that this activity must be clearly finalized to implement technical interventions for the improvement of the ecological status of the wetland.

1.5 Ecological services: Torbiere as a Carbon sink and pre-treatment pond

Apart from the specific value of Torbiere d'Iseo, one of the most important wetlands in Lombardy, there are many reasons to engage in the study of this ecosystem. Wetlands cleanse the earth: they are carbon sinks as they absorb CO_2 and filter human waste, chemicals, and nutrients. They sustain regional water resources and buffer the excess of drought and flood (Proulx A., 2022). They also provide habitat for several fish, bird and insect species.

Torbiere del Sebino is no exception and furthermore, is an important site of recreation as it welcomes more than 100'000 visitors every year (estimated value number from paid entrances, Figure 1.3) and is a controlled fishing venue.

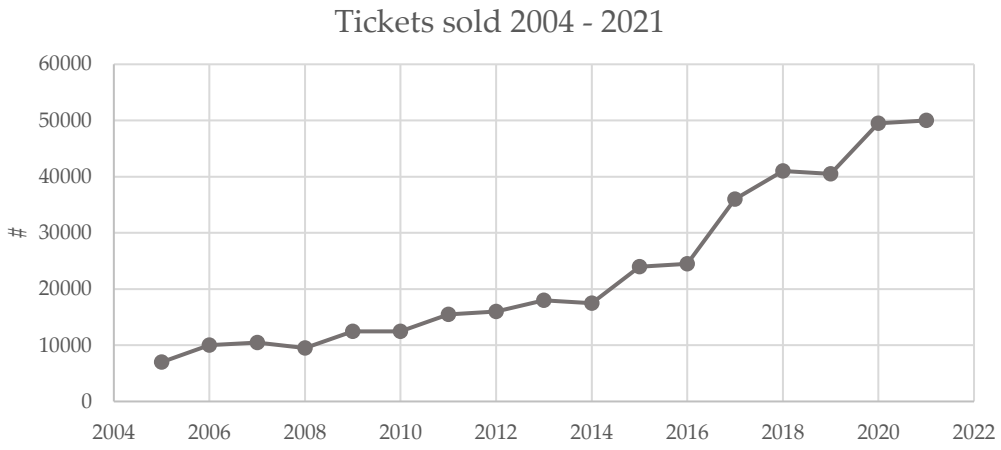

Figure 1.3 Tickets sold from 2005 to 2021. The number does not include the entrances of citizens from Corte Franca, Provaglio d'Iseo and Iseo, which have free entrance. Source: data from Ente gestore per la Riserva Naturale Torbiere del Sebino)

Since the end of excavation of peat, in the 1950s, Torbiere's ponds were no longer man-managed and organic matter started to settle to the bottom of the basin. Given the actual average sediment thickness, estimated at 10 cm (estimation derived from the comparison of the bathymetry of 1960 by Rossi and the present one, see ch. 2.1), and the sediment organic Carbon content measured at 22.9% (ARPA, 2006), one can conclude that Torbiere del Sebino contributes to an average organic Carbon burial rate of around 140 $g/m^2/year$. Given that the area of the system is $1.6 \cdot 10^6$ m^2, this is a significant contribution to the carbon sink on a local scale. This is possibly the only positive outcome of the hypereutrophic state of the system: the high levels of biological productivity enhance the accumulation of organic matter (Skwierawki A., 2022). In a climate change scenario, the rate of carbon sink is expected to increase, enhancing the role of mitigation of Torbiere.

Another important service provided by Torbiere del Sebino is evident if one considers its location along the southern banks of lake Iseo. This wetland receives waters from two main inflow located South: one is a small, natural stream (T. Rì) that drains a 6 km^2 urbanized watershed, which flows in a lowland where the dominant culture are vineyards. This watershed has been subjected to a strong (550%) urbanization since 1954 (*Piano Territoriale Regionale d'Area della Franciacorta*). The second inflow is a combined sewer overflow, which acts as the only flow regulator for the sewer of Provaglio

d'Iseo providing an intermittent discharge during rainy events. Both these inflows bring great amounts of nutrients to the system [ch.2.4.6]. After crossing Torbiere, these waters flow out in lake Iseo, after an average residence time of 1.5 years. Accordingly, currently the wetland acts as a pre-treatment stage, regulating nutrient levels before the final discharge into the lake.

This ecological service has not been recognized and there is only one recent study (ch. 2.4.6) that highlighted the extent of nutrient loading coming from the surrounding watershed of Torbiere. In this document, the construction of a detention pond and of a constructed wetland downstream the Combined Sewer Overflow that discharges in Torbiere is strongly encouraged as a way to mitigate the anthropic pressures on the Natural Reserve. Currently the combined sewer overflow still discharges its untreated waters directly into the Natural Reserve of Torbiere.

Torbiere, in the way we know them, did not exist before the peat-extraction activities that started during the 19th century. Accordingly, it is a production of man-caused disturbance over recent historical times. However, the disruption of the pre-existing equilibria in the drained watershed as well as newer threats from climate change are triggering the rapid degradation of its ecosystem, that might include the disruption of the hydrological cycle, the reduction of biodiversity and the decrease of its ecosystem services.

1.6 Wetland conservation

Attention towards wetland conservation has increased over the past decades and it became clear that the rate at which wetlands are being lost is incredibly fast, particularly in developing countries (Mitsch and Gosselink, 2007). This is easily comprehensible because in the past the emphasis was on land reclamation that had strong economic and sanitary reasons. Nowadays more than 2400 wetlands worldwide are protected under the RAMSAR convention on wetlands of international importance (Scheffers A.M. and Kelletat D.H., 2016). Italy in particular has 57 RAMSAR-sites, as of 2021 (MITE, 2022) and among these is found Torbiere, since 1984.

The Convention was adopted in Ramsar, Iran in 1971 and aims at an integrate wetland protection and conservation into sustainable

development, to halt and reverse wetland loss. The main recommended tools are climate and biodiversity plans, together with national policies and legislation.

In November 2022, the COP14 (Conference of the Parties) was held in Wuhan and Switzerland and the urgency to act of wetlands was reaffirmed, as one of the most useful actions for climate mitigation, adaptation and resilience.

1.6.1 Wetland restoration

Wetland restoration is the manipulation of a former or degraded wetland's physical, chemical or biological characteristic to return to its natural functions (US EPA, 2007). The actions can be distinguished in re-establishment, i.e., the increase of wetland extension through restoration and rehabilitation, i.e., the improvement of natural wetland conditions and functions.

The restoration of natural wetlands, together with the building of constructed wetlands has been recognized as one of the best practices that reduce nutrient loading (Abell J.M. et. Al., 2020) worldwide. The efficiency of wetlands is now common knowledge. In Lake Apopka (Florida) total Phosphorus and Chlorophyll-a concentrations decreased by 40-50% ten years after the building of a constructed wetland for external load reduction (Coveney et al. 2005). Similarly, a wetland creation in 1990s contributed to the decline of phytoplankton biomass in Finnish Lake Finjasjön (Annadotter H. et al. 1999).

However, wetlands are becoming themselves more and more frequently the ecosystems in need to be restored. As explained in ch. 1.4, a shallow lake (or a wetland) can be found in one of the alternative stable states of macrophyte or phytoplankton dominance. Submersed macrophyte dominance is the prevalent condition but as nutrient levels increase, the macrophyte community is first replaced by larger submersed plants, than by tall plants such as water lilies and finally by phytoplankton (Wetlzel, 2001). Phytoplankton communities tend to persist in spite of changing nutrient availability and a restoration to the former macrophyte-dominated stable state is rather challenging.

The restoration techniques to be adopted can be subdivided into three main categories: physical technology, chemical technology and biotechnology (Zhou D. et al. 2020). The first ones include the change in wetland hydrology and land use, together with rewetting techniques and sediment dredging. Chemical techniques refer to the addition of algaecides, precipitation agents or to a rational fertilization of soil. With biotechnology we refer to the addition of microorganisms, plants to increase the degradation process of contaminants and the absorption of nutrients and heavy metals.

Worldwide, phytoremediation and engineering restoration are the most used actions (Moreno-Mateos D. et al., 2015, Zhou D. et al. 2020), as a combination of these techniques might get the best restoration effect and accelerate the recovery process (Williams J.B., 2010). Phytoremediation exploits the natural bioaccumulation abilities of plants (McIntyre 2003, Meagher 2000, Dietz and Schnoor 2001, Salt et al. 1998) and is a solar-driven, passive and poorly intrusive technique; revegetation showed to be particularly efficient in peatlands (Klimkowska et al. 2007), saltmarshes and mangroves. Water engineering can create a favorable water environment and promote self-repair processes (Goodwin P., 1994) through hydrological manipulation. The stability of a wetland is in fact linked to their hydroperiod: the water balance affects the hydraulic residence time, and the seasonality of wetland functions ultimately has a major role on the magnitude of phytoremediation actions.
There is a clear link between the hydrology of a wetland and the rates of remediation reactions occurring, and site-specific hydrological analyses must accompany plant community characterization when applying revegetation techniques (Williams J.B., 2010).

1.7 Research questions

In the present situation, characterized by a substantial lack of data regarding Torbiere d'Iseo, this research aims at paving the way for a systematic monitoring activity at least of some physical parameters of water and of the fundamental meteorological variables that govern water motion. It will also try to provide some answers to the following questions:

Is there any particular spatial pattern in the distribution of the environmental variables within Torbiere that can be a sign of localized biotic or abiotic dynamics?

The question is if there is an environmental gradient defining the distribution of abiotic variables, between different areas of the wetland that are subjected to different hydrodynamic forcings. A positive answer would point to the presence of areas with peculiarity that could be investigated to figure out which elements can influence the dynamics of Torbiere, in contrast with the indication of a perfectly mixed environment that would arise from a negative answer.

Are there ponds with different vertical mixing regimes across the different parts of Torbiere?

Naturally, one could expect that a shallow wetland with average depths in the order of a few meters, are polymictic, i.e. with waters that mix from top to bottom throughout the year. However, in reality Torbiere are a heterogeneous system, with very shallow ponds as well as deeper ones with maximum depth of about 10 m. Accordingly. Also considering the strong sheltering effect exerted by the surrounding trees, one could also expect different mixing regimes. This question will be addressed by both monitoring and modelling tools.

To what extent can numerical modelling help in describing this wetland's functioning?

Numerical modelling tools are the best way to understand the hydrodynamics of Torbiere, which certainly has a controlling effect on the ecological environment. However, there is also a need to calibrate a numerical model and several lessons can be learnt from their application concerning the sensitivity of the model and the delicate matter of their calibration.

Would a restoration of the banks of Torbiere to their pristine condition benefit its water quality by altering the residence time distribution?

After observing this environment for several years, we came to the conclusion that Torbiere del Sebino were negatively impacted by the gradual increase of connectivity that developed over the last 7 decades. The innovative idea behind this question is that a higher degree of connectivity

is not associated to a better quality, if the inflow is polluted. The question, apparently never explored in the literature of wetlands, is addressed by means of a box model and a 3D model, in order to evaluate whether one tool is more suitable for the purpose.

Which type of velocity measurement is best suitable for a shallow system like Torbiere?

We came to the conclusion that drifters are the best tool for measuring horizontal velocity, especially in wind-driven systems with slow velocities. However, the Torbiere being very shallow, we did not find suitable drifters available on the market. By building a new and low-cost drifter, the question to be explored is whether this innovative design is appropriate for this wetland and elsewhere.

What are the priorities for Torbiere in terms of ecological restoration?

Several projects have been carried out on Torbiere throughout the years, each of them addressing a very specific aspect of its environmental issues. In our opinion, an overall view is lacking, that would set a priority list, making each of the interventions, much more effective.

Can a remediation strategy be proposed for Torbiere?

Once the ecological and environmental challenges for Torbiere have been understood, it is possible to think of a suitable remediation strategy that would improve the ecosystem status without disrupting the landscape nor requiring an excessive degree of maintenance.

1.8 References

Abell J.M. et al. (2020). Restoring shallow lakes impaired by eutrophication: approaches, outcomes, and challenges. *Critical Reviews in Environmental Science and Technology*, 52.

Annadotter, H., Cronberg, G., Aagren, R., Lundstedt, B., Nilsson, P.-_Å., & Streobeck, S. (1999). Multiple Techniques for Lake restoration – The Ecological Bases for Lake and Reservoir Management. In D. M. Harper, B. Brierley, A. J. D. Ferguson, & G. Phillips (Eds.), *Proceedings of the Ecological Bases for Management of Lakes and Reservoirs Symposium*, held 19–22 March 1996 (pp. 77–85). Leicester, UK: Springer Netherlands.

Bresciani, M., Rossini, M., Morabito, G., Matta, E., Pinardi, M., Cogliati, S., Julitta, T., Colombo, R., Braga, F., Giardino, C. (2013). Analysis of within- and between-day chlorophyll-a dynamics in Mantua superior Lake, with a continuous Spectro radiometric measurement. *Mar. Freshw. Res*. 64 (4), 303–316.

Bubinas A., Repeeka M. (2003). Distribution of zoobenthos in the bottom sediment of the near-shore zone of the Baltic Sea in Nida-Klaipeda Stretch[J]. *Acta Zoologica Lituanica*, 13(2): 125–134.

Carrick, H.J., Aldridge, F.J., Schelske, C.L. (1993). Wind influences phytoplankton biomass and composition in a shallow, productive Lake. *Limnol. Oceanogr*. 38 (6), 1179–1192.

Chen F. et al. (2020). The importance of the wind-drag coefficient parametrization for hydrodynamic modeling of a large shallow lake. *Ecological Informatics*, 59.

Coveney, M. F., Lowe, E. F., Battoe, L. E., Marzolf, E. R., & Conrow, R. (2005). Response of a eutrophic, shallow subtropical lake to reduced nutrient loading. *Freshwater Biology*, 50(10), 1718–1730. EPA (2007). Environment Science Report.

Cozar A. et al. (2007). Relationships between wetland ecotones and inshore water quality in the Ugandan coast of Lake Victoria. *Wetlands Ecology and Management*, 15, 499-507.

Cyr, H. (2017). Winds and the distribution of nearshore phytoplankton in a stratified lake. *Water Res*. 122, 114–127.

Dietz AC, Schnoor JL. (2001). Advances in phytoremediation. *Environ Health Perspect* 109:163–168.

Dyer K.R. (1986). Coastal and estuarine sediment dynamics. *Wiley*.

Goodwin P. (1994). Physical processes in tidal wetland restoration, In: falconer RA and Goodwin P (eds.), *Wetland management. Proceedings of the international conference organized by the institution of civil engineers*. Thomas Telford, London, U.K.

Hampel, J. J., McCarthy, M. J., Gardner, W. S., Zhang, L., Xu, H., Zhu, G., and Newell, S. E. (2018). Nitrification and ammonium dynamics in Taihu Lake, China: seasonal competition for ammonium between nitrifiers and cyanobacteria, *Biogeosciences*, 15, 733–748.

Hawley, N. (2000). Sediment resuspension near the Keweenaw Peninsula, Lake Superior during the fall and winter 1990-1991. Journal of Great Lakes Research 26(4), 495-505.

Huisman, J., Sharples, J., Stroom, J.M., Visser, P.M., Kardinaal, W.E.A., Verspagen, J.M.H., Sommeijer, B. (2004). Changes in turbulent mixing shift competition for light between phytoplankton species. *Ecology* 85 (11), 2960–2970.

Jiang, L., Xia, M. (2017). Wind effects on the spring phytoplankton dynamics in the middle reach of the Chesapeake Bay. *Ecol. Model*. 363, 68–80.

Kann J., Welch E.B. (2005). Wind control on water quality in shallow, hypereutrophic upper Klamath Lake, Oregon. *Lake and Reservoir Management*, 21(2), 149-158.

Klimkowska, A., Van Diggelen, R., Bakker, J.P. & Grootjans, A.P. (2007). Wet meadow restoration in Western Europe: a quantitative assessment of the effectiveness of several techniques. *Biological Conservation*, 140, 318–328.

Luettich R.A., Harleman D.R., SomlyOdy L. (1990). Dynamic behavior of suspended sediment concentrations in shallow lake perturbed by episodic wind events. *Limnology and Oceanography*, Vol. 35, Issue 5, 1050-1067.

Meagher R.B. (2000). Phytoremediation of toxic elemental and organic pollutants. *Curr Opin Plant Biol* 3:153–162

Mcintyre T. (2003). Phytoremediation of heavy metals from soils. Phytoremediation. *Springer*, Berlin/Heidelberg.

Moreno-Mateos D., Meli P., Vara-Rodriguez M.I., Aronson J. (2015). Ecosystem response to interventions: lessons from restored and created wetland ecosystems. *Journal of Applied Ecology*, 52, 1528-1537.

Moss, B., Kosten, S., Meerhof, M., Battarbee, R., Jeppesen, E., Mazzeo, N., et al. (2011). Allied attack: climate change and eutrophication. *Inland Waters* 1, 101–105.

Rakoczi L., Jozsa J. (1999). On the sediment dynamics in the Hungarian part of lake Neusiedl. *Proceedings of the 28th IAHR World Congress*.

Salt DE, Smith RD, Raskin I (1998). Phytoremediation. *Annu Rev Plant Physiol Plant Mol Biol* 49:643–668.

Scheffer M. et al. (1993). Alternative equilibria in shallow lakes. *Trends in Ecology & Evolution*, Vol.8(8), 275-279.

Sheng Y.P and Lick W. (1979). The transport and resuspension of sediments in shallow lakes. *Journal of Geophysical Research*, Vol. 84, Issue C4, 1809-1826.

Skwierawski A. (2022). Carbon Sequestration Potential in the Restoration of Highly Eutrophic Shallow Lakes. *Int. J. Environ. Res. Public Health*, *19*(10), 6308.

Tammeorg O. et al. (2013). Wind-induced sediment resuspension as a potential factor sustaining eutrophication in large shallow Lake Peipsi. *Aquatic Sciences*, 75(4).

Wang, H., Zhang, Z., Liang, D., du, H., Pang, Y., Hu, K., Wang, J. (2016). Separation of wind's influence on harmful cyanobacterial blooms. *Water Res*. 98, 280–292

Williams J.B. (2010). Phytoremediation in wetland systems: progress, problems and potential. *Critical review in plant sciences*, 21:6,607-635.

Wu, Y., Xiang, Y., Wang, J., Zhong, J., He, J., and Wu, Q. L. (2010). Heterogeneity of archaeal and bacterial ammonia-oxidizing communities in Lake Taihu, China. *Env. Microbiol. Rep.*, 2, 569–576.

Zhou D., Yu J., Guan B., Li Y., Yu M., Qu F., Zhan C., Lv Z., Wu H., Wang Q., Yang J. (2020). A comparison of the development of wetland restoration techniques in China and other nations. *Wetlands*, 40: 2755-2764.

Books

Boqiang Q. et al. (2007). Eutrophication of shallow lakes with special reference to Lake Taihu, China. *Development in Hydrobiology*, Vol. 194.

Dungan P.J. (1990). Wetland conservation: a review of current issues and required action. *IUCN*.

Jòzsa J. (2006). Shallow lake hydrodynamics. Theory, measurement and numerical model applications. Budapest University of Technology and Economics, department of Hydraulic and Water Resources Engineering.

Mitsch, W. J. & J. G. Gosselink, (2007). Wetlands, 4th ed. *John Wiley & Sons, Inc*, Hoboken, New Jersey, USA, 582.

Scheffer M. (2004). Ecology of Shallow Lakes. *Population and Community Biology Series*, Vol. 22.

Scheffers A.M. and Kelletat D.H. (2016), Lakes of the world with Google Earth, Understanding our Environment. *Springer Int. Publishing Switzerland*.

Web Articles

Proulx A. (2022). Swamps can protect against climate change, if we only let them. *The New Yorker, Annals of Nature*, 4th July 2022 Issue.

Havens K.E., Beaver J.R., James T., Lind O.T., Boquiang Q. (2012). Wind effect in shallow lakes. *LakeLine* 32:3, Fall 2012, pp. 17-20.

Others

ARPA Lombardia (2007). Rapporto Osservatorio 2006/2007.

Gentili G. (2020). Progetto di contenimento del siluro (Silurus Glanis) nella Riserva Naturale Torbiere del Sebino e nell'area del basso Lago d'Iseo.

https://www.mite.gov.it/pagina/elenco-delle-zone-umide

2. Field Site

Since 2015 the research group of hydraulics of the Faculty of Engineering of the University of Brescia, which had already focused its research on the subalpine lakes of Garda and Iseo, has extended its area of research including the Riserva Naturale Torbiere del Sebino. To the best of our knowledge, no previous study had ever investigated this wetland's hydrodynamics nor its water quality in an extensive manner. Actually, the existing data set aimed at providing a photograph of some water quality parameters, disregarding the mixing and circulation processes, the thermal evolution and stratification and very little attention was given to the spatial heterogeneity of the system. The discharges entering the system were not monitored and therefore, residence time had never been computed nor estimated. The last measurements of some physical and water quality parameters date back to 2007 [ch. 2.4.4], as ARPA has not yet included the Torbiere within the list of its monitored sites.

This Chapter will provide an overview of the study-case under consideration. Chapter 2.1 presents a general description of the geographical and geomorphological setting of Torbiere. Then, the Chapter 2.3 explains the origin of the wetland and its historical evolution in the last centuries. Chapter 2.4 deals with a review of the past knowledge about this case in terms of data already available. A critical analysis of these data will be then provided in Chapter 2.5.

2.1 Geographical and geomorphological setting

The Riserva Naturale Torbiere del Sebino is located in the Southern banks of subalpine lake Iseo, in Northern Italy, at latitude 45.6° N and longitude 10.1° E (see Figure 2.1). It's the most important wetland for extension and ecological relevance of the province of Brescia and belongs to the municipalities of Provaglio d'Iseo, Iseo and Corte Franca, which share different portions of its territory. Torbiere's borders include a) Lame, a set of highly interconnected ponds of 1.5 - 2 m average depth, whose total area is around $1.6*10^6$ m^2 and that are the focus of this Thesis; b) Lametta, a smaller area located in the Northern portion of the Reserve, close and connected to Lake Iseo, with an average depth of 1.5 m and an area of $9*10^5$ m^2; c) Clay ponds, a set of separated tanks located along the Southern

border of the Reserve, much more recent than Lame (they were excavated in 1960s and 1970s). Their sediment is mainly made of clay, their average depth is 4.5 m, and their total area is $2.5*10^5$ m^2 d). The surrounding fields are either cultivated or fully vegetated, including some portions of this area that used to be ponds then filled by sediments over the years.

As mentioned, the focus of this Thesis has been on Lame, the biggest portion of the system. Lame appears as a set of ponds only partially separated by banks that are the remnants of the floodplain within which, starting in 1860, the ponds were dug for turf extraction. These banks are vegetated. Three visitors' paths were built, that allow tourists and locals to walk around the Reserve and cross it along a central trail. These paths do not block the overall water circulation and currently there is no pond that is hydraulically disconnected from the others in Lame.

Figure 2.1 Location of Torbiere

The main inflow, Rì stream (historically also known as "*Antiquà*", from the name of the mill installed on the river course) is located South and has an average discharge (October 2019 – January 2023) of around 0.04 m^3/s, which corresponds to a theoretical renewal time of 1.5 years. The main outflow is located North at a site known as "*Nedrini*", and is an artificial channel regulated by a pump, that may discharge some of Torbiere's waters into

lake Iseo, in case of strong rainfall events (see ch. 2.4.5). This pumping station was originally set to keep the area of the Torbiere empty during the excavation activities. A second affluent is a combined sewer overflow located in the municipality of Provaglio d'Iseo (see ch.3.4.2). Its volumetric contribution is marginal, but it delivers great loadings of nutrients. Finally, some minor tributaries are present on the west side of Torbiere, coming from Timoline. Along the eastern side of Torbiere there are probably some springs supplied by water flowing down from "Corno di Provaglio". Among these, a documented historical spring is present with a discharge of about 5 L/s according to Cozzaglio.

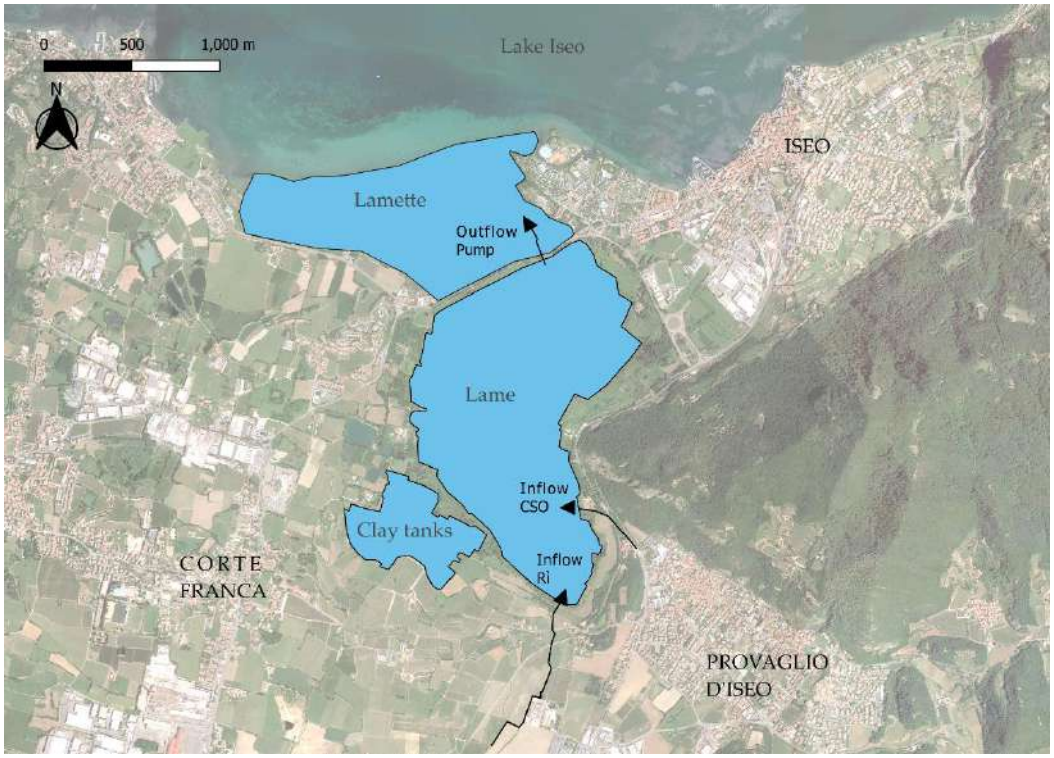

Figure 2.2 the basin of Torbiere, subdivided into Lame, Lamette and clay tanks and the main inflows and outflows of the system

The sediment of Torbiere consists mainly of peat, while it is surrounded by moraine deposits. In the southern portion of its watershed, lake clays are present. The groundwater table is located 130 m asl, around 50 m below the bottom of the wetland (Cozzaglio A., 1932) but some more superficial aquifers are present as well.

Figure 2.3 Bathymetry of Lame and Clay tanks (2019-2022). Accuracy = 0.1 m

To our knowledge, the only available bathymetry of Torbiere was developed by Rossi in 1960 (Consorzio dell'Oglio, Brescia) and his survey was used for all the studies that have followed, without any updating. Although it is difficult to come to clear conclusions without knowing the average water depth that characterized the Rossi's survey, the surveys (> 200 points) during this three-year study confirmed the idea that the progressive, natural silting occurring in Torbiere (figure 2.4a), has very likely increased the height of the sediments, diminishing the total volume of water retained by the basin.

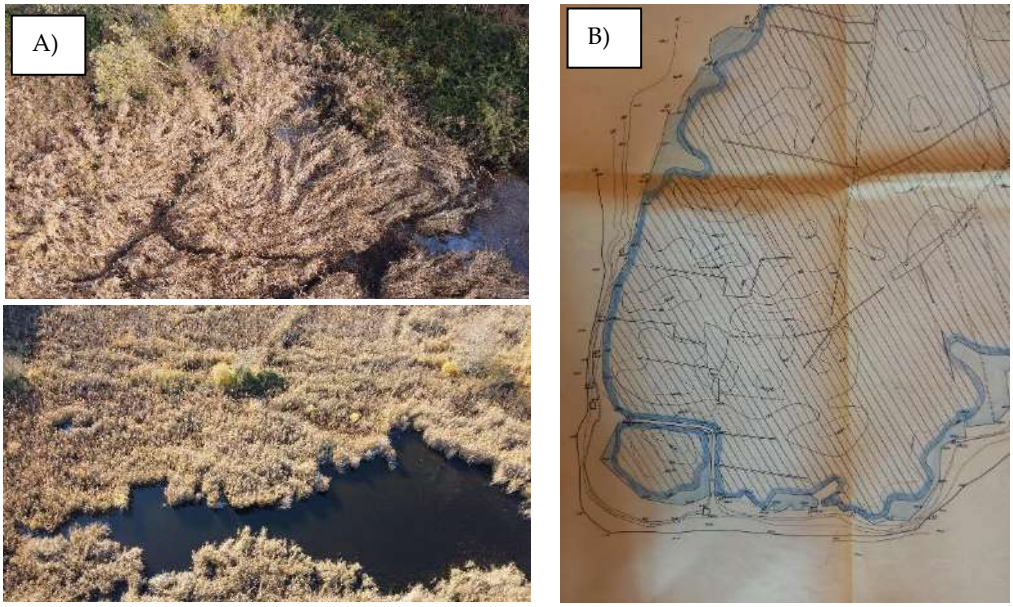

Figure 2.4 a) effects of silting within some ponds located in the eastern side of Torbiere. b) photograph of a detail of the paper map of the bathymetry of 1960

For instance, a maximum 3 m water depth has been detected in the northern ponds of Torbiere during this study, while the 1960 bathymetry indicates the presence of an extended area as deep as 4 m or more. The surveys conducted since 2019, corrected to take into account the water depth variations, were used to produce the bathymetry shown in Figure 2.3 and 2.5a. Even if the map is not expressed in terms of absolute altitude, it provides a representation of the depths that are found in the different areas of Torbiere. Figure 2.5b shows the bathymetry of 1960 by Rossi that we reconstructed from paper documents.

Shallower ponds are found in the southern part of Lame, while deeper points were measured in the middle and northern area. Comparing the results with the bathymetry of 1960s, it seems that once Torbiere were deeper, reaching 4 m of depth in many areas. This is a clear sign of progressive silting due to sedimentation of organic matter. Overall, the biggest difference in the two bathymetries (figure 2.5c) is found in the middle portion of Torbiere, in correspondance of the central area, and in the Southern ponds in general. A zone in the South-East portion, already shallow in the 1960, further decreased its depth. In front of the inlet of the combined sewer overflow (see ch. 2.4.6 and 3.4.2) of the municipality of

Provaglio d'Iseo, the silting is arguably due to the accumulation of great loading of organic matter and sediment coming from that source.

Different depths are found on the sides of the same banks. This is due to a pristine condition where ponds had been excavated down to different depth and also to the effect of the wind, that blows along the direction South-West and North-East, generating the accumulation of sediment in the lateral areas.

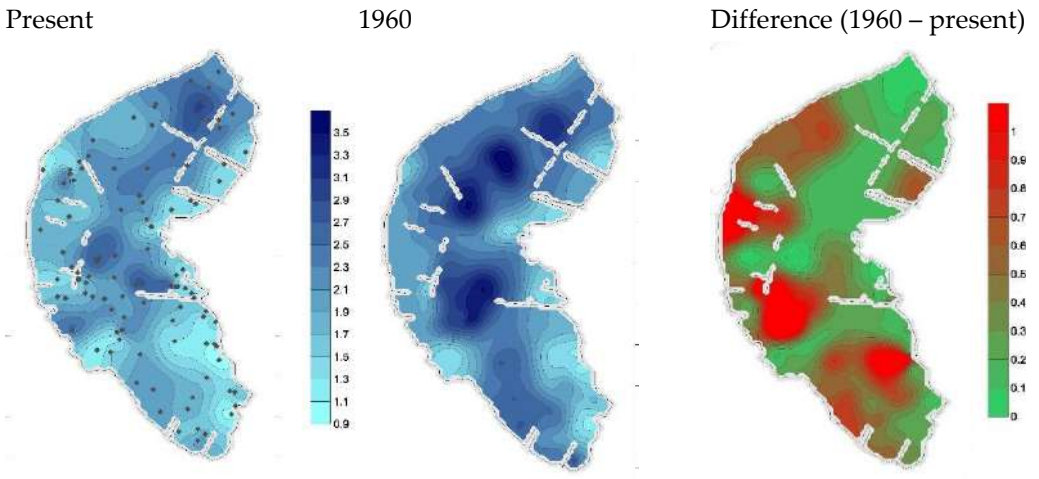

Figure 2.5 Bathymetry (obtained with the minimum curvature interpolation method) of Lame a) nowadays and b) in 1960. c) Difference between the two bathymetries. All the values are in meters. The black dots indicate the location of the points used for the creation of the bathymetric map.

Torbiere del Sebino's hydrometric zero lies at an altitude of 185.23 m asl (Consorzio dell'Oglio). The reserve is situated north of a small morainic hill and is limited eastward by a 600 m asl rocky hill ("Il Corno" di Provaglio). As will be highlighted in ch. 3.1.4, these morphological peculiarities determine the wind regime on the wetland and, consequently, influence its internal circulation.

Figure 2.6 Satellite picture of Torbiere and digital elevation map of the surroundings.

2.2 Land use within the watershed

The watershed of Torbiere has been subject to considerable changes in land use over the recent decades. The increase of population led to an increase of residential, industrial and commercial areas and gradual replacement of fields.

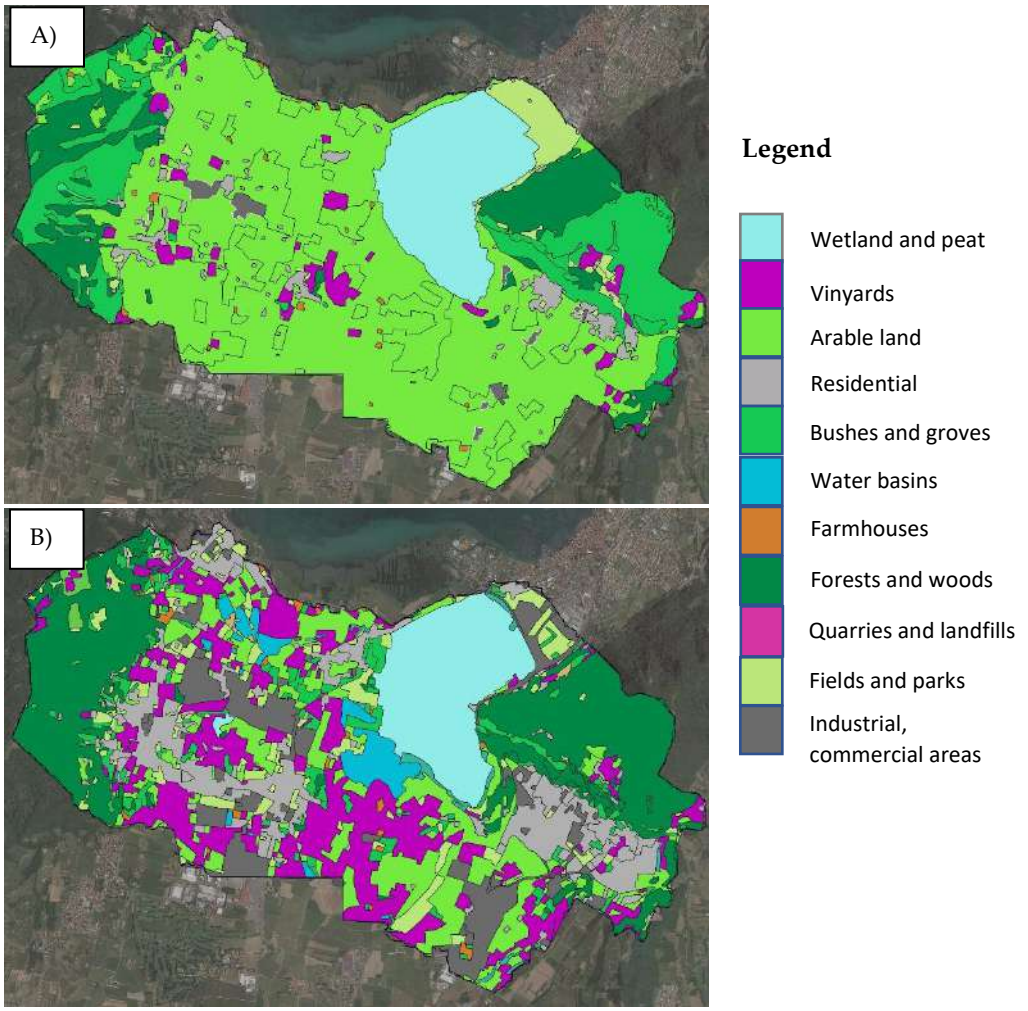

Figure 2.7 land use of the watershed of Torbiere in a) 1954 and b) 2018 (Geoportale della Regione Lombardia)

The watershed of Torbiere is an area of great economic value. In order to identify the perimeter of this watershed, we used a software for the extraction of the drainage network from a Digital Elevation Model. Having an extension of 18.6 km^2 (if we include the watershed of Lamette, 14 km^2 otherwise), it hosts several wineries which produce the typical Franciacorta wine. Their production has increased each year since 2011 (Consorzio per la tutela del Franciacorta, 2022) and so have their revenues. These wineries

benefit from a climate mitigated by the lake, the Natural Reserve of Torbiere and the surrounding hills, and rely on a landscape for attracting tourists every year. At the same time, the use of fertilizers from agricultural practices increases nutrient runoff as well as the loading on the main affluent of Torbiere, worsening the water quality status of Lame and enhancing the eutrophication process.

From 1959 to 2018, the watershed of Rì (land use in figure 2.8), Torbiere's main affluent, decreased its arable land share in favor of vineyards (that occupied only 4% of the total area, while now represent the 37%). The urbanized area in the municipalities of Corte Franca and Provaglio d'Iseo increased by 550% (Piano Territoriale Regionale d'Area della Franciacorta). In ch. 2.4.6, a study by Unibs, Unipr and Acque Bresciane is presented, that estimated the nutrient loading coming from the watershed.

Despite the absence of historical studies on the water quality of the waters coming from Rì, we expect this overall land use change had a strong effect on the chemical profile of the stream's waters, particularly in terms of nutrient loading.

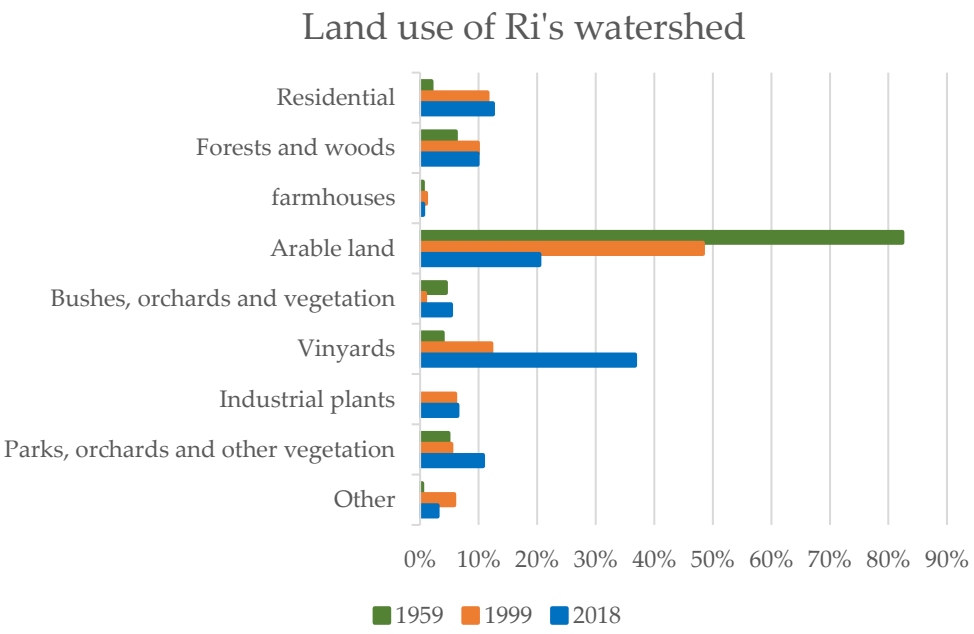

Figure 2.8 Land use of Rì's watershed in the years 1959, 1999 and 2018 (Geoportale Regione Lomabrdia)

2.3 History of the study site

Torbiere's origin dates back to the last glaciation (during the Quaternary), when the glacier of the Camonica Valley retreated, creating a large lake, that included the actual lake Iseo and Torbiere and that was 10 m higher (torbieresebino.it). With time, the outflowing Oglio river eroded its bed, causing a lowering of Lake Iseo level and the emersion of a morainic hill, that now separates the two water bodies. Since then, the stories of lake Iseo and Torbiere diverged and Torbiere developed marsh vegetations that lead to the peat deposits. The term "Torbiere" means, actually, "peat bogs". Until the middle of the eighteen's century, this area was periodically flooded and partially swampy, with some portions used for the cultivation of fodder. In the nineteenth century, peat's potential as a source of energy was discovered and the sediment of this wetland began to be excavated, leaving a landscape similar to that of the post glacier era: a marsh basin. The only difference was the presence of some internal banks that trace the ancient grazing lands, and that were used by workmen to transport the excavated peat. This is the description of the Torbiere layout as given by Cozzaglio (1932), in his study about the possibility of land reclamation of Torbiere and its use as a reservoir (see ch.2.4.7).

Peat excavation completely ended in the 1960s and since then, the wetland has been left to its natural evolution, the only exception being the cutting of some banks at the end of the twentieth century to allow the passage of water from one pond to the other, probably with the aim of increasing the connectivity of the system, as a way to limit the pollution level of the southern pond. We were not able to find any written explanation of the interventions that over the years have progressively taken to the opening of banks between the different ponds. This intervention has been of particular importance for Torbiere, has it changed the mixing processes of the basin and arguably, has had effects on the residence time distribution of the system (see ch.6).

At the end of the productive period of Torbiere, several options were considered on how to exploit the area. One even considered the possibility to build a dump. Eventually, better solution emerged, and it was realized

that the area deserved a special level of protection. The path towards the institution of the Natural Reserve followed several steps (torbieresebino.it):

- 29/04/1960: the Lamette and part of the Lame were included in a Ministerial act, becoming an area of respect, protected by ministerial constraints.
- 20/06/1970: Torbiere are declared "biotope of exceptional importance" by the Consiglio Nazionale delle Ricerche (CNR).
- 27/07/1977: Torbiere are inserted by Lombardy Region in the list of geotopes to be converted into Natural Reserve. The excavation of peat is definitively stopped.
- 15/03/1983: the consortium for the management of Torbiere is approved by the Region and is supported by the municipalities of Provaglio d'Iseo, Iseo, Corte Franca, by the Comunità Montana del Sebino and by the Province of Brescia.
- 30/11/1983: with the regional law n.86 Torbiere becomes a Natural Reserve.
- 11/06/1984: Torbiere is declared area of international interest for migratory birds by ministerial decree in accordance with the Ramsar convention.
- 19/12/1984: the management of the Reserve is entrusted to the Consortium.
- 21/03/1986: the first management plan is created and proposed by the consortium to the Region for its final approval, obtained on 13/09/1988.

Torbiere constituted an important economic source during last century and there were people living within its borders. Their livelihood depended on grass, wood, fish and birds offered by the wetland (see Appendix B when some interviews with local people are presented).

2.4 Overview of the meteorological, hydrological and water quality data already available

In this chapter all the past contributions to the knowledge of the basin and the ecosystem of Torbiere have been collected, with focus on the quantitative environmental data useful for the characterization of the waters of this basin.

2.4.1 Meteorological station data in Iseo

A meteorological station managed by the hydraulic group of the University of Brescia is present in Iseo (45°39'28.8'',10°2',36.24'') and has been active since May 2010 (Valerio G. et al., 2012). It measures wind speed and direction, atmospheric pressure, air temperature, relative humidity, short wave radiation and lake level at a frequency of 1/minute (see also ch.3).

2.4.2 Rain Gauge in Provaglio managed by Consorzio per la Tutela del Franciacorta

Over the years Consorzio per la Tutela del Franciacorta has installed n.40 rain gauges, distributed on the territory of Franciacorta, in the province of Brescia. The aim of these instruments is to give insight on the rainfall spatial patterns on an area that economically relies on vine cultivation. One sensor in particular, *0020547B Provaglio San Carlo* has been chosen for the evaluation of rainfall on Torbiere, due to its proximity to the Reserve. It has been active since December 2017 and records rainfall with an hourly frequency. Figure 2.9 shows the rainfall recorded since June 2020, together with the cumulative value. A study of the previous recordings shows that the average precipitation in this area is 1250 mm/year (consistent with the rainfall measured at Sarnico by ARPA Lombardia).

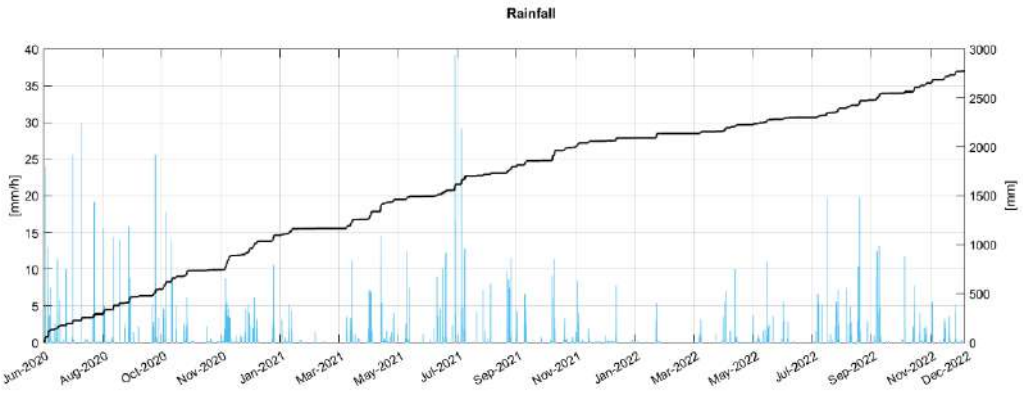

Figure 2.9 Rainfall measured at Provaglio San Carlo (June 2020 – December 2022).

2.4.3 Hydrobiological studies by Barbato

In the context of a LIFE project, from 2000 to 2003, the hydro-biologist Gaetano Barbato took seasonal samples of Torbiere's water at ten different locations: 7/10 from Lame, 2/10 from Lamette and 1/10 at the inlet of Rì's

stream. Samples were analyzed according to Standard Methods for Examination of Water and Wastewater (APHA,1995). Phytoplankton and zooplankton species were monitored as well, in terms of biomass (mm^3/m^3) and of density ($num*10^8/m^3$). Transparency was also measured with a Secchi's disk. The report shows the results of the analysis in tables (here, they are represented through graphs in order to ease their readings).

This study detected a periodic trend in the transparency values of the water of Lame, that showed a minimum of 40 cm during summer seasons and maximum of 210 cm during winter seasons. Conductivity was in the range of 250-450 μS/cm and Dissolved Oxygen was always above 7.5 mg/L. Nitrates and Phosphate were also measured and showed a great variability, with average values of 95 and 12 μg/L, respectively. Measurements at the Rì's stream inlet indicated higher values of Conductivity (> 500 μg/L) and of Nitrates and Phosphates (2025 and 250 μg/L, respectively).

In terms of biomass, these hydrobiological studies indicate that Lame contains high concentrations of phytoplankton. During warm months, cyanobacteria develop starting from the littoral zones and covering big areas of the water surface.

For more information, please consult the original document (Barbato, 2004).

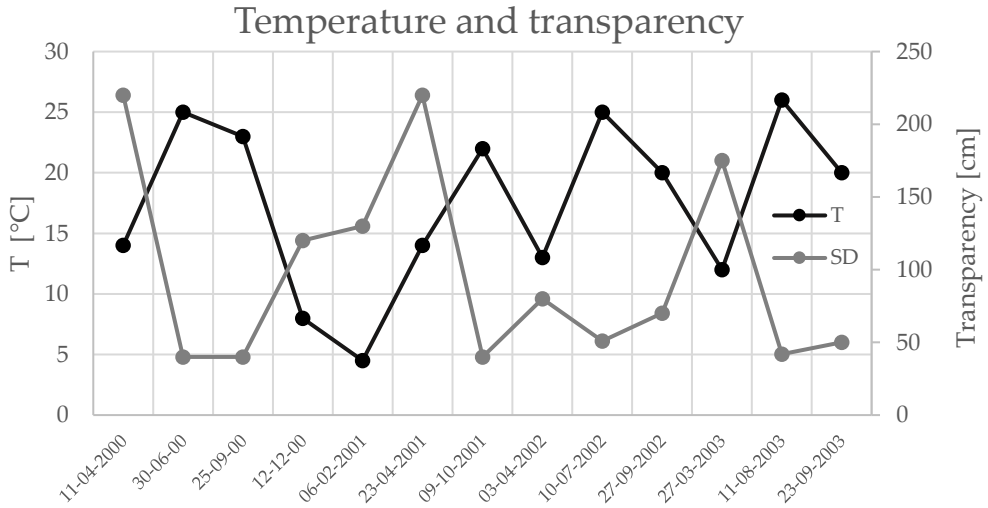

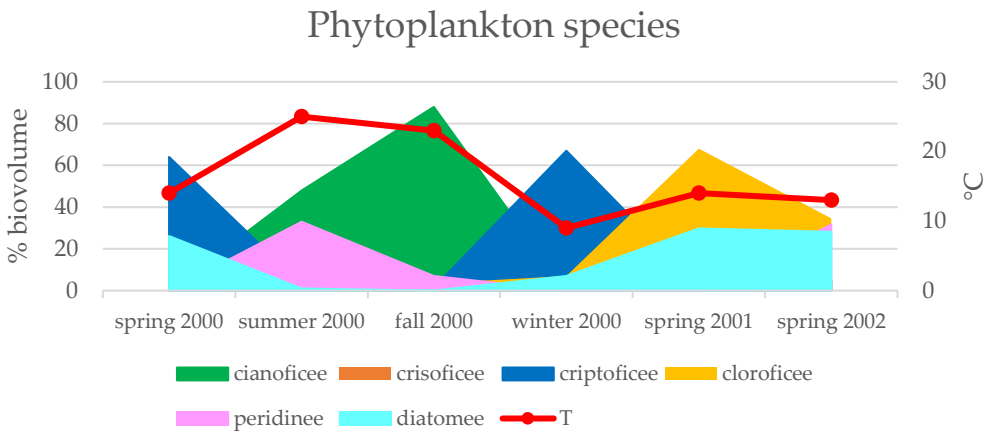

Figure 2.10 a) Trend of water temperature and transparency measured in one of the stations of Lame. b) Phytoplankton species present in a central location of Lame, in terms of percentage of biovolume

2.4.4 ARPA's final report on Lake Iseo's basin

In 2007 the Department of Brescia of ARPA Lombardia published its final report on the survey of the chemical analysis of the waters of Lake Iseo. The report includes also the analysis of some samples taken in Torbiere. Four locations were chosen: 2/4 in Lame, 1/4 in Lamette and 1/4 in one of the clay ponds. The samplings were done in November 2006 and June 2007 and were followed by a complete chemical analysis and quality-quantitative analysis of the phytoplanktonic community. Sediments were sampled as well, to evaluate the concentrations of nickel, brass, zinc, mercury and total chromium.

Dissolved oxygen and conductivity resulted in the same range measured by Barbato. A Phosphate level of 70 µg/L was measured in November 2006. Despite this level being higher than all the others found in the previous years, it looks more reasonable in the view of the author, as it is compatible with a eutrophic system.

A preliminary analysis of the sediments of Lame and Lamette showed that the contamination from heavy metals is higher here with respect to the close lake Iseo. The values of Lamette are particularly worrying as they exceed the regulation limits of Dlgs 152/06, annex 5 for what concerns brass and mercury.

For more information, please consult the original document (ARPA, 2007).

2.4.5 Consorzio dell'Oglio's water gauges' measurements of the water level of Torbiere and pump ON/OFF intervals

Consorzio dell'Oglio has been in charge of the regulation of the water levels of Torbiere since 1970s. To this purpose, the pump originally (1933) installed along the outflowing channel that links Lame to Lamette was revamped in 1985. The pump, that works with an approximately constant discharge of 400 L/s (no characteristic curve is available) is managed by the consortium and keeps the water level of Torbiere within an established range, not to compromise the habitats of the nester species. It is switched ON during intense rainfall events when levels risk getting too high and is turned OFF as soon as ordinary water levels have been reestablished.

Two water gauges were installed by Consorzio dell'Oglio: one is located in the channel upstream of the intake of the pump, the other is located along the southern side of the central trail, in the middle of Lame. Water levels are recorded daily by means of a floating device that writes them with ink on a rotating support. Each month, an operator of the Consortium substitutes the water level sheet and stores the previous one in an archive. All the recordings since 1989 were collected and digitalized and the result is shown in Figure 2.11.

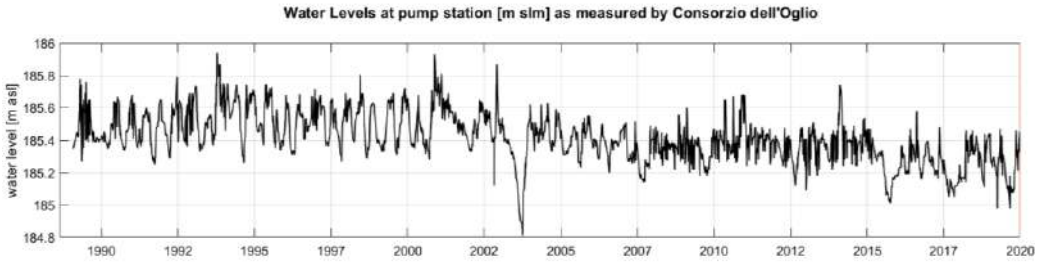

Figure 2.11 Water levels recorded by Consorzio dell'Oglio in the channel upstream the pump. The major drop visible in 2003 corresponds to a long drought period that interested all Europe from May to September.

The water level is kept approximately constant, despite fluctuations of around 50 cm due to the alternation of rainfall events and dry periods. Periods of gentle negative slope are due to evaporation, while a steep negative slope is index of the switching on of the pump.

Pump ON/OFF intervals are recorded by Consorzio dell'Oglio and an example is shown in Table 2.1. During 2022 the pump was kept off due to the scarce precipitation.

Time	On/off
26-sep-2020	ON
29-sep-2020	OFF
03-oct-2020	ON
03-nov-2020	OFF
06-dec-2020	ON
26-dec-2020	OFF
02-jan-2021	ON
17-jan-2021	OFF
23-jan-2021	ON
03-feb-2021	OFF
10-feb-2021	ON
18-feb-2021	OFF
02-may-2021	ON
09-may-2021	OFF
17-may-2021	ON
27-may-2021	OFF
28-nov-2021	ON
05-dic-2021	OFF

Table. 2.1 Pump On/OFF intervals. Source: Consorzio dell'Oglio.

2.4.6 Unibs, Unipr and Acque Bresciane: preliminary study of a natural and evaluation of the nutrient loading.

In compliance with the R.R. 6/2019 that regulates the discipline and administrative regimes of discharges of domestic wastewater and urban wastewater, a first-flush rainwater collection tank (V = 2500 m^3) should be built downstream the sewage system of the municipality of Provaglio d'Iseo, to temporarily stock the water that will be discharged into Torbiere. In this perspective, the University of Brescia and the University of Parma collaborated in 2020 to provide:

- An analysis aimed at the hydraulic design of a sedimentation tank and a constructed wetland in service of the combined sewer overflow of Provaglio d'Iseo (executed by the University of Brescia).

- An analysis of the nutrient loadings reaching the basin of Torbiere through the stream Rì, the combined sewer overflow and the remaining, draining land (executed by the University of Parma).

This study for the first time highlighted the actual extent of the anthropic pressures on Torbiere del Sebino, by carrying out a measurement campaign which led to quantify the overall nutrient load. According to the obtained results, Torbiere receives 7.8 ± 2.2 tP/year and 77.7 ± 13.2 tN/year, 46% of which coming from the Rì's watershed and 30% of which coming from the CSO. Accordingly, the construction of a sedimentation tank and of a constructed wetland was suggested for the containment and the bio depuration of the waters coming from the watershed of Provaglio d'Iseo. The intervention on the waters delivered by Ri is more difficult because the involved watershed is larger. In addition to ordinary control of outfalls along its course and to the possibility of segregating the Ri's outflow in a larger constructed wetland, in general the implementation of runoff control policies from urban and industrial areas of the watershed was suggested.

2.4.7 Cozzaglio's report about Torbiere's hydrological balance

A paper report by Cozzaglio A. was found in the archives of Consorzio dell'Oglio and constitutes one of the few technical documents about Torbiere. It explains the idea of a project to drain the wetland of Torbiere through underground absorption and use it as a reservoir, in the attempt to value an area that had been almost completely exploited in terms of excavation potential. Although the project is now outdated, the document contains some useful information about the hydrological balance of Torbiere. In particular, when listing the affluents of Torbiere, rainfall, runoff, groundwater and infiltration from the lake are named, while the stream Rì, today the main affluent, is not mentioned. For the effluents, a natural channel is described, that delivers waters to lake Iseo unless the lake level is about 50 cm higher than the hydrometric zero, in which case the water flows back to Torbiere.

What we can conclude is that in 1932 the situation was that the stream Rì was channeled directly to the lake and flowed on the eastern side of Torbiere and did not enter the wetland. The levels automatically regulated thanks to a natural channel connecting the wetland to lake Iseo.

2.4.8 Others

Aerial pictures, old maps and drawings together with satellite images have been collected during this three-year research with the aim of reconstructing the geometry of the ponds and the water quality history of the ecosystem. These documents are reported in the supplementary material in appendix A. Despite the low resolution of the images and the maps, they were fundamental for understanding the historical subdivision in ponds and their former depth. The succession of satellite images testifies the progressive collapse of the banks and the decrease of water lilies and other macrophytes cover.

The Regional Biodiversity Observatory of Lombardy published in 2016 a report of the habitat of Torbiere, containing a description of its littoral areas and its vegetation. This document was revised and is presented in appendix D.

Further information has been collected about the system thanks through the testimony of guides to the Reserve and of people that once inhabited this place. A summary of these interviews is provided in appendix B. Overall, they confirmed a decrease in biodiversity and in transparency since 1960s, while invasive species have incremented their presence.

Since 2018, botanical, fish and ornithological reports have been drawn up by Canzoneri, Bricchetti, Munari, Biagi and Mazzotti and published on the official website of the institution of Torbiere. Although the analysis of these documents is beyond the scope of this Thesis, their reference should be included for completeness. A general conclusion of these studies is that the presence of birdlife is well below the receptive possibilities of Torbiere. However, the creation of the Natural Reserve in 1983 lead to an increase in birdlife and biodiversity in general between 1970s and 1993, confirming the positive outcome of the habitat protection.

2.5 Some conclusions on data availability

As seen from the previous chapter, no study was ever carried out on the hydrodynamics and hydrology of this indeed extremely interesting system. The only studies available regard botanical, fish or ornithological research. We believe that a better understanding of the water exchange within

Torbiere would provide useful information not only to engineers and water supply institutions, but also to the botanists and ornithologists themselves. Water is the fundamental element in the ecosystem of Torbiere, constitutes the habitat for most of the species and its quantity and quality have a direct influence on the biodiversity of this Natural Reserve.

In this perspective, the hydrobiological relations of Barbato (2000-2003), together with the final report of ARPA (2006-2007) constitute the only reference when talking about the water quality of Torbiere. These analyses give an idea of the range of certain parameters inside the basin of Torbiere. However, they do not provide a precise measure and cannot be considered more than a general indication of the state of the art of the water quality in a period that was already affected by the pollution caused by the growing anthropic pressure but that probably was only at the beginning of the expansion phase of invasive species that now besets the area of Torbiere. In the view of the author, these data contain a considerable level of uncertainty related to the fact that:

- Samples of water are taken at different locations, sometimes at the "surface", sometimes at the "bottom", but no indication about the depth of the sample is given. This might be a problem in the case of parameters such as temperature, oxygen and conductivity.
- Dates of the samples are given but no further information is added. One would like to know something about the weather of the previous days, as it might influence some parameters such as temperature, conductivity, algal populations. For example, a rainfall event is able to suddenly decrease the Conductivity both in Lame and in the Rì's stream. On the other hand, one can expect that nutrients level is lower in dry periods when the overflow weir of Provaglio is inactive.
- Taking four or even less samples per year does not provide an accurate picture of the system as every sample might be extremely time-, condition- and site-specific.
- G. Barbato highlighted himself the limits he encountered in the evaluation of the phytoplankton biomass of Torbiere: during summer seasons, the amount of cyanobacteria differently spatially distributed on the surface of Lame, made it impossible to make a

count of the single phytoplankton units. To bypass this problem, he decided to give only a qualitative indication of the amount of cyanobacteria that was present at the time of the sampling.

- The water levels measurements by Consorzio dell'Oglio needed to be filtered as many of them presented problems due to the humidity of the location where the hydrometer was installed. For this reason, there are some gaps in the time series. Furthermore, this data gives an idea of the overall trend of the water levels, but no sub-daily scale type of reasoning can be done, as the water levels were recorded daily. Moreover, to our knowledge the measured level is not coherent with the level of the lake measured in Sarnico, making it impossible to understand the relation between the two water bodies.

In general, this lack of intentional surveys may be attributable to a poor collaboration between the different institutions that gravitate around Torbiere. This led to the fact that the few studies were carried out mostly because they were required by a regulation or by the opportunity of an external funding.

We believe that there is the need to put in order all the information about Torbiere and organize them keeping in mind the purpose: understanding a wetland whose main features, in the end, are all dependent on the state and condition of its waters. The next chapter is an attempt in this direction.

2.6 References

ARPA – Dipartimento di Brescia (2007) Rapporto finale 2006/2007 lago di Iseo.

APHA (1995) Standard Methods for the Examination of Water and Wastewater. 19th Edition. *American Public Health Association Inc*., New York.

Cozzaglio A. (1932). Sulla possibilità di un impinguamento dei fontanili bresciani occidentali con le acque di recupero del lago di Iseo e sulla bonifica della Torbiera.

Valerio, G., Pilotti, M., Marti, C.L., and Imberger J. (2012). The structure of basin scale internal waves in a stratified lake in response to lake bathymetry and wind spatial and temporal distribution: Lake Iseo, Italy, *Limnology and Oceanography*, 57(3): 772–786.

Websites

https://www.torbieresebino.it/management/?lang=en

https://www.geoportale.regione.lombardia.it/

Others

Barbato G. and Consorzio per la Gestione della Riserva Naturale Torbiere del Sebino, progetto LIFE (2004). Relazione sui risultati delle analisi chimico-fisiche eseguite sulle acque della Riserva negli anni 2000, 2001, 2002, 2003.

Nizzoli D., Scibona A. (2020). Analisi dei carichi di nutrienti generati e veicolati nel bacino drenante le Torbiere di Iseo nell'ambito del progetto di Acque Bresciane denominato "Torbiere", Relazione finale.

Pilotti M., Valerio G., Farina G., Volpini S. (2020). Analisi finalizzate al dimensionamento di un'area umida a servizio dello sfioratore della fognatura mista di Provaglio, Relazione finale.

3. Monitoring activities accomplished in this study

As explained in Chapter 2, before the beginning of this study no continuous monitoring effort had been done to understand the hydrodynamics and the ecology of Torbiere. With a view to model the hydrodynamics of Lame, to understand the reasons of the deterioration of the quality of its waters and to supply future studies with a solid set of data, the following activities were developed:

- Installation of water level and temperature probes in three locations of Lame (MWS1, MS2 and MS3)
- Installation of two water level probes on the stream Rì and on the combined sewer overflow to calculate their discharges (IS1 and IS2).
- Installation of a specific conductivity probe on the stream Rì (IS1).
- Installation of a weather and water quality monitoring station inside Lame (MWS 1, see Fig. 3.2)
- Measurement activities of transparency in Lame (MS2).
- Measurement of vertical profiles of temperature, specific conductivity, turbidity, dissolved Oxygen and a proxy of chlorophyll-a in several locations of the area of Lame by means of a multiparametric CTD probe RINKO-Profiler.
- Measurement of vertical profiles of temperature, specific conductivity, turbidity, dissolved Oxygen and a proxy of chlorophyll-a in several locations in the clay ponds.
- Installation of two temperature probes at different depths inside the deepest of the clay ponds (MS4).
- Drone (DJI Mini2) surveys on the areas of Lame and clay tanks.
- Velocity measurements with the drifter (see ch. 5).
- Bathymetric measurements in Lame and clay ponds.

Besides the above-mentioned monitoring data, in this chapter, the recordings of the monitoring station located at Iseo will be presented.

The position of the probes is depicted in Fig. 3.1. and a list of the variables measured at each location, together with the respective time interval of the installation, the frequency of acquisition and the accuracy is provided in Table 3.1.

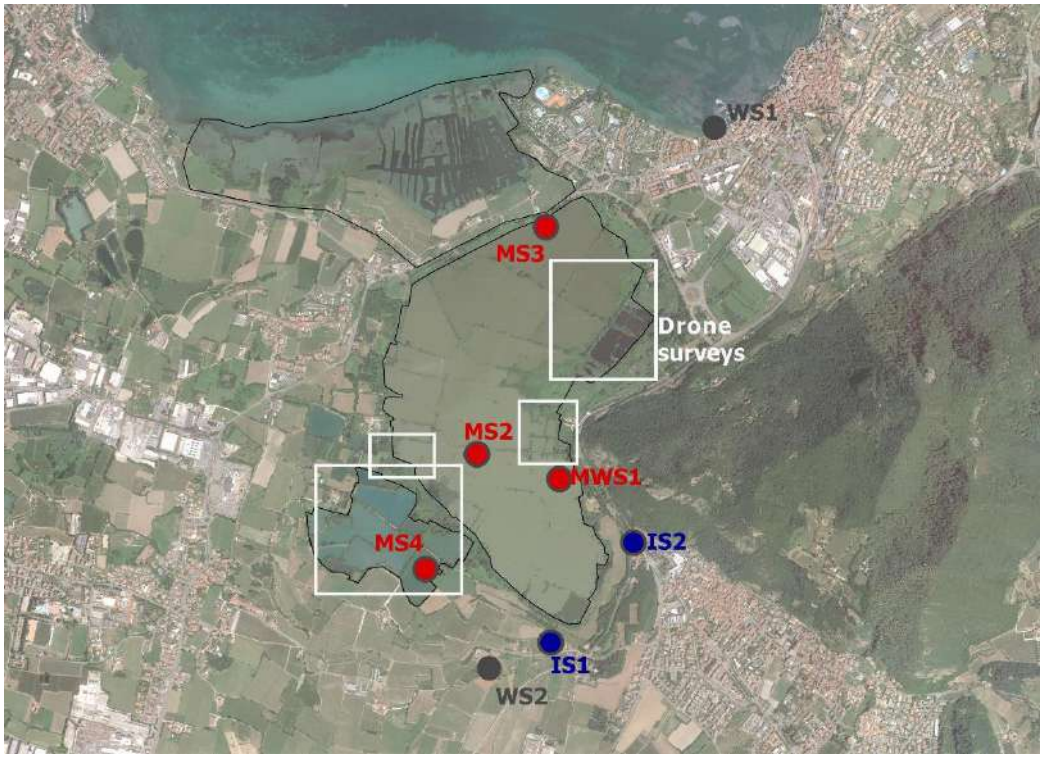

Figure 3.1 Location of different installations and campaigns. MS = Monitoring Station (where variables related to water are measured). WS = Weather station. MW = Monitoring and Weather station. IS = Inflow Station.

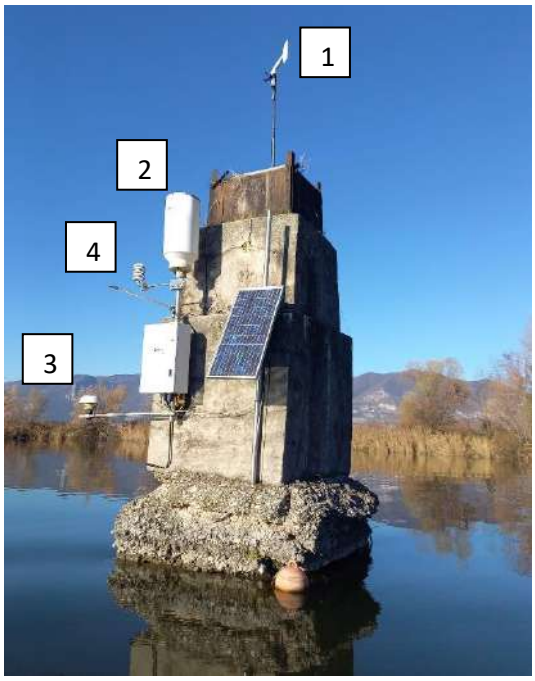

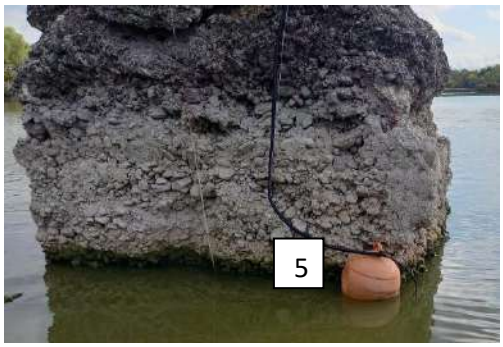

1 : Anemometer
2: Rain gauge
3: Water level probe
4: Net total radiation probe
5: Buoy to which water temperature and specific conductivity probes are attached

Figure 3.2 Monitoring station MWS1

	Measured Parameters	Acquisition frequency	Time interval	Instrument	Accuracy
WS1	Air temperature	1/minute	May 2010 – CURRENT	Campbell 107	± 3°
	Air humidity	1/minute	May 2010 – CURRENT		
	Shortwave solar radiation	1/minute	May 2010 – CURRENT	Apogee SP110	N/A
	Wind speed	1/minute	May 2010 – Apr 2019, Oct 2019 – CURRENT	Young Wind Monitor 05103	± 0.3 m/s
	Wind direction	1/minute	May 2010 – CURRENT		± 3°
WS2	Rainfall	1/hour	Dec 2017 – CURRENT	N/A	N/A
MWS1	Air temperature	1/minute	Nov 2021 – CURRENT	HygroVUE5	± 0.4 °C
	Air humidity	1/minute	Nov 2021 – CURRENT		± 3%
	Net total radiation	1/minute	Nov 2021 – CURRENT	Campbell NR-LITE2-L	± 25 mV
	Wind speed	1/minute	Nov 2021 – CURRENT	Campbell 05103-L	± 0.3 m/s
	Wind direction	1/minute	Nov 2021 – CURRENT		± 3°
	Rainfall	1/minute	Nov 2021 – CURRENT	N/A	N/A
	Lake level	1/minute	Nov 2021 – CURRENT	Mobrey MSP series-ultrasonic liquid level transmitter	0.005 m
	Water temperature -0.2 m	1/minute	Nov 2021 – Aug 2022	Campbell CS547A-L	N/A
	Water temperature -0.6 m	1/minute	Sep 2022 – CURRENT		N/A
	Water specific conductivity -0.2 m	1/minute	Dec 2021 - Aug 2022		±5% (0.44 – 7 mS/cm)
	Water specific conductivity -0.6m	1/minute	Sep 2022 – CURRENT		
MS2	Water Level	1/10 minutes	Feb 2021 – May 2021, Oct 2021 – Dec 2021, Feb 2022 – Mar 2022	Hobo U20-001-04 Data Logger	0.004 m
	Water Temperature -0.25 m	1/ 10 minutes	Feb 2021 – May 2021, Oct 2021 – Dec 2021, Feb 2022 – Mar 2022		0.44 °C
	Water transparency	1/ 2 weeks	Jan 2020 – CURRENT	Secchi's disk	-
MS3	Water Level	1/10 minutes	Feb 2021 - Dec 2021, Apr 2022 – May 2022	Hobo U20-001-04 Data Logger	0.004 m
	Water Temperature -0.25 m	1/10 minutes	Feb 2021 - Dec 2021, Apr 2022 – May 2022		0.44 °C
MS4	Water temperature -1 m	1/10 minutes	Mar 2022 – CURRENT	Hobo U20-001-04 Data Logger	0.44 °C
	Water temperature -6 m	1/10 minutes	Mar 2022 – CURRENT	Hobo Water Temperature Por v2 data logger	0.2 °C
IS1	Water level	1/ 15 minutes	Oct 2019 – Nov 2020, Apr 2021 – Nov 2021, Dec 2021 – CURRENT	Sofrel Ultrasonic LT-US Data Logger	± 0.003 m
	Specific conductivity	1/ 2 minutes	Apr 2021 – May 2022 (With gaps)	YSI 600 LS	0.5 mS/cm
IS2	Water Level	1/10 minutes	Sept 2017 – CURRENT	Vega WL S61	± 0.005 m

Table 3.1 Time interval, acquisition frequency and accuracy of the different probes installed on the monitoring stations of Torbiere del Sebino

Together with some ad-hoc investigations, this monitoring activity assured a full coverage for weather parameters, water levels and temperatures in Lame.

These data provide for the first time a quantitative picture of the thermal and hydrodynamic behavior of this system. For the purpose of this Thesis,

these data also provide the model forcing and a set of data to compare the model results with, in order to evaluate the accurateness of the simulations.

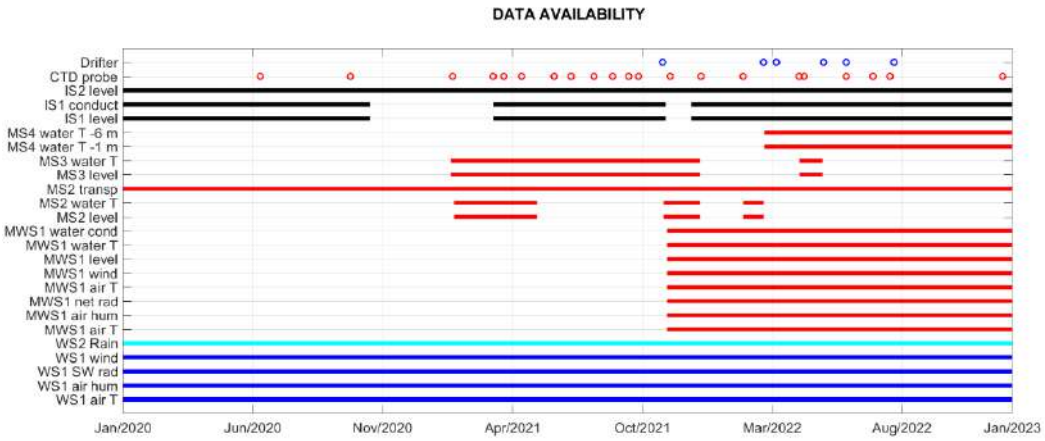

Figure 3.3 Periods of time when the different stations installed on Torbiere were working.

This chapter aims at giving a detailed description of the monitoring set up of Torbiere. Ch. 3.1 is dedicated to Lame and the measurements of their water levels, water temperature, transparency, and wind. In ch. 3.2 the data of the multi-parametric probe are presented to show the heterogeneity of Torbiere and point out the key features of each pond. Ch. 3.3 explores the water temperatures of one of the clay ponds and uses them to estimate the vertical diffusion coefficient. Finally, ch. 3.4 is dedicated to the data collected at the inflow station: the specific conductivity measurements were used to detect the plume of the stream Rì and the discharge data provided the information needed to compute the first water balance of Lame (ch. 3.5).

3.1 Lame

3.1.1 Water Levels

Water levels of Torbiere have been monitored by Consorzio dell'Oglio since 1989 with a hydrometer located upstream the pump at *Nidrì* location, as explained in ch. 2.4.5. At the beginning of this research, three water level data loggers were installed to measure the water levels of Torbiere at MWS1, MS2 and MS3. The loggers were a HOBO U20-001-04 Data Logger with a typical accuracy of 0.4 c m. With these new instruments, water levels

were acquired with a temporal resolution of 10 minutes and then averaged over the hour to obtain an average time series. The number of water level probes was reduced to one since no significant difference was recorded among the three locations in three months of observations. It is important to underline that the accuracy of these loggers is not enough to detect differences in water levels < 0.4 cm, therefore they cannot be used to measure wind setups in a small basin like Torbiere (see ch. 4.1 for more information about the setup).

In November 2021 a fixed monitoring station was installed, with an Ultrasonic Liquid Level Transmitter (Mobrey MSP Series) with an accuracy of 5 mm that allowed to obtain real time data with a 1 minute- temporal resolution. For accuracy reasons, daily averages are taken of the ultrasonic transmitters.

In September 2022 the probe was substituted with a more precise, RADAR probe. The series of water levels recorded by the HOBO probes, by the Mobrey transmitter and by the radar probe are presented in Fig. 3.4. For consistency, daily averages have been extracted for both.

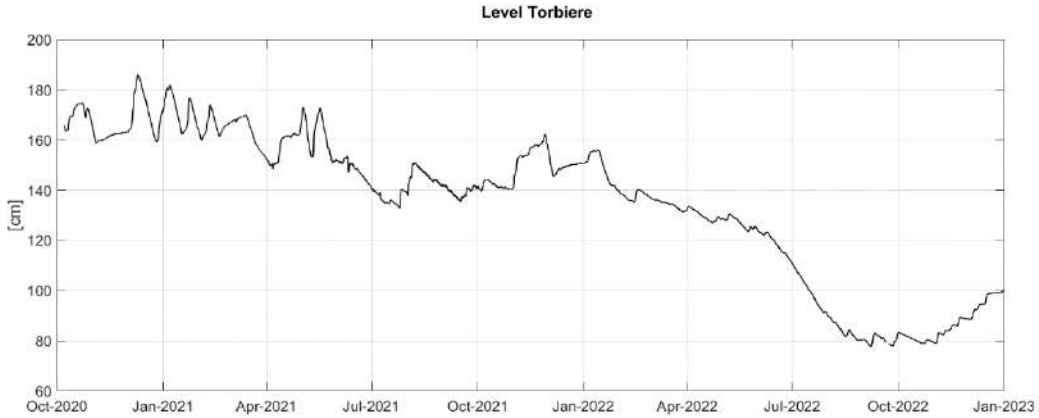

Figure 3.4 Daily-averaged water levels at Torbiere monitoring station – series of Hobo and Mobrey measurements from October 2020 to January 2023

These instruments were installed at the beginning of a long dry period that started in autumn 2021 and continued throughout 2022, until the month of September. While the usual precipitation regime of the area is 1350 mm/year (climatedata.org), during that period only 900 mm fell in 9 months. As a consequence, a constant decrease (up to -60 cm) in water levels

was observed due to evaporation. Fig 3.5 summarizes all the water level recordings and shows the anomaly of the 2021-2022 years.

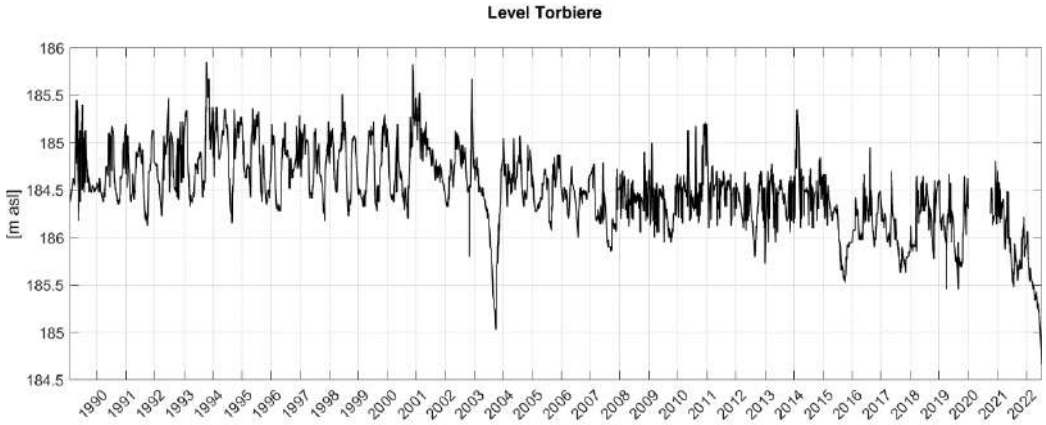

Figure 1.5 Water Level recordings of Consorzio dell'Oglio, HOBO probes and Mobrey Level Transmitter (1989-2022)

The level varies between the historic minimum of 184.7 m a.s.l. and the maximum of 185.8 m a.s.l. Sharp reductions are due to the switching on of the pump (which induces a decrease of 25 mm/day) while mild decreases are attributable to evaporation (2-5 mm/day). Generally, the level oscillates within 1 m every year and there is no seasonality in this change.

3.1.2 Water Temperatures

Water temperature in Torbiere was continuously measured for the first time during this project.

In October 2020 three HOBO U20-001-04 Data Logger were installed, that recorded temperature with an accuracy of 0.44 °C at a temporal resolution of 10 minutes. The probes were installed at MWS1, MS2 and MS3. Recordings were then averaged over 1 hour to obtain the average time series. The instruments were installed in the surface layer, approximately 20 cm below the water surface to detect the major daily temperature fluctuations.

In November 2021 a fixed monitoring station was installed at MWS1, with a Campbell CS547A probe with a typical error < 0.1 °C. For consistency with the Hobo measurements, this probe was installed at 20cm depth as well. With the unforeseen drop of water levels occurred in the spring and

summer 2022, the water temperature probe at MWS1 remained outside the water (this is the reason for the gap of recordings between August and September 2022). On 22nd September 2022 the same instrument was installed directly to a buoy (see Figure 3.2), so that its depth remains constant despite the water level fluctuation of Torbiere. Since then, the instrument records water temperature at 60 cm depth. The time series of the recorded temperatures is presented in Figure 3.6.

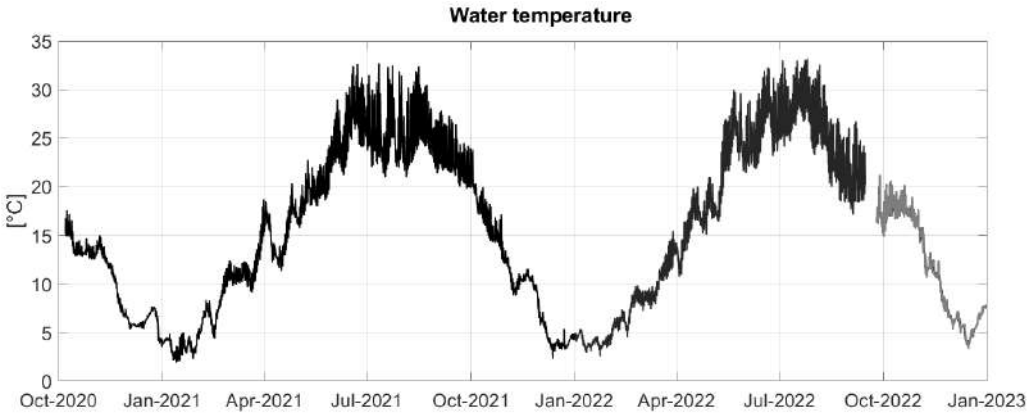

Figure 3.6 Hourly-averaged temperature measurements from October 2020 to January 2023. The grey series is referred to the period when the probe was moved down to a depth of 60 cm.

The temperature series shows the yearly thermal regime of Torbiere. Higher daily fluctuations occur in summer, with a daily ΔT of 6 °C, due to the high incoming short wave solar radiation. In winter, temperatures reach 3°C, but a thin ice layer was observed during some days (for example on 13th January 2022).

In addition to this surface measurement, other investigations were carried out to investigate thermal stratification in Lame. Understanding the way stratification forms and disrupts is of fundamental importance in the characterization of the mixing regime of a system. At this purpose, several campaigns were carried out using a multiparametric probe (Rinko, JFE Advantech Co, Japan) to collect profiles of water temperatures during different seasons.

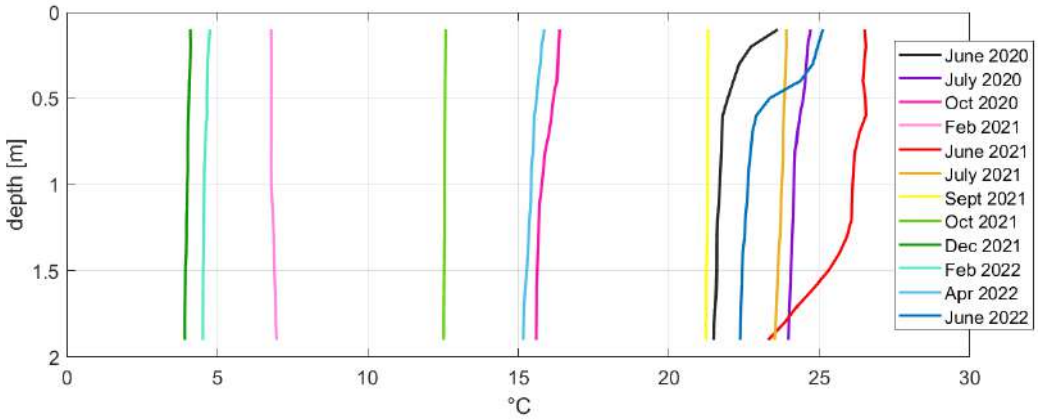

Figure 3.7 Profiles of water temperatures measured with the multiparametric probe at MS2

The profiles shown in Figure 3.7 are chosen among the ones taken in the central part of Torbiere (around MS2). In this location water is 1.8 m deep, allowing for the thermal stratification to occur.

In the mornings and in winter Torbiere is not thermally stratified. Only during June 2020, July 2020 June 2021 and June 2022 there is a slight stratification with temperatures that decrease towards the bottom sediments. As it could be expected, lower and constant temperatures are found in October, December and February.

In addition, during August and September 2022, two HOBO U20-001-04 Data Loggers were installed at MWS1 at 15 cm and 50 cm depth respectively, to obtain the time series of water temperatures at two depths.

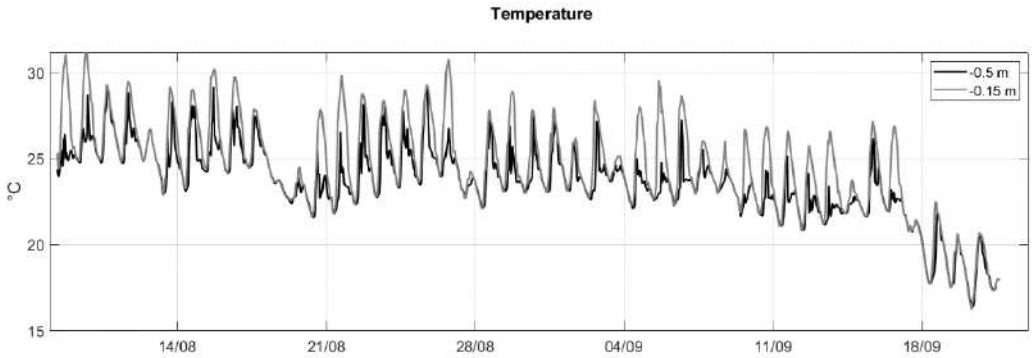

Figure 3.8 Hourly-averaged water temperatures at 0.15 and 0.5 m depth at MWS1 (August – September 2022)

Given the shallow nature of the system, Torbiere responds very fast to weather variations and changes reach the bottom of the water column within a few hours. Compared to deep lakes at similar altitudes, Torbiere exhibits small characteristics of diurnal mixing. Taking September 4th, 2022, as an example, water is at homeothermy from 12 am to 8 am, a stratification than builds up, with a difference of about 4°C between surface and middle of the water column, followed by a second homeothermy at 4 in the morning of the next day.

3.1.3 Water Transparency

Water transparency is very easy to measure and can give an insight on the trophic state of a system. The trophic state index of a lake can be estimated from (Carlson ,1977):

$$TSI(SD) = 60 - 14.41 \ln(SD) \quad [3.1]$$

Where SD is the Secchi's Depth or water transparency.

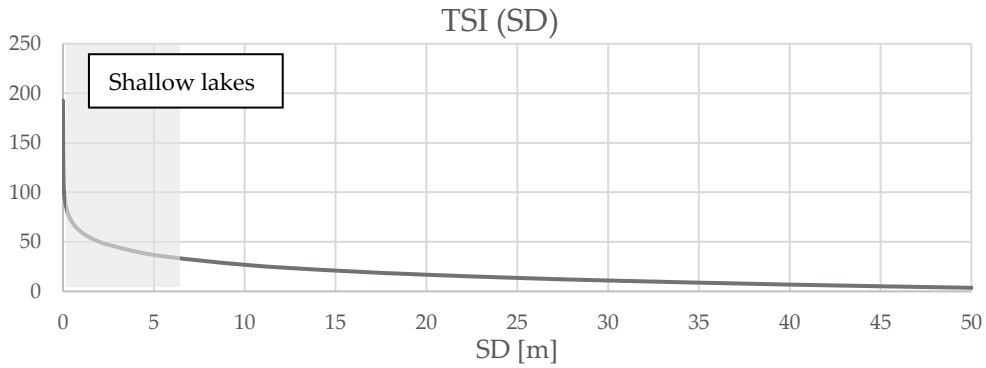

Figure 3.9 Trophic state index estimated from Secchi's depth according to eq. 3.1.

And the following ranges apply (Chapra and Dobson, 1981):

TSI < 5: Oligotrophic

TSI = 5 – 10: Mesotrophic

TSI > 10: Eutrophic

However, for shallow lakes, the ranges for trophic state are not applicable in a straightforward way: the water level is so shallow that even if the Secchi's depth is equal to the maximum depth, one would obtain that the lake is eutrophic (see Fig 3.9). This should be kept in mind when evaluating

the Secchi's depth of Torbiere, a shallow system where sediment resuspension plays an important role.

In Torbiere, transparency was measured with a Secchi's disk starting from January 2020 with a biweekly frequency, at MS2, where the water level is around 2 m. At the beginning of this survey, transparency was measured in different points of Lame but, as results were the same, it was established to measure it at MS2, a central station, representative of the waters of Lame.

The time series of measured water transparency are given in Figure 3.10.

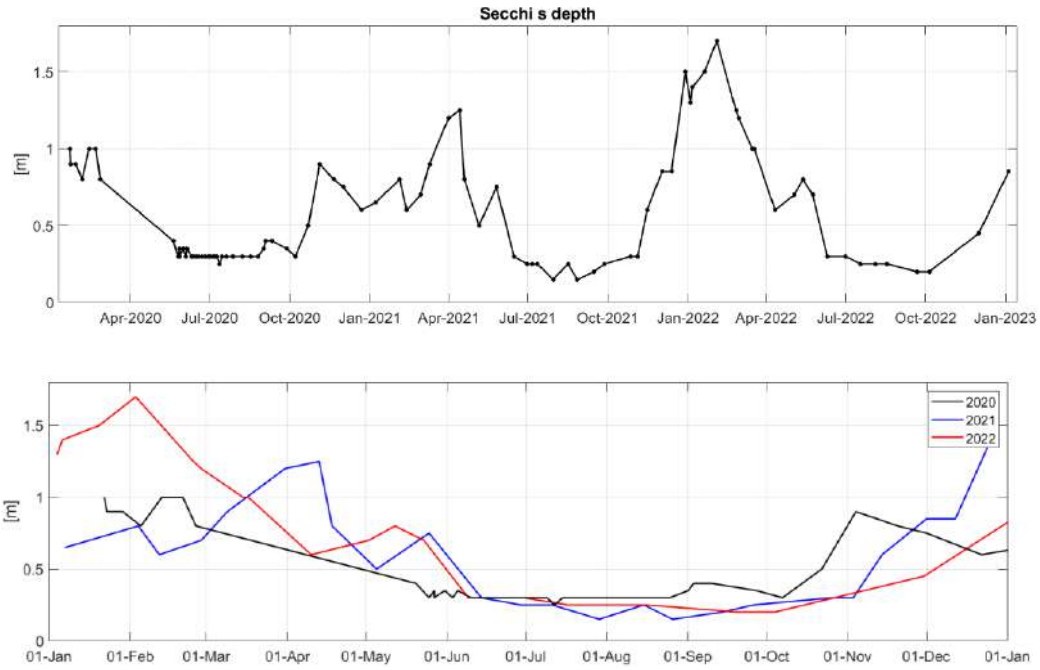

Figure 3.10 a) Time series of water transparency as measured at MS2 with a Secchi's disk. b) Comparison of the three years of recorded data.

Water transparency shows a sinusoidal behavior, with maximum levels in winter months and lowest levels in summer. With respect to Barbato's measurements of 2000 - 2003 (see ch. 2.4.3), current values appear lower, indicating a worsening condition of the trophic state of Lame. Water transparency is, in fact, directly related to Total Phosphorus and Chlorophyll-a concentrations, and values of Secchi's depth lower than 1 m are an index of hypereutrophic system. This condition of very low transparency is caused by multiple factors:

- The nutrient loading coming from the affluents, that favors the primary productivity in the system and the proliferation of phytoplankton.
- The absence of substantial aquatic vegetation (Jeppesen et a., 1990)
- The shallow nature of Torbiere, whose sediments, as a result, can be easily mobilized by the wind and increase the particle matter concentration.
- The presence of benthivorous fish that mobilize the sediment themselves.

The implications of the lack of clearness go beyond the aesthetically unpleasant aspect of Torbiere's waters. The lower the transparency, the harder it is for light to pass through water; as a result, sunlight can never reach the bottom of Torbiere and macrophytes cannot grow. This might be the reason why water lilies are found only in the shallowest area of Torbiere, where depths are lower than 1 m and sunlight can somehow penetrate towards the bottom.

3.1.4 Wind stations

Wind is the main hydrodynamic driving force in Torbiere, due to the high ratio between the water surface length along the wind main direction and the mean depth of this basin (Nutz et al., 2016). It triggers inner circulation and influences nutrient transport, sediment resuspension, mixing (Madsen et al., 2001) and therefore has a key role on the development of the water environment and the ecosystem, even changing the alternative stable states (Scheffer M. et al, 2001).

The wind acting on Torbiere can be represented by the recordings of two weather stations:

- Iseo weather station WS1: it was installed in 2010 and completed in 2013 and since then it measures wind speed, wind direction and wind gust at a one minute – temporal resolution.
- Torbiere weather station MWS1: it was installed in November 2021, and it measures wind speed, wind direction and wind gust at a one minute – temporal resolution.

The two stations are as important to describe the wind on Torbiere, as the morphology of the territory is such that a steep mountain ("il Corno")

located to eastern side of the wetland, diverts the wind, that changes its direction when blowing on the Southern ponds (ch. 2.1). Furthermore, a small hill is located to the South of Torbiere, diverting the wind as well.

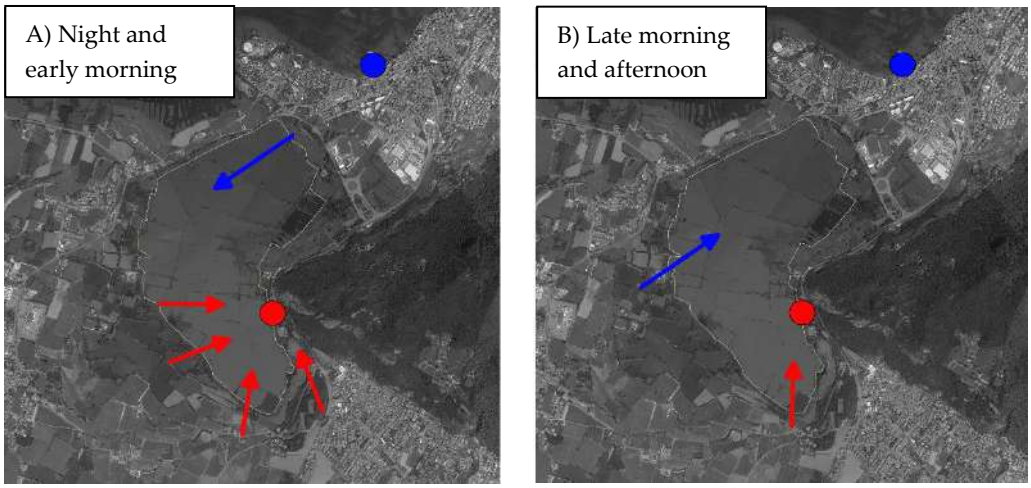

Figure 3.12 Sketch of the wind pattern of Torbiere. A) When the strong wind "Vet" of Iseo (blue arrow) blows from North – East, at Torbiere a weaker wind is recorded, coming from West, South-West, South or South – East (red arrows). B) During the Ora wind measured at Iseo from South-West, at Torbiere station a wind from South is recorded.

The analysis of the wind speed and wind direction time series showed that the series of wind speed at the two locations are correlated ($R^2 = 0.68$), while the ones of the direction are not (Fig 3.12 a, b).

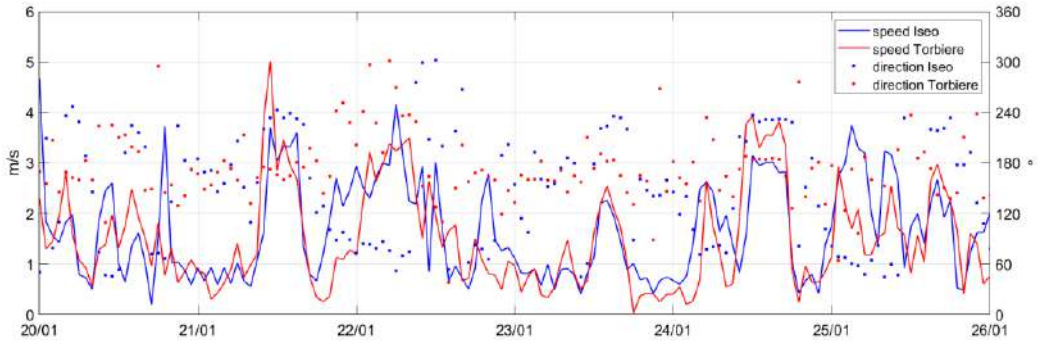

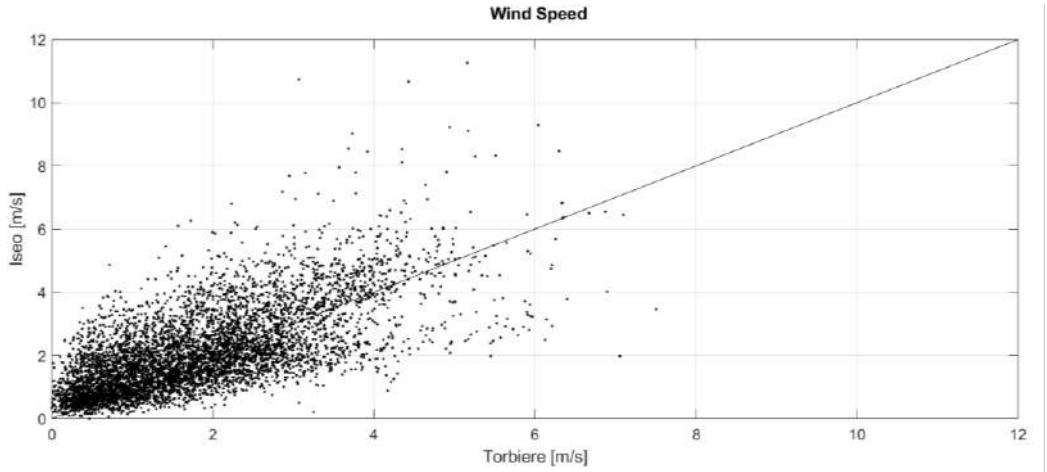

Figure 3.12 a) Example of one week (January 2022) series of wind speed and direction. The wind intensity is the same, but the directions do not match. b) correlations between the series of wind speed at Iseo and at Torbiere

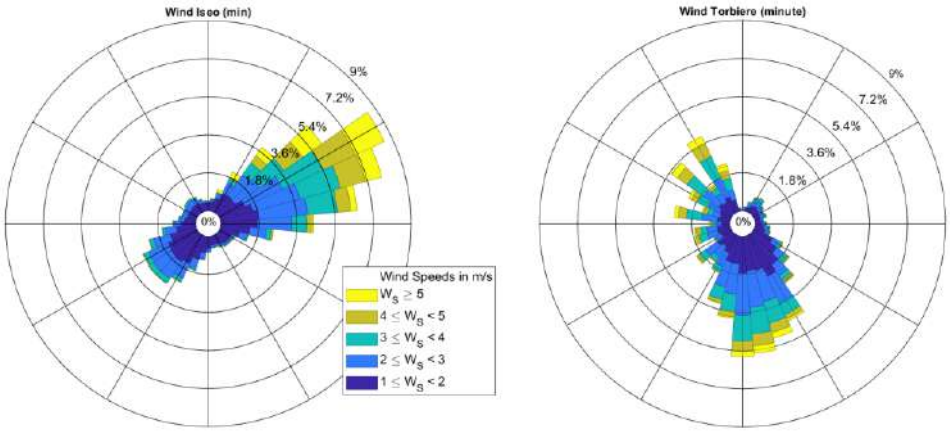

Figure 3.13 Wind roses of minutely data measured in Iseo and Torbiere. Data refer to the period November 2021 - January 2023. In a polar coordinate system, these diagrams indicate the relative frequency, proportional to the length of each spoke, of the winds blowing from a certain direction; the shade-coded bands indicate the velocity range to which the wind belongs.

The wind field measured at Iseo is characterized by a regular daily alternation of an afternoon (''Ora'') and a nightly northerly (''Vet'') wind. The "Ora" is weaker and blows from South-West, the "Vet" is typically stronger and blows from North-East. More than half of the volume of Torbiere experiences this regular pattern, while the shallower, Eastern and Southern ponds are subjected to the wind field measured at the Torbiere's station, which is characterized by a principal blowing direction from South.

Given that the larger volume of Lame is influenced by Iseo's wind, the weaker wind at Torbiere is not able to establish its own currents. Overall, it is possible to say that Torbiere is mainly influenced by the wind measured at Iseo station.

Monthly-averaged wind in Torbiere.

To analyze the wind at Iseo and Torbiere's station, for every month the average wind velocity and direction over the different hours of the day were computed. 24 wind roses were obtained per month, each of them corresponding to one of the hours of the day. Standard deviation was used to analyze the degree of dispersion of the data.

In the following, the analysis of one month, December 2021 is presented as an example.

Wind in December 2021

December 2021 is the first month when data from both monitoring station was available, as the Torbiere's one was installed in November 2021.

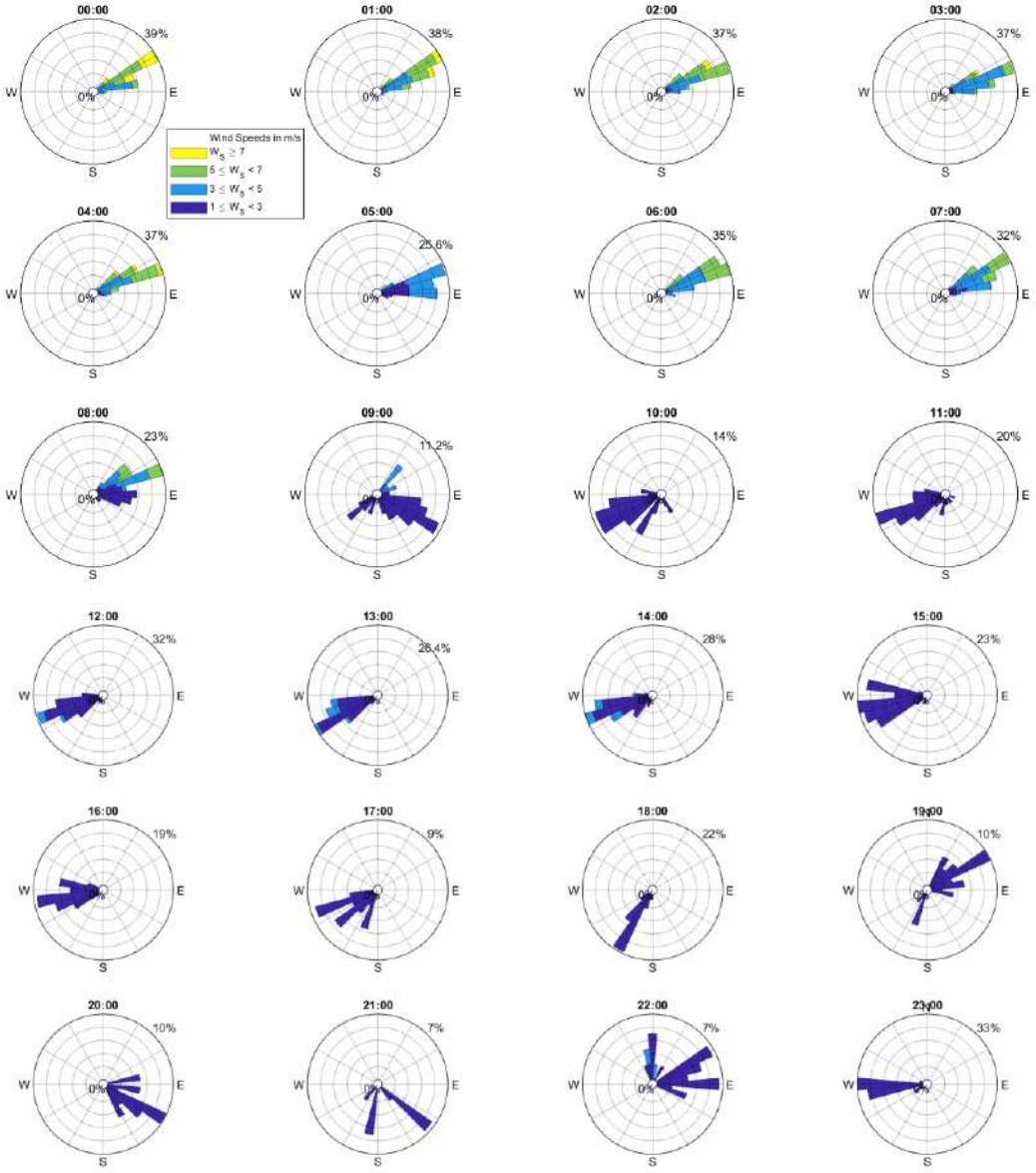

Figure 3.14 Wind Roses of Iseo measurements relative to the Month of December 2021

Wind measured at Iseo is particularly stable during night and early morning hours, when high wind intensities (> 5 m/s) coming from North-East ("Vet") are recorded. Figure 3.16 shows that the standard deviation for these data is very low (15), indicating a low degree of dispersion. For the

same moments of the day this is not true for Torbiere's station (Fig. 3.15) where weaker winds are present, without a principal direction (STD ≈ 70).

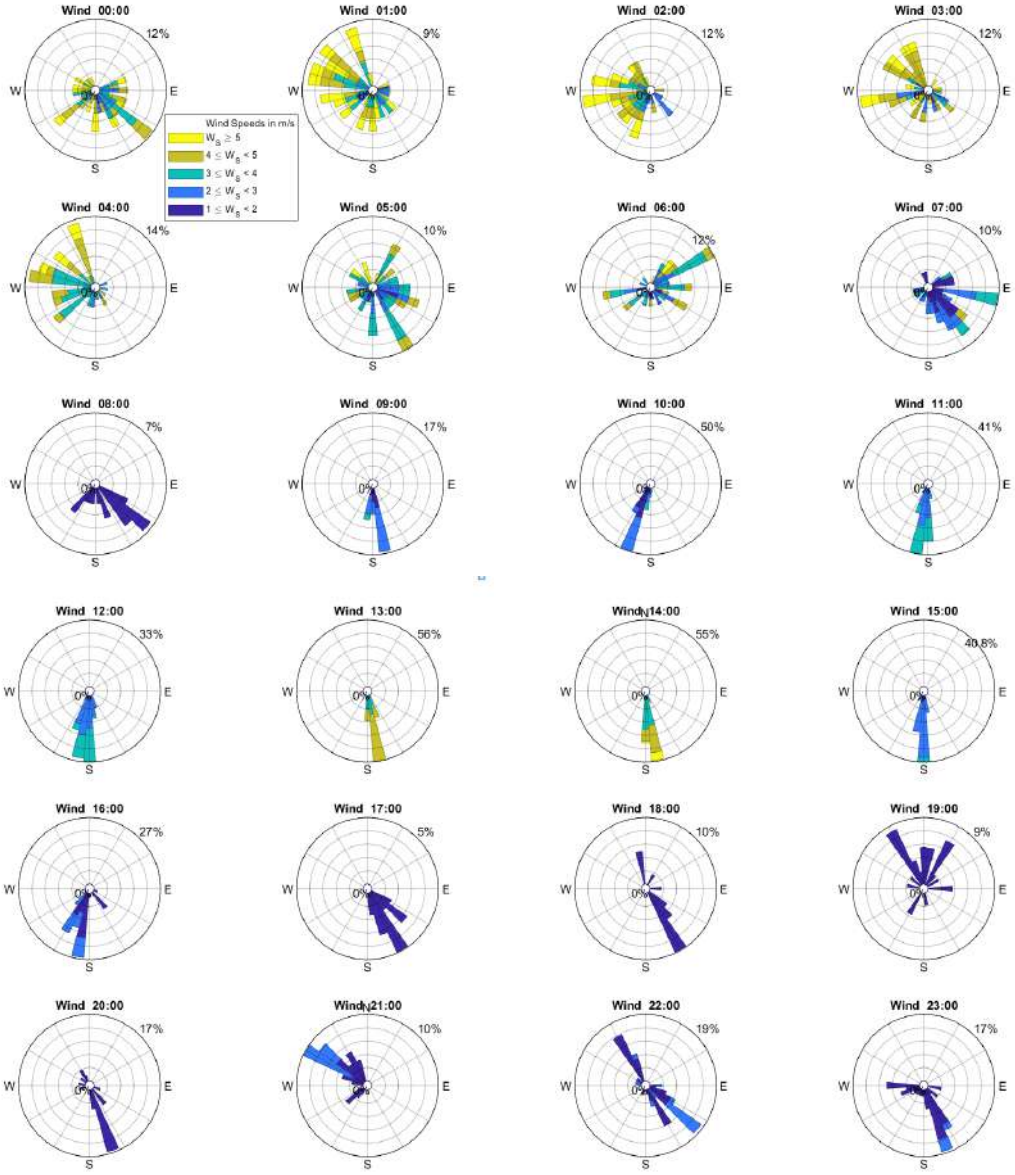

Figure 3.15 Wind Roses of Torbiere measurements relative to the Month of December 2021

Despite this being the example of one month only, this is a recurring situation: the wind at Iseo is periodic and predictable, while the wind in Torbiere is weaker and more dispersed.

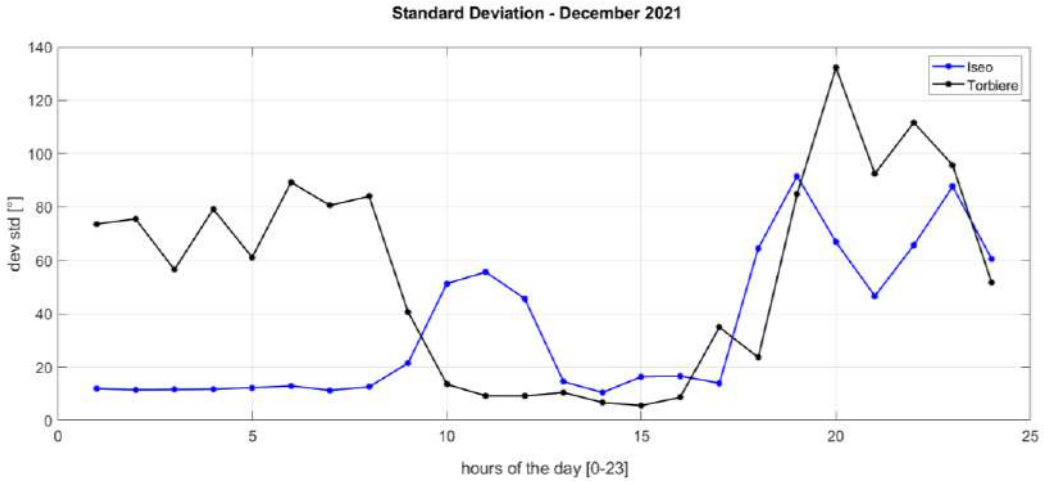

Figure 3.16 Comparison of standard deviation (in degrees) of the direction of the wind for the month of December 2021 for Iseo and Torbiere station

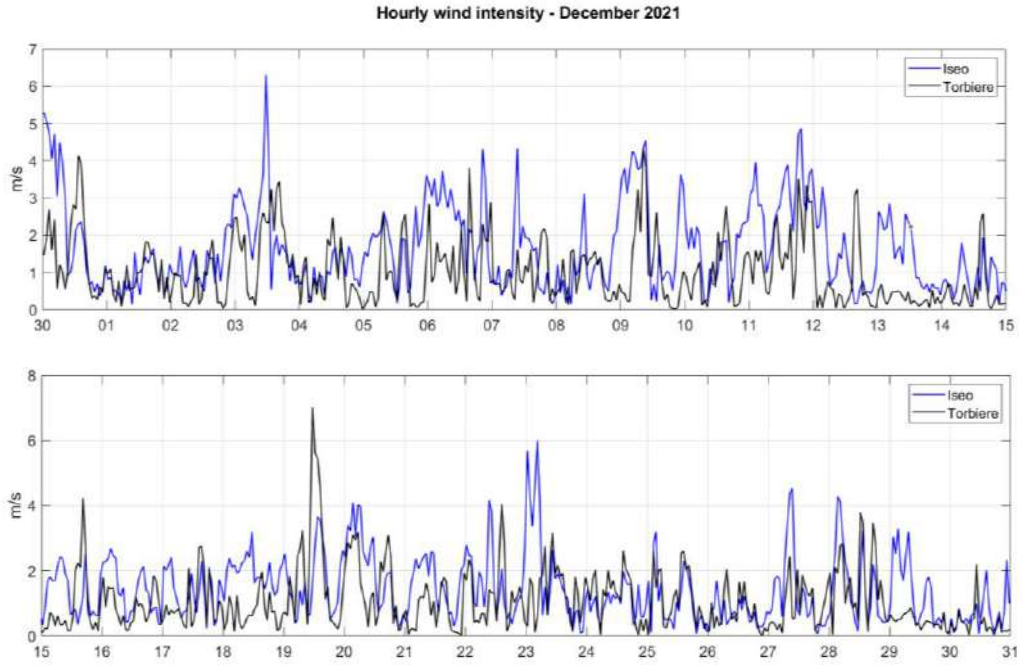

Figure 3.17 Comparison of hourly wind intensities measured at Iseo and at Torbiere during the month of December 2021

3.2 Sparse samplings

A quick look at any satellite image of Torbiere is enough to understand that, besides the big volume of the completely mixed Lame, there is a multitude of smaller ponds, generally located to the sides, which experience different degrees of water quality and therefore appear of different colors. Some of them are more turbid, others are of a bright blue color, others are greener, and others contain water lilies. Suspension of large amounts of organic materials and abundance of cyanobacteria or diatoms impart a *seston* color that will be yellow to brown or blue-green or yellowish-brown, respectively (Wetzel, 2001). After the frequent visual observation of this heterogeneity (Fig. 3.18 and 3.19 A,B and C), several campaigns were conducted to characterize the different ponds, by means of a multiparametric CTD probe. For a more detailed description of these campaigns, and to consult all the data acquired, please refer to Appendix D. For some campaigns, the drone pictures acquired were used as a support for the detection of spatial patterns.

Figure 3.18 The colors of eutrophication. Picture of Torbiere that won the 1st prize of the Photo Contest SIL2021 – Korea

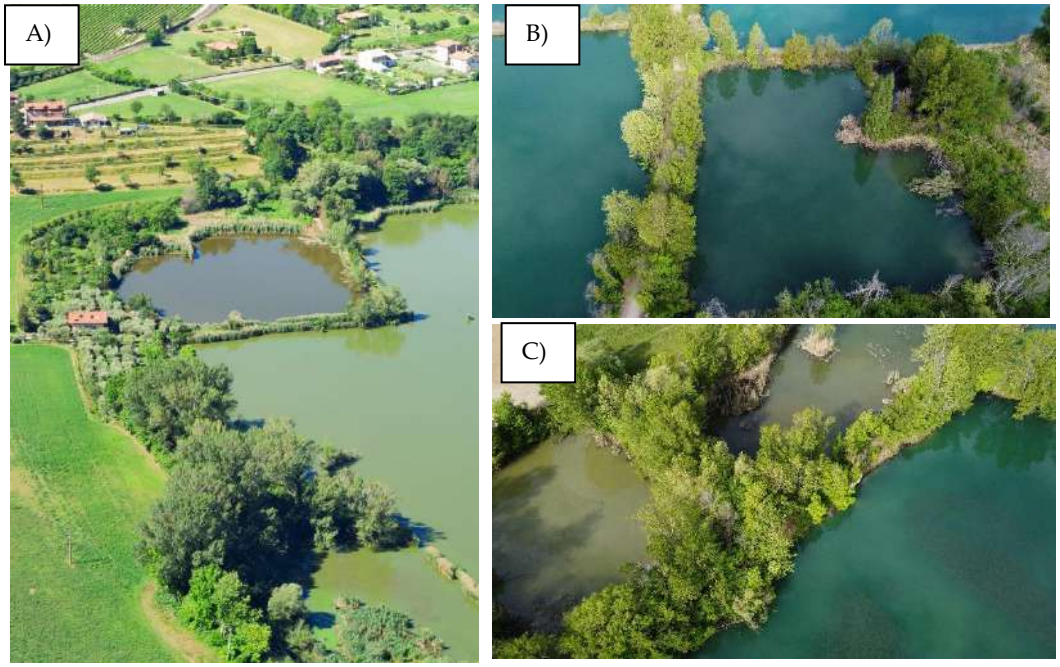

Figure 3.19 A) The pond where the main affluent, Rì, enters Torbiere and B) Clay ponds in the Southern part of the Reserve (credits: drone pictures of UniBS hydraulic group 29/04/2022)

A total number of 18 campaigns was conducted by means of three small boats. The boat of Ente Gestore della Riserva was used to explore all the ponds of Lame, while a rubber raft belonging to the Sebino Carp Team was used for the campaigns in the clay ponds. An exception is the deepest clay tank (see Fig. 3.30), that was explored thanks to the rowboat of some fishermen who benefit from a land concession.

After several campaigns, the conclusion is that in the territory of Torbiere, different cases might be distinguished. Fig. 3.20 shows a map representing the different ponds. Please note that a grey color refers to a pond that has not been explored, mainly for logistical reasons.

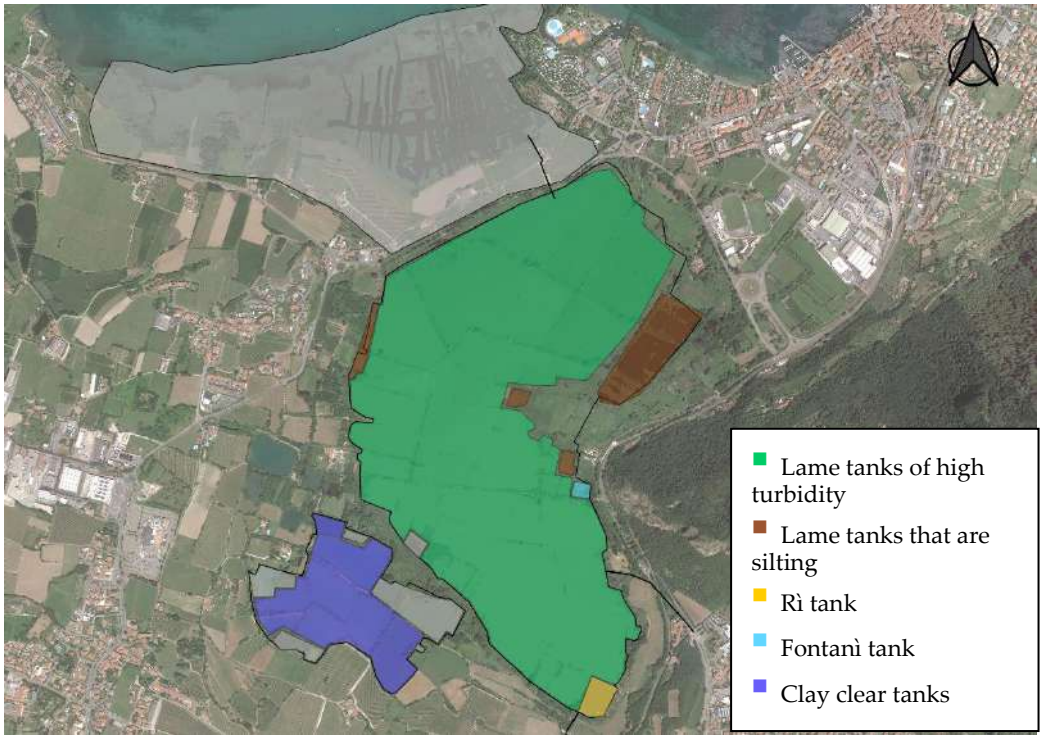

Figure 3.20 Ponds of Torbiere grouped according to their appearance and water quality

The main characteristics of the campaigns are summarized in Tab. 3.2.

Pond name	Average number of points per campaign	Dates of the campaigns
Lame	40	18/06/2020 27/07/2020 07/10/2020 15/06/2021 30/07/2021 15/09/2021 28/10/2021 13/12/2021 03/02/2022 13/04/2022 10/06/2022
Rì's pond	8	06/07/2021
Fontanì's pond	7	06/07/2021
Clay ponds	10	26/08/2021 13/07/2021
Deep clay pond	9	03/08/2021 01/03/2022 19/04/2022 03/08/2022

Table 3.2 Campaigns with the multiparametric probe

During each campaign, a certain number of points, suitable for representing the spatial distribution of the parameters, was measured by means of a multiparametric probe. Each point was associated with the time at which it was sampled and its coordinates. Profiles of the following parameters were obtained:

- Temperature
- Dissolved Oxygen (concentration and saturation)
- Specific conductivity
- Turbidity
- Proxy of Chlorophyll-a

The above-mentioned parameters, together with a measure of Secchi's disk transparency, were used to characterize the different ponds. In the following, vertical profiles and 2D - interpolated maps, representing the average of each parameter over a certain depth, are used to discuss these measurements.

The following considerations should be kept in mind when reading the data of the campaigns:

- Temperature measurements are extremely time-dependent in shallow systems. Therefore, when campaigns lasted several hours (e.g. the campaigns of Lame), the water column had the time to warm up or cool down according to the time of the day and the season when the campaign took place. In those cases, only single profiles of temperature should be considered, and no conclusion should be done about differences in temperature among different points. For this reasons, 2D maps of temperatures are either absent or should be viewed with a critical eye.
- When creating 2D – interpolated maps, the value of the parameter chosen for the interpolation, was selected equal to the average of the profile over a certain depth. The depth is a fraction of the maximum depth and was chosen to best represent each pond. For Lame, the parameters are averaged over the first 80 cm of water column. The only exception was the procedure for the proxy of Chlorophyll-a, where it was decided to represent the maximum value over the 80

cm depth, in order to better represent the presence of an algal bloom, that is usually confined to a few centimeters in the water column.

- The range indicated for dissolved oxygen saturation has a maximum value equal to 200%. Any value detected above that threshold should not be considered reliable because it is over the functioning range of the probe.
- Any outliers detected in the profiles was eliminated from the series. This occurred mainly with turbidity measurements, in silting ponds: when the probe approached the sediments, it recorded unphysical and extremely high, values of turbidity.
- In case of shallow ponds and homogeneous water column, only the vertically averaged value is shown.

3.3.1 2D – interpolated maps

Maps of the different parameters were obtained using Surfer, a 2D & 3D mapping, modeling & analysis software. The minimum curvature method was chosen for the interpolation and faults were used to show discontinuity when gridding. A fault is a two-dimensional boundary file defining a line acting as a barrier to information flow. When gridding a data set for the interpolation process, data on one side of a fault is not directly used when calculate grid node values on the other side of the fault (Surfer Full User's Guide, 2019).

The 2D maps were created for all the different areas of Torbiere (Figure 3.20). However, only the maps of Lame are shown, where several campaigns are available, and the most interesting spatial heterogeneities are detectable.

Fig. 3.21 shows the interpolated maps of dissolved oxygen saturation, specific conductivity, turbidity, and proxy of chlorophyll-a for the 10 campaigns that were done in Lame from 2020 to 2022. A unique range of parameters was chosen to ease the reading of the maps and allow for comparisons. For a more detailed description of these campaigns, please refer to Appendix D.

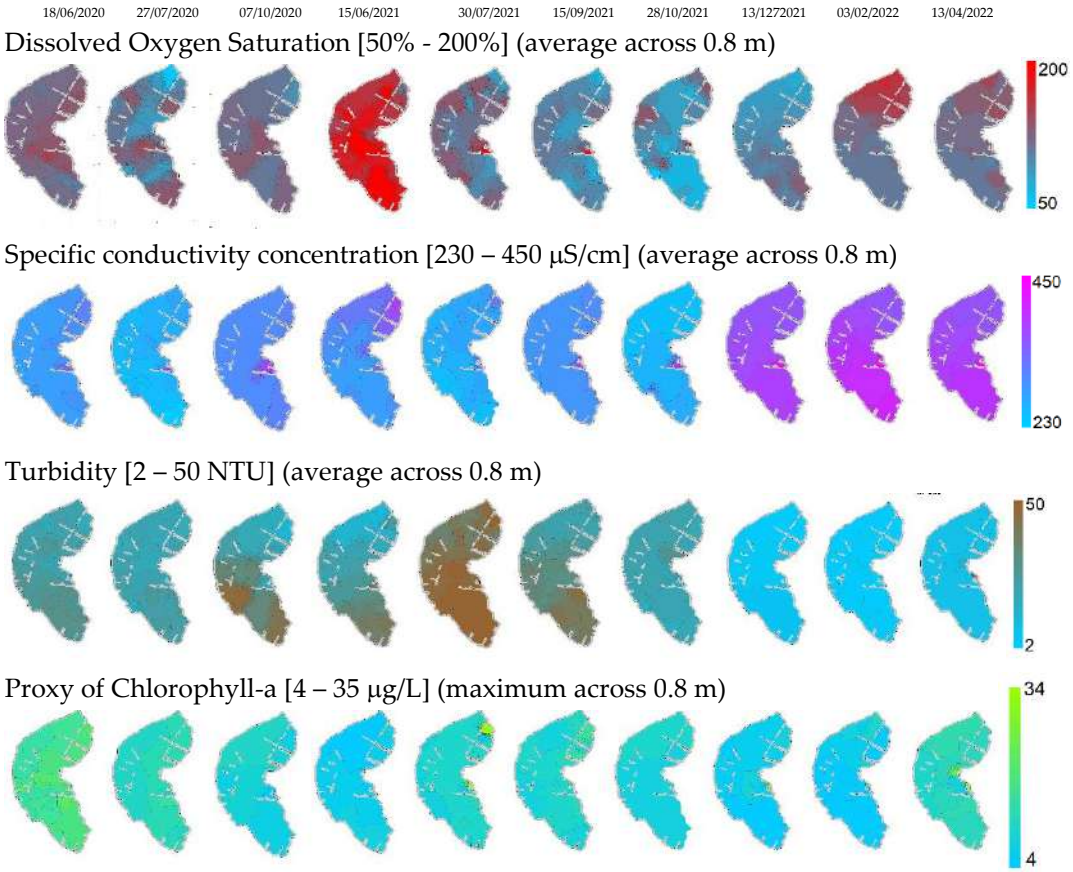

Figure 3.21 2D-interpolated maps of the Lame's campaigns

Dissolved Oxygen values show a great temporal and spatial variability. Higher values are often found in littoral zones, where phytoplankton might accumulate due to the lack of turbulence. Despite the high turbidity, oxygen depletion hardly occurs, due to the shallow nature of the waters and the wind pattern that favor reoxygenation.

Specific conductivity is spatially less variable with respect to oxygen but shows a maximum in the Eastern ponds closer to the Fontanì pond, where a groundwater source is present.

Turbidity is generally higher in the southern pond, probably due to presence of the two inflows and to the shallower depths.

Proxy of Chlorophyll-a is often above 10 µg/L, a threshold for eutrophic lakes.

What emerges is that Torbiere, being a shallow, polymictic system, is extremely weather dependent and no similar features are found in the same

period in different years. A change in the precipitation, in air temperature and in solar radiation might quickly affect the entire water volume of Torbiere.

3.2.2 Vertical profiles

If 2D – interpolated maps are more suitable for describing the spatial distribution of the measured parameters in Lame, in the case of the Fontanì pond, the Rì tank and the clay tanks, vertical profiles are more appropriate. Fontanì and Rì tanks are spatially uniform and therefore, a unique, vertical profile is enough for their description. In the case of clay tanks, a vertical profile is the best solution as it well depicts the stratification of these deep ponds.

Fontanì pond

On July 6th, 2021, a campaign took place to characterize the Fontanì tank, which could not be reached during the regular campaigns in Lame as it is separated from the main body of Torbiere. The connection between this pond and Lame is a one-way communication: water can only leave the Fontanì pond. This singularity is what makes it peculiar with respect to the other ponds: it is fed by a groundwater source and not, as the rest of the Lame, by the (polluted) Rì's discharge.

Fontanì is a small pond of 1120 m^2 with average depth 0.8 m. The groundwater source once provided an incoming discharge of 5 L/s (Cozzaglio A., 1932), now it is estimated to be lower.

Differently from the other ponds, its waters are clear; transparency equals the entire water depth and water lilies cover the whole area (Fig. 3.22 B and C). Recalling the classification of Scheffer (2004), Fontanì tank is found in a clear, macrophyte-dominated state. During winter, when the rest of Lame might freeze, this pond never does, as the incoming discharge, being of groundwater nature, has a fairly constant temperature (around 14°C) throughout the year.

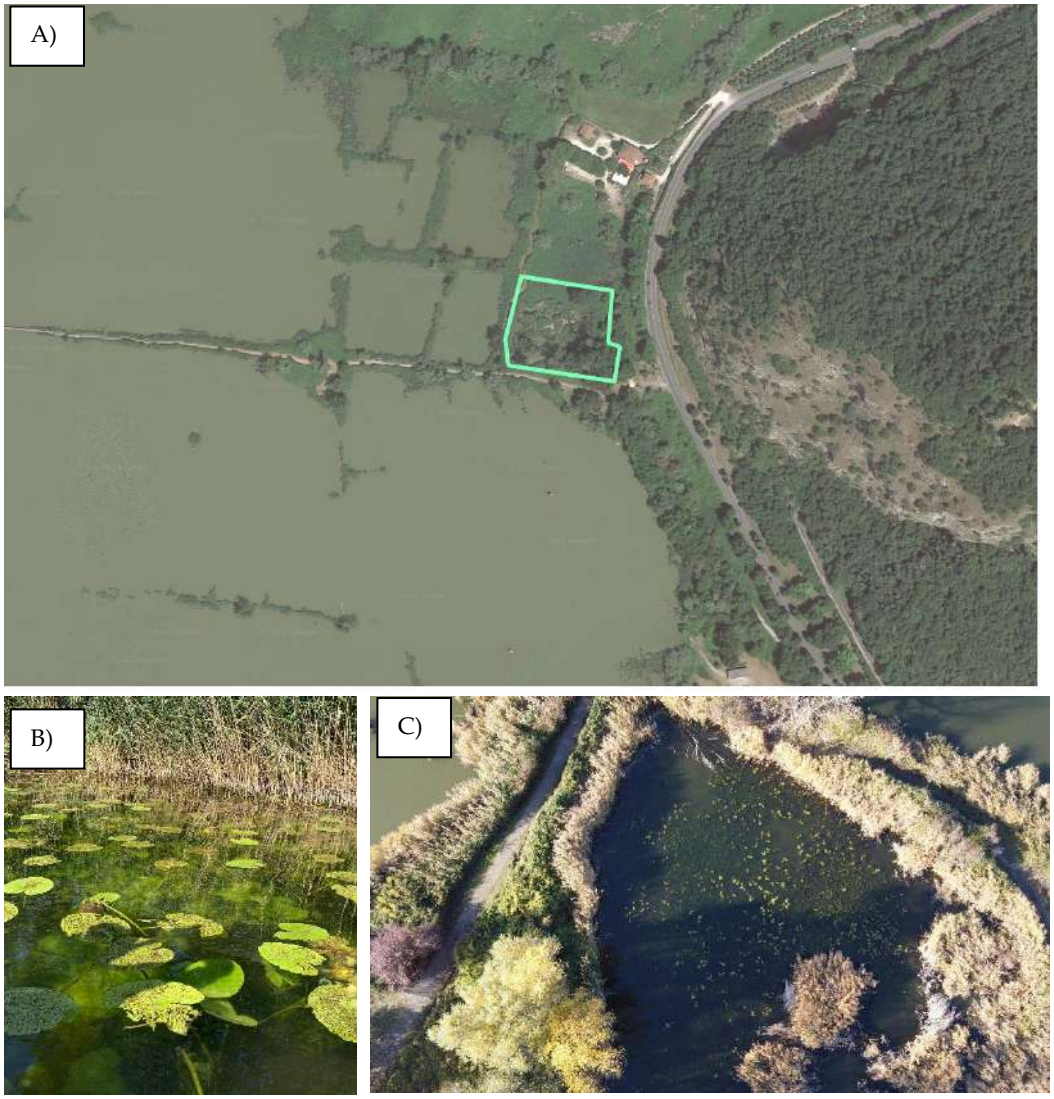

Figure 3.22 Fontanì tank: A) location and B) water lilies in July 2021 C) Water lilies in November 2021 (credits: drone pictures of UniBS hydraulic group 18/11/2021)

Given the small size of the pond, the campaign lasted 30 minutes (starting from 09:45 am), during which the water was found at 19 °C, a cooler temperature with respect to Lame (23°C). This is due to the cooling effect of the groundwater discharge, that was measured to be around 16°C. The water column was partially stratified, with $\Delta T = 1.5$ °C between the surface and the bottom

Specific conductivity was 710 µS/cm, due to a groundwater discharge conductivity equal to 750 µS/cm. Dissolved Oxygen saturation was around 65 % (6 mg/L), a low value compared to the rest of Lame, which might be caused by the groundwater nature of the tank, the lack of phytoplankton

biomass and the absence of wind. Proxy of chlorophyll-a, as well of turbidity, were extremely low: 3.5 μg/L and 1.5 NTU, respectively, indicating an oligotrophic state.

Rì tank

On 06th July 2021 a measurement campaign was conducted in the Rì tank, the pond where Rì enters first, before reaching the main volume of Lame. It is a small tank of 1000 m^2 and average depth 1.2 m. Satellite images of this tank, together with pictures taken from the surrounding hills (Fig. 3.19A) show that this pond often appears of a different color with respect to Lame. Receiving the polluted discharge of Rì, this tank is place of higher turbulence, conductivity and suspected nutrient concentration.

The campaign lasted 20 minutes (starting at 11:50 am), during which the pond appeared stratified, with 26.5 °C at the surface and 23°C at the bottom. Specific conductivity was fairly constant and equal to 425 μS/cm, while 250 μS/cm are found in the rest of Lame. Chlorophyll and turbidity were measured equal to 35 μgChl-a/L and 30 NTU, respectively. Dissolved Oxygen concentrations decreased towards the bottom due to high sediment Oxygen demand (11 mg/L at the surface vs 6 mg/L at the bottom).

Figure 3.23 Rì tank

There is a need to measure the nutrient content in the Rì stream, in this tank and in Lame, right outside this pond, to assess the extent of the nutrient removal exerted by this pond. In this way only the value of this pond will be recognized.

Bersi Serlini #1 and #2 tanks

Bersi Serlini tanks are the biggest of the clay tanks (extension of around 62'000 m^2), their average water depth is 4 m, and they receive water mainly from rainfall and runoff (coming from South). An outlet activates when the water level is too high and some water is discharged northward (into Vasca Bagni tank, see next paragraph) by means of an overflow pipe.

These two tanks appear as separated systems from satellite images, but the boundaries between them are labile and consist of reefs, allowing for the hydraulic communication between the ponds. Profiles that were measured confirmed this idea and therefore they are presented as a unique system. The name "Bersi Serlini" refers to the famous winery that is located South and that owns some vineyards whose slope generates a runoff directly into these tanks.

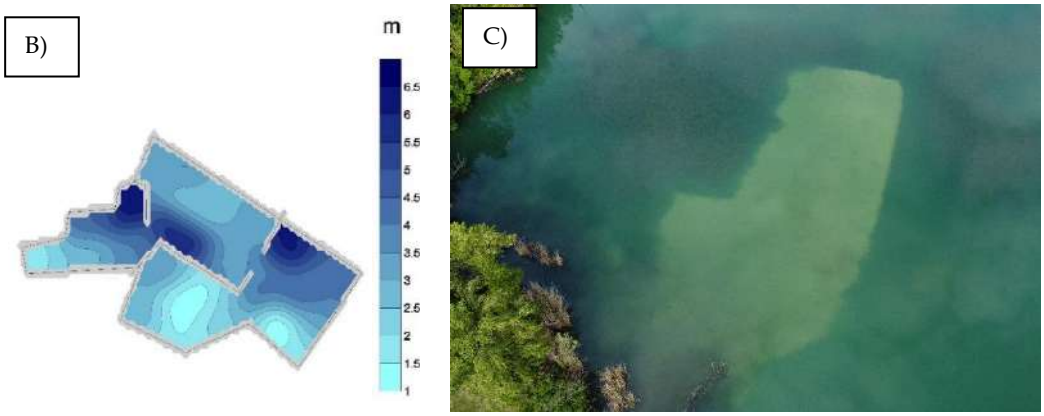

Figure 3.24 A) Bersi Serlini tanks, B) Bathymetry, C) drone picture of submerged grassland (credits: drone pictures of UniBS hydraulic group 29/04/2022)

Fig. 3.25 shows the comparison between the profiles measured during the two summer campaigns of 2021 and 2022. Transparency was measured during both campaigns and was equal to 1.2 m (during the same period in Lame the transparency was 0.2 m)

The tank appears deeply stratified, with a thermocline located at 1 m depth (in correspondence of the Secchi's depth), then temperature decreases with a constant slope until 4 m depth, where the profile changes the slope and temperature decreases more steeply towards the bottom. From the profiles one can conclude that the mixed layer consists of the first 4 m of water column, where specific conductivity is lower (around 300 μS/cm) and Oxygen concentration is higher (6 mg/L). The hypolimnion consists of the last two meters at the bottom, where specific conductivity is higher (> 350 μS/cm) and no Oxygen is present. Given the similarities between this tank and the one presented in figure 3.30, it is reasonable to believe that in winter this pond is able to mix completely. Therefore, the bottom isolated layer present in summer, is here called "hypolimnion" and not "monimolimnion", as one might believe given its higher conductivity concentrations.

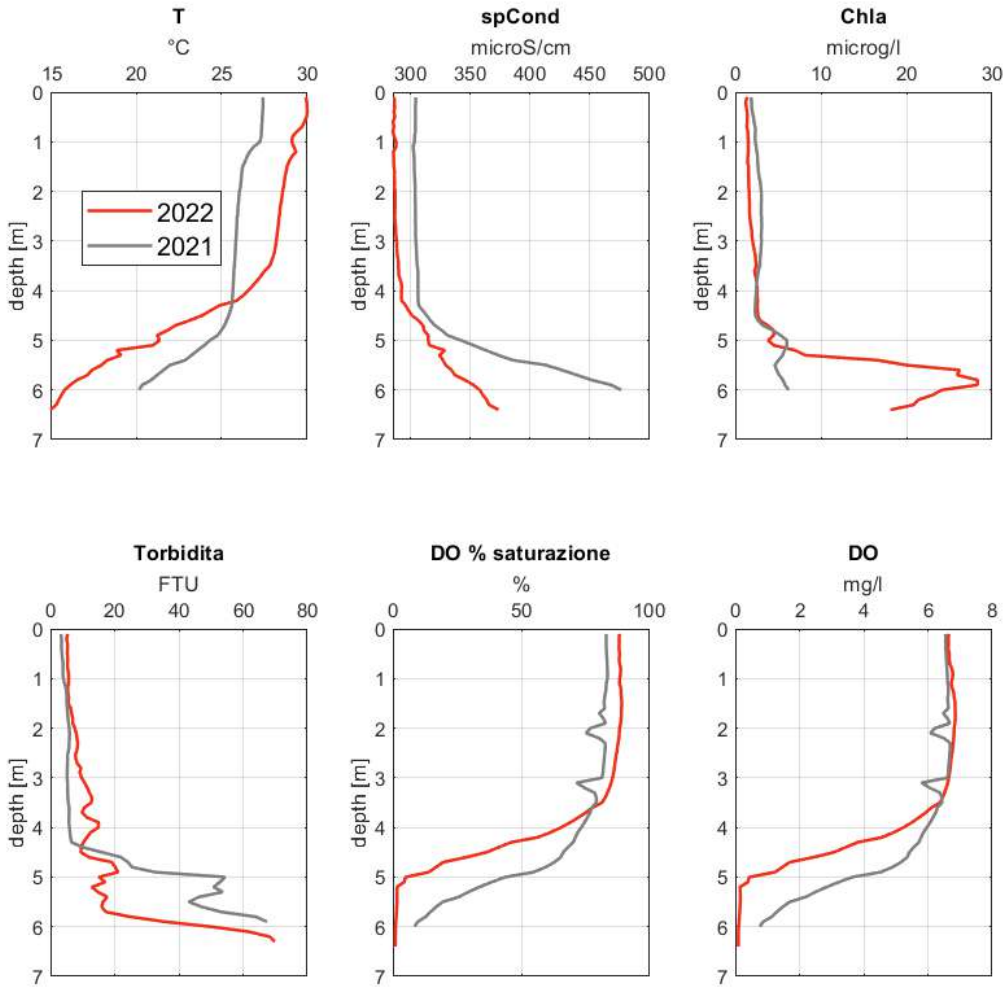

Figure 3.25 Profiles collected in the deepest point of the clay tank.

Oxygen levels below 4.5 m depth are such that life cannot occur. This, together with transparency values, is the reason why the only submerged grassland (coordinates 45°38'21.2"N 10°01'16.1"E) present in this tank, lies in the sole area where water levels are around 1 m (see Fig. 3.24 C).

The high values of conductivity at the bottom raise the suspicion that these tanks receive some kind of volumetric contribution from groundwater.

Proxy of chlorophyll-a concentration values are low (< 3 µg/L) and are typical of an oligotrophic system.

Vasca bagni tank

Vasca Bagni is a 38'000 m² tank of 6 m average depth. A shallower area is found in the Eastern portion and a deeper area (up to 8 m) is found in the

western area (Fig. 3.26 A). Two summer campaigns in 2021 and 2022 were conducted in this tank, where transparency was equal to 1.5 m and 1.75 m, respectively.

Vasca Bagni receives water from the Southern tanks, during overflow, from the northern Extra tank (see next paragraph) from rainfall and probably from groundwater.

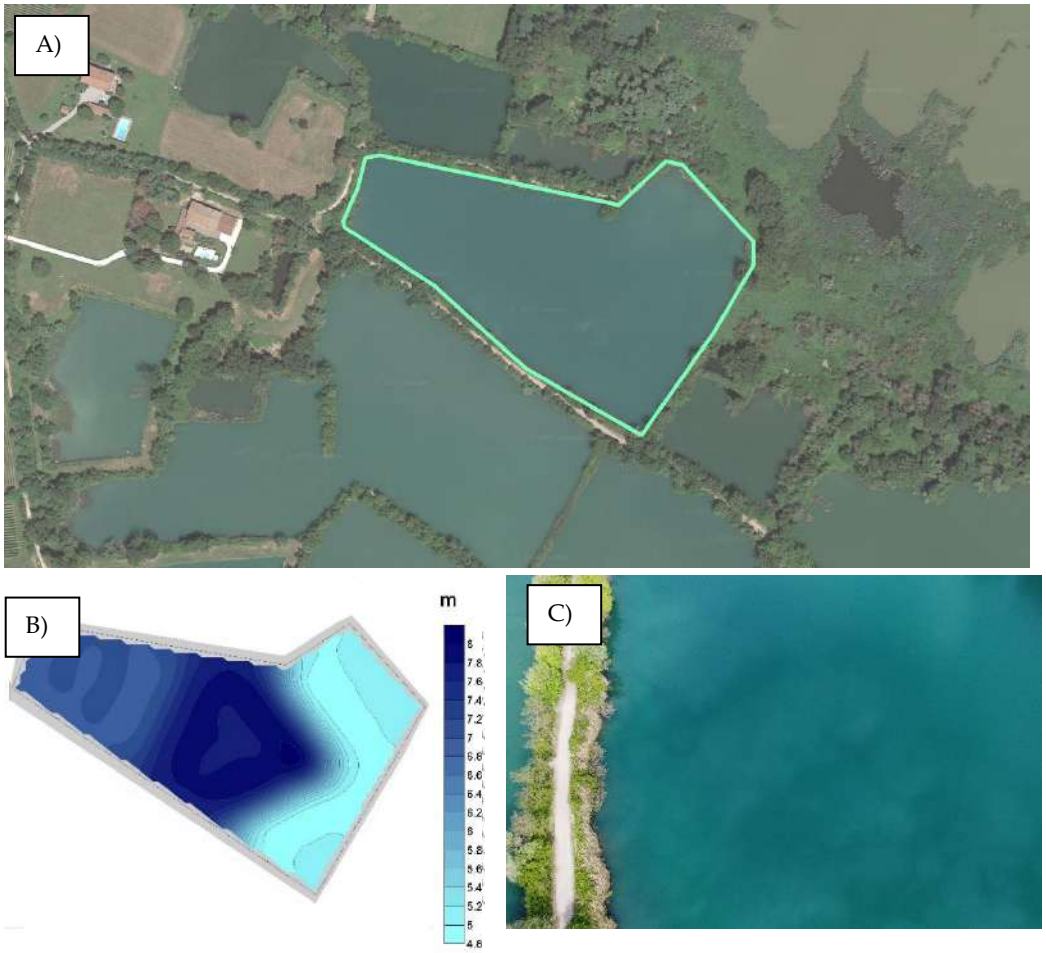

Figure. 3.26 A) Vasca bagni tank B) Bathymetry C) credits: drone pictures of UniBS hydraulic group 29/04/2022)

Fig. 3.27 shows the comparison between the profiles measured during the two summer campaigns of 2021 and 2022. Most of the considerations done for Bersi Serlini tanks in the previous paragraph apply also to this one. The mixed layer in Vasca Bagni is slightly thicker and the chemocline occurs at 4.5 m depth. Chlorophyll-a concentrations are even lower than the ones

found in Bersi Serlini tank. This pond appears to be of a light blue, milky color (Fig. 3.26C).

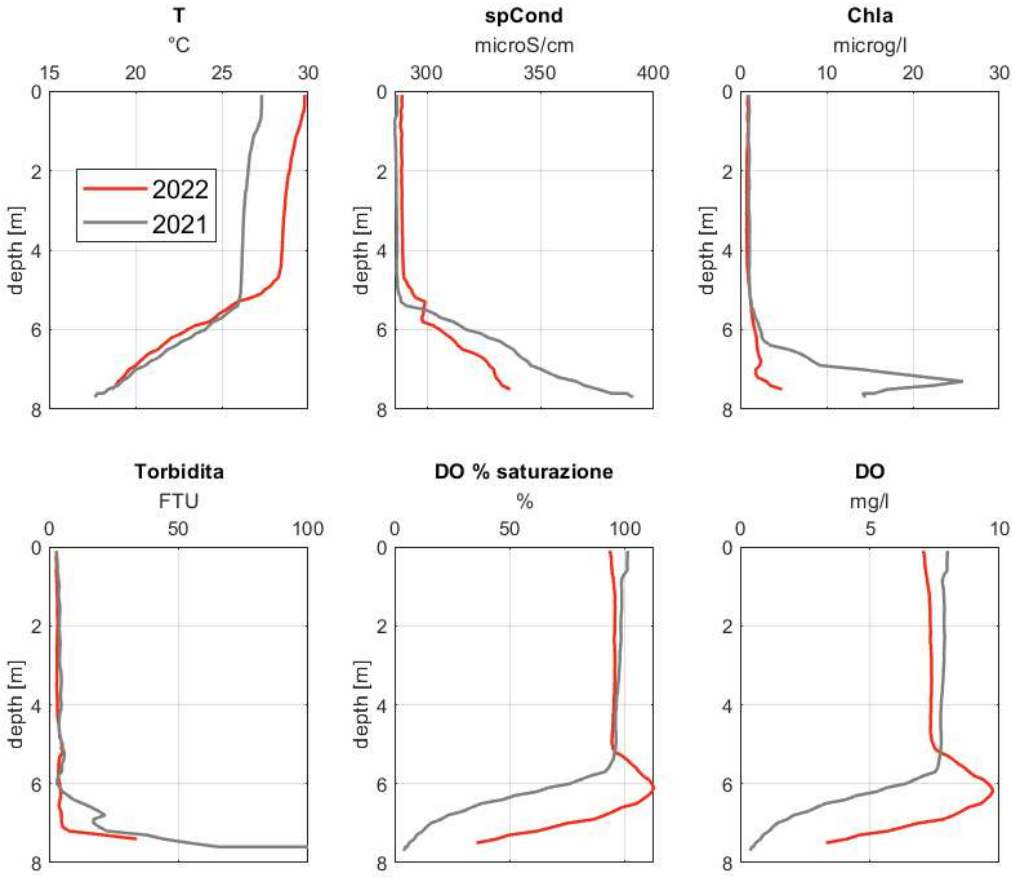

Figure 3.27 Profiles collected in the deepest point of the clay tank.

Extra tank

One campaign was possible in this smaller (Area = 5'000 m^2) tank and was done in July 2022. This pond has an average depth of 5 m and receives waters mainly from runoff (from West and North), rainfall and groundwater. The only evident outflow is a natural overflow directed towards Vasca Bagni tank, when water levels are high.

Despite the darkest color of this pond, the highest transparency of the period was recorded here: 2.6 m. The upper mixed layer is 4 m deep and is characterized by very low chlorophyll-a concentrations and turbidity. Specific conductivity shows the highest values among the surveyed clay tanks, indicating the extent of the groundwater contribution to the mass balance of this tank.

Figure 3.28 Extra tank

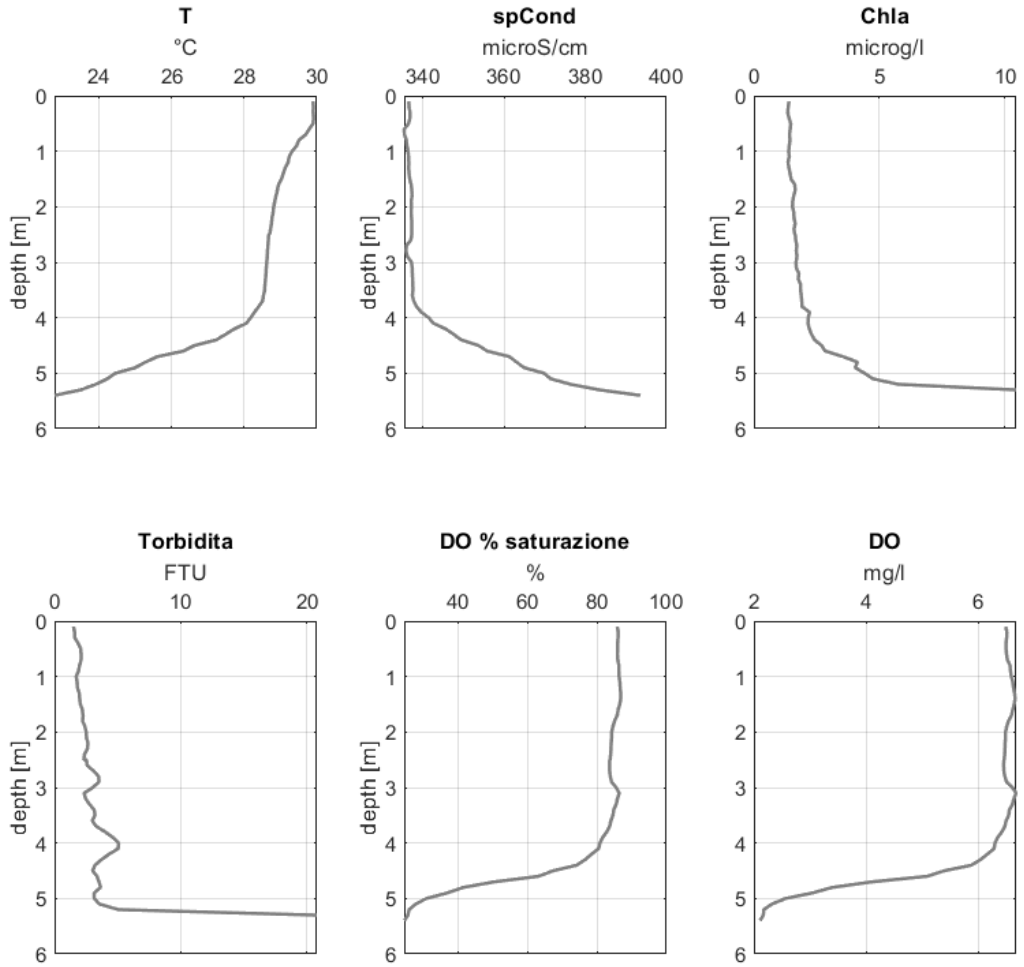

Figure 3.29 Profiles collected in the deepest point of the clay tank.

Deep clay tank

This tank is the deepest among the clay tanks and is therefore subjected to a specific monitoring of the water temperatures as described in ch. 3.3. It is characterized by a northern part being deeper (around 7 m average depth), and a Southern part being shallower (around 3.5 m average depth). This tank one consisted in fact of two separated ponds of different depth. A submerged sill, at the pristine boundary, was still visible during a drone survey (29th April 2022), during which transparency was 4 m (see Fig. 3.31).

Figure 3.30 Deep clay tank

Figure 3.31 Drone picture of the submerged sill between the Southern pond (low portion of the picture) and the Norther pond (top portion of the picture). Credits: UniBS hydraulic group 29/04/2022)

Five campaigns were done to characterize this pond. Due to the limited differences among the observations in the different profile locations, only one, unique profile is depicted for each campaign. Deep profiles, taken in the northern portion of the pond, are shown in Figure 3.32.

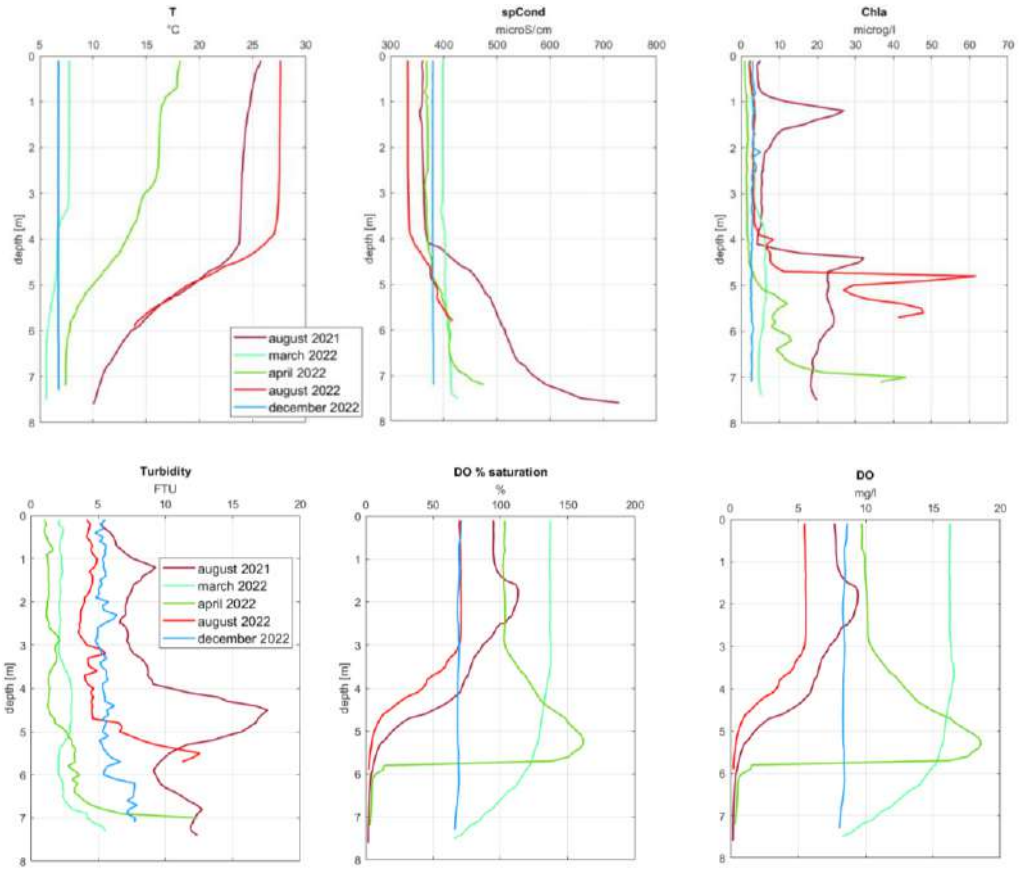

Figure 3.32 Profiles collected in the deepest point of the clay tank.

Profiles measured from March to August show the progressive stratification, while measurements in December show a uniform profile in terms of all the monitored parameters. During cold months, the difference in density established by the gradients of temperature and specific conductivity is not enough to keep the hypolimnion isolated. An overturn occurs, mixing the whole water column and oxygenating the bottom waters previously hypoxic.

3.3 Clay Tanks: water temperatures

This chapter is dedicated to the analysis of water temperature data that was obtained after the installation of two probes in one of the clay tanks located in the Southern part of Torbiere. Among all the clay ponds the one in Fig. 3.30 was chosen because it is in concession to some private fishermen, that have a little boat that could be easily used for the installation of the instruments.

This pond is surrounded by trees and is protected from tourists' sight, so that a buoy would not attract too much attention.

Some analysis, containing an indication of some water quality parameters, were done in this tank in 1990 by Istituto di Entomologia agraria of the University of Milan, directed by prof. Vighi (see Appendix D Additional materials).

Two loggers of water temperature installed at 1 m and 6 m depths, in the epilimnion and in the hypolimnion, respectively. Water temperatures were acquired at the time resolution of 10 minutes starting from March 1st, 2022.

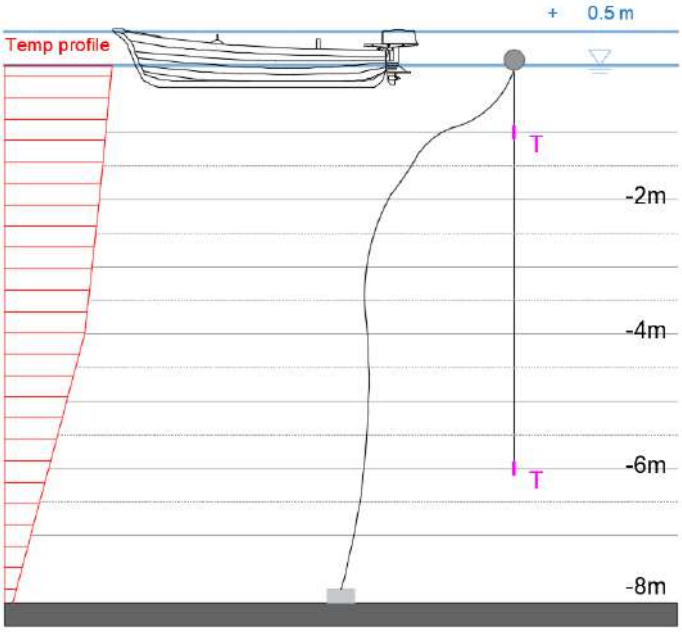

Figure 3.33 Scheme of the installation

Fig 3.33 shows the set-up of the installation, with a dead weight at the bottom of the pond to keep the probes in place. Two rows are attached to

the floating buoy, one connected to the dead body and one with the two temperature probes. The first row is loose to ensure that for an increase of water level of +0.5 m the probes are still found at the designed depth.

The temperature data series that were collected are shown in Fig. 3.34. At the beginning of March 2022 this pond was at the onset of a stratification period that lasted all summer until November 2nd, 2022. While the surface layer experienced thermal oscillations due to daily temperature fluctuations, the bottom probe recorded a fairly constant signal, that increased more slowly as summer approached.

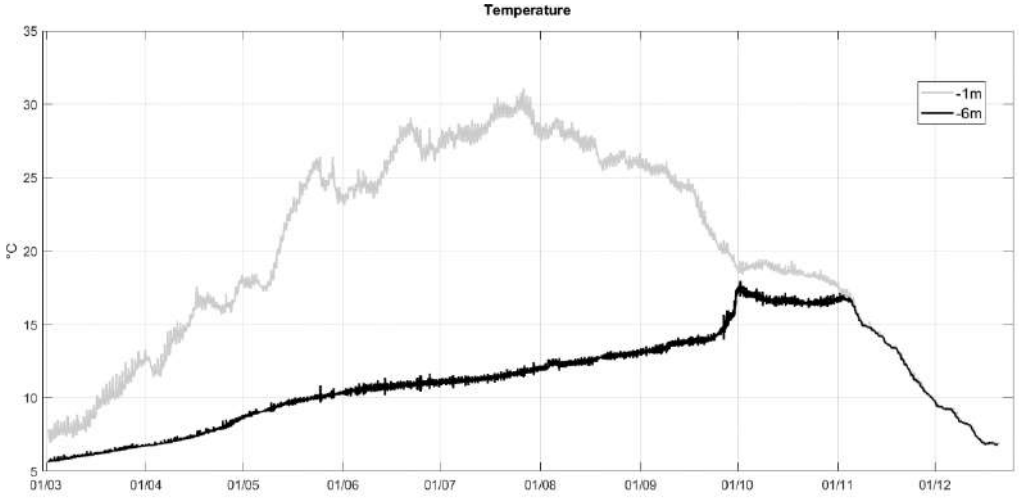

Figure 3.34 Temperature recordings at -1 m depth and -6 m depth

A remarkable event occurred towards the end of September 2022, when 70 mm of rain fell in three days, determining simultaneously a drop in the surface temperature and a warming of the deeper layer, due to a convective heat exchange. This pond is usually well shaded, especially from the wind coming from North, as it is surrounded by trees. When the difference in temperature between the two layers is great, the stress induced by the wind is not enough to trigger a circulation. The precipitation event of late September 2022 however, cooled the top layer and decreased the thermal gradient, making it possible for the wind to mix the water column. A portion of the top layer dropped and finally, on November 2nd, complete mixing was reached.

3.3.1 Estimation of diffusion coefficient

The phenomenon responsible for the transport of heat from the surface layer to the bottom layer is diffusion, a process through which substances

like heat, momentum, and matter, are spread within a water body from region of higher to regions of lower concentrations (Boehrer & Schultze, 2008). The (vertical) diffusivity is a key parameter when studying thermal stratification in a water body. It is the sum of two contributions: one is the molecular diffusivity, negligible with respect to the second one, the turbulent diffusivity. The latter is a property of the turbulent fluid and does not depend on the physio-chemical property of the water.

The time series of water temperatures in the epilimnion and hypolimnion allow for the estimation of the diffusion coefficient. Starting from the turbulent diffusion equation (Fick's Law):

$$\frac{\partial T}{\partial t} = (D_T + K_z)\frac{\partial^2 T}{\partial z^2} \qquad [3.2]$$

Where T is a function of time t and depth z, D_T is the molecular diffusivity and K_z is the vertical turbulent diffusivity. Considering that the turbulent diffusivity is orders of magnitude larger than the molecular diffusivity, the latter can be neglected. The turbulent diffusivity can therefore be estimated as:

$$K_z = \frac{\frac{\partial T}{\partial t}}{\frac{\partial^2 T}{\partial z^2}} \qquad [3.3]$$

Equation 3.3 has been applied at each time step to the series of water temperature from March to December 2022. The second derivate of temperature in the vertical direction was obtained by fitting a second order polynomial to the available profiles of water temperatures (profiles are shown in Figure 3.32).

The procedure led to an average value for the turbulent vertical diffusivity of 2.9 x 10^{-7} m^2/s.

3.4 Inflow stations

3.4.1. Rì: discharge, conductivity, and plume dynamics

Station IS1 consists of two separated, but close, installations: one (Fig. 3.35 B) is located at the inlet of a 1 m – diameter concrete pipe, within which a LT-US Sofrel ultrasonic water level probe is installed and records water levels with a frequency of 15 minutes since October 2019. A stage discharge

relationship was obtained during the project described in ch. 2.4.6 for this channel, in order to get an expression of the discharge. It was derived by finding the roots of the Chezy equation:

$$Q(h) = A(h) * k_s R_h^{2/3} \sqrt{Sb} \qquad [3.4]$$

, considering a channel of bed slope Sb = 0.06 and Strickler's roughness coefficient k_s = 50 $m^{1/3}/s$.

This probe is managed by Acque Bresciane. The second installation is located 200 m upstream and is in a private garden. Here, a YSI conductivity probe (Fig.3.35 C) was installed for some months (See tab. 3.1), to study the ranges of variability of conductivity in Rì and its behavior with respect to rainfall events.

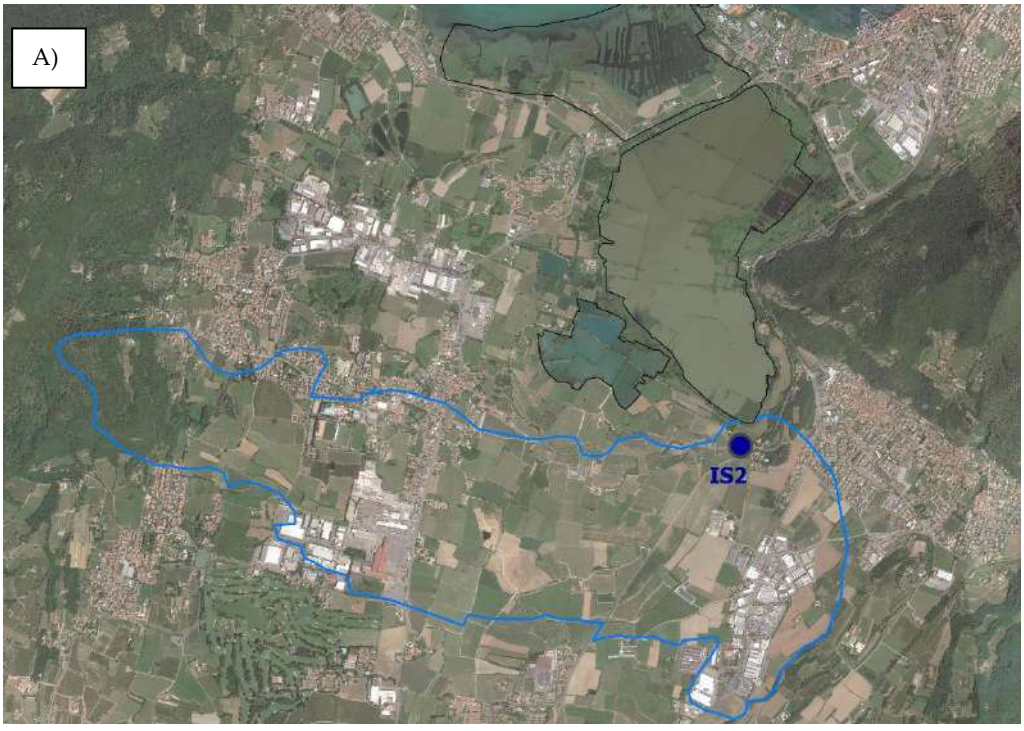

Figure 3.35 A) Watershed of Rì and location of the station B) location of IS1 where the water level probe is installed (a black wire is visible entering the pipe) C) YSI probe for specific conductivity

Rì is a rather small stream, that drains a big watershed of 6 km^2, consisting of urban areas (the municipality of Corte Franca), vineyards, quarries, arable land, and industrial areas.

The discharges that were obtained are represented in Fig. 3.36. two regimes can be distinguished:

- Dry regime: when few-to-no precipitation occurs on the watershed of Rì, the discharge is very low and equal to underlying value of 40 L/s.
- Wet regime: during a precipitation event the discharge increases very quickly and reaches 300-1000 L/s.

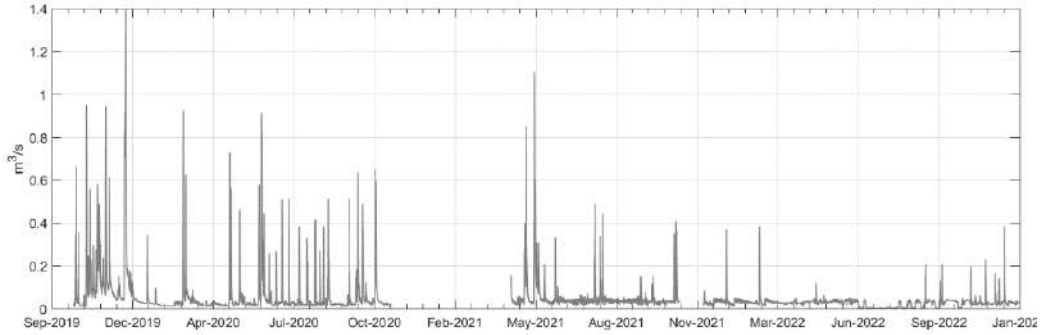

Figure 3.36 Discharges of Rì as obtained from the stage-discharge relationship of eq. 3.4

Records of specific conductivity (Fig. 3.37) in Rì show that very high values are reached during dry periods (500 to 800 μS/cm), while the levels drop as soon as there is a rainy event, down to 300 to 400 μS/cm. This decrease in conductivity is due to the dilution effect of rainy water. During precipitation, the discharge of Rì is mainly due to the precipitation volume, which consequently has a great effect on the conductivity levels.

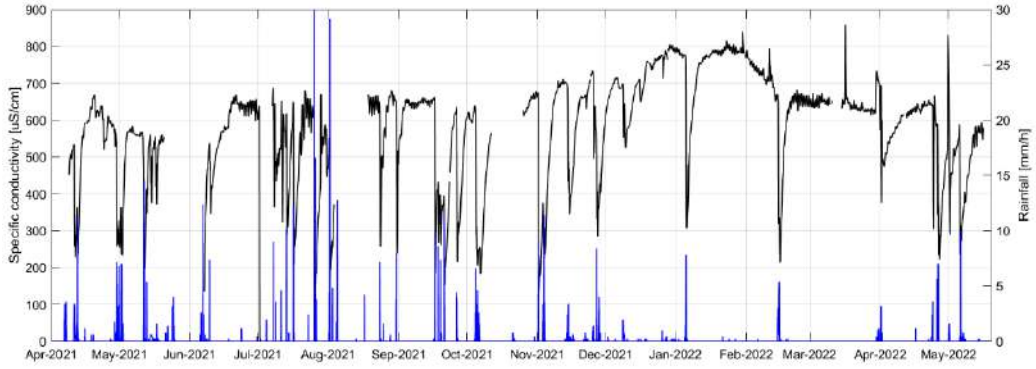

Figure 3.37 Specific conductivity in Rì and precipitation

Plume dynamics

Given the discharge regime of Rì, with very low dry discharge but sudden spikes during rainy events, it makes sense to investigate the creation of a plume during rainfall times. During the flood regime, discharge increases as well as the velocity with which the inflow enters first the Rì tank and then the rest of Lame. Specific conductivity is low, arguably even lower than the underlying value inside Lame.

Some campaigns were (see Tab 3.3) were conducted with the multiparametric probe, in order to measure vertical profiles in the area of Lame just outside the Rì tank, trying to detach the plume after a rain event.

Date	**Number of profiles**	**Rainfall in previous 10 days [mm]**	**Peak discharge [m3/s]**	**Δ conductivity (Lame – Rì) [µS/cm]**
14/04/2021	42	90	≃ 0.6	460 – 220
27/09/2021	36	65	0.15	290 – 200
05/11/2021	36	100	0.4	325 - 200

Table 3.3 Plume-detection campaigns

2D-interpolated maps were created for each parameter, to visualize the presence of any plume. In only one measurement campaign (14th April 2021) it was possible to identify the plume outside Ri tank, probably thanks to the greater gap between conductivity in Lame and in Rì. The results of this campaign are therefore shown in the following.

Location of the profiles

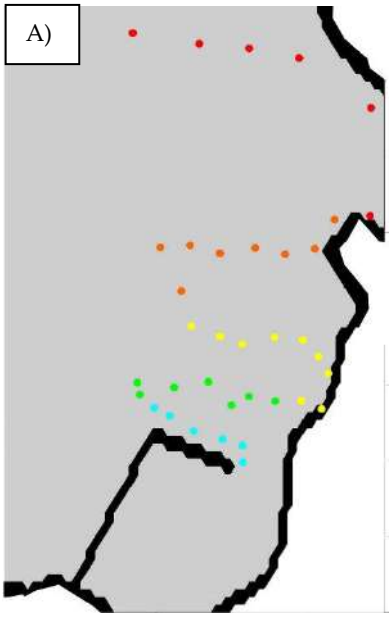

Specific conductivity (average over the first 80 cm) [µS/cm]

Temperature (average over entire water column) [°C]

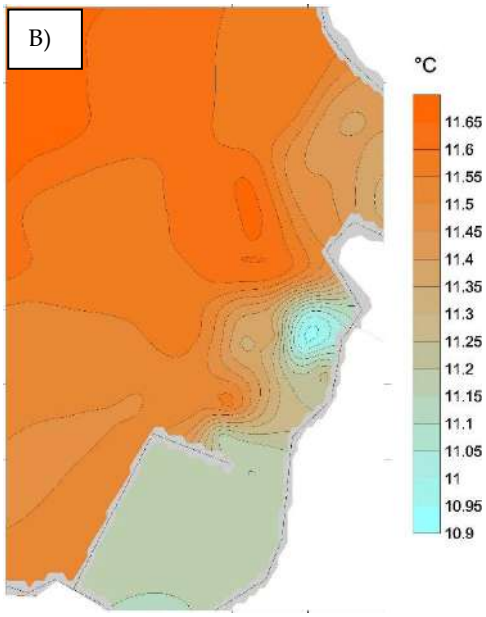

Dissolved Oxygen saturation (average over the first 80 cm) [%]

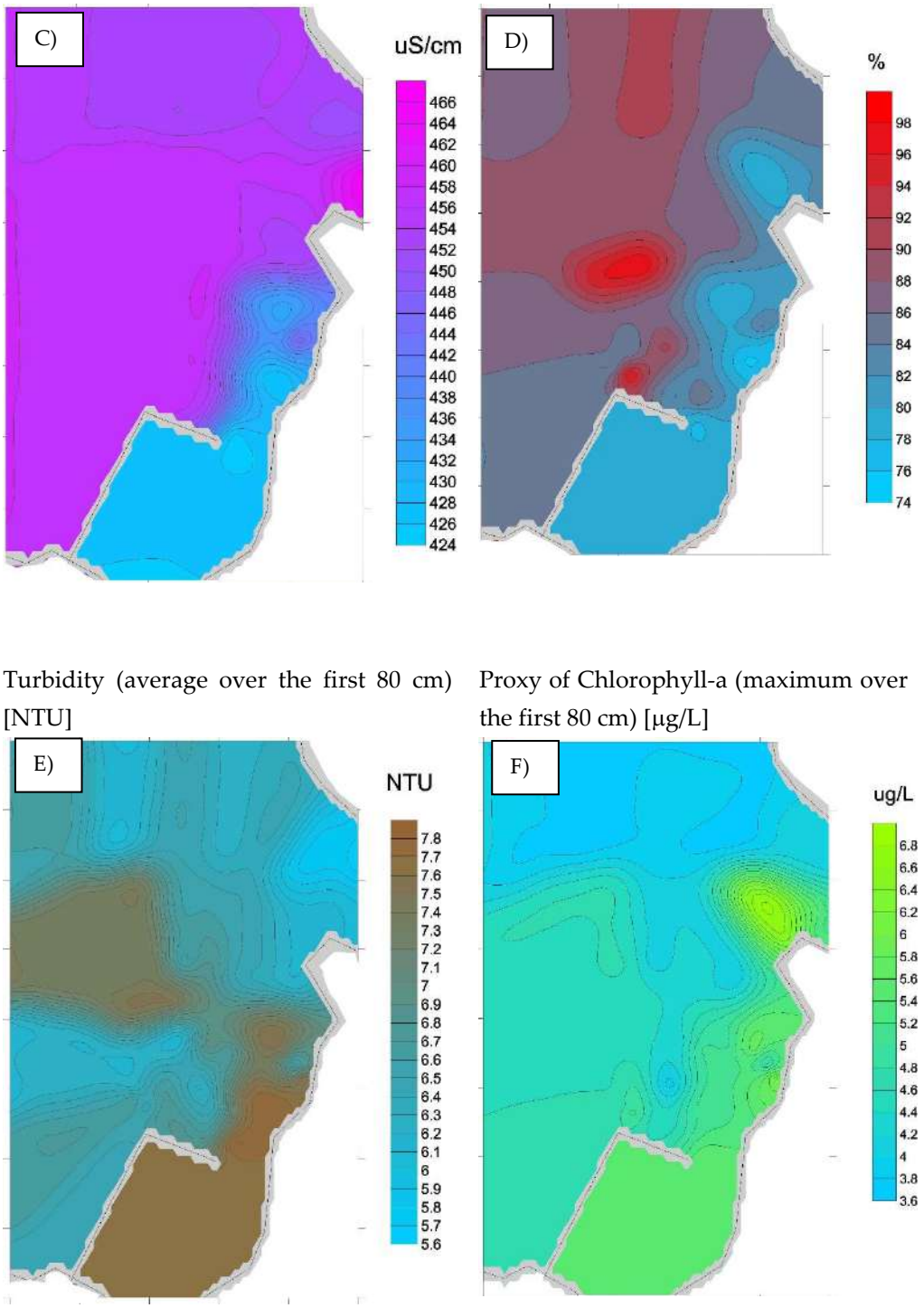

Turbidity (average over the first 80 cm) [NTU]

Proxy of Chlorophyll-a (maximum over the first 80 cm) [µg/L]

Figure 3.38 2D – interpolated maps obtained from the plume campaign of 14th April 2021

The measurements were taken following parallel transect, orthogonal to the direction of the plume, of increasing length (starting from 80m up to 250 m), in order to represent the edges of the plume as well as its inner part (Fig. 3.38 A). Overall, the measurements covered a cone of 31'000 m^2. During the

campaign, there was no thermal stratification: profiles of temperature were constant all over the water column. Rì's water was slightly cooler than the one of Torbiere (Fig. 3.38 B).

The maximum of Chlorophyll-a across the first 80 cm of water column is around 6 mg/L, indicating a mesotrophic state. A slight gradient depending on the distance from the inlet of Rì can be seen and higher values are found closer to the affluent (Fig. 3.38 F).

Specific conductivity is the best parameter to look at when trying to detect the plume as seen from Fig. 3.38 C: it behaves like a tracer, with lower concentrations close to the Rì's inlet. During rainy periods, Rì's conductivity drops due to the dilution effect of rain. As a result, the high discharge of these periods has a cleaning and flushing effect on the waters of Torbiere. While the main tanks of Torbiere have a conductivity of 460 μS/cm, Rì is entering with 400 μS/cm (Fig. 3.39 E).

Dissolved Oxygen is quite variable over space, but a plume is detectable from DO concentrations as well: Rì's waters are less oxygenated than the tanks of Torbiere (Fig. 3.38 D).

Turbidity is higher in the surroundings of Rì's inlet. In terms of absolute values, turbidity was quite low during this campaign (Fig. 3.38 E).

Overall, the plume was visible from all the parameters measured, not only for specific conductivity.

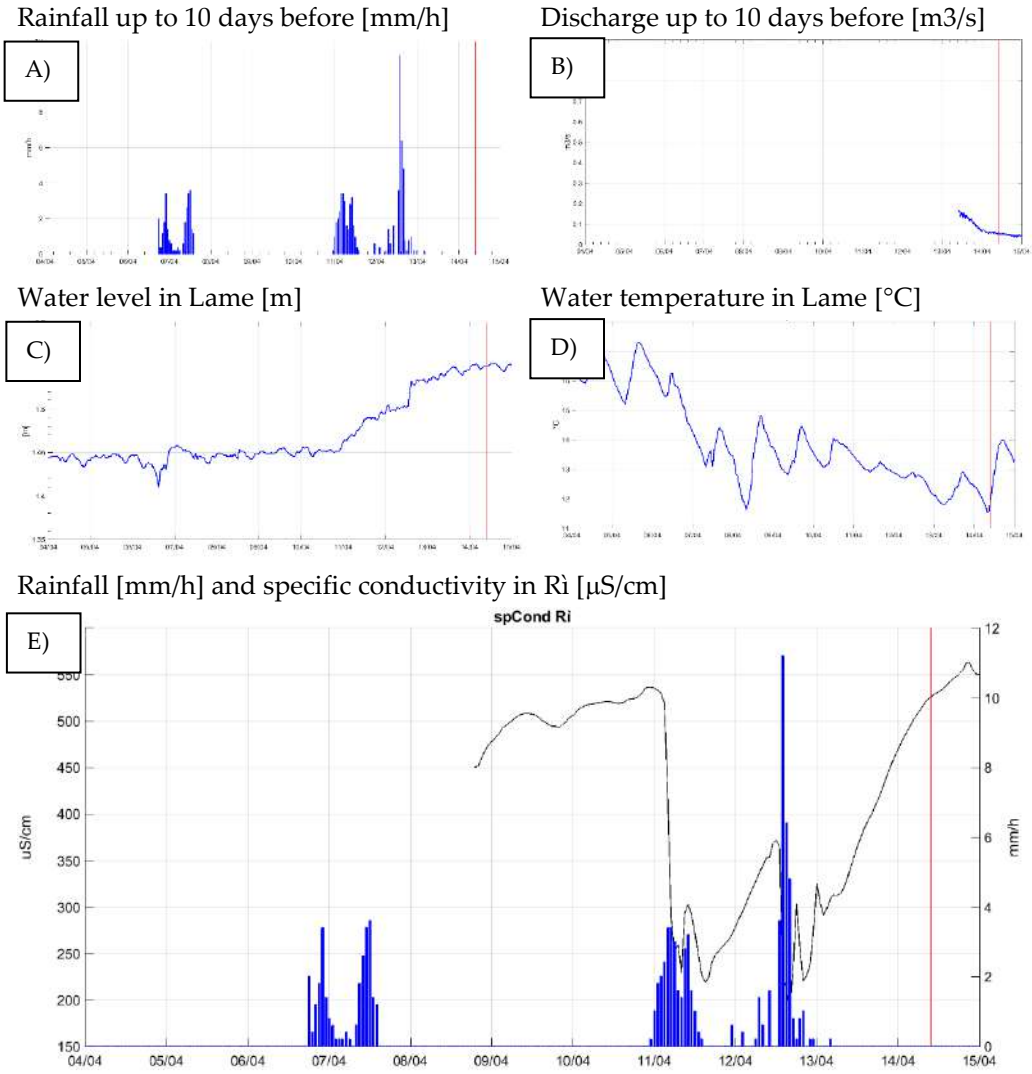

Figure 3.39 Precipitation, discharge in Rì, water level and temperature in Lame and specific conductivity in Rì, 10 days before and during the campaign. The red vertical line indicates the time when the campaign was done.

The measurements were done after 10 days of quite intense rains, with a cumulative precipitation of 90 mm (Fig. 3.39 A).

The main affluent Rì was not being monitored in terms of discharge during these days, but with tis rainy event, values of 0.5-0.7 m^3/s of peak discharge are expected.

When looking at the specific conductivity in Rì as measured by the YSI probe located in station IS1, one should consider that the conductivity value measured at the time of the campaign is shifted in time: the value influencing the measured profiles is that of the conductivity ≃10 hours

before, with 10 hours being the time it takes to the water of Rì to travel from IS1 to the location of the campaign.

The way the plume of Rì spreads inside Lame in space and time strictly depends on the horizontal viscosity and diffusivity, two parameters that govern the transport in the horizontal direction. In ch. 4.4 the above showed measurements will be used to calibrate a numerical model and assign the values of horizontal eddy viscosity and diffusivity.

3.4.2 Combined sewer overflow: discharge

The combined sewer overflow of the village of Provaglio d'Iseo is located at 45.638655, 10.039659 under a flower bed below the road level. A stage discharge relationship was developed for this channel to obtain the flowrates shown in figure 3.40 starting from the water level measurements of a VEGA WL S61 radar level meter (Barone et al., 2019).

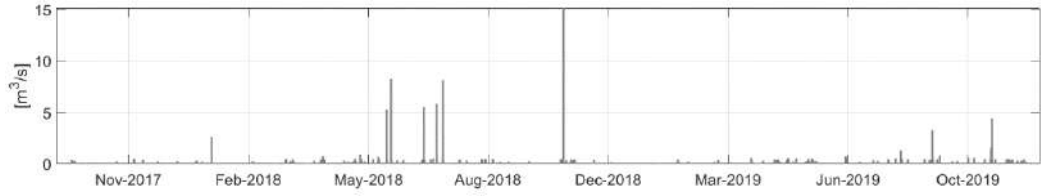

Figure 3.40 Time series of discharge at the CSO of Provaglio (Sep 2017-Nov 2019)

The CSO delivers a discharge (up to 5-10 m^3/s) only during rainy period, corresponding to a total flood volume that is below 2000 m^3 in 90% of the events (Unibs preliminary study, 2019).

Some samples collected on this CSO allowed for an estimation of the load of nutrients coming from this affluent. Despite the low average discharge, it delivers 770 kg of Phosphorous per year and 3860 kg of Nitrogen per year. (Pilotti M. et al., 2020).

3.5 Water balance of Lame

The monitoring data of water levels of Torbiere, the discharges of Rì and CSO, the precipitation, the evaporation rate derived from weather station measurements as well as the pump ON/OFF time intervals, all contribute to the assessment of the water balance of Lame:

$$A\frac{dh}{dt} = Q_{Rì} + Q_{CSO} + A * i_{rain} - Q_{evap} - Q_{pump} \quad [3.5]$$

At this purpose, the years 2020, 2021 and 2022 were considered, where all the above-mentioned hydrodynamic data was available. It is important to stress that a more appropriate estimation would require a longer time series, since one or two years might be influenced by exceptional weather and climate conditions (e.g., 2022 was a particularly dry year where the pump was exceptionally hardly never switched on).

Evaporation (m^3/day) was estimated using the Penman-Monteith equation (Monteith J.L., 1965):

$$ET_0 = A * \frac{0.408\Delta(R_n - G) + \gamma\frac{900}{T+273.15}U_{wind}VPD}{\Delta + \gamma(1+0.34U_{wind})} \quad [3.6]$$

Where A is the area of Torbiere, R_n is the net radiance (W/m^2), G is the ground net flux (W/m^2) and γ is the psychrometric constant (Pa/K). Δ is the slope vapor pressure curve (kPa/°C) obtained through the Tetens- Murray equation (Tetens O., 1930):

$$\Delta = \frac{4098[0.6108e^{\frac{17.27+T}{T+237}}}{(T+237)^2} \quad [3.7]$$

VPD is the vapor pressure deficit (kPa):

$$VPD = \frac{(100-RH)SVP}{100} \quad [3.8]$$

With *SVP* being the saturated vapor pressure (kPa).

The required data were provided by the hourly-averaged time series of air temperature, relative humidity, short wave radiation and wind speed during the two periods in exam.

This chapter presents the main volume contributions. The author is aware that other elements of the water balance might be involved (see list below), but they have been assessed as negligible, with respect to the other contributions. This choice eases the task of evaluating the mass balance as these contributions would be particularly difficult to measure or estimate.

In particular, the mass balance presented here will not take into account:

- Groundwater sources: the Eastern portion of Lame receives some sort of groundwater contribution of difficult estimate. Fontanì tank is the only pond whose volume is actually created by this contribution, but the discharge is in the order of a few litres per second, making it negligible.
- Runoff: the surrounding fields discharge water into Lame either directly or through ditches. The ditches have been inspected several times: during dry periods no water is present, and during rainy periods the water still does not show a detectable flow.
- Secondary discharges coming from the surrounding municipalities: there are minor discharges coming from single houses or from wider residential areas of Provaglio d'Iseo, Corte Franca and Iseo. The volume conveyed by these discharges is of secondary importance and was considered negligible in this evaluation.

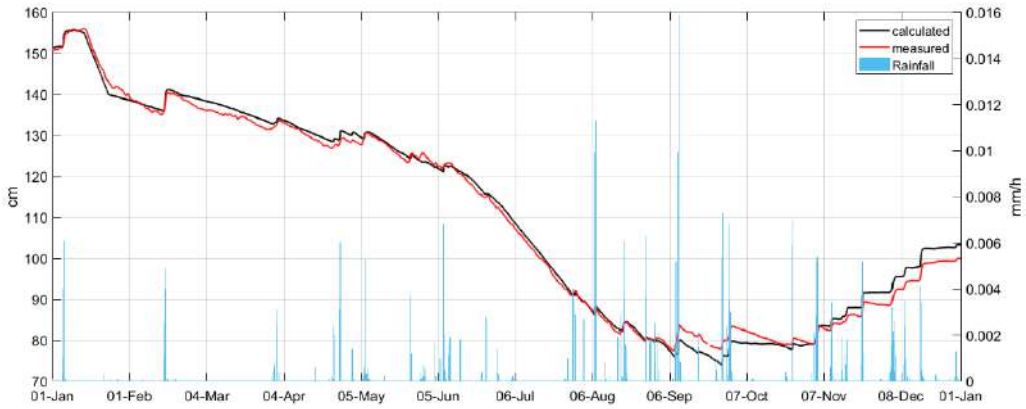

Figure 3.41 results of the dynamic water balance for the year 2022 by means of a comparison between the computed and the measured water levels

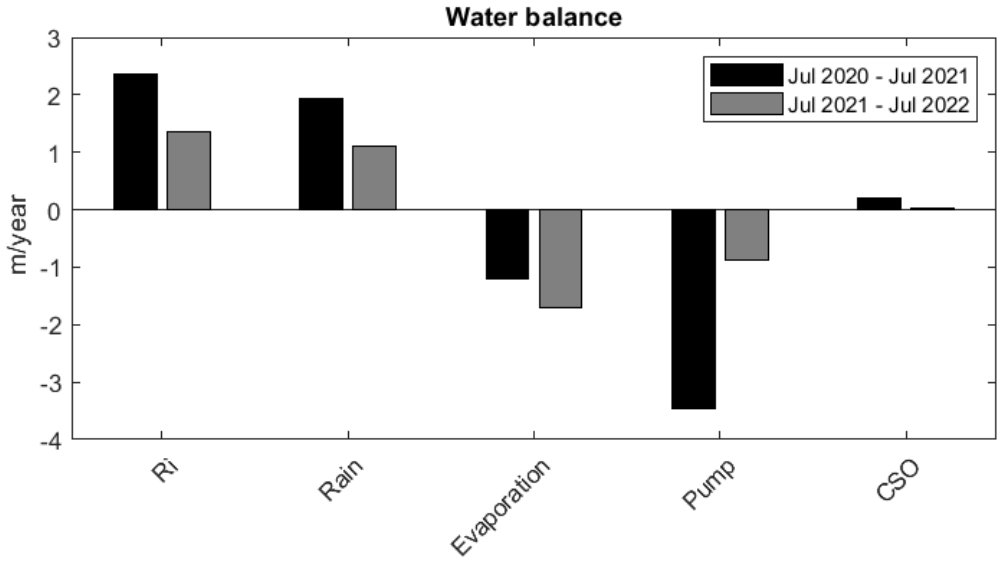

Figure 3.42 Annual incoming and outflowing volumes (specific volumes per area) during the two years of observations.

Figure 3.41 represents the dynamic computation of the mass balance of Torbiere for the year 2022. The mass balance was resolved for the whole year to obtain the computed water levels (black line). The comparison with the measured water levels (red line) shows a good agreement ($R^2 = 0.991$), meaning that the terms of the mass balance considered are correct and there is no extra relevant contribution. The cumulated error after one year of computation was 3.31 cm.

Figure 3.42 shows the results of the computation of the water balance for 2020-2021 and 2021-2022. There is a large variability between the years that have been considered and the recording of a longer time series is required in order to obtain an average yearly water balance. Despite the low amount of data, some observations can be done:

- Torbiere is fed similarly by the affluent Rì (101% of total volume of Torbiere in July 2020 – July 2021) and rainfall (82%) and one would expect that these two contributions will show similar behaviors across the years, as Rì's discharge is mainly composed by the watershed runoff and, therefore, rain. Also, Rì's basin is rather small and located close to Torbiere, meaning that the two pluviometric regimes are the same.

- CSO delivers a negligible volume (8% in July 2020 – July 2021 and 1% in the following year) but is shown because of its relevance with respect to nutrient loading.
- Evaporation is the only natural effluent of Torbiere, it is a fundamental element of the water balance due to the shallow nature of the system (a large area is exposed for evaporation with respect to the effective volume of the system). In the period July 2020 – July 2021 evaporation's contribution corresponded to 52% of the total volume of Torbiere, in the following period its contribution rose up to 72%.
- Despite its importance, evaporation alone is not enough at regulating the water levels of Lame. The addition of an artificial channel regulated by a pump is of key importance when balancing the water depth throughout the year. Without the pump, levels would increase. During a rainy year like the one of July 2020 to July 2021, the pump removed 147% of the total volume of Torbiere, while in the following period its contribution was only 37%.

3.6 References

Barone L., Pilotti M., Valerio G., Balistrocchi M., Milanesi L., Chapra S.C., Nizzoli D. (2019). Analysis of the residual nutrient load from a combined sewer system in a watershed of a deep Italian lake. Supplementary material II. *Journal of Hydrology*, Vol. 571, 202-213.

Boehrer, B., and M. Schultze (2008). Stratification of lakes. *Rev. Geophys*., 46, RG2005.

Carlson R.E. (1977). A trophic state index for lakes. *Limnology and Oceanography*, Vol 22(2), 361-369.

Chapra S.C., Dobson H.F.H. (1981). Quantification of the lake trophic typologies of Naumann (surface quality) and Thienmann (oxygen) with special reference to the Great Lakes. *Journal of Great Lake Research*, Vol 7(2), 182-193.

Cozzaglio A. (1932). Sulla possibilità di un impinguamento dei fontanili bresciani occidentali con le acque di recupero del lago di Iseo e sulla bonifica della Torbiera.

Jeppesen E. et al. (1990). Fish manipulation as a lake restoration tool in shallow, eutrophic, temperate lakes 2: threshold levels, long-term stability and conclusions. *Hydrobiologia*, Vol 200, 219-227.

Madsen J.D., Chambers P.A., James W.F., Koch E.W., Westlake D.F. (2001). The interaction between water movement, sediment dynamics and submersed macrophytes. *Hydrobiologia*, Vol 444 (1-3), 71-84.

Monteith, J. L. (1965). Evaporation and environment. *Symposia of the Society for Experimental Biology*. 19: 205–234.

Nutz A., Schuster M., Ghienne J.F., Roquin C., Bouchette F. (2018). Wind-driven waterbodies: a new category of lake within an alternative sedimentologically-based lake classification. *Journal of Paleolimnology*, Vol 59, 189-199.

Scheffer M, Carpenter S., Foley J.A., Folke C. and Walker B. (2001). Catastrophic shifts in ecosystems. *Nature*, Vol 413, 591-596.

Scheffer M. (2004). Ecology of Shallow Lakes. *Population and Community Biology Series*, Vol. 22.

Tetens, O. (1930). Über einige meteorologische Begriffe. *Z. Geophys* 6: 297-309.

Books

Wetzel R. (2001). Limnology, Lake and River Ecosystems. *Elsevier Inc*. Third Edition.

Others

Pilotti M., Valerio G., Farina G., Volpini S. (2020). Analisi finalizzate al dimensionamento di un'area umida a servizio dello sfioratore della fognatura mista di Provaglio, Relazione finale.

Surfer User's Guide (2019).

4. Numerical simulations

This chapter describes the numerical simulation of the thermal regime and the internal hydrodynamics of Torbiere del Sebino. Chapter 4.1 is dedicated to the water level and setup modeling. In chapter 4.2 and chapter 4.3 the issue of temperature modeling in Lame and in clay tanks is assessed. Chapter 4.4 shows the sensitivity of the used model to the turbulence parameters and explains the process of their calibration.

The choice of a modelling technique should depend on the objectives, on scientific and technical aspects as well on the availability of resources and data (Wester S.J. et al., 2018). Several modelling approaches have been successfully applied for wetland hydrologic and hydrodynamic simulations. These include 1D models (Gu et al.,2014), quasi 2D models (Zanobetti et al., 1968, Garcia et al., 2015 and Wester et al., 2018), 2D models (Schumann et al., 2013 and Haines, 2013) and 3D models (Marsooli et al., 2016, Bricheno et al., 2016, Popescu et al., 2015). 1D and 2D models are preferred in larger deltaic systems, while for smaller areas, 3D models usually show a good performance and are reliable.

To model the hydrodynamics and thermal regimes of Torbiere, DELFT3D was chosen. It is an integrated open-source modelling software developed by Deltares for coastal, river and estuarine areas that best suits wetlands and shallow basins in general. The DELFT3D suite is composed of several modules grouped in a common interface that can be easily linked to each other. DELFT3D-FLOW, one of the modules of this suite, is a multidimensional (2D or 3D) hydrodynamic/transport simulation program that calculates non-steady flows and transport phenomena resulting from tidal and/or meteorological forcing (Deltares, 2020). Delft3D solves the Navier-Stokes and transport equations under the Boussinesq assumption:

$$\frac{\partial u}{\partial t} + u\,\frac{\partial u}{\partial x} + v\,\frac{\partial u}{\partial y} + w\,\frac{\partial u}{\partial z} - \frac{1}{\rho_0}\frac{\partial \tau_{xj}}{\partial x_j} = \frac{\rho}{\rho_0}F_x - \frac{1}{\rho_0}\frac{\partial p}{\partial x} + \nu\nabla^2 u \qquad [4.1]$$

$$\frac{\partial v}{\partial t} + u\,\frac{\partial v}{\partial x} + v\,\frac{\partial v}{\partial y} + w\,\frac{\partial v}{\partial z} - \frac{1}{\rho_0}\frac{\partial \tau_{yj}}{\partial x_j} = \frac{\rho}{\rho_0}F_y - \frac{1}{\rho_0}\frac{\partial p}{\partial y} + \nu\nabla^2 v \qquad [4.2]$$

$$\frac{\partial w}{\partial t} + u\,\frac{\partial w}{\partial x} + v\,\frac{\partial w}{\partial y} + w\,\frac{\partial w}{\partial z} - \frac{1}{\rho_0}\frac{\partial \tau_{zj}}{\partial x_j} = \frac{\rho}{\rho_0}F_z - \frac{1}{\rho_0}\frac{\partial p}{\partial z} + \nu\nabla^2 w \qquad [4.3]$$

In which τ_{ij} are the Reynolds or turbulent stresses, p is the normal pressure and F are the external forces.
For the transport of scalar quantities, Delft3D solves the transport equation:

$$\frac{Dc}{Dt} = \frac{\partial}{\partial x}\left(D_h \frac{\partial c}{\partial x}\right) + \frac{\partial}{\partial y}\left(D_h \frac{\partial c}{\partial y}\right) + \frac{\partial}{\partial z}\left(D_v \frac{\partial c}{\partial z}\right) + s \qquad [4.4]$$

Where D_h and D_v are the horizontal and vertical eddy diffusivity, respectively, c is the transported scalar quantity and s is the source or sink term.

Wetland schematization and grid construction

A 2D grid was built for the study area, as defined in Fig. 4.1. The size of each cell is 5 ± 3 m, considered suitable in view of topographical characteristics and computational time. The total number of cells is around 24'000, allowing for the representation of both big and smaller tanks. The feature "thin dams" is used to represent the banks subdividing the tanks, which therefore will have no dimensions and will not allow any kind of communication between the sides of the dam itself.
The vertical grid schematization was selected differently for each simulation according to the need to represent different phenomena. For this reason, the choice of the vertical grid will be described each time a new simulation is presented.

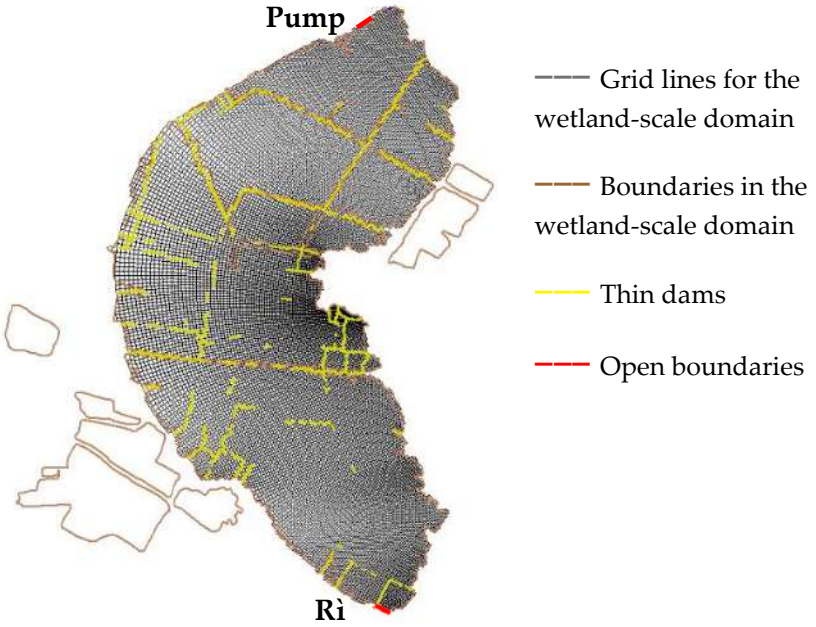

Figure 4.1 2D Grid construction of Torbiere with Delft-3D

Boundary conditions and rainfall

After evaluating the relative importance of tributaries' discharges, one inflow and one outflow were considered and depicted through the "open boundaries" feature. The time-series of incoming discharges from Rì (obtained from the stage – discharge relationship described in ch. 3.4.1) and of outflowing discharges of the pump (whose time intervals are given by Consorzio dell'Oglio, ch. 2.4.5) are entered in the model. Temperature of Rì has been measured from July 2019 to October 2020 and the extended time series has been obtained from a linear correlation derived between Rì's daily average water temperature and air daily average temperature:

$$T_{Rì} = 3.7°C + 0.8T_{air} \quad [4.5]$$

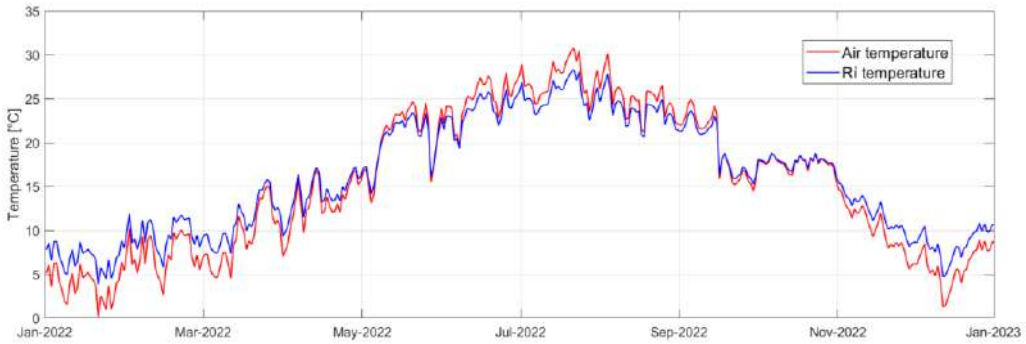

Figure 4.2 Time series of daily average water temperature for the affluent Rì for 2022, derived from the linear correlation obtain from the series of air temperature measured at MWS1.

The relationship 4.4 gives back $R^2 = 0.77$ between the measured and the derived water temperatures.
Rì's temperature, however, is only relevant in the surroundings of the inlet, due to its low volumetric discharge and momentum.
Rainfall is measured at WS2 (ch.2.4.2) and can be added to the model through an "additional parameters" flag as a time series containing its intensity and temperature. Rainfall temperature is calculated from the air temperature as described in eq. 4.5.

Heat flux model

Five heat flux models are available in Delft 3D, each of them requiring different input parameters. The choice of the heat flux model should be driven towards the most complete one that can be applied considering the available data. In the case of Torbiere the most complete heat flux model was chosen, i.e the Ocean model. This model allows to insert, as time-dependent input data: air temperature, relative humidity, cloud cover and net solar radiation, as well as a constant value of Secchi's depth. By means of this model it is possible to take into account the evaporative mass flux, which plays an important role in Torbiere (see ch. 3.5).
In general, the total incoming heat flux is given by (Deltares, 2020):

$$Q_{tot} = Q_{sn} + Q_{an} - Q_{br} - Q_{ev} - Q_{co} \quad [4.6]$$

Where Q_{sn} is the net incident short-wave solar radiation and is measured at WS1 station. Q_{an} is the net incident long-wave atmospheric radiation and Q_{br} is the longwave back radiation and are computed together as:

$$Q_{an} - Q_{br} = \varepsilon\sigma T_a^4(0.39 - 0.05\sqrt{e_a}(1 - 0.6F_c^2) \quad [4.7]$$

With T_a being the air temperature (K), ε being the emissivity factor, σ is the Stefan-Boltzmann constant(J/m^2/s/K), e_a is the actual vapor pressure:

$$e_a = r_{hum}10^{\frac{0.7859+0.3477T_a}{1+0.00412T_a}} \quad [4.8]$$

Q_{ev} is the evaporative heat flux (latent heat):

$$Q_{ev} = L_v\rho_a f(U_{10})\{q_s(T_s) - q_a(T_a)\} \quad [4.9]$$

With $q_s(T_s)$ and $q_a(T_a)$ being the specific humidity of respectively saturated air and remote air (10 m above water level). L_v is the latent heat of vaporization in water (J/kg), $f(U_{10})$ is the wind speed function:

$$f(U_{10}) = (3.5 + 2U_{10})\frac{(5x10^6)^{0.05}}{S_{area}} \quad [4.10]$$

With S_{area} being the exposed water surface (m^2).
Q_{co} is the convective heat flux (sensible heat):

$$Q_{co} = \rho_a c_p g(U_{10})(T_s - T_a) \quad [4.11]$$

c_p is the specific heat of air, $g(U_{10})$ is the wind speed function:

$$g(U_{10}) = c_H U_{10} \quad [4.12]$$

With c_H being the Stanton number (c_H = 0.00145).
All terms are in W/m^2. The total incoming heat radiation is absorbed according to depth.

All the above-mentioned terms are calculated internally by Delft-3D. The results of the calculation of the annual heat balance for 2022 are shown in Figure 4.3a. The computed fluxes are plotted together with the water temperature recorded at the MWS1 station.

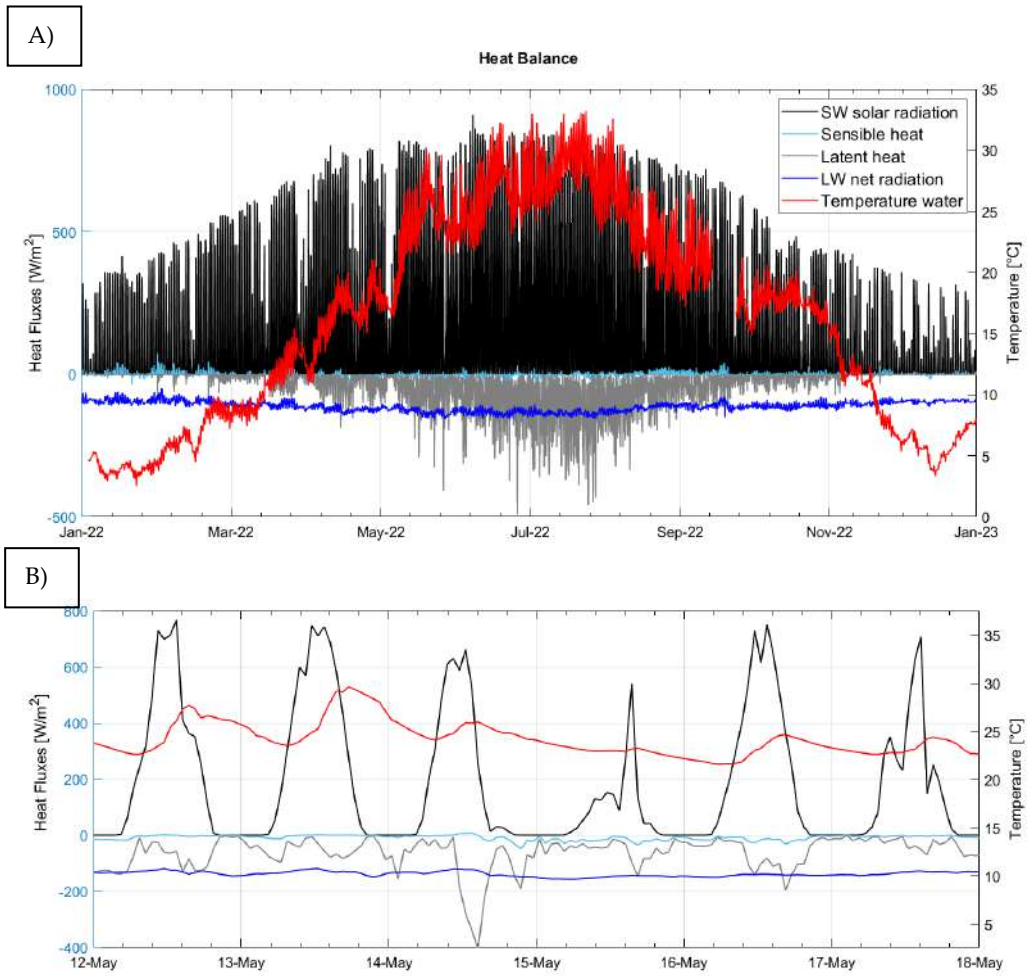

Figure 4.3 a) Heat fluxes calculated for Torbiere for the year 2022. The net longwave radiation is the result of Q_{an} - Q_{br}. b) zoom in for the period of May 12th to May 18th.

	Short wave radiation	Sensible heat	Latent heat	Long-wave atmospheric	Long-wave water rad
January	63.22215	0.909803	-0.39114	228.4122	-321.441
February	102.5609	2.850882	-4.77717	240.4878	-334.591
March	145.612	-1.42788	-14.8418	246.0147	-352.834
April	188.0904	-6.27749	-30.3483	259.8274	-381.281
May	212.5633	-4.66013	-55.3235	287.4289	-416.063
June	258.3831	-3.50234	-88.9497	305.1124	-437.545
July	284.2693	-2.75441	-133.945	316.2205	-451.703
August	219.04	2.595902	-81.1447	304.6751	-422.428
September	155.9922	1.218621	-23.6297	285.8003	-394.385
October	105.0699	0.537089	-15.8901	277.3528	-388.926
November	58.24106	0.382962	-3.56057	251.0587	-353.959
December	32.5488	0.269121	-0.00132	235.6938	-330.612

Table 4.1 Average heat flux (W/m^2) per month

The short-wave solar radiation peaks during midday and is zero through the night and has a strong seasonality. Figure 4.3 b shows that temperature (red line) has a delayed response of some hours with respect to the SW solar radiation, and peaks in late afternoon.

Although the net long-wave radiation peaks in July, it is stably negative and around 115 W/m^2, meaning that the back radiation from the water is larger than the incoming LW radiation from the atmosphere. This occurs because, even if the water temperatures of water and air are fairly similar, water has a greater emissivity factor. Furthermore, atmospheric radiation also depends on cloud cover and part of it is reflected by the air-water interface itself.

Overall, the short-wave radiation contributes to 20% of the total heat fluxes in spring and summer, while in winter its contribution drops down to 5-10%. Long-wave radiation dynamics are the opposite and peak during winter months.

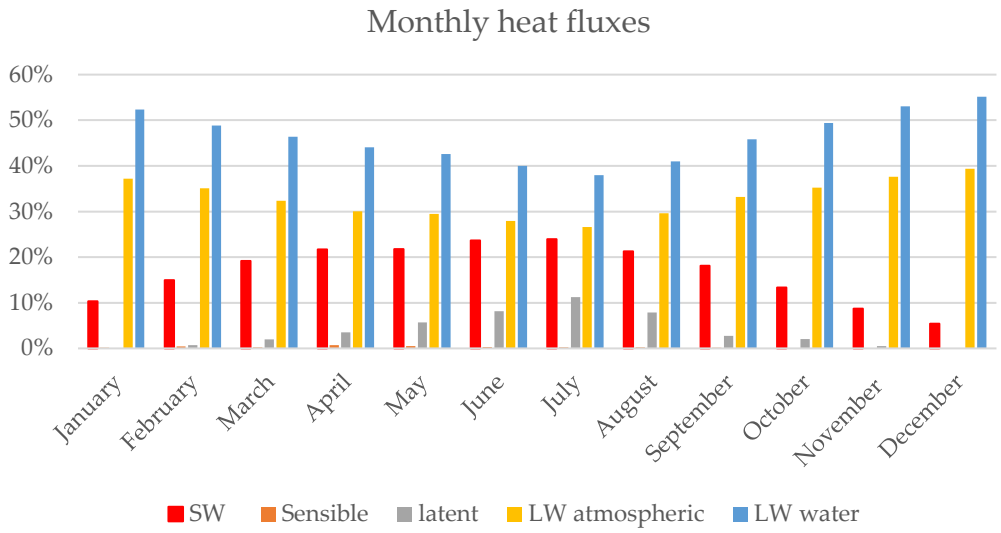

Figure 4.4 Monthly contribution of each of the heat flux term expressed as a percentage of the total heat flux

Turbulence model (k-ε)

Delft3D-FLOW implements four separate turbulence closure models in order to determine the vertical eddy viscosity and diffusivity coefficients (Deltares, 2020): the constant coefficient model, the algebraic turbulence closure model, the k-L turbulence closure model and the k-ε turbulence closure model.

k-ε is chosen as the turbulence closure model as it is the most common model used in computational fluid dynamics (Rodi, 1980) and it solves the transport equations for both the turbulent kinetic energy k and the dissipation rate of turbulent energy ε, providing higher level of accuracy than the other three models (Lesser, 2000).

$$\frac{\partial(\rho k)}{\partial t} + \frac{\partial(\rho k u_i)}{\partial x_i} = \frac{\partial}{\partial x_j}\left[\frac{\mu_t}{\sigma_k}\frac{\partial k}{\partial x_j}\right] + 2\mu_t E_{ij}E_{ij} - \rho\varepsilon \quad [4.13]$$

$$\frac{\partial(\rho \varepsilon)}{\partial t} + \frac{\partial(\rho \varepsilon u_i)}{\partial x_i} = \frac{\partial}{\partial x_j}\left[\frac{\mu_t}{\sigma_\varepsilon}\frac{\partial \varepsilon}{\partial x_j}\right] + \frac{C_{1\varepsilon}\varepsilon}{k}2\mu_t E_{ij}E_{ij} - \frac{C_{2\varepsilon}\rho\varepsilon^2}{k} \quad [4.14]$$

Where u_i is the velocity component in the i-direction, E_{ij} is the strain tensor component, μ_t is the turbulent viscosity.

The mixing length L is the determined as:

$$L = \frac{c_D k\sqrt{k}}{\varepsilon} \qquad [4.15]$$

With c_D being an empirical constant determined by calibration and relating mixing length, turbulent kinetic energy and dissipation, c_D = 0.1925 Uittenbogaard et al., 1992).

In a 3D shallow water flow, the stress and diffusion tensor are anisotropic and the horizontal terms of eddy diffusivity D_H and viscosity ν_H are much larger than the vertical coefficient (Deltares, 2020). Due to the coarse grid size specified in Delft-3D, the closure model is unable to resolve the above-mentioned parameters. One must therefore specify a background value for the horizontal mixing coefficients, which otherwise would be reduced to zero. The process of calibrating D_H and ν_H is described in ch. 4.4. For the vertical direction, the coefficients are computed by the turbulence closure model.

Other parameters

To take into account the resistance of the flow at the bottom, a Manning coefficient is chosen, equal in the U and V direction to 0.015 s/m$^{1/3}$, after a calibration process shown in chapter 5. A no slip condition is defined at the walls.

Wind drag coefficient is proportional to the wind shear stress and is dependent on the wind velocity. The relationship is taken from Wuest and Lorke (2003):

$$C_d = \begin{cases} 0.01, & U_{10} = 0\ m/s \\ 0.001, & U_{10} = 4\ m/s \\ 0.002, & U_{10} = 20\ m/s \end{cases} \qquad [4.16]$$

In this way one is able to take into account for the additional friction that occurs at low intensity winds. Due to the absence of large scale upwind topographic features and the fact that the extension of the study area is relatively small compared to typical cyclonic scales, the input of wind speed and direction over the lake is considered spatially constant.

4.1 Water levels and setup

Fluctuations of lake water level depend on time series that are the results of several hydrological and climatological parameters including rainfall, runoff, evaporation, temperature, and groundwater exchange (Li et al. 2007; Doulgeris et al. 2012).

Water Levels in Torbiere are influenced mainly by the discharge coming from the stream Rì, the outflowing discharge delivered by the pump and evaporation (See ch. 3.5). According to whether the year has been rainy or dry, one term might be predominant.

Figure 4.5 shows two months of water level simulations (October - December 2020). This period was chosen because there were several rainfall events, and the pump was switched on twice. Therefore, it was suitable to check whether the different water balance terms were computed correctly. As shown, the model satisfactorily (R^2 = 0.98) reproduces the changes in water level of these months. The model was tested for other periods, leading to similar results.

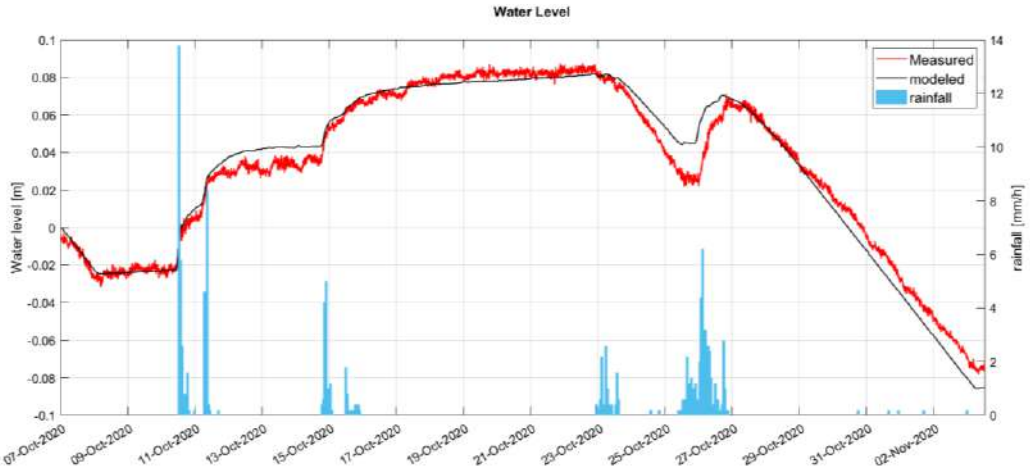

Figure 4.5 water levels measured at MWS1 and computed with Delft-3D (October 2020 – December 2020).

During 2022 the modeling of water levels reduced to the calculation of the evaporation term present in the heat flux model. The shortage of precipitation events meant that the incoming discharge was very low and mostly equal to the background value and that the pump was kept switched off throughout the whole year.

Wind setup

In a homogeneous (unstratified) lake, the set up along the n-th direction can be estimated as: (Spigel R. and Imberger J., 1980):

$$\frac{\partial h}{\partial x} = \frac{u_*^2}{Hg} = Fr^2 \qquad [4.17]$$

Where H is the average water depth along the n-th direction and u_* is the water friction velocity and is equal to

$$u_* = \sqrt{\tau/\rho_w} \qquad [4.18]$$

With τ being the surface boundary layer stress and ρ_w being the density of water.

$$\tau = \rho_a C_d U^2 \qquad [4.19]$$

Considering the North-South direction of Torbiere, along which the strongest wind usually develops, if there is a sustained wind o 3 m/s intensity, a surface stress of 0.0135 N/m^2 is generated, leading to a setup of $8.6 \cdot 10^{-7}$ m/m. As the fetch is 2.4 km, this leads to a runup of 2 mm.

Similarly, along the East-West direction, an equal wind would work on a much smaller fetch (550 m), leading to a runup of 0.4 mm only.

As mentioned in ch. 3, the accuracy of the water level probes does not allow to detect such small differences of water levels and therefore, wind setup cannot be measured in this system. However, one could simulate different wind conditions to ensure the model is able to reproduce reasonable values of set up, according to different intensities.

A simulation was performed forcing Torbiere with a simplified wind with similar features of the real one measured at WS1 station. It blows with 5 m/s intensity from North during the night and with a 1.5 m/s intensity from South during the day. Water level was monitored in three points located North, South and in the middle of the basin. Due to wind's duration and intensity, a setup establishes every evening, where the water level in the northern and southern stations decreases and increases, respectively (figure

4.6). The point in the middle acts as a node in this oscillation pattern. The extent of this modeled setup is 2.4 mm, which is compatible to the theoretical values.

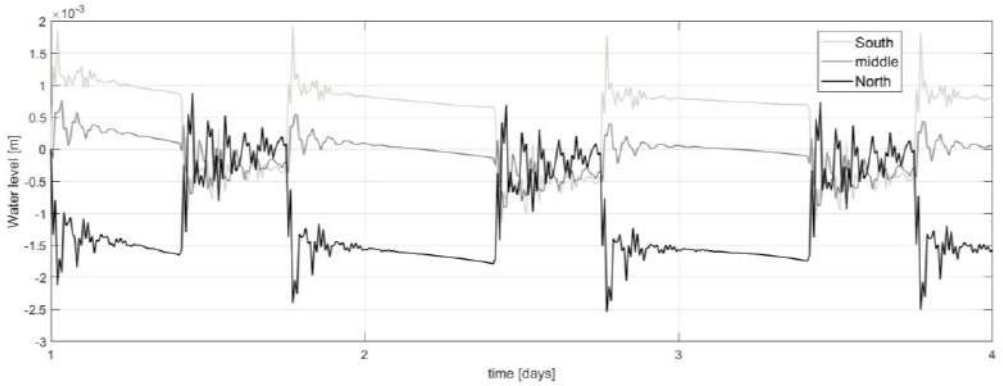

Figure 4.6 wind set up obtained by forcing Torbiere with an alternate simplified wind. Water levels are monitored in three points of the basin.

4.2 Temperatures

Changes in water temperature have impacts on the aquatic ecosystem, algal growth and the spread of fishes (Wetzel, 2001).

A correct water temperature modeling is key for the water balance as well, since evaporation plays an important role, especially during summer months.

Being a very shallow system, Torbiere responds quickly and strongly to climatological variations, increasing the complexity of the modeling of its temperature.

Simulations of water temperature carried out for the time span 1/1/2021 – 1/1/2022. The model is initialized with a uniform condition of T = 4.7 °C and the first 10 days are considered spin-up time. Torbiere is modeled by means of a z-model considering 15 layers in the vertical direction, each occupying 6.7% of the water column. The Secchi's depth is uniform and set equal to 50 cm, an average value observed throughout the year.

Results are shown in Fig. 4.7.

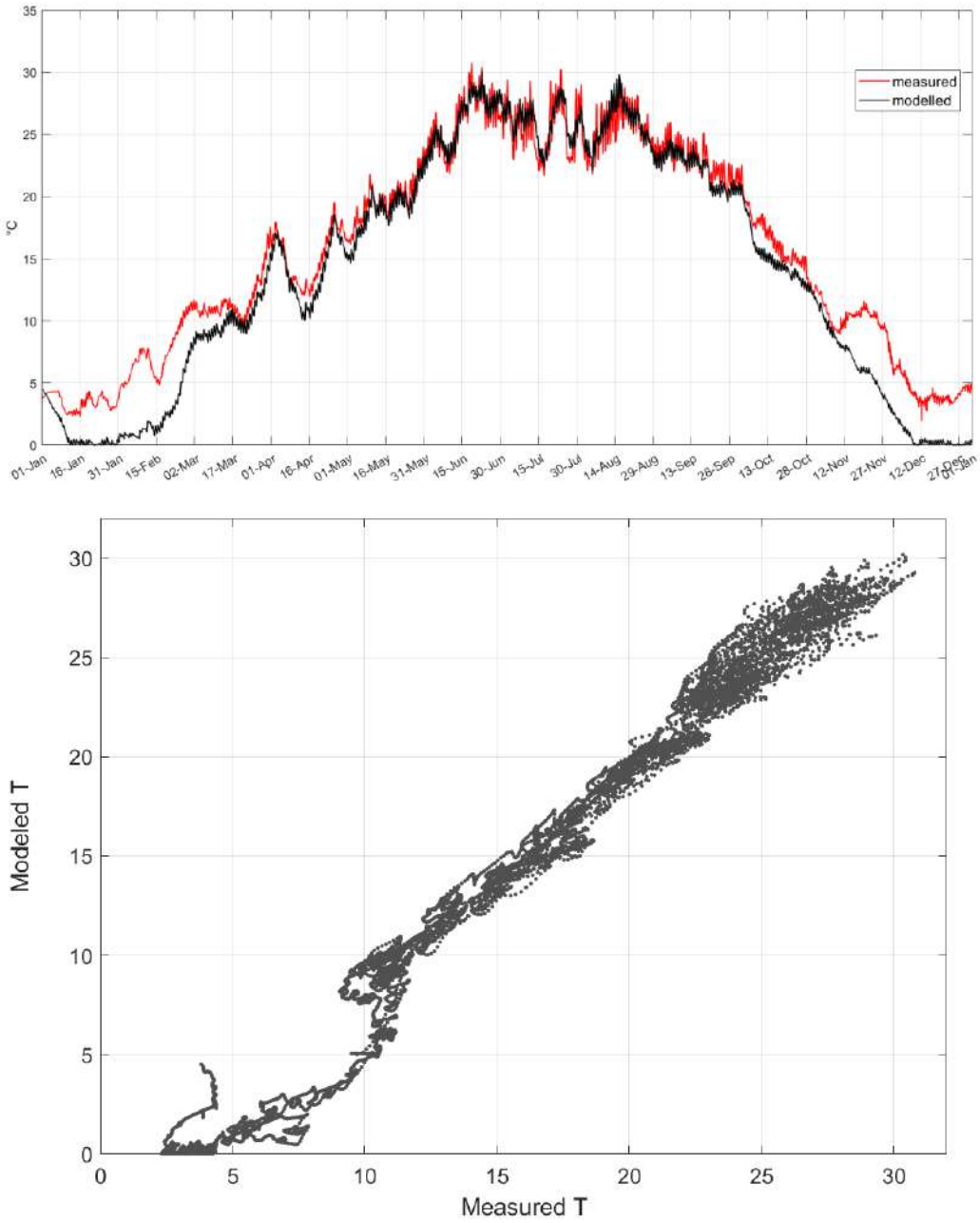

Figure 4.7 a) Time series of modeled and measured water temperature, b) Comparison between the two series.

The model well catches ($R^2 = 0.981$) the overall temperature trend from mid-March to November but fails to capture the wide daily fluctuations and underestimates temperatures in the cold months.

Torbiere, being so shallow, is a polymictic lake, with a water column characterized by great thermal excursions through the day and along the year. Water temperatures reach up to 30 °C in the summer and a gradient

of 6°C might establish between the surface and the bottom waters in the warmest hours of the day.
In winter months, Torbiere might experience ice cover on the surface.

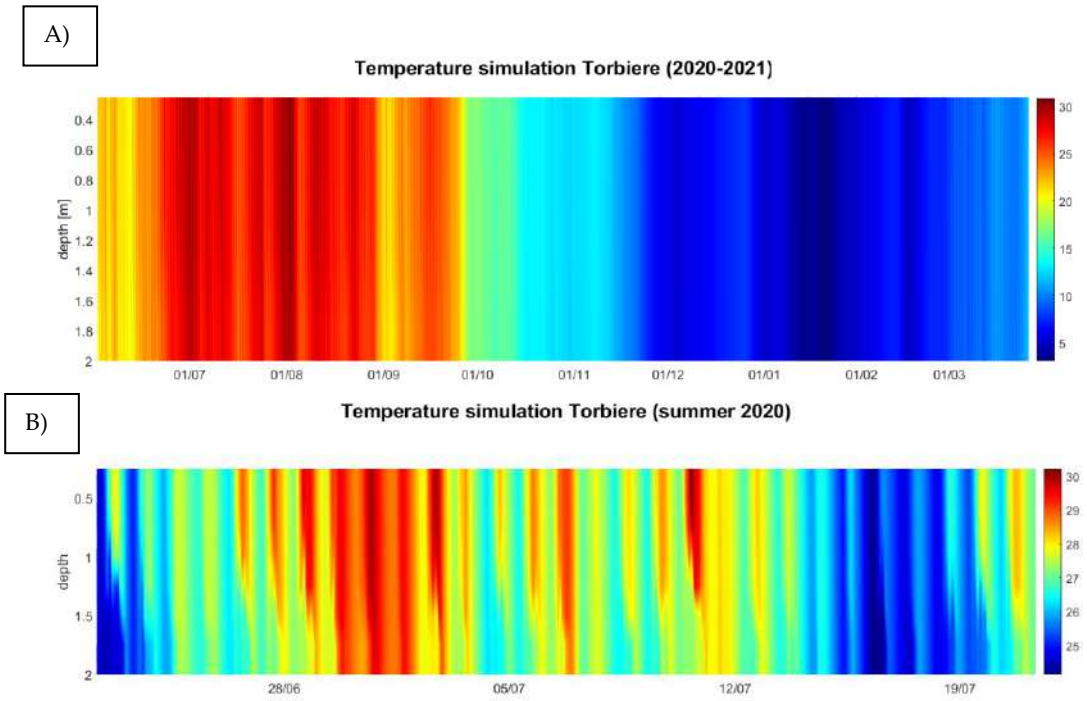

Figure 4.8 a) Temperature plot for the water column of Torbiere (January 2021-January 2022) as modeled with Delft-3D. b) Focus on the summer period

In summer (Figure 4.8b) stratification establishes in the first hours of the morning and disrupt in late evening, when stronger winds occur.

4.3 Clay tank temperature simulation

The setup of a monitoring station in one of the clay tanks in March 2022 (ch.3.3) allowed for an investigation of the thermal regime of the tanks. The model Delft-3D was applied to reproduce the temperature stratification over the period March 2022-December 2022.

For this simulation, a grid with 5 x 5 m cells was built and bathymetry was derived from a campaign done with the multiparametric probe in August 2021. In the vertical direction, a z-grid is adopted, with 20 layers of 5% thickness each. This vertical grid schematization is more suitable for reproducing thermal stratification. As seen from Ch.3.3, this tank stratifies in summer due to a combination of thermal and chemical effects. In this chapter we describe a simulation not taking into account the chemical

stratification, but we argue it is advisable to better represent the seasonal dynamics of the bottom layer especially.

Due to its limited area and the presence of trees all around its perimeter, it is not clear *a priori* whether the wind plays an important role in the disruption of thermal stratification of this tank. For this reason, the thermal simulation was run both with and without the forcing of the wind. If one considers a wind acting with the same drag coefficient as used for Torbiere, he will obtain a homogeneous water column throughout the year, which is not correct. On the other hand, the results with no winds resemble reality much more closely. This is why a reduced drag coefficient (50% reduction) was set for this tank, to take into account the shading effect of the trees.

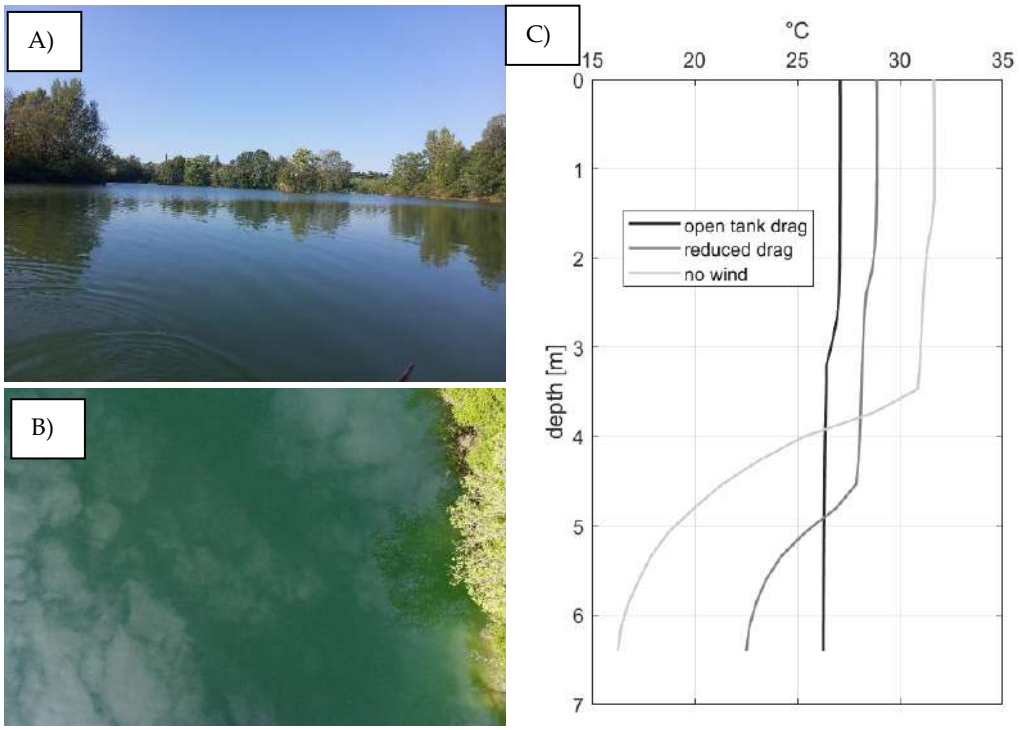

Figure 4.9 a & b) pictures of the clay tank showing the edges covered in trees and the calm surface c) effect of the wind drag coefficients on temperature profiles in mid-June 2022

Secchi's depth was set uniform to 3 m and the Ocean Flux model (ch. 4) was used. No salinity stratification was introduced and a constant temperature of 5 °C was set as initial conditions everywhere. For this reason, the first week is considered spin up time.

A time step of 30 seconds was used for this simulation.

Figure 4.10 shows the results of the temperature simulation of the clay tank. During the spin up time, a thermal stratification establishes and on March 1st a difference of 2 °C between the two layers is present, equal to that measured by the two probes. The daily fluctuations of the surface layer are well reproduced by the model ($R^2 = 0.994$), but it overestimates the warming of the top layer in the summer season (figure 4.11).

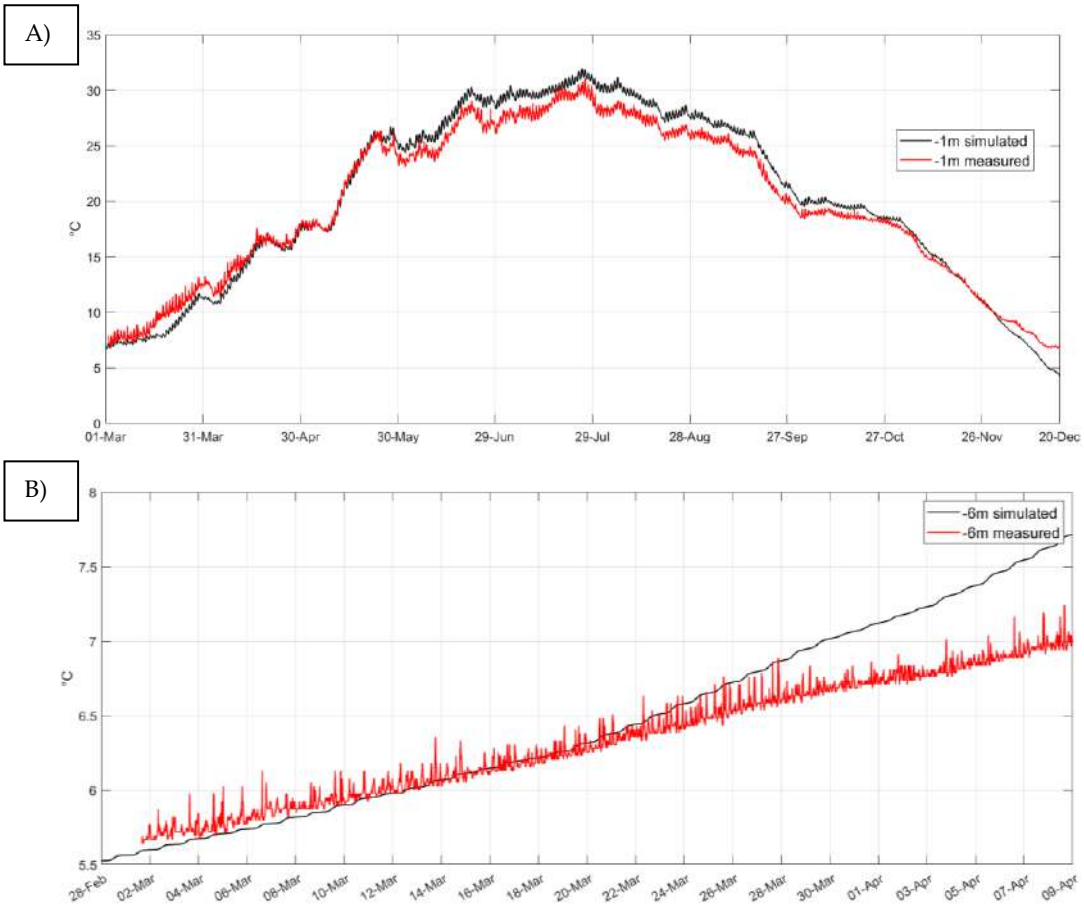

Figure 4.10 a) Temperature time series (measured and modeled) of the a) surface layer for the whole monitored period and b) of the bottom layer for the spring period.

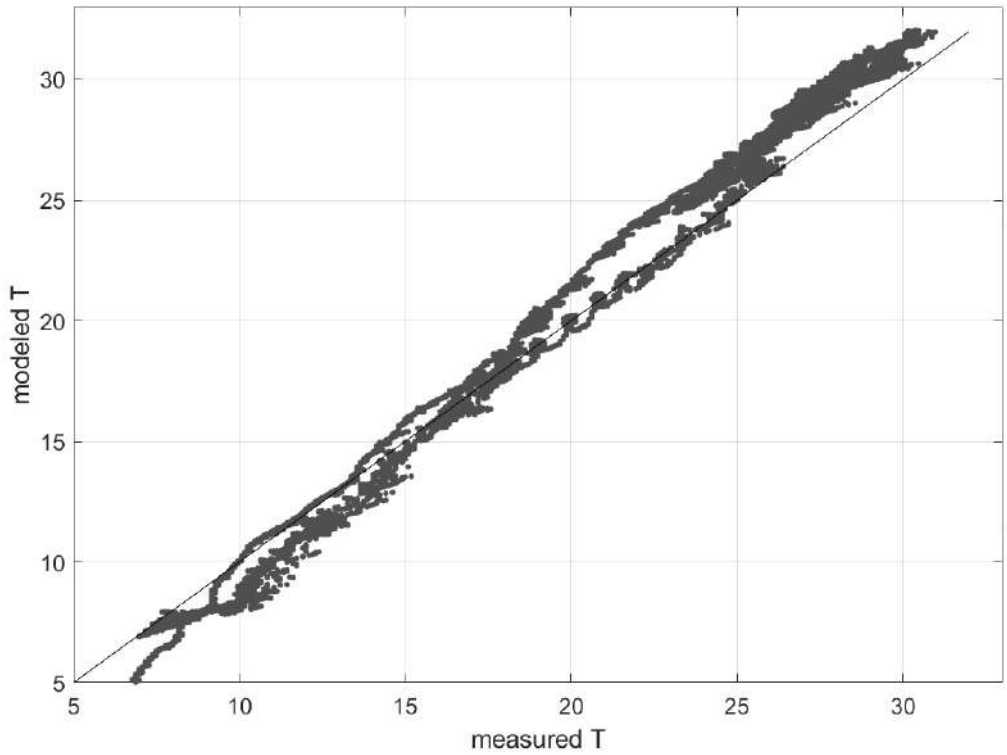

Figure 4.11 Comparison between the series of measured and modeled temperature.

The temperature simulation of the bottom layer (Figure 4.10b) generates a progressive warming that is not actually occurring in the tanks.

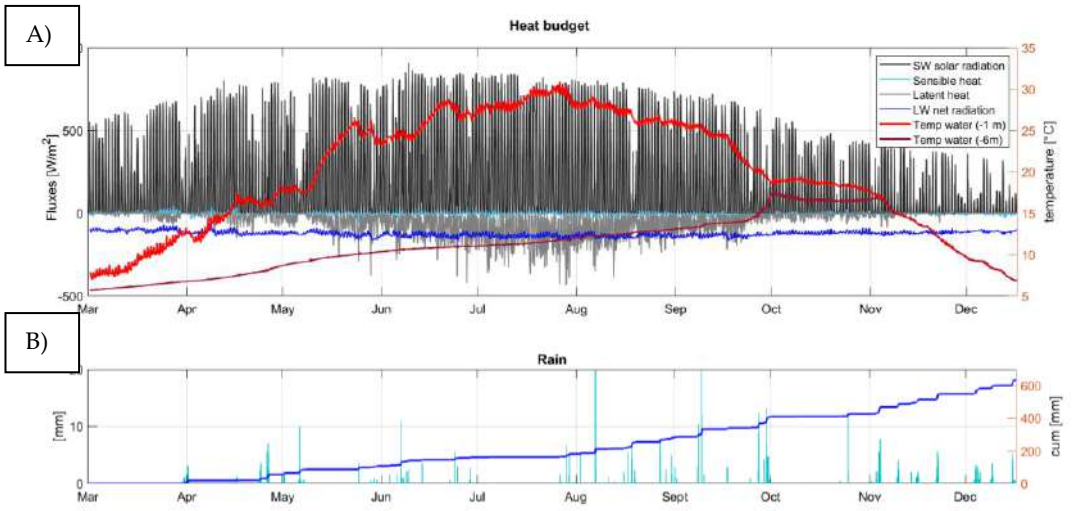

Figure 4.12 a) Heat fluxes computed for the clay tank and displayed with the measured surface and bottom temperature. b) time series of rainfall.

Considering that the model captures a correct trend for the surface layer and that the greatest term in the heat budget is represented by the short-wave solar radiation (figure 4.12a), the reason for the overestimation of the rate of warming of the bottom layer has to be found in the layered structure of the water column. In particular, the quick heat transfer may be attributable to the absence of a chemical stratification in the model, while in the real tank the gradient of conductivity might act as a barrier for heat fluxes to the bottom. This finding arises the need for a more complex modeling setup for this tank, that admits salinity profiles variations.

4.4 Plume dynamics

One of the main ways nutrients, sediments and other land-based pollutants are transported into lake waters is through river plumes (Qin et al., 2007, Rao and Schwab, 2007). Fluvial discharges modify the concentrations and ratios of nutrients in waters near the river mouth. Effects of river plumes are evident in case of high discharge following heavy rainfall (Chen et al. 2011) and are influenced by freshwater discharge, wind stress, coastline shape and local bathymetry (Avila R.A., 2018). As the dynamics of the near-field region are governed by turbulent mixing (Hetland, 2005, 2010), which is linked to lateral spreading, the plume phenomenon offers the possibility to calibrate turbulent eddy viscosity and diffusivity, two fundamental parameters in the turbulence closure of hydrodynamic models (Bricker J.D., 2006) and that are introduced in Delft3D by the user as direct input.

The sensitivity of the hydrodynamic model Delft-3D to the choice of eddy viscosity and eddy diffusivity was tested in the simulation of a generic plume where the domain is filled with a unitary tracer concentration and the affluent enters with a constant discharge (70 L/s) and null tracer concentration. Wind is present and forced with direction and intensity measured at WS1.

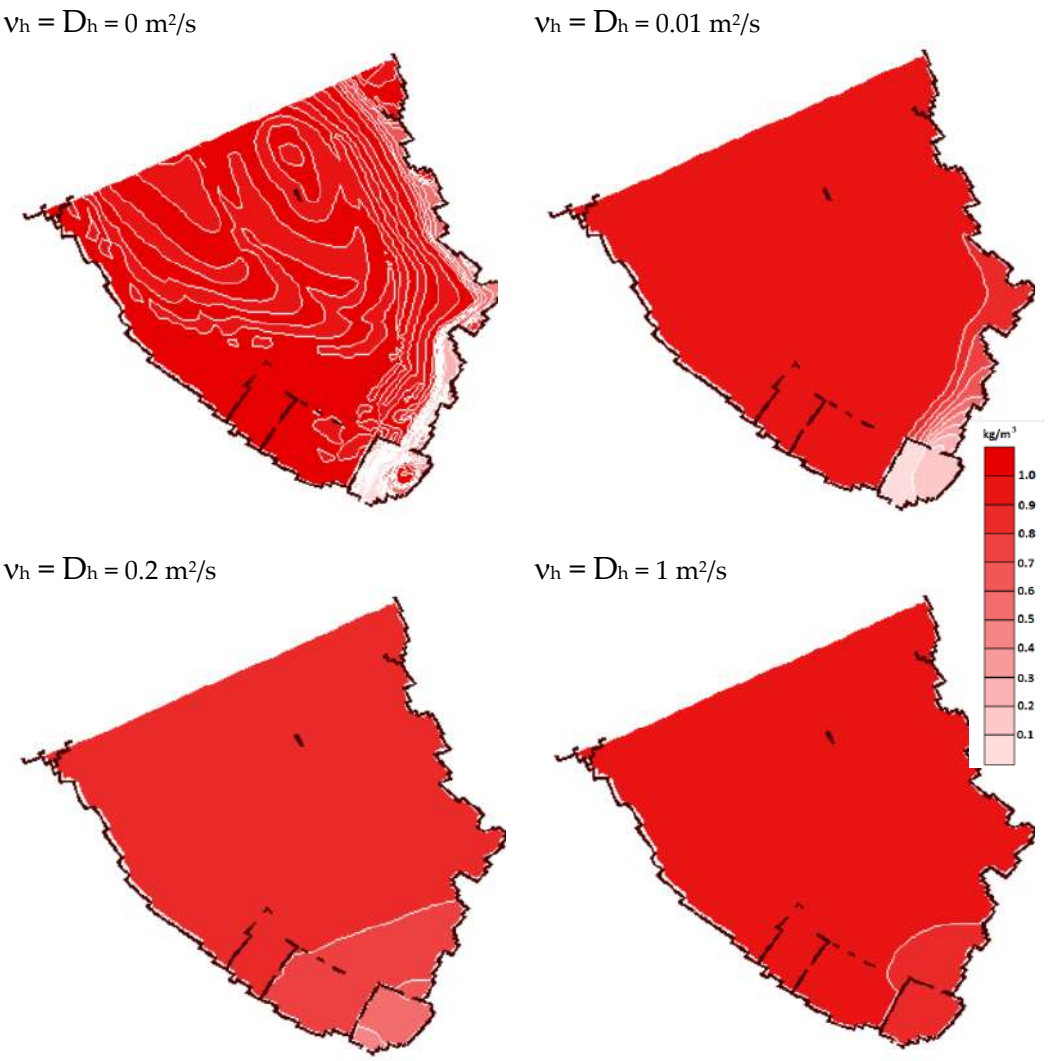

Figure 4.13 Snapshots of tracer concentration in the near field region of the plume of Rì in Torbiere with different values for the eddy viscosity and diffusivity parameters.

Figure 4.13 shows the results of the sensitivity analysis of the model with respect to eddy viscosity and eddy diffusivity. These parameters have a great influence on the lateral dispersion of the tracer. If diffusion is set, unphysically to zero, there is no lateral dispersion, and the distribution of the tracer only occurs because of advective reasons. Gradients of tracer concentrations are particularly sharp. In case of high eddy diffusivity (e.g. 1 m²/s), the inlet of a zero-concentration inflow has almost instantaneous effects in the domain and the water volume gets diluted quickly.

The observation of this tracer maps led us think that the reality might lie somewhere in between these extreme conditions. Yet there still is a wide range of values for these parameters that should be tested.

As described in ch. 3.4.1, on April 14th, 2021, a campaign was carried out in Torbiere, near the inlet of the main affluent Rì. The campaign was performed after 10 days of intense rains, with a cumulative precipitation of 90 mm. 24 hours after a rainy event, the momentum of the Rì river is expected to be higher and therefore, it is likely that a measurable plume will form. The peak discharge of Rì was estimated at 0.6 m^3/s, much bigger than the usual discharge of dry period (80 L/s). From the 2D interpolated maps, a plume is present, with the following characteristics: it is cooler than the rest of the waters of Torbiere, presents a lower specific conductivity, higher turbidity and chlorophyll-a concentrations and lower dissolved oxygen levels. Compared to the dry regime, after heavy rainfalls the discharge of Rì is cleaner, due to the dilution effect of rainwater.

Among the above-mentioned parameters, specific conductivity is the one that behaves like a tracer: it is advected with currents and can be diffused in the horizontal direction. For this reason, a simulation was performed using Delft 3D to reproduce the phenomenon of this specific plume with the aim to calibrate two parameters present in the model: the horizontal eddy viscosity and diffusivity.

For the purpose of this calibration, a new grid was created, with cells of size 2 x 2 m and more depths measurements were acquired in the area in order to define bathymetry more precisely. The simulation was run from April 10^{th} to April 14^{th} with a 30 seconds time step, and the first 24 hours were considered spin up time.

The system is force with the wind measured at MWS1, as this is a particular area of Torbiere, shaded from the wind coming from Iseo.

Time series of specific conductivity are available as measured at IS1, while the discharges were reconstructed by creating a Nash model for the basin, considering the series of rainfall (MS2), a number of 2 tanks, 10 hours as retention parameter and a background discharge of 0.03 m^3/s. The time series of water levels in IS1 presents, in fact, a gap and does not cover this event (Fig 3.36).

The calibration was performed by varying ν_h and D_h in order to minimize the RMSE between the measured and the simulated values of specific conductivity in the area of the plume. The values that were tested were: 0.005, 0.02, 0.03, 0.05, 0.08, 0.1, 1.

The value of 0.05 m^2/s was obtained for both horizontal eddy viscosity and diffusivity, corresponding to a RMSE of 6.9 µS/cm. Higher values lead to a greater spread of the plume, especially in the lateral direction, while lower values (below 0.03 m^2/s) lead to a situation where the plume could not be reproduced at all.

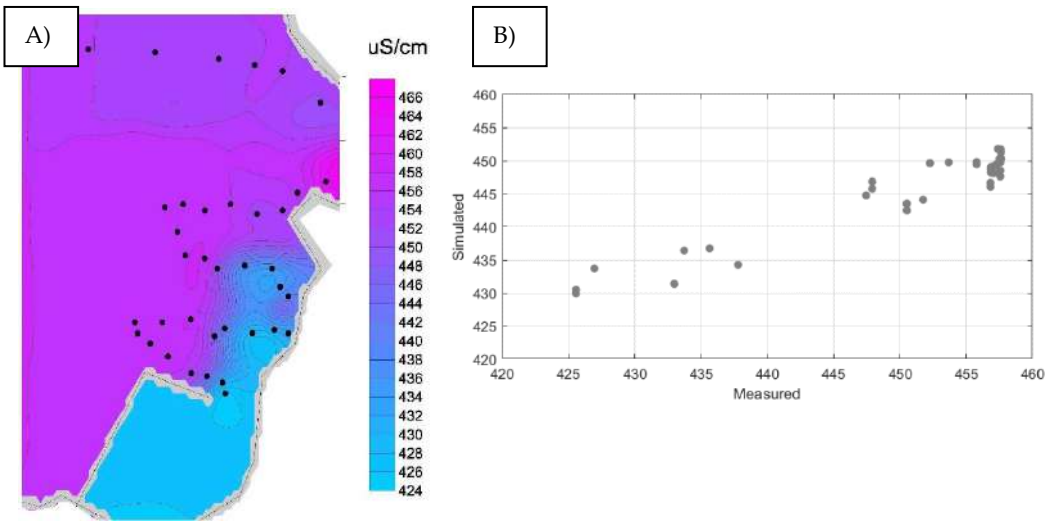

Figure 4.14 a) 2D interpolated map of the measurements (black dots) obtained with the multiparametric probe at 09:00 am, April 14th. b) Simulated vs Measured values of specific conductivity.

Figure 4.15 shows the development of the plume in the hours prior to the survey. The tracer spreads as time passes, mostly towards North, while the lateral diffusion is limited. The particular shape of the plume (Figure 4.14a) is probably due to bathymetric reasons and a more detailed description of the bottom altimetry is recommended to improve the modeling of this phenomenon.

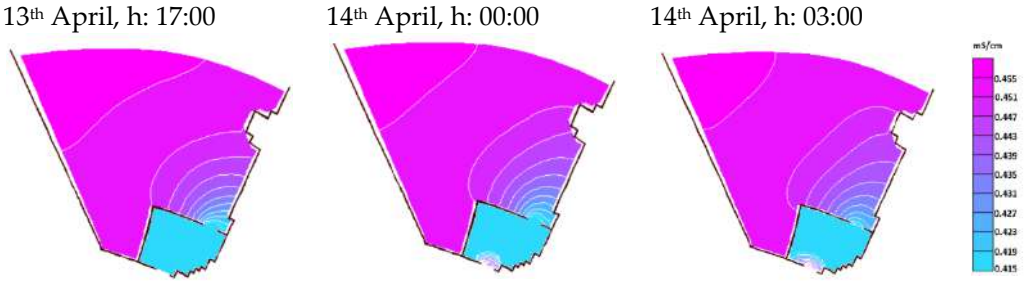

Figure 4.15 Tracer (specific conductivity) values obtained with Delft-3D, at three-time steps before the measurements.

4.5 References

Ávila, R. A. and Calil, P. H. R. (2018). Buoyancy-driven effects on turbulent diffusivity induced by a river plume in the southern Brazilian shelf, *Ocean Sci. Discuss*. [preprint].

Bricheno L.M., Wolf J., Islam S. (2016). Tidal intrusion within a mega delta: an unstructured grid modelling approach. Eastuar. Coast. Shelf S., 182 A, 12-26.

Bricker J.D. and Nakayama A. (2006). Estimation of far-field horizontal and vertical turbulent diffusion coefficients from the concentration field of a wastewater plume near the Akashi Strait. *Environ. Fluid Mech*., 7: 1-22.

Bye, J.A.T. (1965). Wind-driven circulation in unstratified lakes. *Scripps Institution of Oceanography*, University of California, San Diego, La Jolla, California.

Chen S. et al. (2011). Remote sensing analysis of rainstorm effects on sediment concentrations in Apalachicola Bay, USA. Ecological Informatics, 6, pp- 147-155.

Deltares, 2020. Delft3D-FLOW User Manual.

Doulgeris C, Georgiou P, Papadimos D, Papamichail D (2012). Ecosystem approach to water resources management using the MIKE 11 modeling system in the Strymonas River and Lake Kerkini. *J Environ Manag* 94:132–143.

Garcia M.L., Basile P.A., Riccardi G.A., Rodriguez J.F. (2015). Modelling extraordinary floods and sedimentological processes in a large channel-floodplain system of the Lower Parana River (Argentina). *Int. J. Sedim. Res*., 30 (2), 150-159.

Gu X.W., Yang W.L., Dong G.T., Dang S.Z. (2014). Application of one-dimensional hydraulic model for flood simulation in Yellow River Delta. *Adv.Mater.Res*., 955-959.

Haines P. (2013). Hydrological modelling of tidal re-inundation of an estuarine wetland in south-eastern Australia. *Ecol. Eng*., 52, 79-87.

Hetland, R. D. (2005). Relating river plume structure to vertical mixing. *J. Phys. Oceanogr.* 35, 1667–1688

Hetland, R. D. (2010). The effects of mixing and spreading on density in near-field river plumes. *Dyn. Atmos. Oceans* 49, 37–53.

Lesser, G.R. (2000). Computation of Three-Dimensional Suspended Sediment Transport within the Delft-3D Flow Module. MSc Thesis. UNESCO-IHE. Delft, the Netherlands.

Li XY, Xu HY, Sun YL, Zhang DS, Yang ZP (2007). Lake-level change and water balance analysis at lake Qinghai, West China during recent decades. Water Resour Manag 21:1505–1516.

Marsooli R., Orton P.M., Georgas N. and Blumberg A.F. (2016). Three-dimensional hydrodynamic modeling of coastal flood mitigation by wetlands. *Coast. Eng*., 111, 83-96.

Murbach D.E. (2011). SBFCA's feather River West Levee strengthening EIP project – wind setup and runup analysis. *Technical memorandum.*

Popescu I., Cioaca E., Pan Q., Jonoski A., Hanganu J. (2015). Use of hydrodynamic models for the management of the Danube Delta wetlands: the case study of Sontea-Fortuna ecosystem. *Environm. Sci. Pol.,* 46, 48-56.

Qin B., P. Xu, Q. Wu, L. Luo, Y. Zhang (2007). Environmental issues of Lake Taihu, China. *Hydrobiologia*, 581, pp. 3-14.

Rodi, W. (1980). Turbulence Model and Their Application in Hydraulics. IAHR. State of the Art Paper. Delft, The Netherlands.

Schumann G.J.P., Neal J.C. and Voisin N. (2013). A first large-scale flood inundation forecasting model. *Water Res. Res*., 49(10), 6248-6257.

Spigel R. and Imberger J. (1980). The classification of mixed-layer dynamics of lakes of small to medium size. *Journal of Physical Oceanography*, Vol. 10, 1104-1121.

Uittenbogaard R.E., Van Kester J.A.TH.M., Stelling G.S. (1992). Implementation of three turbulence models in TRISULA for rectangular horizontal grids (including 2DV test cases), Delft Hydraulics.

Y.R. Rao, D.J. Schwab (2007). Transport and mixing between the coastal and offshore waters in the Great Lakes: A review. *Journal of Great Lakes Research*, 33, pp. 202-218

Wester S.J., Grimson R., Minotti P.G., Booij M.J., Brugnach M. (2018). Hydrodynamic modelling of a tidal delta wetland using an enhanced quasi 2D model. *Journal of Hydrology*, Vol. 559, 315-326,

Wuest A., Lorke A. (2003). Small-scale hydrodynamics in lakes. *Annual Review of Fluid Mechanics,* Vol. 35(1): 373-412.

Zanobetti D., Lorgeré H., Preissmann A., Cunge J. (1968). Le modèle mathématique du delta du Mékong. *La Houille Blanche*, 1, p.17.

Books

Wind set-up and waves in shallow water. Technical memorandum n.27, beach erosion board, corps of engineers, 1952

Wetzel R. (2001). Limnology, Lake and River Ecosystems. *Elsevier Inc*. Third Edition.

5. Drifter design and experiment

Wind blowing over the surface of shallow lakes or estuaries can drive flows, surface waves and sediment resuspension (Schoen J.H et al, 2014). Given the high ratio between the water surface length along the wind main direction and the mean depth, big and shallow basins (e.g. wetlands) are very likely to behave as wind-driven systems (Nutz et al, 2016), receiving their major energy input from the surface air-water interaction (Hutter et al., 2011; MacIntyre et al., 2020; Rey et al., 2021).
The inner circulation that develops with the wind influences nutrient transport, sediment resuspension, mixing (Madsen et al., 2001), and therefore has a key role on the development of the water environment and the ecosystem, even changing the alternative stable states (Scheffer M. et al, 2001).
As wind transfers momentum from air to water, generating currents, waves and turbulence, understanding its role on a specific basin is key when trying to represent the inner circulation of a lake through a hydrodynamic model. In a shallow system, flow resistance under wind shear action due to bottom roughness becomes of great importance, consuming energy and momentum from the flow, changing the flow structure. A hydrodynamic model requires the calibration of a bottom roughness parameter in order to compute the flow field of a basin (Holden J. et al., 2008).
Drifters represent a valuable tool for measuring current velocities and understanding mixing characteristics in basins based on a Lagrangian approach. The increasing popularity in the past decades of these systems lead to several low-cost drifter designs being proposed and applied to fluid dynamics for oceans, lakes and coastal areas (Johnson D. et al, 2003, Boydstun D. et al, 2015, Gerin R. et al, 2017). Drifters for shallow basins are becoming of wide use as well (Suara K. et al, 2015, Nasello C. et al, 2016). However, despite the clear interest in making drifters for shallow water systems, the rationale behind their design is rarely explained. In addition, it would come in handy to use a low-cost drifter suitable for shallow basins of depth < 1 m (while most drifters on the market have a depth of >1.5 m).

In this contribution, we propose a low-cost (< 200 euros) GPS drifter that can be deployed in a shallow system for 5 days. The instrument can log its position in time and is able to send to the user its current position, making it easier to recover at the end of the campaign. We argue that the hardware component of this drifter could find application in deeper basins as well.

Chapter 5.1 describes the design of the drifter, and its verification, allowing any scientist with a basic background in electronics, to reproduce it and adapt it to his own needs. In chapter 5.2 the deployment scheme is presented, together with an example of the measurements campaign. Chapter 5.3 shows the use of the drogue's measurements for the calibration of the Manning coefficient for the model Delft3D.

5.1 Drifter design

In Torbiere del Sebino, flow velocities are in the order of magnitude of few centimeters per second at the surface, and millimeters per second at the bottom, making it hard to measure them with ordinary instruments such as current meters. The objective of this work is to propose the design of a low-cost drifter suitable for shallow waters (< 2 m). To get reliable current measurements, the best design is the one that maximizes ease in handling and scales it up, to obtain the largest drogue possible (Monhan E.C et al., 1973). This allows to minimize the slip between the drogue and the moving water parcels, making the drifter moving at nearly the same velocity as the water at the same depth. Therefore, making a drifter for shallow waters is challenging in itself and every design choice should be justified.
To reduce the costs of the drifter, on the other hand, the mechanical structure must be as simple as possible, made of easily available materials and with low power consumption. In a drifter like this, the electronic components tend to be the ones that increase the costs of the entire equipment. In this chapter we propose the setup of the electronic compartments in order to make the reader autonomous in making its own drifter from scratch. Thanks to the use of the open-source electronic platform of Arduino, the system can be adapted to different needs, without specific high-level competences in electronics.

5.1.1 Hardware

The drifter consists of an aluminum cylinder topped with a plastic cap. The height of the cylinder is 0.73 m, and the diameter is 0.16 m (Figure 5.1a). Inside, there are two separate compartments: the lower one is used to adjust the buoyancy of the device, in our case bags of gravel were used to obtain the desired height above water. For our purposes, the total weight of the instrument resulted to be 13.7 kg. The top compartment, separated by a plate at the bottom, contains the main hardware of the drogue. The hardware is relatively simple and consists of the following components:

- **Arduino MKR GSM 1400**: it is the brain of the instrument, thanks to the Arm Cortex-M0 32-bit SAMD21 built-in processor (Arduino Store website) and the u-blox SARA-U201 module which enables low power GSM / 3G connectivity for the board. GSM connectivity takes advantage of the cellular network to send and receive data; such a feature is especially useful when no other connectivity options (like Wi-Fi or LoRa) are available in operating conditions. The board is lightweight (32 g) and compact (plane dimensions 67.64 mm x 25 mm) making it easy to fit in all sensor like applications.
- **SIM card**: the board requires a SIM card and a cellular network coverage to send and receive data. In this application a regular SIM operated by Vodafone is used.
- **GSM antenna**: any GSM antenna with a U.FL connector is required to maintain a stable connection. The connector is already built-in into the board, no soldering is necessary.
- **LiPo battery**: cellular network GSM handshake may require up to 2 A of current depending on signal strength, which is too high for standard USB ports which are limited to 0.5 A as a regulation. For this reason, the board is equipped with a JST connector in which a LiPo battery can be attached as a separate power supply to account for power hungry operations. After testing different batteries, we choose to adopt a 3.7 V LiPo battery with 3 Ah of capacity.
- **Power bank**: the board is equipped with a type-C USB port for serial communication and for power supply. An external 5 V power bank with 20 Ah of capacity is used to ensure durability and resilience to

the sensor. The board comes with an internal charging circuit able to recharge the installed Li-Po battery while running on the external power bank battery. The switch from one power source to the other is done automatically and internally (Arduino website).

- **GPS module**: while it is possible to obtain an estimate of the position just using GSM information, usually such information is not precise enough for our purposes. For this reason, we used an external GPS module to obtain the position of the device continuously. The module adopted is the NEO-6M (GY-GPS6M) module capable of a horizontal accuracy of 2.5 m in clear sky conditions. The connections and pins used are displayed in figure 5.2A. A flashing blue LED will indicate if the module is working properly and if the module was able to obtain the GPS coordinates.
- **GPS external antenna**: the operating conditions must ensure at all times that the GPS antenna is placed in a way to maximize the number of observed satellites. A cable with an external antenna in plastic able to withstand the effects of the weather has been used in this application. The antenna is placed on top of the instrument together with the GSM antenna to ensure better reception.
- **SD card module + SD card**: using GSM communication the position and speed of the device are sent in real time to the cloud. To avoid loss of data due to possible GSM signal attenuation the generated data are also stored as a backup option into an SD card. This component is entirely optional.
- **Breadboard + cables**: all the connections are made using jumping wires and a regular breadboard.

Component	Cost [€]
Arduino MKR GSM 1400	71.90
SIM card	10.00
GSM antenna	5.00
LiPo battery, 3.7 V, 3 000 mAh	23.00
Power bank, 20 000 mAh	18.00
GPS module	4.00
GPS external antenna	12.00
SD card module (optional)	2.00
SD card (optional)	10.00
Breadboard + jumper wires	5.00
TOTAL	**160.90**

Table 5.1 list of the components and their costs

The external casing was adapted from an existing aluminum cylinder, which was divided in two compartments (see figure 5.1A): the lower one was filled with gravel pebbles to adjust the buoyancy of the device while the top compartment holds in place the hardware of the instrument. A plastic cap provides a watertight seal in which two holes have been drilled to expose the two antennas (GPS and GSM). Two grommets were positioned inside the holes and later sealed with silicone to avoid water intrusion. Previous designs showed that the positioning of the antennas inside the instrument (separated from the outside by the plastic cap) drastically impaired the signal reception in the field, therefore drilling the cap was mandatory. All the components described are connected as depicted in figure 5.2.

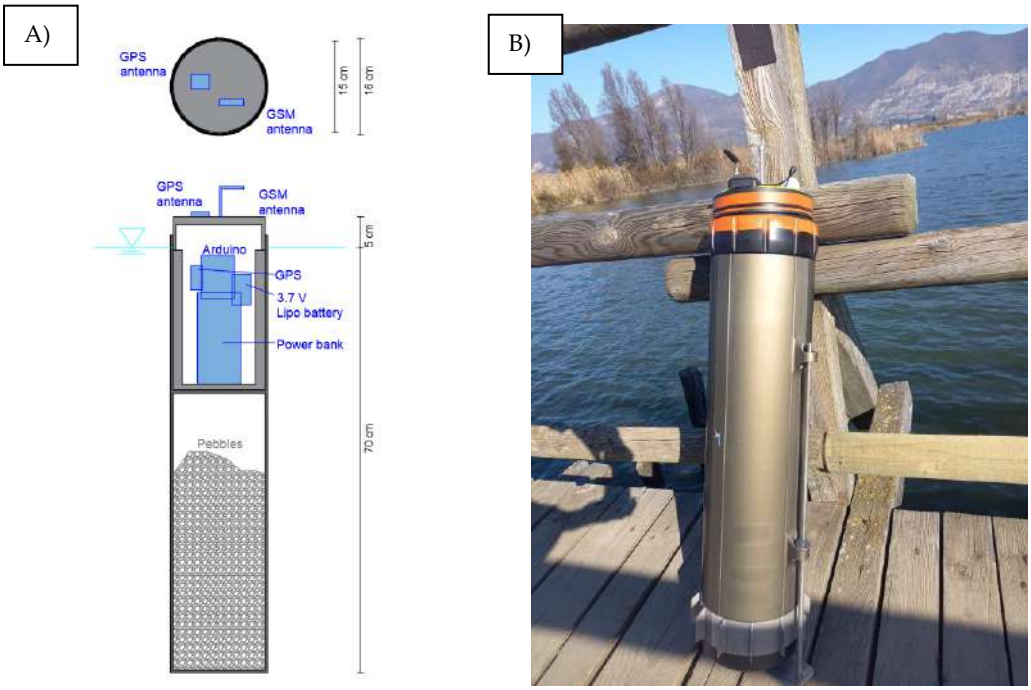

Figure 5.1: a) Design and b) picture of the drogue.

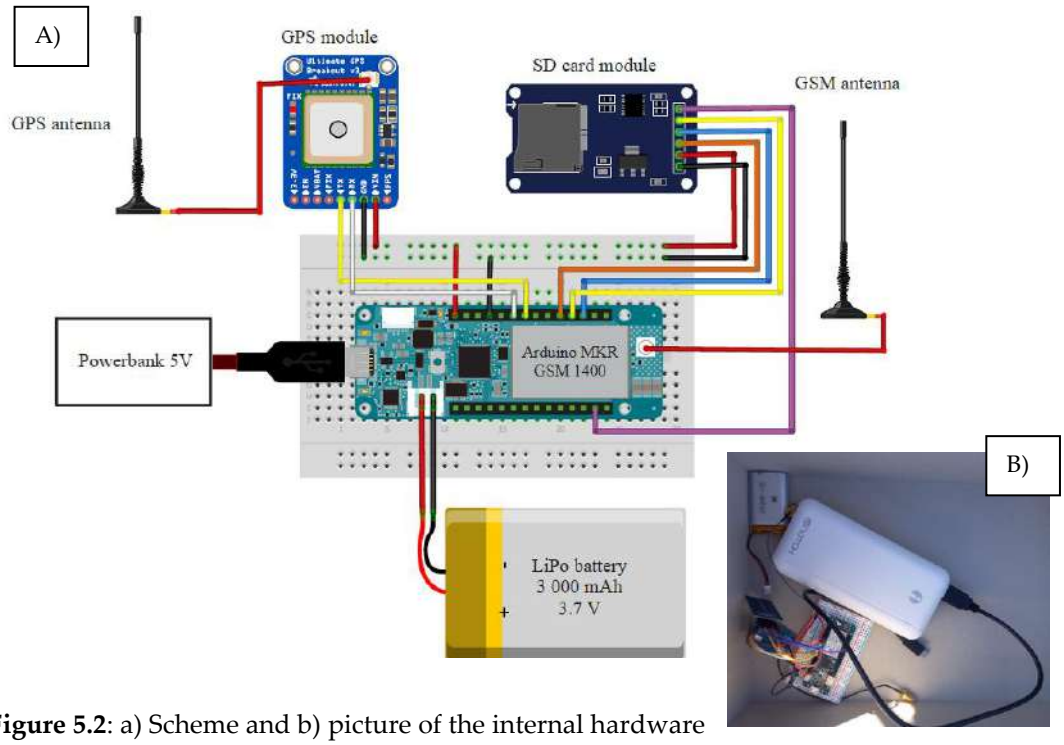

Figure 5.2: a) Scheme and b) picture of the internal hardware

5.1.2 Software

The microcontroller present on the board is responsible for holding all of the compiled code and executing the command specified by the programmer. All the data generated by the drogue is sent to a website named Arduino Cloud which is naturally supported by the board. Arduino Cloud allows the visualization of the generated data and offers a programmable interface to offer custom plots to better visualize the data in real time. The user can track the drogue movement and see its position on the map, just by connecting to the website. Real time data is necessary to ensure the retrieval of the device once it has been deployed on the field since it would otherwise be lost.

Arduino Cloud offers different subscription plans for the project specifications, for the present application the free subscription was enough for the purposes described. The source code (*.ino* file) responsible for the drogue routine will be briefly summarized in this section. After importing the necessary libraries, the device tries to connect to the Arduino Cloud services; if successful, the device listens for the data registered by the GPS module and, if it is valid, it is sent to the cloud and registered on the SD card for backup. The board is able to store the device's position, speed, number of visible satellites at the time of the measurement and the Horizontal Dilution Of Precision (HDOP) which is a parameter reflecting the planimetric quality of the GPS measurement. Values of HDOP close to or less than unity indicate the highest quality of data possible. The raw data provided by the GPS is handled using the library TinyGPS++ available freely on GitHub (TinyGPS++ library). A built-in debug LED will signal if the writing of the data to the SD card was successful. After a delay of 5 seconds, the device will send the stored data to the cloud, then wait again for other 5 seconds to finish all cloud related communications. The time lag between measurements can be adjusted to the application needs.

The loop then ensures that the procedure described so far continues forever. On the cloud, accessible both via desktop and smartphone, while the device is functioning, the user can access a dashboard in which all data retrieved is displayed for real time monitoring.

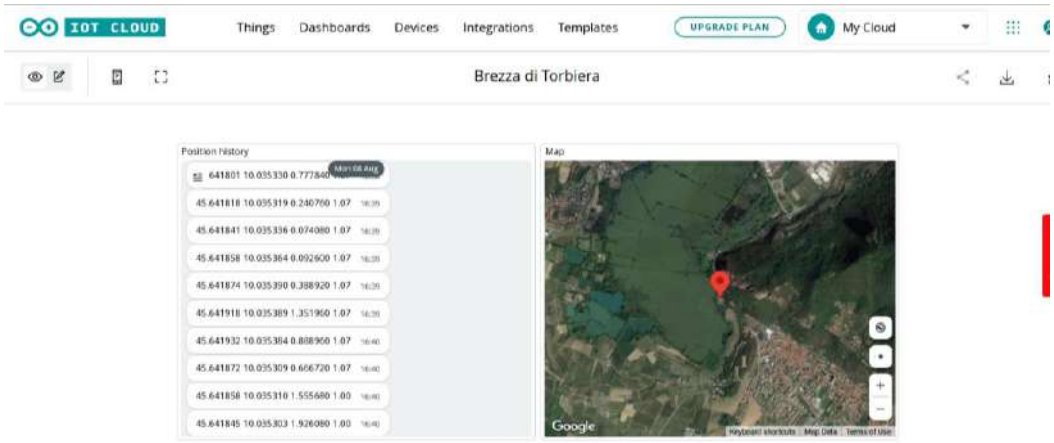

Figure 5.3: cloud dashboard of the device. On the left panel called "position history" the user can see the stream of data fetched every 10 seconds. The numbers reported are: Latitude, Longitude, speed in kilometers per hour and HDOP value of the single measurement. On the right panel a satellite map displays the last recorded position for clarity

5.1.3 Verification

During the design process of the container, it was crucial to minimize as much as possible the wind action on the emerged portion of the instrument. The drogue must be put in motion by the water currents and not be influenced theoretically by the wind field. Typically, in deep water applications, this is achieved simply by increasing the submerged area. On the contrary, in shallow water contexts, this is made challenging by the limitations of the water depth, which can cause the device to be stuck over local shoals or to behave inappropriately. It was thereby necessary to verify the effect of the wind on the overall force balance of the drogue by means of a 3D CFD simulation. The geometry modelled is depicted in figure 5.4, where all dimensions are reported. The entire domain is divided into two parts: water at the bottom and air at the top, each phase is treated automatically using the ANSYS FLUENT 2022 VOF model (ANSYS, Theory Guide). An average water depth of 1.8 m is used in this scenario which is representative of the average level of Torbiere. The cylindrical drogue is fixed in the middle of the domain throughout the simulation. The cap of the drogue emerges 0.05 m from the initial free surface while the remaining 0.68 m is submerged. The plastic antennae present on the cap are not considered in this simulation due to their small size. Air enters from one end of the domain with a logarithmic profile which was calibrated using the wind

speed data available from the WS1 station. Following Bañuelo-Ruedas et al. (2011) the following expression was used as boundary condition for the air inlet:

$$u_{inlet} = u_1 \left(\frac{y}{y_1}\right)^p \quad [5.1]$$

where u_1 is the velocity recorded at height y_1, u_{inlet} is the unknown inlet velocity at height y and p is a friction coefficient which is function of the topography of the study site. The meteo station measures the wind speed at 3.8 m from the free surface and a representative recorded value of 1.2 m/s was selected to perform the numerical test. Following Bañuelo-Ruedas et al. (2011) a value of 0.12 was adopted for the exponent, considering the context of the landscape site which consists predominantly of a lake but includes hedges as well.

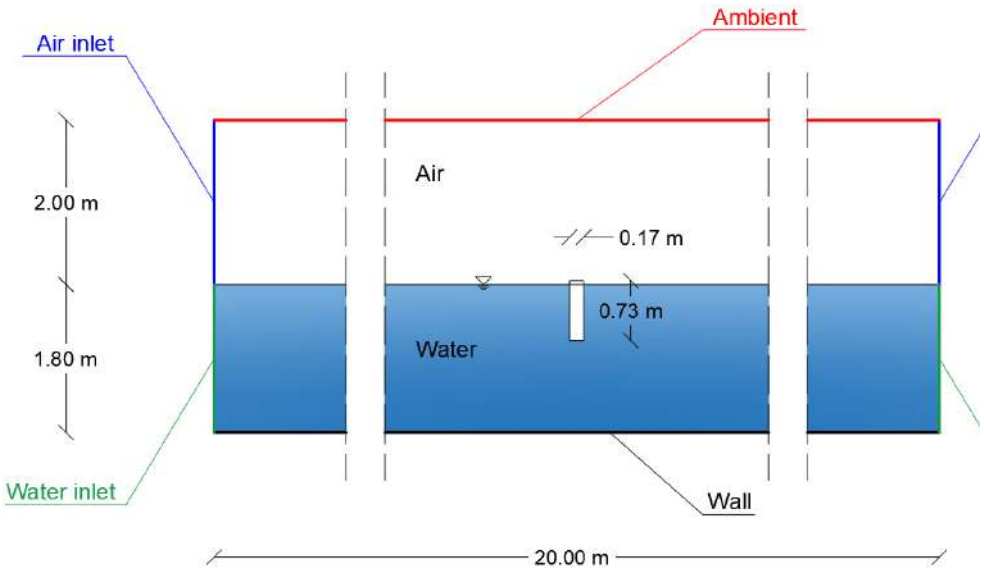

Figure 5.4: Geometry description of the numerical simulation. Two phases are being modelled, air and water respectively, and they are separated by a free surface located at 1.8 m from the bottom. The out-of-plane dimension is 4 m.

With reference to figure 5.4, water inlet and outlet surfaces are set as periodic boundary conditions, i.e. the flow across one periodic surface is treated as the opposing periodic plane is a direct neighbor to the cells adjacent to the first periodic boundary (ANSYS, User Guide). This condition is enforced in order to numerically replicate an ideally infinite domain in the direction of the flow. Air inlet surface is set as a velocity inlet with the

custom logarithmic reported in eq. 5.1 and exits through either the ambient or the air outlet surface (both set as a pressure outlet). At the bottom wall and on the drogue surface a no-slip condition is enforced. Finally, the lateral surfaces are modelled as zero shear walls to replicate symmetry in the out-of-plane direction.

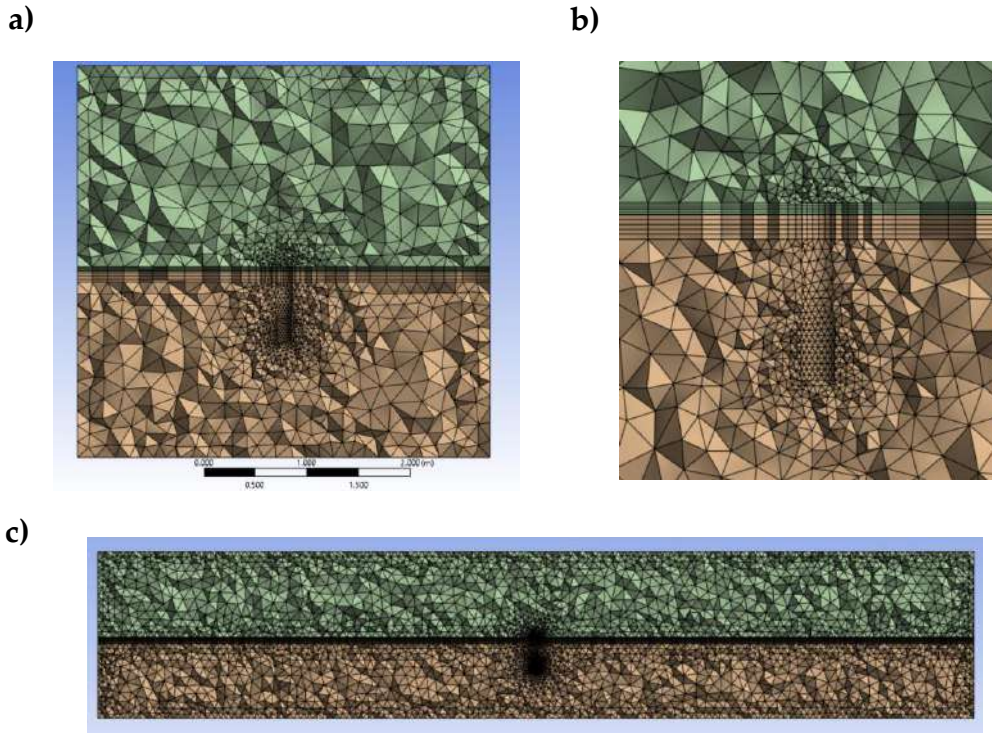

Figure 5.5 a) mesh detail in the vicinity of the drogue, transverse cross section. An inflation layer is placed directly above and below the free surface to better capture both the behavior of the flow near the drogue as well as the free surface location in the vertical direction. b) mesh detail near the drogue. c) longitudinal mesh cross section, highlighting the underlying unstructured mesh used in the computations

As reported in figure 5.5 an unstructured mesh was created, made of 497 426 elements (average spacing 0.15 m), where a match-control algorithm has been enforced on the inlet and outlet faces in order to ensure the consistency of the periodic boundary conditions applied. Near the position of the free surface two inflation layers are inserted to accurately model both the interface between air and water and the limited area of the cap of the drogue emerging from the water. The portion of the drogue in contact with air has been divided into 5 slices of 0.01 m thickness. Similarly, the first 0.1 m of the drogue which is submerged has been divided into 5 slices of 0.1 m. The initial condition was still water with a constant water depth of 1.8 m

across the domain. The Semi-Implicit Method for Pressure-Linked Equations (SIMPLE) (ANSYS, User Guide) solution method was chosen to resolve the problem so far described together with the $k-\omega\ SST$ turbulence model. It is well known that the steady state solver implemented in the software may fail to converge if the initial state of the flow is not sufficiently close to the steady solution still to be computed. For this reason, an unsteady simulation is first adopted and then, after the initial setup of the flow has occurred, switched to steady state for better performance and convergence. The parameters which assess the convergence of the solution are the forces released by the two phases on the drogue. The simulation is considered converged if the difference between two successive iterations does not exceed a threshold of 10^{-6}. The converged solution shows that the ratio between the forces released by the two phases on the drogue is given by:

$$\frac{F_{water}}{F_{air}} = \frac{2.85 \cdot 10^{-2}\ N}{5 \cdot 10^{-4}\ N} = 57 \qquad [5.2]$$

Thus, verifying that the designed geometry ensures that the force exerted by the water on the submerged part is far greater than the air contribution on the emerged part.

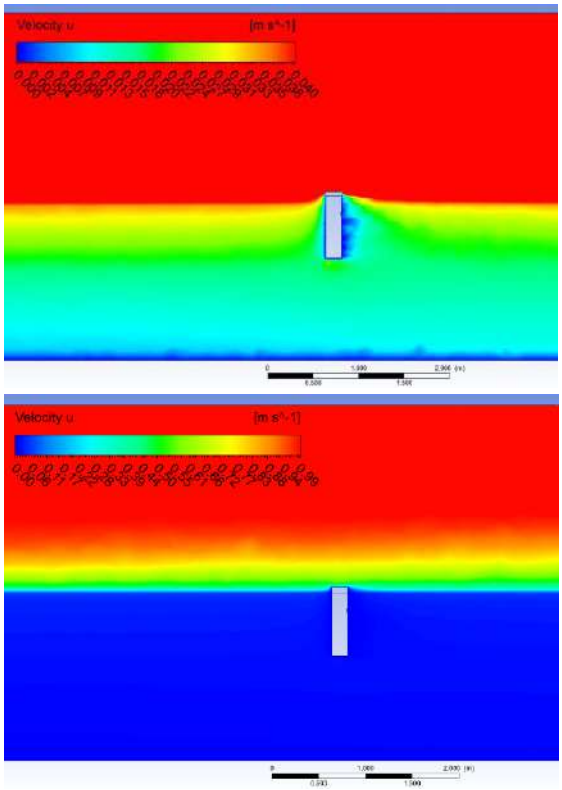

Figure 5.6: Velocity field of the converged solution, longitudinal cross sections. In the top panel the color scale has been adjusted to emphasize the flow field inside the water while in the bottom one the color scale is modified to show the velocities present in the air phase.

5.2 Deployment analysis

When the casing is still open, the drifter is started manually by the user by pushing a button, at the beginning of each deployment. A light shows that the instrument has been switched on and on the website the operator can check that the GPS module is receiving data, recording and writing. The cap of the casing can be shut, and the drifter can be placed in the study site in a sufficiently deep area (we suggest > 1.2 m).

Figure 5.7 a) the cap of the casing, b) the drifter seen from above, right after the deployment from one of the piers, c) the recovery 1 day after, after reaching the drifter with a boat.

When deployed, the operator can check real-time the position of the drifter. After the recovery of the drogue, the data file with the positions in time of the drifter can be downloaded withing 24 hours-time in a comma-separated values format (.CSV).

The drifter was tested in 10 deployments, whose main features are summarized in table 5.2. Most of the releases were done in the bigger tanks, where chances for the instrument to get stuck are lower (figure 5.8).

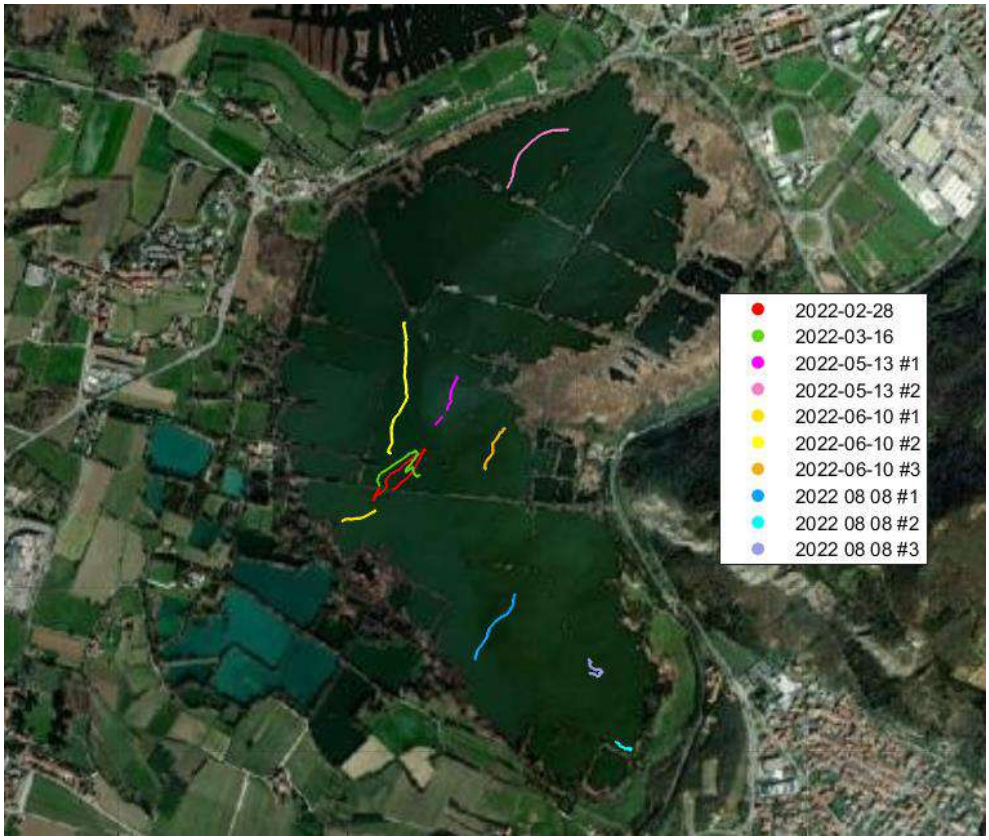

Figure 5.8: Map of all the releases of the drifter

As seen in table 5.2, all the deployments have a duration comprised between 30 minutes and 48 hours. The batteries allow to make deployments that last up to 5 days, but in case of Torbiere, the presence of separating banks makes it difficult for the instrument to float freely: it is very likely to get stuck, making it useless to implement longer deployments. To optimize the logistics of the campaigns, more deployments per day were performed: the drifter was left in the middle of a tank with the help of a boat, and it was left floating. After it got stuck in reefs and banks, it was re-floated in a different location. The result is a series of successive deployments, with a minimum amount of time spent by the drifter stuck.

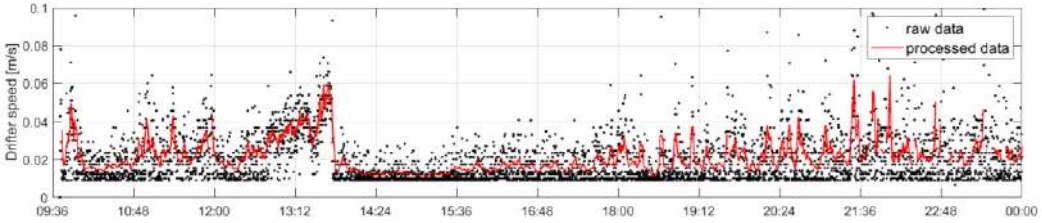

Figure 5.9 Example of raw and processed data

Despite the GPS sensor calculates internally its instantaneous speed, the velocity was calculated starting from the recorded coordinates and the elapsed time to get a much more accurate estimate. To take into account the accuracy of the GPS, which is around 3 m, a pre-processing of the data was needed. A new data set of data was created, with each velocity data being a moving mean over a window of +- 3 m. The result is a much more stable series (figure 5.9), where the unphysical fluctuations due to GPS accuracy are dumped.

Release				Recovery				Duration	Distance Travelled	Drifter av Speed [m/s]	Wind average speed [m/s]
Date	Time	Lat	Long	Date	Time	Lat	Long				
28/02	10:40	45.6442	10.02611	01/03	10:20	45.64417	10.02662	23 h 30 m	700 m	0.0082	2.059
16/03	15:20	45.6443	10.02616	18/03	09:45	45.64451	10.02757	42 h 25 m	400 m	0.0037	1.09
13/05	10:50	45.6458	10.0282	13/05	11:28	45.64703	10.02898	0 h 40 m	140 m	0.0583	1.566
13/05	12:00	45.6518	10.03081	13/05	13:15	45.6533	10.03299	1h 15	220 m	0.0438	1.982
10/06	09:30	45.6436	10.026	10/06	10:30	45.64336	10.02482	1h 0 m	130 m	0.0288	1.87
10/06	10:35	45.64508	10.02655	10/06	15:30	45.64839	10.02708	4h 55 m	486 m	0.0203	1.657
10/06	15:40	45.64468	10.03	10/06	17:25	45.64571	10.03072	1h 45 m	178 m	0.0171	1.712
08/08	09:25	45.64142	10.03228	08/08	11:25	45.63985	10.02964	2 h 0 m	252 m	0.025	1.94
08/08	11.30	45.63764	10.0348	08/08	12:40	45.63753	10.03527	1h 10 m	140 m	0.0037	2.08
08/08	14:00	45.63962	10.03374	08/08	16:30	45.63985	10.03378	2h 30 m	190 m	0.0091	1.746

Table 5.2: List of the deployments: category of the deployment, date, time and position of the release and recovery, total duration of the campaign and distance travelled, drogue average speed and wind average speed during the deployment period

The drifter moved with an average speed of 2.2 cm/s with 34% of the recorded velocities under 2.5 cm/s and only 15% above 6 cm/s. The maximum recorded velocity was 8.5 cm/s.

5.2.1 An example of application: deployment of Feb 28th, 2022

The data acquired from the analysis of the deployment done on February 28th, 2022, is presented as an example. The drifter was left at 10:40 am from the main wooden pier located in the center of Torbiere (yellow-shaded rectangle in figure 5.10). Here the average depth is 2 m. The drifter was left floating for 23 hours and 30 minutes. The drifter trajectory followed the Iseo wind pattern, due to the location of the experiment, that is found in the area influence by Iseo's wind (as argued in ch. 3.1.4). In the first hour, the "Vet" wind was present, that blew from North-East, resulting in the drifter going South-West. Then, the "Ora" wind started, and the drifter changed direction. It then remained stuck for several hours during the night, due to the presence of reefs, it was able to move again in the morning, under the action of "Vet". Overall, it has travelled a distance of 700 m, with an average speed of 0.8 cm/s.

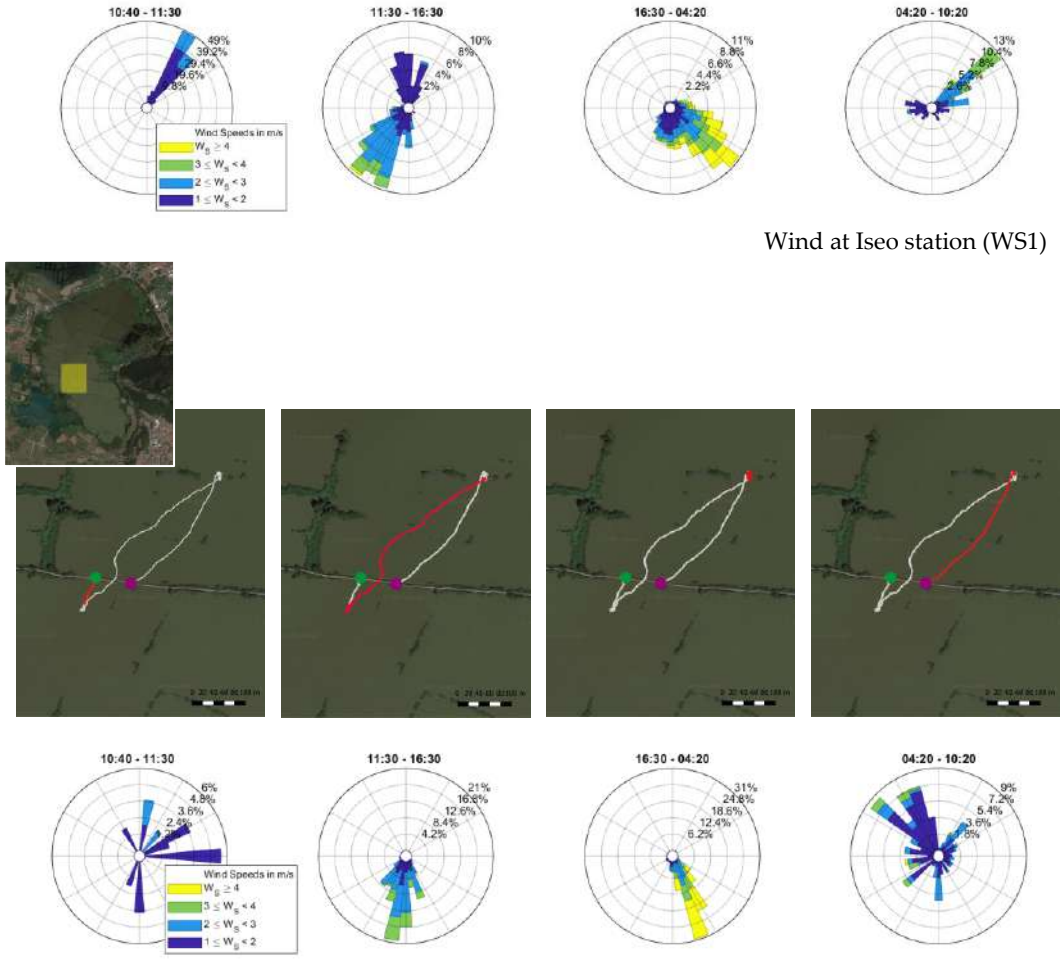

Figure 5.10: Wind roses of Iseo (top row) and Torbiere (bottom row) and maps of the deployments of 28th Feb 2022. The campaign is subdivided into four subsections in order to visualize the wind intensity and direction acting during each sub-period. Please note that the subsections do not correspond to the same duration; for visualization purposes, the period during which the drifter was stucked is represented in one frame only (c), while the first 6 hours, when the wind changed direction, are depicted in two distinct frames (a and b). In the maps the green dot represents the point of release while the purple one the point of recovery of the drifter.

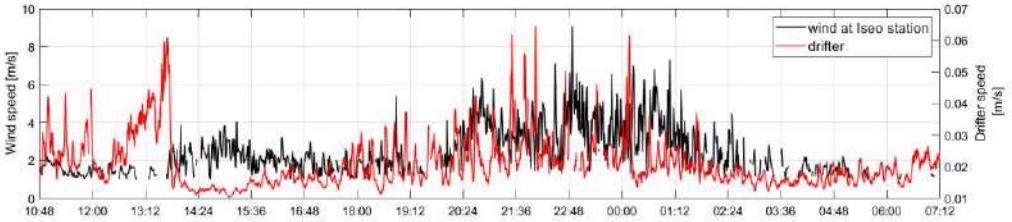

Figure 5.11: Time series of wind intensities at Iseo and drifter speeds.

To see the maps of the other nine deployments and the correspondent wind roses, please refer to Appendix C.

5.3 Model calibration

The velocity of the surface layer obtained with the drifter deployments in the 10 campaigns was compared to the results of 3 – D hydrodynamic model Delft-3Din order to calibrate the manning coefficient. A 2D grid was built for the study area, as defined in Figure 4.1. The size of each cell is 5 ± 3 m, considered suitable in view of topographical characteristics and computational time. The total number of cells is around 24'000, allowing for the representation of both big and smaller tanks. The feature "thin dams" is used to represent the banks subdividing the tanks, which therefore will have no dimensions and will not allow any kind of communication between the sides of the dam itself.

For the vertical grid schematization, a z-model was selected so that the first layer is 70 cm thick, equal to the size of the drogue. In this way, the horizontal velocity modeled in that layer can be directly compared to that measured by the drifter. Delft-3D allows for a feature called "drogue" which consists in placing a floating device in a specific point of the domain at a certain time step and then record its velocity over time. Despite this being extremely convenient to understand trajectories of particles, it does not suit our application, as the forward displacement of the drogue implies an increase of the location error, i.e., as time passes, the comparison of the velocities would be done between points of increasing distance, and not between point in the same location. To overcome this issue, a series of "Observation points" was used in the model, located retrospectively along the registered drogue path. The horizontal velocity in the two components in these points was recorded and extracted at the time when the drogue had passes through them. In this way it is possible to compare a Lagrangian measure to a Eulerian one.

The model was forced using the wind recorded at Iseo station WS1 and the main parameters values are shown in Table 5.3.

Parameter	Value	Units
Horizontal eddy viscosity and diffusivity	0.05 all over the domain 0 at inlet and outlet cells	m^2/s
Slip condition	No slip	
Wind drag coefficient	$\begin{cases} 0.01 & \text{for } u = 0 \text{ m/s} \\ 0.001 & \text{for } u = 4 \text{ m/s} \\ 0.002 & \text{for } u = 20 \text{ m/s} \end{cases}$	-

Table 5.3 Summary of the parameters used in Delft 3D simulations

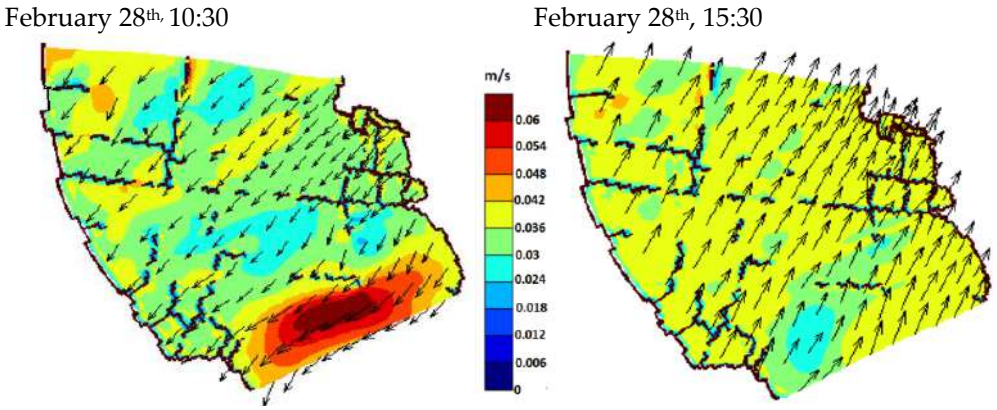

Figure 5.12 Contour patches of velocity magnitudes of the top layer, together with arrows, obtained with Delft 3D. In the left panel is a snapshot obtained at 10:30, when the drifter was moving Southward. The right panel corresponds to the 15:30 time, when the drifter was moving North-Eastward.

Once verified the velocity vectors' directions were consistent between model and measurements (Figure 5.12), a comparison between the velocity magnitudes was possible. The comparison between observed and simulated velocities was used to fine tune the bed roughness coefficient through the Manning's coefficient n. The values of 0.01, 0.012, 0.015, 0.02, 0.05, 0.1 for the Manning coefficient were tested and the final value of 0.015 $s/m^{1/3}$ was chosen as it is the one that gives back the most satisfying results in terms of linear correlation, low dispersion of data (Nash-Suitcliffe coefficient NSE as close to 1) and minimizes the RMSE. As expected from the Manning's equation, where the flow velocity is inversely proportional to the Manning's coefficient, the greater this roughness parameter, the slower the velocities in the model.

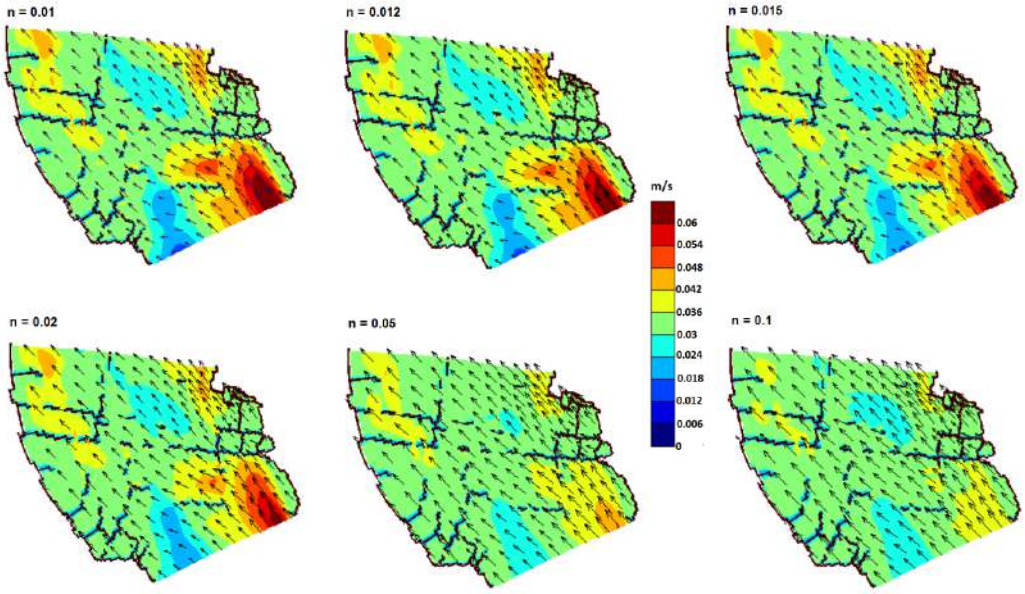

Figure 5.13: horizontal velocities in the top layer obtained for February 28th at 20:30, according to different values of Manning coefficient.

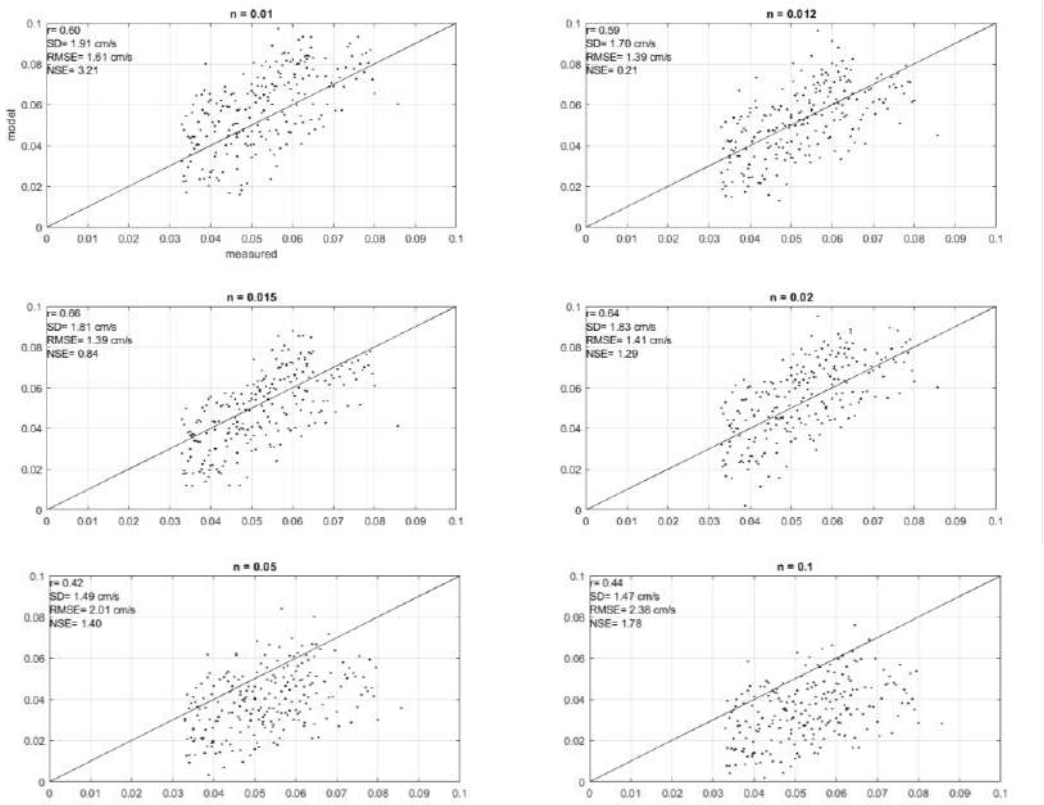

Figure 5.14: Correlation between simulated and measured horizontal velocities during the 10 drifter deployments according to Manning coefficient. The panel in the middle-left corner corresponds to n = 0.015. For each panel, the values of linear correlation coefficient *r*, standard deviation in cm/s and RMSE are given.

Figure 5.14 shows the correlation between the measured and simulated velocities in Torbiere during all the 10 deployments. The model well catches the velocities in the range of 4 to 8 cm/s, while it is less precise (negative R values) when the drifter is moving at 1-3 cm/s. The overall linear correlation coefficient is 0.82 and the standard deviation of the dataset is 0.015 m/s. The modeled velocities are in a reasonable agreement with the measured drifter velocities and the deviation is around 1.9 cm/s. The levels of correlations obtained are consistent with similar comparisons found in literature (Abascal et al., 2009, Huhn et al., 2012, Mardani N. et al., 2020).

5.4 Discussion

A low-cost drifter has been designed for the measurement of surface currents in shallow waters. The ability of this design to capture flow velocities and not wind speeds has been demonstrated by means of Fluent Ansys. The ratio between the drag forces acting on the submerged portion of the device and the one acting on the air-exposed cap is greater than 50, ensuring that the drifter is actually measuring flow velocities and is not being drifted by the wind.
This work represents the first contribution where a drifter designed for shallow waters has been verified in terms of drag forces, while this task has been often neglected due to the challenges imposed by the limited depths of shallow waters (Nasello C. et al., 2016).
The total cost of the drifter is below 200 euros and requires very few, if not null, maintenance costs.

The main applications of this device could be the study of surface currents in deep lakes, the dispersion of multiple drifters in open waters and the study of flow velocities in very shallow systems. In case of application to deep lakes, the hardware components should be placed in a bigger, deeper device as there would not be a depth limitation anymore.

The drifter was tested in Torbiere del Sebino, where flow field is triggered by the wind, and where horizontal velocities lie in the range of a few millimeters – 10 centimeters per second. Ten deployments were done to test the device under different wind conditions and in different areas of the basins and the acquired data was processed and compared to simulations

performed with the hydrodynamic model Delft3D. By comparing measured and modelled flow velocities in the same domain locations, the RMSE was minimized in order to obtain a calibrated value for the Manning coefficient. It can be concluded that a suitable manning coefficient for Torbiere would be 0.015, resulting in a $R^2 = 0.82$.

During the experience gained with the several deployments in Torbiere the device resulted extremely handy and manageable. On the other hand, it showed some limitations. The device could not be deployed in a basin with high waves: the antennas present on the cap might only exceptionally be wetted, but their submergence must be avoided. Before the application, an accurate observation of the flow field is advisable: if the vertical velocity profile shows an inversion, one must ensure that the depth of the inversion does not involve the drifter height: the device captures the integral of the velocity along its depth and the presence of an inversion of the velocity would compromise the measurements. The specific design presented in this work has a battery life of 5 days, therefore one must ensure that within that time, the device can be recovered. Otherwise, there is the risk of losing it as it is not able to send its real-time position.

5.5 References

Abascal, A.J.; Castanedo, S.; Medina, R.; Losada, I.J.; Alvarez-Fanjul, E. (2009). Application of HF radar currents to oil spill modelling. *Mar. Pollut. Bull*, 58, 238–248.

ANSYS Fluent Theory Guide Release 2022 R2.

ANSYS Fluent User Guide Release 2022 R2

Banuelos-Ruedas F., Angeles-Camacho C., Rios-Marcuello S. (2011). Methodologies Used in the extrapolation of wind speed data at different heights and its impact in the wind energy resource assessment in a region. *Wind Farm*.

Boydstun D., Farich M., McCarthy III J., Rubinson S., Smith Z., Rekleitis I. (2015). Drifter sensor network for environmental monitoring, 12th Conference on Computer and Robot Vision.

Gerin R., Zennaro M., Rainone M., Pietrosemoli E., Poulain P.M., Crise A. (2017). On the design of a sustainable ocean drifter for developing countries. *EAI Endorsed Transactions on Internet of Things*, Vol 4(13).

Holden J. et al. (2008). Overland flow velocity and roughness properties in peatlands. *Water Resources research*, Vol.44.

Huhn, F.; von Kameke, A.; Allen-Perkins, S.; Montero, P.; Venancio, A.; Perez-Munuzuri, V. (2012). Horizontal Lagrangian transport in a tidal-driven estuary—Transport barriers attached to prominent coastal boundaries. *Cont. Shelf Res*, 39, 1–13.

Hutter K., Wang Y. and Chubarenko I.P. (2011). Physics of Lakes, Volume 1: foundation of the mathematical and physical background. *Advcances in Geophysical and Environmental Mechanics and Mathematics*.

Johnson D., Stocker R., Head R., Imberger J., Pattiaratchi C. (2003). A compact low-cost GPS drifter for use in the oceanic nearshore zone, lakes and estuaries. *Journal of Atmospheric and Oceanic Technology*, Vol. 20.

Liu S. (2020). Wind driven circulation in large shallow lakes: Implications for Taihu Lake.

Macintyre S., Bastviken D., Arneborg L. and Karlsson J. (2020). Turbulence in a small boreal lake: Consequences of air-water gas exchange. *Limnology and Oceanography*, Vol 9999, 1-28.

Madsen J.D., Chambers P.A., James W.F., Koch E.W., Westlake D.F. (2001). The interaction between water movement, sediment dynamics and submersed macrophytes. *Hydrobiologia*, Vol 444 (1-3), 71-84.

Mardani N., Suara K., Fairweather H., Brown R., McCallum A., Sidle R.C. (2020). Improving the accuracy of hydrodynamic model predictions using lagrangian calibration. *Water*, 12(2), 575.

Monhan E.C., Monhan E.A. (1973). Trends in drogue design. Limnology and Oceanography, Vol.18 (6), 981-985.

Nasello C., Armenio V. (2016). A new small drifter for shallow water basins: application to the study of surface currents in the Muggia Bay (Italy). *Journal of sensors*, Vol. 2016.

Niler P.P., Davis R.E., White H.J. (1987). Water-following characteristics of a mixed layer drifter. *Deep Sea Research part A. Oceanographic Research Papers*, Vol 34(11), 1867-1181.

Niler P.P., Sybrandy A.S., Bi K., Poulain P. M., Bitterman D. (1995). Measurements of the water-following capability of holey-sock and TRISTAR drifters. *Deep Sea Research Part I: Oceanographic Research Papers*, Vol 42(11-12), 1951-1964.

Nutz A., Schuster M., Ghienne J.F., Roquin C., Bouchette F. (2018). Wind-driven waterbodies: a new category of lake within an alternative sedimentologically-based lake classification. *Journal of Paleolimnology*, Vol 59, 189-199.

Rey A., Mulligan R., Ferreira A.M., Filion Y., Champagne P. and Boegman L. (2021). Three-Dimensional hydrodynamic behaviour of an operational waste-stabilization pond. *Journal of Environmental Engineering*, Vol 147(2).

Scheffer M, Carpenter S., Foley J.A., Folke C. and Walker B. (2001). Catastrophic shifts in ecosystems. *Nature*, Vol 413, 591-596.

Schoen J.H., Stretch D.D. and Tirok K. (2014). Wind-driven circulation patterns in a shallow estuarine lake: St. Lucia, South Africa. *Estuarine, Coastal and Shelf Science*, Vol 146, 49-59.

Suara K., Wang C., Feng Y., Brown R.J. (2015). High-resolution GNSS-tracked drifter for studying surface dispersion in shallow water. *Journal of Atmospheric and Oceanic Technology*, Vol. 32(3), 579-590.

Wetzel R.G. (2001). Limnology: Lake and River Ecosystems. *San Diego: Academic Press*.

Wu T., Qin B., Huang A., Sheng Y., Feng S. and Casenave C. (2022). Reconsideration of wind stress, wind waves, and turbulence in simulating wind-driven currents of shallow lakes in the Wave and Current Couple Model (WCCM) version 1.0. *Geoscientific Model Development*, Vol 15, 745-769.

Wuest A. and Lorke A. (2003). Small-Scale Hydrodynamics in Lakes. *Annual Review of Fluid Mechanics*, Vol 35, 373-412.

Others

Arduino store website https://store-usa.arduino.cc/products/arduino-mkr-gsm-1400?selectedStore=us

Arduino website https://www.arduino.cc/

TinyGPS++ library https://github.com/mikalhart/TinyGPSPlus

6. Residence time simulation

Large shallow wetlands like Torbiere del Sebino provide a multitude of ecosystem services and are an important ecological, social and touristic resource for the area where they are located. A fundamental role played by wetlands is that they also represent a natural solution for the treatment of pollutants, by means of the processes that control contaminant distribution, such as sedimentation, oxidation, disinfection, and stabilization (Reddy K.R. et al. 1997).

Actually, the expected efficiency of the nutrient removal processes acting in a wetland is related to its flushing time, or residence time, as it describes its waters renewal ability (e.g., Nguyen et al. 2014). The residence time is defined as the time is takes for any water parcel of the sample to leave the lagoon through its outlet to the sea (Dronkers and Zimmerman, 1982).

Many studies have analysed the water renewal in terms of residence time (Bravo et al. 2020, De Brauwere A. et al 2011, Thackston et al. 1987) and water age (Qi et al. 2016, Liu et al. 2012, Li et al. 2011) or both (Shen et al. 2011). The main tools used to reach insights on residence time include the calculations of residence time using hydrodynamic models and lake particle transport models, as well as the use of isotope-tracer experiments (Dincer, 1968) and drifter experiments (Sanderson, 1987, Pal et al., 1998). It is important to observe that the use of isotope-tracer experiments is typical for systems smaller than Torbiere, where, in addition, the use of tracers (e.g. fluorescein and, better, rhodamine dye) is limited due to its natural reserve status. Whereas the effects of variable discharge (Huang et al. 2016), variable wind regimes (Liu et al. 2020) and variable water levels (Li et al. 2010) have been evaluated, to our knowledge, little is known about the effect of different bank configurations on renewal timescales and the consequent water quality of a wetland.

From the ecological point of view, there is wide consensus on the positive role of connectivity, that is usually associated to a better environmental quality. However, in the particular situation of Torbiere d'Iseo, that are stressed from a considerable and localised pollutant load and that have undergone the negative effects of invasive species proliferation, we believe that restoring the original separation between the ponds could be beneficial. The physical separation could limit the diffusion of pollutants and make

biomanipulation practices more viable. However, to our knowledge there are very little studies that discuss the trade-off between connectivity, as a source of biodiversity, and the worsening of water quality in areas that were originally isolated (De Paggi 2008).
Accordingly, in this work we directed the hydrodynamic study of this important wetland to investigate the variation of its residence time in response to the demolition of the separating banks. The idea that led this research is that in some cases, a lower level of connectivity might improve the water quality of a basin. Furthermore, given that the only outflow of Torbiere is headed towards lake Iseo, one can consider it as a pre-treatment basin (see ch. 1.5) and the inner disposition of the banks might influence the removal efficiency of any pollutant discharged in the system.

6.1 Reactor analogy

Torbiere del Sebino can be assimilated to a reactor, that receives waters from the affluent Rì and from the Provaglio's sewer and delivers an effluent through an artificial channel that discharges into Lake Iseo. In this perspective, its behavior in terms of removal and emission of polluted substances, should be compared with the regimes of two ideal reactors: the Completely Stirred Tank Reactor (CSTR) and the Plug Flow (PF) reactor (Schmidt L.D.1998).

There are two, complementary approaches to investigate the residence time in a system through tracer concentrations. The first would be to consider a clear system, with zero concentration of pollutant at time t = 0 s, where a polluted inflow of known concentration enters and contaminates the domain. This approach is the one typically followed from the experimental point of view. The second one consists of considering a polluted system, with known pollutant concentration everywhere, where an inflow of null concentration enters and clears the domain. This second approach is the one usually followed in numerical simulations and was chosen for our purpose, as it allows to evaluate residence time by means of the average pollutant concentration left in the domain at a certain time t. In the completely stirred tank reactor analogy, the time at which 63% of the initial pollutant has left the system, is considered as the residence time of the water body (Bolin B. et al,1973) and as a convenient convention, could be used as a definition of

this quantity also for other types of incompletely mixed reactors (e.g., Pilotti et al, 2014).

The remaining concentration in time in a real mixed reactor is a monotonically decreasing curve that lies in between that of a CSTR and a PF of analogous geometry. To allow for a comparison, the CSTR and PF should be chosen to have the same area and average depth of Torbiere, they should be supplied with the same discharge and the distance between inlet and outlet should be the same. In this case, for a CSTR:

$$C = C_0 e^{-kt} \qquad [6.1]$$

With $k = V/Q$, where V is the volume of the reactor and Q is the average discharge entering the system.

In case of a PF reactor, the average concentration in the pond is given by:

$$C = C_0 (1 - u/L * t) \qquad [6.2]$$

Where u =Q/A is the average horizontal velocity with which the sharp front of the pollutant propagates in the system, A is the cross section of the pond and L is the distance it has to travel, from inlet to outlet, being $V = A*L$.

Equations (6.1) shows that a non-reacting pollutant concentration in a CSTR decreases following an exponential curve of initial slope equal to Q/V, while eq. (6.2) shows that in a PF it decreases linearly, with a constant slope that is the same as that found at t = 0s for the CSTR ($u/L = Q/V$).

Figure 6.1a shows the average concentration of a conservative pollutant left in the two ideal reactors where geometry and boundary conditions are set equal to those of Torbiere (i.e. same area and volume and incoming discharge equal to the average value of the main affluent). By fixing a dummy initial mass concentration of 1 kg/m^3 everywhere, it decreases with a constant rate in the PF reactor, while it decreases with a diminishing rate in the case of CSTR. The shaded area in between the two curves is where the real reactors curves can lie. Neglecting systems with meromictic behavior, there is no reactor faster in the removal than a PF nor slower than a completely mixed (Sperling M.V., 2020).

The CSTR curve lies above the PFR line, meaning that a mixed reactor increases the time needed for the completion of a reaction.

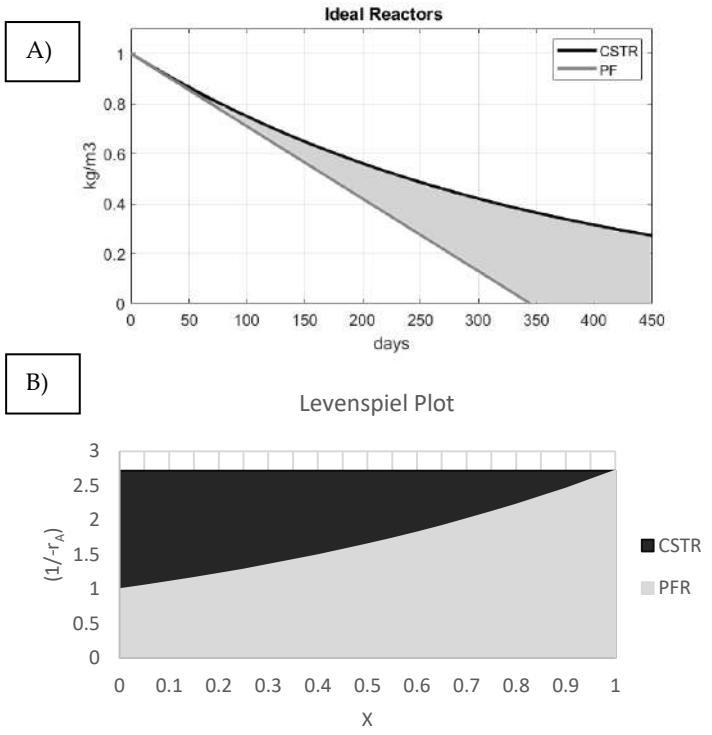

Figure 6.1 a) CSTR and PFR ideal reactors curve of average tracer concentrations under the action of a clear inflow. b) Levenspiel plot for ideal CSTR and PFRs. The shaded area under each curve represents the volume required to reach a 100% conversion X.

As in the field of chemical engineering one would design a real reactor so that its flow approaches one of the two ideal behaviors, the behavior of Torbiere will be compared to that of a CSTR and a PFR. The PFR behavior will be considered desirable, as it allows for a higher degree of conversion (i.e. the fraction of a certain reactant converted to something else or reacted away) for the same volume as the CSTR (Levenspiel O. 1999). The Levenspiel plot in Figure 6.1.b shows the area required by each reactor to reach a certain degree of conversion *X*: it is proportional to the inverse of the reaction rate and to the target efficiency *X* itself. Another way to understand this concept is by looking at the plot in Figure 6.2 proposed by Dimian (2003). At low conversions ($1-X_A \sim 1$), the difference in volume between CSTR and PFR is small; however, it becomes considerable at

conversions higher than 90% (1-X_A~0.1). For a first order reaction at X_A = 0.99, V_{CSTR}/V_{PFR} = 20.

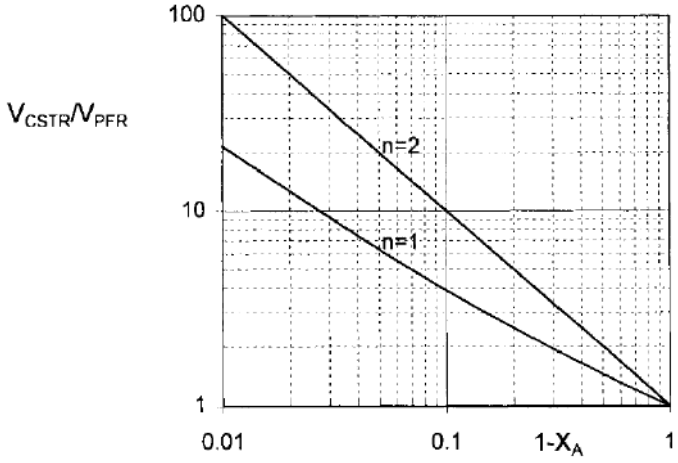

Figure 6.2 Comparison of CSTR and PFR for first and second-order reactions (Dimian A.C., 2003)

In the following, in order to investigate the residence time of Torbiere, two modeling approaches were chosen, of increasing completeness, and complexity. The setup of the models is presented in the next paragraphs. In particular, the two historical configurations of Torbiere were studied: one corresponding to the present situation, the other to the 50s/60s configuration. Accordingly, by focusing on the layout changes that have occurred in this 70-80 years period, the scope of this investigation is the understanding of the role of the disconnection between the different ponds operated by the inner subdivision of the banks, neglecting any changes in the two systems related to bathymetry and forcings.

The present configuration is known thanks to site-inspections, while the 50s/60s was reconstructed through old maps and satellite images (see figure 6.3 for a comparison).

6.2 The models

Two different models have been implemented for the analysis of the distribution of residence time in Torbiere del Sebino: a multiply connected box model that has been implemented *ad hoc* and programmed in the DELPHI language and a 3D model, using the Delft3D-FLOW package.

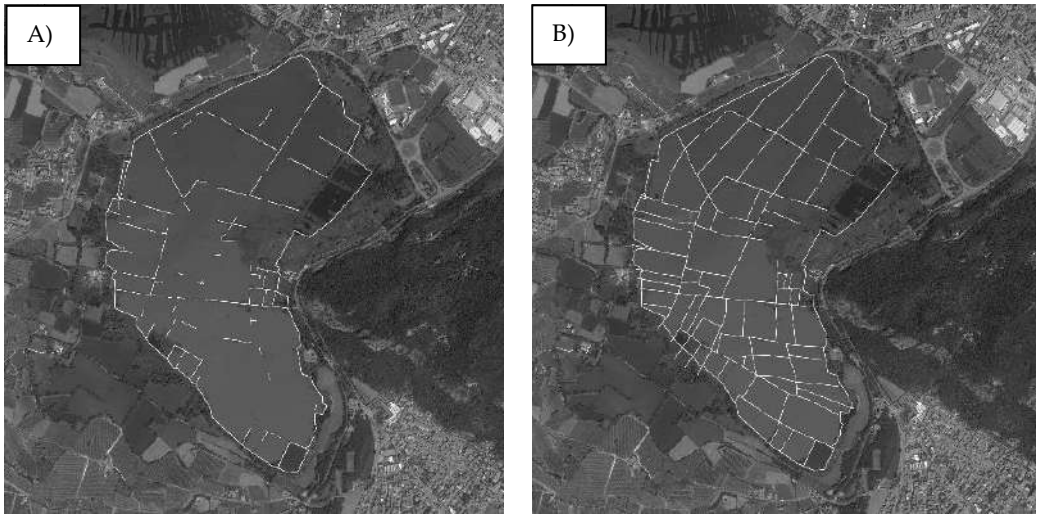

Figure 6.3 a) Present (2022) vs b) 50s/60s configuration as reconstructed from satellite images (see Appendix A).

6.2.1 Box model setup

In the following a simple differential balance model that takes into account the dynamics of the "old water", seen as the overall water within the wetland at time t = 0 is proposed. In order to compute the concentration of the old water in the wetland as a function of time, a mass balance of the old water during the years is made, using basic information regarding the wetland connectivity and dynamics. Due to the typical shallowness of a wetland, its shape can be simplified as cylindrical and only its area and initial depth is needed. Similarly, due to the likely polymictic condition, each pond of a wetland can be regarded as perfectly mixed, and its vertical thermal profile is not needed. On the other hand, it would be necessary to have the time series of the tributaries discharge, rainfall, evapotranspiration and groundwater exchanges.

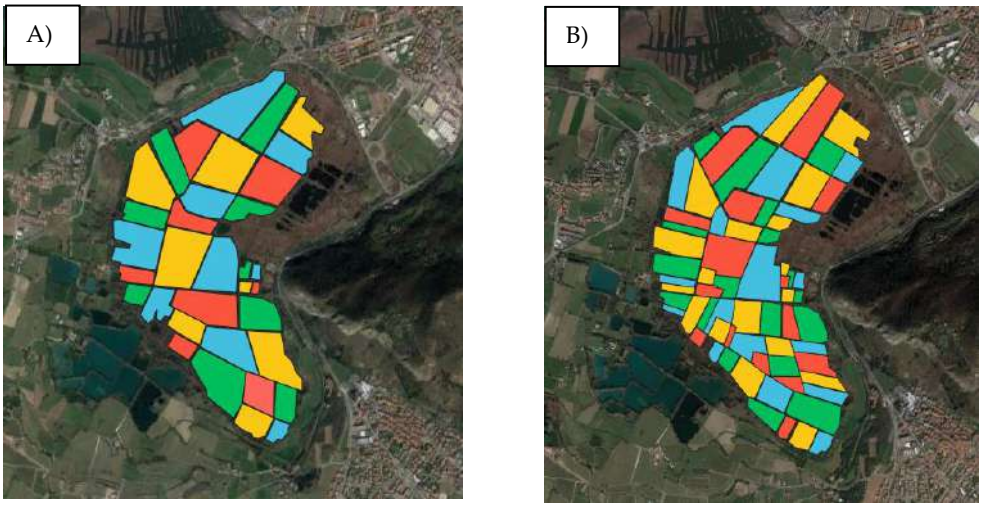

Figure 6.4: Subdivision of Torbiere in a) 34 ponds for the present configuration and b) in 68 ponds for the 50-60s configuration

We subdivide the wetland into n ponds that make up its overall area (see Figure 6.4, where the colors show the 2 different considered layouts), each pond being of volume *Vj* and having homogeneous old water concentration *Cj*. The initial depth of each pond is provided along with the initial "old water" concentration, set equal to 1.

Two mass balances are needed. The first is a hydrological volumetric balance of water within the *j-th* pond making up the wetland. The balance is provided by the system of n equations:

$$\frac{dV_j}{dt} = \sum_{i=1}^{n} Q_{i,j\ in} - \sum_{i=1}^{n} Q_{i,j\ out} + q_{j\ in} - q_{j\ out} + R_j - E_j + G_j \qquad [6.3]$$

where *n* is the overall number of ponds in the wetland and the symbols have the following meaning: $Q_{i,j\,in}$ is the entering discharge from pond *i* to pond j. $Q_{i,j\,in}$ is 0 if no connection is present between pond *i* and *j*, if the water elevation in cell *i* is less than the water elevation in pond *j* and when *i = j*.

$Q_{i,j\,out}$ is the outflow from pond j to pond *i*; it is 0 if no connection is present between pond j and *i*, if the water elevation in pond *j* is less than the water elevation in pond *i* and when *i=j*.

If present, $q_{j\,in}$ is the inflow entering pond j from outside the wetland, typically provided by a tributary or by a spring.

If present, $q_{j\,out}$ is the outflow from pond *j* flowing out of the wetland.

R, *E* and *G* are the rainfall, evaporation and groundwater exchange for pond *j*, computed as m^3/s. *G* is positive if the groundwater feeds the pond and negative otherwise.

Considering that V_j, $Q_{i,j\,in}$ and $Q_{i,j\,out}$ are functions of the water depth Y_j and Y_i, the solution of system (6.3) provides the volume of water (i.e., the water depth) in each pond of the wetland as a function of time.

In order to compute the renewal time of water in the wetland, one can study the variation in time of the mass of water M_j originally present in each pond (the so-called *old water*). Accordingly, a second system of equations governs the mass conservation of the *old water*, that is gradually substituted by the new water coming from rainfall, groundwater and external inflows and that exits from the system due to outflows and to evaporation. If $C_j = M_j/V_j$ is the average old water concentration within each *j-th* pond, the variation in time of the amount of old water M_j can be described as:

$$\frac{dM_j}{dt} = \sum_{i=1}^{n} C_i Q_{i,j\,in} - C_j \sum_{i=1}^{n} Q_{i,j\,out} - C_j q_{j\,out} - C_j E_j + \delta_j C_j G_j \qquad [6.4]$$

where δ_j is 1 if G_j is negative and 0 otherwise. On the other hand, considering the definition of concentration and the volumetric balance (6.3), one can write:

$$\frac{dM_j}{dt} = \frac{d(C_j V_j)}{dt} = \frac{V_j dC_j}{dt} + \frac{C_j dV_j}{dt} = \frac{V_j dC_j}{dt} + C_j\left(\sum_{i=1}^{n} Q_{i,j\,in} - \sum_{i=1}^{n} Q_{i,j\,out} + q_{j\,in} - q_{j\,out} + R_j - E_j + G_j\right) \qquad [6.5]$$

And by substituting into equation 6.4:

$$\frac{V_j dC_j}{dt} = \sum_{i=1}^{n}(C_i - C_j)\, Q_{i,j\,in} - C_j(q_{j\,in} + R_j) + (\delta_j - 1)\, C_j G_j \qquad [6.6]$$

that can be solved to provide the old water concentration C_j for the *j-th* pond being $V_j(t)$ and $Q_{i,j\,in}(t)$ known from the solution of system (6.3) and being $C_{j,0} = 1$ the initial old water concentration.

The system of equations (6.3) and (6.6) can be used for the computation of the time distribution of old water mass in the wetland. By knowing the hydraulic connectivity between the different ponds, the functional relations

$Q_{i,j\,in}$, $Q_{i,j\,out}$ and G_j, that are a function of the water depth, and the time variation of the other input/output to the *j-th* pond, the system (6.3) can be solved to provide the volume (i.e., the water depth) in each pond as a function of time. Then, the system (6.6) is solved to provide the old water concentration mass C_j in the pond. The product of the two variables provides the old water mass M_j remained in each pond and in the wetland, $M = \sum_{j=1}^{n} M_j$. Finally, the variation in time of the ratio $M_j / M_{j,0}$ provides the local and overall distribution of residence time in the wetland.

It is particularly convenient to introduce a connectivity matrix that reflects the topology of the interconnection between the different ponds in the wetland (figure 6.5a). In this way it is possible to write the two systems of equation (6.3) and (6.6) in a more efficient vectorial way. If n ponds are present in the wetland, the connectivity matrix $\boldsymbol{K}$ is a n x n sparse matrix whose element K_{ij} is 1 if the *i-th* and *j-th* ponds are connected and 0 otherwise; the diagonal values are 0. $\boldsymbol{A}$ is a n x n diagonal matrix whose A_{ij} element is the area of the *i-th* pond and $A_{ij} = 0$ when $i \neq j$.
$\boldsymbol{Q}$ is a n x n matrix whose elements are the volumetric flow between pond i and j and whose diagonal elements are 0. Q_{ij} is computed as a function of the water depth Yi and Yj and is positive when it is entering pond i and negative otherwise. Let $\boldsymbol{y}$ be the n x 1 vector of water depths in the n ponds of the wetland and $\boldsymbol{i}$ is a n x 1 vector with all elements equal to 1. Finally, $\boldsymbol{q}_{in}$, $\boldsymbol{q}_{out}$, $\boldsymbol{r}$, $\boldsymbol{g}$, and $\boldsymbol{e}$ are n x 1 vectors of external input, output, rainfall, groundwater exchange and evaporation. Accordingly, system (6.3) can be written as:

$$\mathbf{A}\dot{\mathbf{y}} = \mathbf{K} \circ \mathbf{Q}\mathbf{i} + \mathbf{q}_{in} - \mathbf{q}_{out} + \mathbf{r} - \mathbf{e} + \mathbf{g} \qquad [6.7]$$

where $\dot{\mathbf{y}}$ is the time derivative and $\circ$ is the elementwise Hadamard product between $\boldsymbol{K}$ and $\boldsymbol{Q}$.
System (6.7) can be integrated in time using standard numerical techniques for ordinary differential equations, such as a Runge-Kutta variable-step method.
In a similar way, one can write system (6.6) as:

$$\mathbf{V}\dot{\mathbf{c}} = \mathbf{K} \circ \mathbf{Q}\mathbf{c} - (\mathbf{K} \circ \mathbf{Q}\mathbf{i}) \circ \mathbf{c} - \mathbf{c} \circ (\mathbf{q}_{in} + \mathbf{r}) + \mathbf{c} \circ \bar{\mathbf{g}} \qquad [6.8]$$

where $\mathbf{V}$ is a n x n diagonal matrix whose V_{ii} element is the volume of water at time t in the *i-th* pond and $V_{ij} = 0$ when $i \neq j$; $\mathbf{c}$ is the n x *1* vector of old water concentration in the n ponds of the wetland. Finally, $\bar{\mathbf{g}}$ is the groundwater exchange vector which includes the quantity $(\delta_j - 1)$.

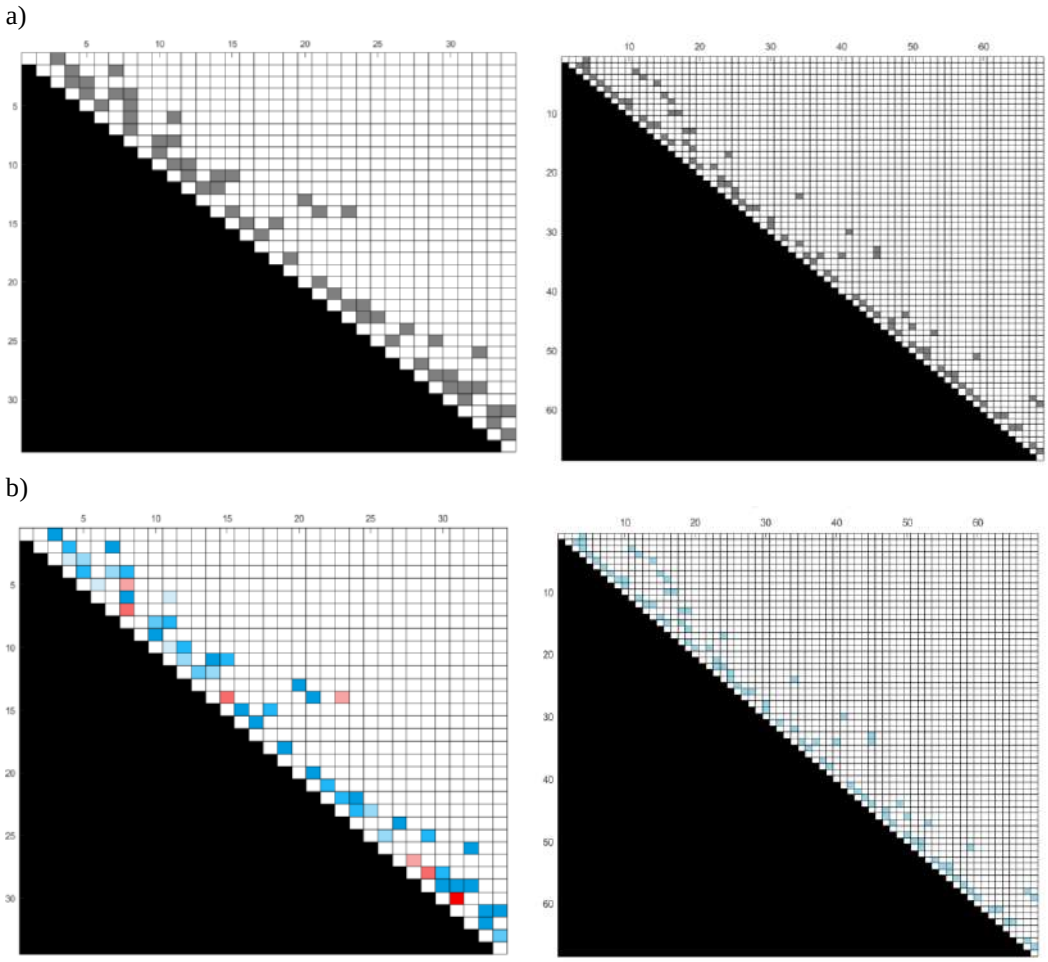

Figure 6.5: A) connectivity matrixes of the actual situation (left panel) and the situation of the 50s-60s (right panel). B) the colored cells represent a connection between the *i-th* (column) and the *j-th* pond (row). The red color indicates a higher degree of connectivity, the blue a lower degree. The degree of connectivity is built as a function of the geometry of the connection itself: the larger the opening between the ponds, the higher the degree of connectivity. In the 50s-60s configuration, all the ponds present the same level of connectivity due to the absence of a clear cartography of the time.

In order to solve systems (6.7) and (6.8), the initial conditions must be given. For system (6.7) this is provided by the initial water depth vector $\mathbf{y}(0)$. For system (6.8), it is provided by the initial concentration vector, $\mathbf{c}(0) = \mathbf{i}$, reflecting the condition that initially all the water within the wetland is *old water*. Note that system (6.7) is decoupled from system (6.8). Accordingly,

the variation in time of the water depth in the wetland is computed first. Then, using the computed volume and the water depth, the old water concentration **c** in each pond is computed as a function of time t.
The overall average old water concentration in the wetland can then be obtained as the volumetric average as

$$C = \frac{\mathbf{c}^{\mathrm{T}} \cdot (\mathbf{Vi})}{\mathbf{i}^{\mathrm{T}} \cdot (\mathbf{Vi})} \qquad [6.9]$$

In the following, some simple examples of use of the proposed equations are shown.

In the case of an isolated pond j where only a constant rainfall rate is present, eq. 6.3 is simplified as

$$\frac{dV_j}{dt} = R_j, \qquad V_j(t) = V_{j,0} + R_j t \qquad [6.10]$$

where $Vj,_0$ is the initial volume in the pond. The old water balance (6.4) gives:

$$\frac{V_j dC_j}{dt} = -C_j R_j \qquad \left(V_{j,0} + R_j t\right)\frac{dC_j}{dt} = -C_j R_j \qquad [6.11]$$

That provides:

$$C_j = \frac{C_{j,0}}{\left(1+\frac{R_j}{V_{j,0}}t\right)} \qquad [6.12]$$

i.e., C decreases due to the volume increase but the old water mass, M_j,

$$M_j = C_j V_j = \frac{C_{j,0}}{\left(1+\frac{R_j}{V_{j,0}}t\right)}\left(V_{j,0} + R_j t\right) = \frac{C_{j,0}V_{j,0}}{\left(1+\frac{R_j}{V_{j,0}}t\right)}\left(1 + \frac{R_j}{V_{j,0}}t\right) = C_{j,0}V_{j,0} = M_{j,0} \qquad [6.13]$$

Remains constant in the pond.

Similarly, in the case of an isolated pond where only the groundwater is present, the two balance equations simplify as:

$$\frac{dV_j}{dt} = G_j, \qquad [6.14]$$

$$V_j \frac{dC_j}{dt} = \left(\delta_j - 1\right)C_j G_j \qquad [6.15]$$

Let us suppose that the volumetric flux j G is constant. If it is positive, the case is similar to the one considered above. If j G is negative, the volumetric balance provides:

$$\frac{dV_j}{dt} = -|G_j| \qquad V_j(t) = V_{j,0} - |G_j|t \tag{6.16}$$

And the old water balance shows that the concentration does not change:

$$V_j \frac{dC_j}{dt} = 0 \quad C_j = C_{j,0} \tag{6.17}$$

But the old water mass in the pond, M_j

$$M_j = C_j V_j = C_{j,0}(V_{j,0} - |G_j|t) = M_{j,0} - C_{j,0}|G_j|t \tag{6.18}$$

Decreases linearly in time.

6.2.2 3 – D model setup

To model the hydrodynamics of Torbiere, the DELFT3D-FLOW module was chosen. The module solves the following equations…

The 2D grid with which the domain was reproduces has been described in chapter 4. For the vertical grid schematization, 5 σ-layers (20% of depth) were selected, leading to a thickness comprised between 0.24 and 0.55 m according to the location in the domain. The decision of using a 3D model in place of the 2D Shallow Water Equations was initially motivated by the idea of better understanding the flow situation close to the bed, where anoxic conditions could develop during the summer. Moreover, considering that a wind set-up was expected under the action of the periodic winds blowing in the area, the possibility of backflow with a velocity inversion close to the bottom was sometimes expected. Neither of these situations could have been explored with a 2D approach.

As mentioned, two configurations were considered that only differ in their geometry and, in particular, in the number and position of the "thin dams", features in Delft3D that were used to represent the banks subdividing the ponds.

After the flow field has been computed, the feature "pollutants and tracers" allows to investigate the fate of a conservative substance that is present all over the domain at time t = 0 s with a given initial concentration (in this case we arbitrarily set $C(0) = 1$ kg/m^3). For an arbitrary control volume, one may simulate the dynamics of the concentration in time, which is governed by the mass balance:

$$\frac{dM}{dt} = C_{in}Q_{in} + C_{rain}Q_{rain} - C_{out}Q_{out} - C \cdot E \tag{6.19}$$

Where $M=M(t)$ is the mass of the conservative tracer [kg], C_{in} and C_{rain} are the tracer concentrations of incoming discharge and rain [kg/m^3], in this case set equal to zero. C_{out} is the tracer concentration at the cell closest to the outlet, C is the average tracer concentration in the domain. Q_{in}, Q_{rain}, Q_{out} and E are the incoming discharge from affluents, from rainfall, the outflowing discharge of the effluent and the evaporation term [m^3/s].

For the transport equation solved by the model we recall equation 4.4.

After initializing the domain with unitary concentration of tracer, and considering a null concentration for the inflow terms, C is a representation of the "old water" concentration present in the system. Therefore, the variation in time of the ratio $M(t)/M(0)$ provides the overall distribution of residence time in the wetland.

The current absence of macrophytes within the Torbiere led to the choice of a spatially uniform bottom roughness (Manning coefficient), set equal to 0.015 after a calibration performed with drifter measurements as explained in chapter 5. A no slip boundary condition is used at the walls. Horizontal eddy-viscosity and diffusivity play an important role in the transport of substances; their value, set equal for both parameters as suggested in the manual (Deltares, 2020), was calibrated using measurements of the spread of a plume of specific conductivity that occurred in April 2021 as explained in paragraph 4.4. The identified value, constant all over the domain, is 0.05 m^2/s, with the exception of the inlet and outlet cells, where it is forced to be zero, to avoid the unphysical diffusion of the tracer outside the domain through the open boundaries.

The flow field within Torbiere was simulated from June 2020 to August 2021, with a time step of 1 min chosen for the stability and accuracy of the solution. Considering the short duration of the available time series and its strong variability, we eventually decided to make reference to an average equivalent situation characterized by steady forcings, to get a view of the flow field in an ideal reference condition. In this way one is able to assess the behavior of Torbiere in the long term, without the affection of the unsteady Ri's and pump's regimes. Accordingly, the Delft-3D model was forced using wind speed and direction from WS1, recomputed at 10 m elevation, and constant incoming and outflowing discharge. The incoming

discharge is equal to the average discharge measured in the observation period at Rì's inlet; the outflowing discharge is set equivalent to the sum of the Rì's discharge and the contribution of rain. A constant rainfall, equal to the net (rainfall-evaporation) average throughout the year, is introduced and has a diluting effect on the waters, having a tracer concentration equal to 0 kg/m^3.

The alternating daily wind direction causes a slight set-up in the water depths of the Torbiere, that can be evaluated in the order of few millimeters (ch. 4.1). When the wind is turned off, the system is stationary and shows constant water levels.

6.3 Results

The two different geometries produce different results in terms of water levels, flow field and tracer concentration. As seen from chapter 4.1, a typical wind setup for Torbiere can be reckoned to be about 2 mm and the simulations presented in this chapter confirm that evaluation. However, larger overall setup values (2.5 mm) are found in the present configuration of Torbiere, due to the bigger size of its ponds, that allow the wind stress to develop with a longer fetch (Figure 6.6a). In the 50-60s configuration, in contrast, the presence of a much greater number of banks prevents a complete wind setup. Furthermore, given the absence of internal connections, some ponds that, under the action of a strong wind coming from North, in the present configuration, would increase their water level, in the 50-60 configuration remain at a much lower level.

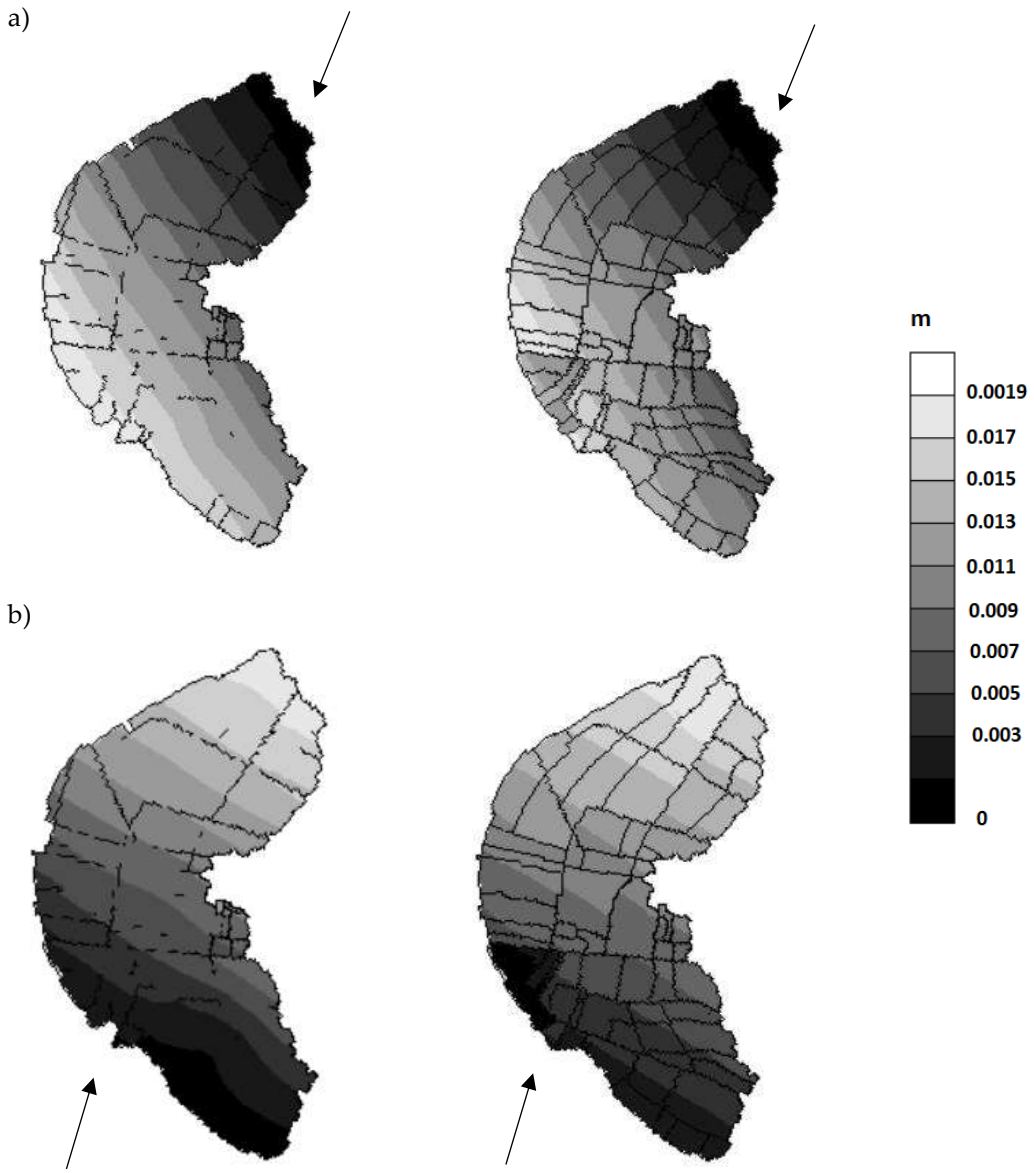

Figure 6.6 Relative water level differences in the present (left panel) and the 50-60s (right panel) configuration, during a sustained wind from a) North and b) South. The arrows indicate the direction of the wind.

The time-series of pollutant concentrations left in Torbiere obtained with Delft 3D are shown in Fig 6.7 and the snapshots of the tracer's spatial distribution at different times are shown in Figure 6.8, for both the box model and Delft3D. When commenting on the plots, we recall the analogy between the tracer concentration left in the domain and the *old* water, used in paragraph 6.1. Moreover, it should be taken into account that, although each pond in the box model is a CSTR, the mixing action of wind is not considered.

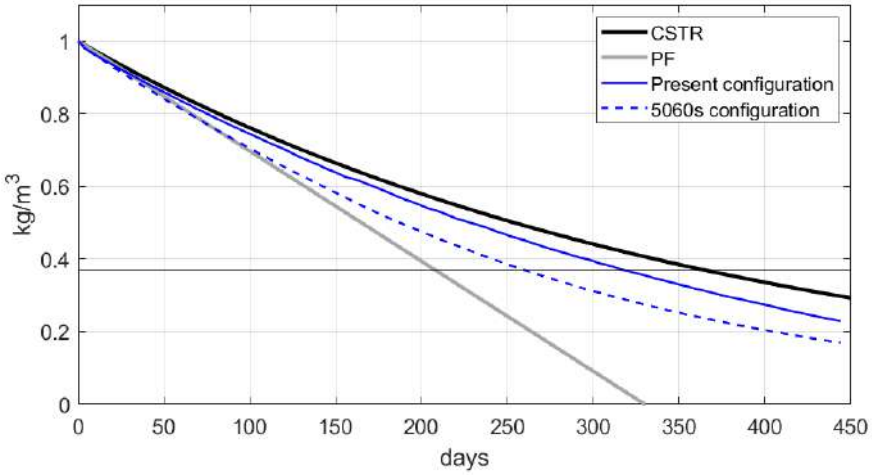

Figure 6.7 Comparison between the average tracer concentration within the basin in the present and in the 50s/60s configuration. The horizontal thin line indicates that only 37% of the initial tracer is still in the system, and corresponds to the residence time

The *old* water concentration, represented by the conservative tracer, varies spatially and in time during the simulations, as the main direction of the flow is from South to North. The distribution of the old water in the present configuration (Fig. 6.6a) is rather homogeneous between the ponds, with a tendency to a greater accumulation of old water in the north-eastern side. In the 1950s-1960s configuration (Fig. 6.6 b), the flow is driven from pond to pond, with some parts of the basin being significatively reached by the flushing only after 6 months of simulation. Despite this, the flow is more efficient in flushing one pond at a time and the overall concentration of tracer at each time step is lower in the 1950s-1960s configuration (dashed blue line in Fig 6.7).

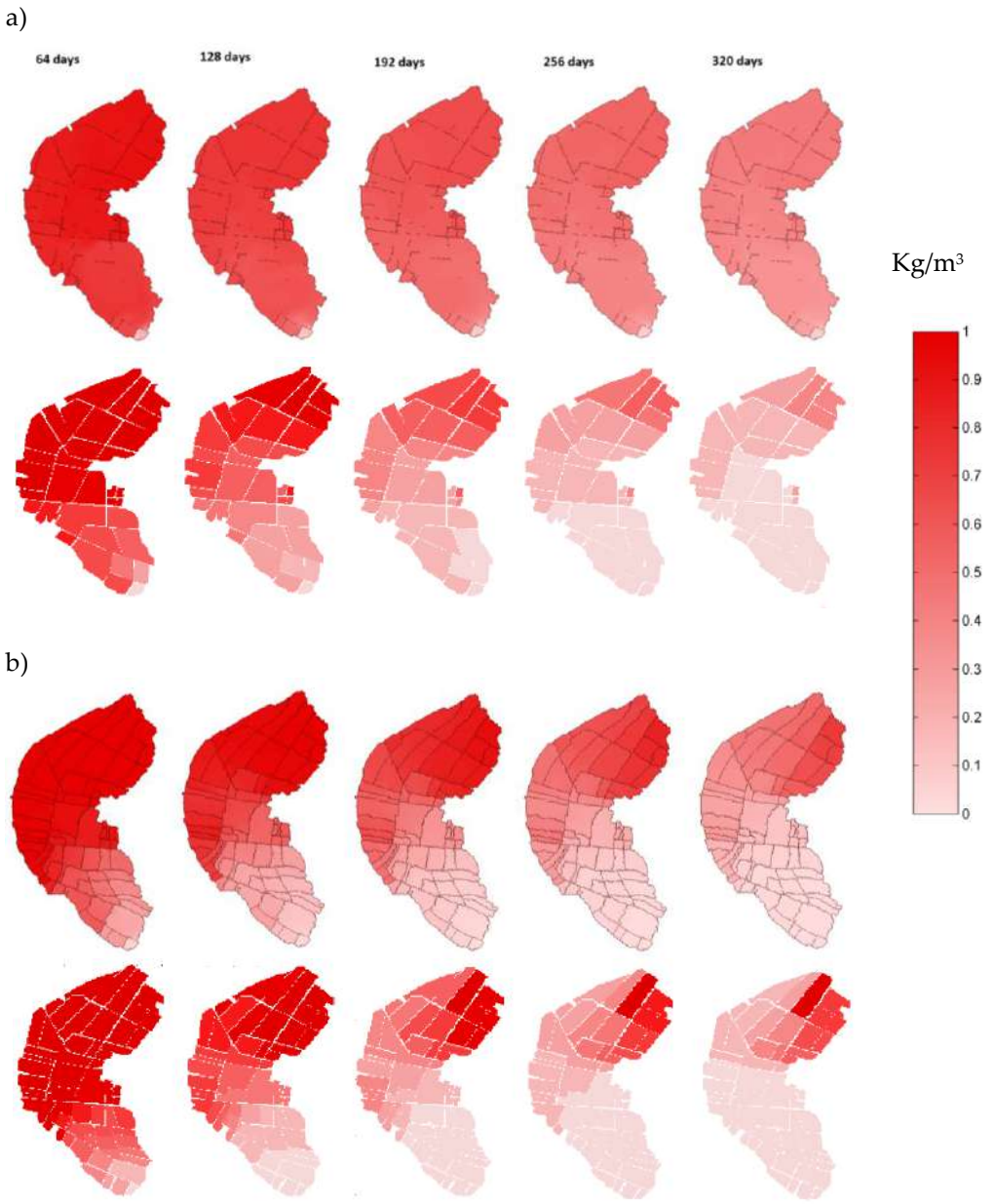

Figure 6.8 Snapshots of tracer concentration at 5 different time steps within the basin in the a) present and b) in the 50s/60s configuration. The top row of each panel refers to the Delft3D simulation, the bottom row shows the results of the box model.

As expected, the more isolated ponds (namely the northern-eastern ones) show an accumulation of the tracer in the old configuration: the system has altogether a lower residence time (the conventional time T_{37} decreases from 310 days to 255 days). However, in the 1950s-1960s configuration there are wider differences between the concentration of the ponds and several ponds have a much longer renewal time.

Overall, the present configuration more closely resembles a CSTR, while the 50s/60s's behavior approaches that of a PFR. The present system of Torbiere takes approximately 55 days longer to remove 63% of the initially present pollutant.

Comparing the results obtained with the box model and the 3D model, one can observe that the conceptual model is, by construction, less diffusive and the differences between old water concentrations between ponds are much sharper. Whereas this was an obvious consequence of the simplified approach, one can also observe that the model shows a stronger persistence of *old water* in the more peripheral areas, leading to an overall higher residence time. This is due to one of the limits of the box model: as the transport of old water is only due to differences in water levels, once a parcel is found at a dead end, due to the stationary regime, there is no way it can flow out. Furthermore, it does not include wind, which in Torbiere, by creating an alternating setup, is the main driving force of the inner circulation.

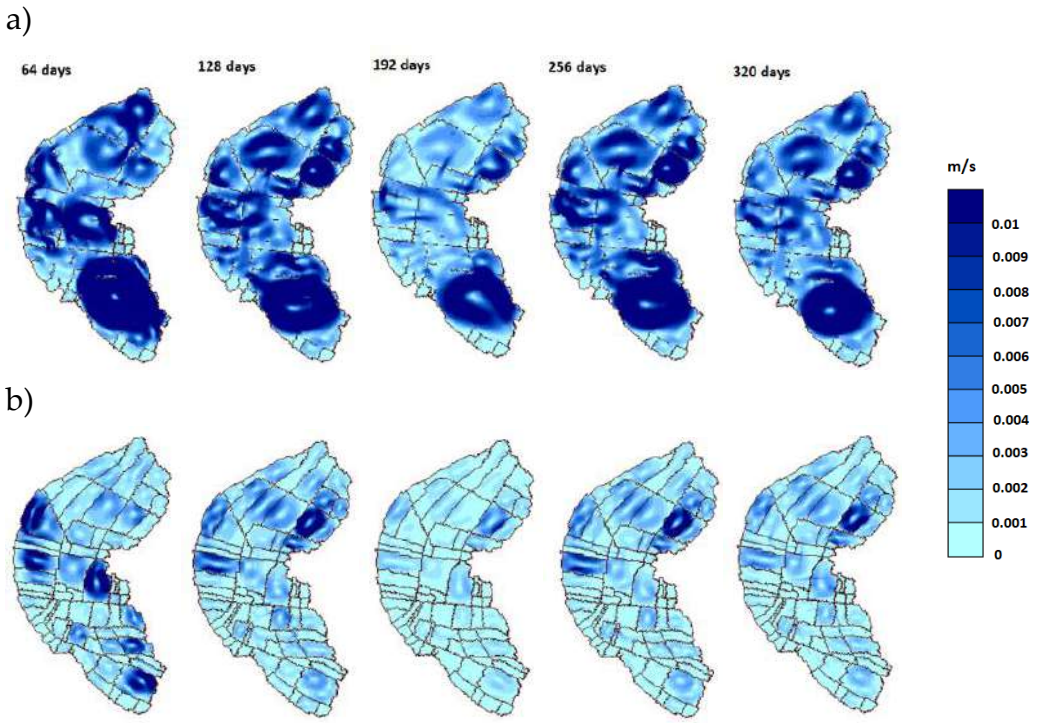

Figure 6.9 a) Comparison between the depth-average horizontal flow velocity within the basin in the present and in the 50s/60s configuration at 5 different time steps.

Another way to look at the results is by observing the maps of the flow field obtained with Delft3D (figure 6.9). Large open ponds favour the development of currents of higher velocities thanks to the higher fetch along which the wind can act. For this reason, flow velocities, even if forced by the same wind, are overall higher in the present configuration and recirculation within each pond is enhanced as also shown in the enlarged figure 6.10a. In the 50-60s configuration, the flow is channelled from pond to pond and undergoes smaller local velocities. Weaker vortices form only in the biggest ponds and overall, the transport in the South-North direction is more efficient.

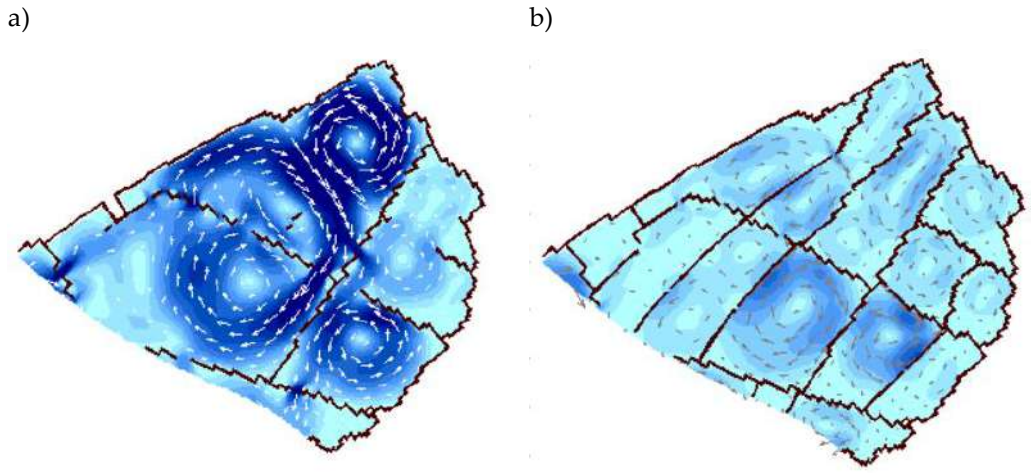

Figure 6.10 Flow field in the northern portion of the basin after 64 days of simulation in the a) present configuration and in the b) 50-60s configuration

In conclusion, the evaluation of residence time of Torbiere was done by observing the decaying concentration of a conservative tracer that has a unitary concentration constant all over the domain at time t_0. This approach proved to be effective and simple, as it allows to extract the residence time, here identified as T_{37} in analogy to the CSTR theory, by simply looking at the time when 37% of the initial concentration is still present in the basin, as it is representative of the *old* water concentration. This analysis was done comparing two approaches: a box model, implemented *ad hoc*, and a 3D model, using Delft3D -FLOW module. Although the box model showed quite similar results as the 3D model – and at a much lower computational burden - it cannot include the effect of the alternating wind and is not reliable when it comes to reproducing what happens at a dead end, so that it should be improved in these directions. For instance, we argue that the

introduction of a turbulent diffusion effect at the interface between two boxes, by which the old water concentration can be transported even if the level between two neighboring ponds is the same, would overcome the issue of old water accumulation at dead ends.
By using the average values of current discharges, rainfall and evaporation, we found that the present residence time of Torbiere is 310 days, 55 days longer than it would be if the internal bank configuration was that of 1950s-1960s. The tracer removal curves obtained with these two different geometries show that at the moment, Torbiere's basin more closely resembles the behavior of a completely stirred tank reactor, which is known in literature for not being the most efficient in terms of removal capacity of an incoming pollutant. On the other hand, the more tortuous path that the flow undergoes in the 50s-60s configuration, resembles a plug flow reactor: a minimum contact time is guaranteed for the removal of the pollutant and the tracer is driven towards the outlet in a more controlled way. Areas close to the inlet are found with much lower concentrations, while towards the outlet there are ponds with greater concentrations. Considering that often the pollutants are not passive, and their kinetic and reaction rates are also controlled by the concentration, in a real system, this leads to a higher removal rate.

Overall, the comparisons of the two behaviors confirmed the idea that the demolition of the internal banks of Torbiere, thought as a way to improve the degree of connectivity, actually decreased the removal capacity of the basin and arguably has worsened its water quality.

We believe that this changes, however dramatic, are not irreversible and, thanks to these findings, a remediation strategy can be proposed for the case study of Torbiere del Sebino, as presented in the following chapter.

6.4 A proposal for a remediation strategy

As a PFR allows to reach the same fractional conversion with a lower volume than a CSTR, a suitable remediation strategy can be deduced, that would at the same time increase the conversion process and protect some ponds from the incoming pollution of the inflow. It consists of the creation of a channel-shaped wetland that will receive the waters of the Rì's channel and the CSO, while the ponds to the sides will remain isolated and

protected from the incoming nutrient loading. Thanks to the combination of the inner channel geometry, resembling a plug flow reactor, and the plantation of cattails covering 50% of its whole area, the two affluents' pollutant load may be treated more efficiently than in the current situation.

For the evaluation of this remediation scenario, a dynamic numerical box model in the MatLab environment is used, that solves the following differential equations for the Nitrogen cycle (Chapra S.C, 1997):

$$\begin{cases} \frac{d(PON)}{dt} = -v_{0PON}[PON]\frac{A}{V} - k_{hPON}{\theta_{PON}}^{T-20}[PON] & [6.20] \\ \frac{d(DON)}{dt} = k_{hPON}{\theta_{PON}}^{T-20}[PON] - k_{hDON}{\theta_{DON}}^{T-20}[DON] & [6.21] \\ \frac{d(NH_4)}{dt} = k_{hDON}{\theta_{DON}}^{T-20}[DON] - \frac{[DO]}{[DO]+H_{DO}}k_{nitr}{\theta_{DO}}^{T-20}[NH_3] - \left(\frac{[NH_4][NO_3^-]}{(Pamp+[NH_4])(Pamp+[NO_3^-])} + \frac{[NH_4]+Pamp}{([NH_4]+[NO_3^-])(Pamp+[NO_3^-])}\right) * a_{na}k_{gM}{\theta_M}^{T-20}[\phi M]\frac{A}{V}\frac{[NH_4]}{[NH_4]+H_{NH_4}} & [6.22] \\ \frac{d(NO_3^-)}{dt} = \frac{[DO]}{[DO]+H_{DO}}k_{nitr}{\theta_{nitr}}^{T-20}[NH_4] - (1-Pap_1)a_{na}k_{gM}{\theta_M}^{T-20}[\phi M] \frac{A}{V}\frac{[NO_3^-]}{[NO_3^-]+H_{NO_3^-}} - (1-\frac{[DO]}{[DO]+H_{sodn}})k_{dn}\theta_{dn}^{T-20}[NO_3^-] & [6.23] \end{cases}$$

Where all the parameters are described in Table 6.1.

Whereas the actual nutrient removal process should include a model comprehensive also of the Phosphorous cycle and of other sink effects, the simpler nitrogen cycle can be selected as a simplified back-of-the-envelope evaluation of the remediation scenario.

Moreover, nitrates are chosen as the target pollutant to be removed, as they are the most common form in the affluent waters and present the furthest concentration from the receiving waters of Lake Iseo. The removal efficiency of nitrates, in order to obtain a good quality outflow (according to the Limeco index, DM 260/2010) is 90%.

To this purpose, two forms of organic Nitrogen are modeled, together with ammonium and Nitrates, while cattails represent the only uptake and are considered to have a constant biomass per unit area. Although, among different plants, cattails are some of the least efficient, they are the only species already present in Torbiere. Therefore, one can assume they will be

able to develop if a suitable habitat is created. This requires a depth shallower than 1 m and slow running waters.

Equation 6.20 describes the dynamics of the particulate organic Nitrogen, which is removed by settling and through hydrolysis, which converts it into its dissolved form. The hydrolysis term becomes positive in the Dissolved Organic Nitrogen equation (6.21), while it is removed by its own hydrolytic reaction, which transforms it into ammonium. Ammonium is removed (equation 6.22) by nitrification and by the cattails' uptake. The portion of nitrified Nitrogen constitutes a positive term for the balance of nitrates (equation 6.23), which are removed by cattails as well as denitrification.

Parameter	**Description**	**Value**	**Unit**
v_{oPON}	Settling velocity of PON	0.3	m/day
k_{hPON}	Maximum hydrolysis rate of PON	0.03	1/day
θ_{PON}	Temperature coefficient for PON hydrolysis	1.07	-
k_{hDON}	Maximum hydrolysis rate of DON	0.03	1/day
θ_{DON}	Temperature coefficient for DON hydrolysis	1.07	-
H_{DO}	Half-saturation constant for Oxygen for nitrification	1.7	µg/L
k_{nitr}	Maximum rate of nitrification	0.04	1/day
θ_{Nitr}	Temperature coefficient for nitrification	1.07	-
$Pamp$	Preference of phytoplankton for ammonia	20	µg/L
k_{gM}	Maximum uptake rate for cattails	0.167	1/day
θ_{M}	Temperature coefficient for cattails uptake	1.07	-
ϕ	Fraction of bottom area covered in cattails	[0.3,0.4,0.5]	-
M	Cattails biomass in dry weight	$3*10^7$	µg/m^2
a_{na}	Fraction of N in dry cattails biomass	0.025	gN/g
H_{NH4}	Half-saturation constant for ammonium uptake	0.01	µg/L
$H_{NO3\text{-}}$	Half-saturation constant for nitrate uptake	0.01	µg/L
H_{sodn}	Half-saturation constant for denitrification	1.7	µg/L
k_{dn}	Maximum denitrification rate	0.05	1/day

θ_{dn}	Temperature coefficient for denitrification	1.7	–

Table 6.1 Parameters and their value for the dynamic model (Chapra S.C, 1997)

The Nitrogen cycle simulated by the model is shown in Figure 6.11. The removal of nitrates is eventually reached by means of the uptake of cattails and denitrification. However, being the system so shallow and mixed, we did not measure any Oxygen depletion, and denitrification could never be triggered, but within the sediments.

The initial conditions are set so that the reactor is filled with water coming from a potential flood event of both Rì and CSO. The initial concentrations of the Nitrogen compounds were reconstructed based on the work of Nizzoli et al. (2020) and are shown in Table 6.2.

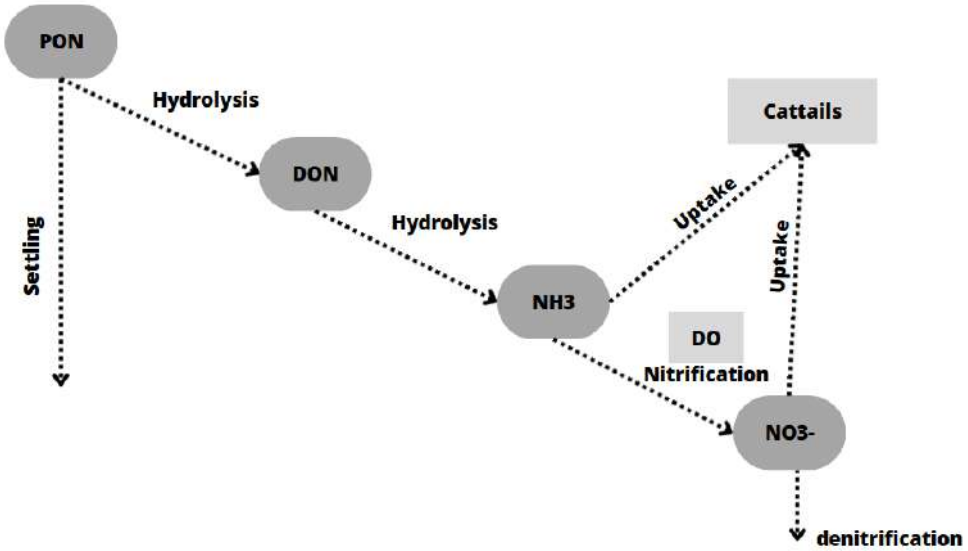

Figure 6.11 Schematic of Nitrogen Cycle model

Parameter	Value
Particulate Organic Nitrogen (PON)	125 µg/L
Dissolved Organic Nitrogen (DON)	26 µg/L
Ammonium (NH4)	41 µg/L
Nitrates (NO_3^-)	1600 µg/L

Table 6.2 Initial concentrations of Nitrogen compounds

The simulation is run without inflow and outflow, in order to single out the effects of the inner kinetics. Temperature in the system was chosen to be equal to 10°C, as in the coldest months of the year of Torbiere, in a

conservative approach that considers the period where reaction rates are the slowest.

Four scenarios are modeled, considering cattails covering 30%, 40%, 50% and 60% of the bottom area of the wetland. Results show that a removal of 90% of nitrates can be reached with a contact time T of 80, 60, 50 and 40 days, respectively. The area of the constructed wetland can be therefore derived as (Crites R.W., 1994):

$$A_{CW} = \frac{QT}{h\phi} \qquad [6.24]$$

Where h is the average depth of the wetland and ϕ is the void ratio (0.3, 0.4, 0.5 and 0.6 according to the scenario).

Considering a daily average discharge of 5000 m^3/day and a water depth of 1 m, suitable for the cattails' growth, this leads to a wetland area of 1'400'000, 760'000, 510'000 and 410'000 m^2.

As an example of this strategy, a wetland layout is proposed in figure 6.12 with a wetland of extension 610'000 m^2 that collects the waters of the two tributaries transferring them along a channeled path towards the outlet to Lake Iseo.

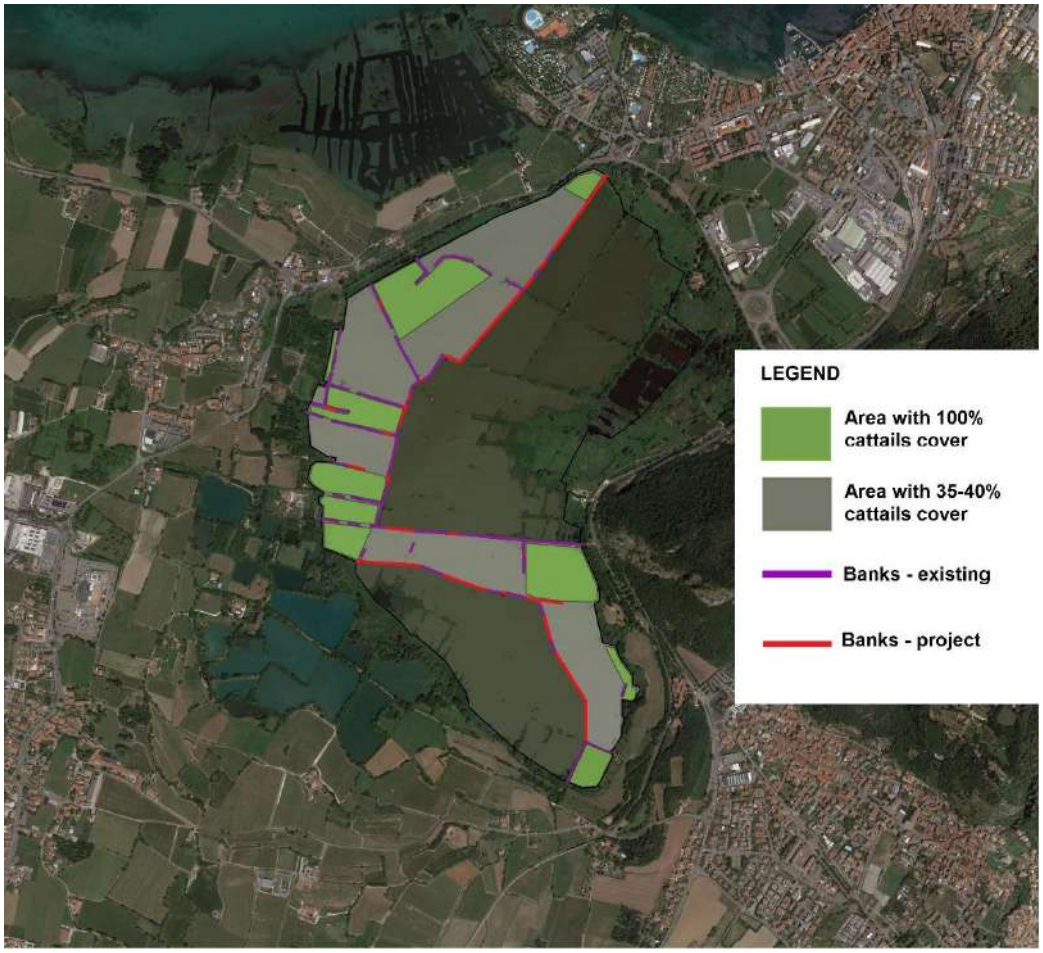

Figure 6.12 Design of the constructed wetland

The design follows the present and the former configurations of the banks of Torbiere. In this way, no major changes are made to the appearance of the wetland, and the costs of the interventions are strongly limited (controls on the banks' structure and periodic mowing of the cattails). The ponds involved in the constructed wetlands are the shallowest ones, so that depth is as constant as possible, and plants are able to grow. Cattails cover an area equivalent to 50% of the total wetland: some areas (23% of total) are covered for 90-100% by cattails, the remaining area is occupied by cattails for 35-40%. The average depth of the constructed wetland is 1 m, while the side ponds keep their current bathymetry. The new banks would be at least 1.4 m high, to reduce the possibility of wave overtopping and erosion during windy periods. The pump located downstream would be no longer needed and would be replaced by a broad-crested weir of length L = 2 m and height 1.15 m so that Torbiere would naturally deliver to lake Iseo a discharge, according to the stage-discharge relationship:

$$Q_{out} = 0.385 * L\sqrt{2g}(h_{water} - h_{weir})^{3/2} \quad [6.25]$$

The hydraulic franc of 15 cm is chosen to laminate the peak discharges of Rì and the CSO during flood events, which might deliver a volume of 2300 m^3 (as from the study of the University of Brescia described in chapter 2.4.6) and 60000 m^3, respectively.

The ponds that would remain isolated are the ones on the side of the wetland and their water balance would now be only governed by rainfall and evaporation. Based on meteorological data (figure 3.42), rainfall is enough to overcome the losses by evaporation throughout the year and these ponds would not dry out even if they stop receiving the contribution of the affluents. Once they become isolated, they will not receive the current nutrient loading anymore and other forms of bioremediation strategies could be undertaken. These might even involve sediment removal or capping, to prevent internal loading.

6.5 References

Bolin B. and Rodhe H. (1973). A note on the concepts of age distribution and transit time in natural reservoirs. *Tellus*, Vol.25, 58-62.

Bravo H.R., Hamidi S.A., Anderson E.J., Klump J.V. and Khazaei B. (2020). Timescales of transport through Lower Green Bay. *Journal of Great Lake Research*, Vol.46(5), 1292-1306.

Chapra S.C. (1997). Surface Water-Quality Modelling. *WCB McGraw-Hill*.

De Brauwere A., De Brye S, Blause S. and Deleersnijder E. (2011). Residence time, exposure time and connectivity in the Scheldt Estuary. *Journal of Marine Systems,* Vol.84(3), 85-95

Crites R.W. (1994). Design criteria and practice for constructed wetlands. *Wat. Sci. Tech*., Vol. 29, 1-6.

De Paggi S.B.J. and Paggi J.C. (2008). Hydrological connectivity as a shaping force in the zooplankton community of two lakes in the Paranà river floodplain. *International Review of Hydrobiology*, Vol.93(6), 659-678.

Deltares, 2020. Delft3D-FLOW User Manual.

Dimian A.C. (2003). Integrated Design and Simulation of Chemical Processes. s.l. *Elsevier*, 0-444-82996-2.

Dincer, T. (1968). The use of oxygen-18 and deuterium concentrations in the water balance of lakes. *Water Resources*, 4: 1289-1306.

Dronkers J. and Zimmerman T.F. (1982). Some principles of mixing in tidal lagoons. *Oceanologica Acta, Proceedings of the International Symposium on Coastal Lagoon*, Bordeaux, France, 107-11.

Gao X., Xu L., and Zhang C. (2016). Estimating renewal timescales with residence time and connectivity in an urban man-made lake in China. *Environmental Science and Pollution Research*, Vol. 23, 13973-13983.

Huang J., Yan R., Gao J., Zhang Z. and Qi L. (2016). Modelling the impacts of water transfer on water transport pattern in lake Chao, China. *Ecological Engineering*, Vol.95, 271-279.

Kadlec R.H and Wallace S.D. (2009). Treatment wetlands, second edition.

Li Y., Acharya K., Chen D. and Stone M. (2010). Modelling water ages and thermal structures of lake Mead under changing water levels. *Lake and Reservoir Management*, Vol.26, 258-272.

Li Y., Acharya K. and Yu Z. (2011). Modelling impacts of Yangtze River water transfer on water ages in Lake Taihu, China. *Ecological Engineering*, Vol.37, 325-334.

Liu S., Ye Q., Wu S. and Stive M.J.F. (2020). Wind effect on the water age in a large shallow lake. *Water*, Vol.12(5), 1246.

Liu Z., Wang H., Guo X., Wang Q. and Gao H. (2012). The age of Yellow River water in the Bohai Sea. *Journal of Geophysical Research*, Vol.117.

Monsen, N.E., Cloern J.E. and Lucas L.V. (2002). A comment on the use of flushing time, residence time, and age as transport time scales. *Limnology and Oceanography*, Vol.47(5), 1545-1553

Nguyen T.D., Pramod T., Anderson E.J., Phanikumar M.S. (2014). Summer circulation and exchange in the Saginaw Bay-Lake Huron systems. *Journal of Geophysical Research*, Vol.119(4), 2713-2734.

Nizzoli D., Scibona A. (2020). Analisi dei carichi di nutrienti generati e veicolati nel bacino drenante le Torbiere di Iseo nell'ambito del progetto di Acque Bresciane denominato "Torbiere", Relazione finale.

Pilotti M., Simoncelli S. and Valerio G. (2014). A simple approach to the evaluation of the actual water renewal time of natural stratified lakes. *Water Resources Research*, Vol.50, 2830-2894.

Reddy K.R. and D'Angelo E.M. (1997). Biogeochemical indicators to evaluate pollutant removal efficiency in constructed wetlands. *Water Science Technology*, Vol. 35(5), 1-10.

Pal, B. K., Murthy, R. & Thomson, R. E., 1998: Lagrangian measurements in Lake Ontario. *J. Great Lakes &s*. 24(3): 681--697.

Pilotti, M., Simoncelli, S., Valerio, G. (2014). A simple approach to the evaluation of the actual water renewal time of natural stratified lakes. *Water Resources Research,* VOL. 50, Issue 4, pages 2830–2849.

Qi H., Lu J., Chen X., Sauvage S. and Sanchez-Pérez J.M. (2016). Water age prediction and its potential impact on water quality using a hydrodynamic model for Poyang Lake, China. *Environmental Science and Pollution Research*, Vol.23, 13327-13341.

Sanderson, B. G., 1987: An analysis of Lagrangian kinematics in Lake Erie. *Great Lakes &s*. 13(4): 559-567.

Shen Y.M., Wang J.H., Zheng B.H., Zhen H., Feng Y., Wang Z.X. and Yang X. (2011). Modeling study of residence time and water age in Dahuofang Reservoir in China. *Science China*, Vol.54(1),127-142.

Thackston, E.L., Shields F.D. and Schroeder P.R. (1987). Residence time distribution of shallow basins. *Journal of Environmental Engineering*, Vol.113(6).

Books

Levenspiel O. (1999). Chemical Reaction Engineering (Third Edition). *John Wiley & Sons*.

Schmidt, Lanny D. (1998). The Engineering of Chemical Reactions. *New York: Oxford University Press.*

Sperling M.V., Verbyla M.E., Oliveira S.M.A.C. (2020). Assessment of treatment plant performance and water quality data. *IWA Publishing*, London, UK.

Others

DM 260/2010, Regolamento recante i criteri tecnici per la classificazione dello stato dei corpi idrici superficiali, per la modifica delle norme tecniche del decreto legislativo 3 aprile 2006, n. 152, recante norme in materia ambientale, predisposto ai sensi dell'articolo 75, comma 3, del medesimo decreto legislativo

7. General conclusions

This chapter contains the discussion of some of the findings previously presented, showing the importance of the monitoring and modelling activity accomplished during my research on Torbiere del Sebino. The key aspects of this complex ecosystem are summarized and the potential of 3D hydrodynamic modelling in this particular case is shown. Finally, some of the limits of this research are presented, together with some recommendations for future research.

Heterogeneity of the habitats and homogeneity in the abiotic parameters

Torbiere are a heterogeneous system, with ponds that differ in their mixing regimes and abiotic variable distribution. These differences depend on the depth of the ponds and the nature of their inflow. This is why Lame, characterized by a fairly constant bathymetry and by the same inflow, present the same abiotic parameters everywhere.

Lame, which represent the greatest portion of Torbiere, are characterized by shallow ponds (< 2 m average depth). They are polymictic and thermal stratification can establish only for some hours during the warmest months of the year, but it is always disrupted during each night. These ponds are directly fed by the stream Rì, which drains a 6 km^2 urbanized watershed, and are affected by the CSO of the municipality of Provaglio di Iseo. Their volumetric discharges contribute to half of the yearly entering volume of Lame (the other half is represented by rainfall); therefore, they have a great influence on the water quality of the ponds. Lame's waters are turbid, especially in the Southern ponds where the two inflows enter Torbiere, and transparency remains below 40 cm during several months of the year due to the frequent recurrence of algal blooms (which have been recorded also during winter months). Furthermore, the extension of these Southern ponds, with very few separating banks, allow for the action of the wind that can easily resuspend the sediments.

The influence of the nature of the inflow on the water quality of the receiving waters is clear when observing the only pond of Lame, so called Fontani's pond, that is fed by the groundwater. Its waters are transparent and water lilies cover its surface; turbidity is extremely low while specific

conductivity shows a maximum, due to the karst origin of the waters. Fontani's pond is the only example of a macrophyte-dominated pond in Lame and raised the hypothesis that a different source of inflow can actually trigger a different equilibrium in the waters.
Contrary to our original idea of a possible anoxic situation in the waters, suggested by the eutrophic nature of Lame, there's plenty of Oxygen in their waters, an idea based also on the lack of systematic measurements before of our research. On the contrary, Oxygen levels turned out to be generally high and usually above the saturation level, due to both the photosynthetic contribution and the re-aeration exerted by wind on this shallow system. The polymictic nature of Lame ensures that an Oxygen gradient hardly establishes during the day and the reaeration process compensates for the sediment Oxygen demand.
A different situation is found in the Southern clay ponds. They are much deeper (up to 8 m) and fed mostly by precipitation, runoff and probably some groundwater springs, with very small discharges coming during heavy rainfall events. A summer survey on the vertical profiles of temperature, dissolved Oxygen and specific conductivity in one of these ponds revealed a strong stratification, where the surface 4 m were separated from the bottom layer by a steep gradient in the above-mentioned parameters. Oxygen was below 3 mg/L at the bottom and the presence of a salinity gradient that could not be won by the wind was evidenced by the measured profile of specific conductivity. By monitoring water temperature at two different depths for a year-long period, we concluded that these ponds are actually monomictic and reach vertical uniformity during winter months, when bottom waters re-oxygenate.

Numerical modelling of Torbiere

Even in this case 3D hydrodynamic modelling proved to be a powerful tool for learning more about a complex system like Torbiere.
Temperature and water level modelling were used to reproduce diurnal stratification and to check the accuracy of the mass balance terms, respectively. Delft3D-FLOW package was used, and its sensitivity was tested against several parameters, revealing the need for a proper

calibration of the horizontal eddy viscosity and diffusivity and of the Manning's roughness coefficient.
Being the flow field of Torbiere characterized by low velocities (few cm/s), advection has a minor role and the transport and mixing of substances are strongly influenced by diffusive terms, that must be correctly parametrized. Again, due to the shallow nature of its waters, the bottom, although devoid of macrophites, strongly controls the magnitude of the velocities, and a correct estimation of the Manning's roughness coefficient is needed. To this purpose, for its calibration the measurements of a specifically designed drifter were used to compare the horizontal velocity values to the modelled ones. By minimizing the RMSE, the final value of n = 0.015 s/m$^{1/3}$ was eventually chosen.

Horizontal eddy viscosity and diffusivity were calibrated using the measurements of a natural plume of specific conductivity detected in April 2021. After an intense rainfall event, a plume formed in the near-field area of the affluent Rì and was measured in several points; after an interpolation, a 2D map of specific conductivity in that area was obtained. The event was then reproduced in Delft3D, using a tracer to simulate specific conductivity. By minimizing the RMSE between measured and simulated values of specific conductivity, the value of the eddy viscosity and diffusivity coefficients (which affect the lateral dispersion and transport of a tracer) was calibrated, obtaining an equal value for the two parameters of 0.05 m^2/s, similar to the one used in literature for other similar inland waters.

Drifter's design for shallow waters

Driven by the necessity of measuring flow velocities in a shallow system, where currents are very weak and there is not a principal direction of the flow, as it is mainly governed by the wind field, a drifter was designed for Torbiere. This device exploits the flexibility of the hardware Arduino, that can also host a GPS and a GSM antenna and is able to record its position in time during several measurement sessions. Despite the presence of several drifters available on the market, most of them are suitable for deep waters only. In other cases, if they are usable for shallow basins, their efficiency was not demonstrated and it is unclear how much their movements are

affected by the surface wind. Accordingly, we decided to verify the design of this drifter using Fluent ANSYS to compare the drag forces acting on the submerged portion of the device and the drag exerted by the wind on the emerged cap. The results show that the water drag is much stronger of the one exerted by wind, demonstrating that the device's motion actually reflects the average water velocity profile along the drifter height rather than being drifted by the wind.
The drifter was deployed ten times inside Lame's ponds and recorded flow velocities for an overall period longer than 70 hours. These data were used, after being pre-processed, in the calibration of the Manning's roughness coefficient.

Assessing connectivity

The observations and the monitoring campaigns of Torbiere revealed the link between the water quality of a single pond and its degree of connectivity with the others and, in particular, with the affluents' waters. Despite connectivity being a desirable feature in many natural systems, in the case of a polluted inflow, the trade-off between connectivity and water quality is not as clear in the literature. In this research, we explored our idea that, in this situation, connectivity, in place of an asset, is a flaw of the system. The historical reconstruction of the geometry of Torbiere has directed the research in this direction as well: Torbiere used to be a system of separated ponds in the 1950s, while now most of the banks have collapsed or have been demolished. Simultaneously, water quality has worsened over time, and we argued that the change in the inner geometry might have had an active role in this direction.
To investigate the effects of this change, two 3D model simulations were performed, which differed only in the geometry, in order to isolate the effects of connectivity only. A unitary tracer concentration was set as the initial condition and the systems were flushed with the average inflow discharge, characterized by a null tracer concentration. Observing the decrease in average tracer concentration in the domain over time, equals studying the percentage of the water left in the system. By comparing these decreasing curves with the theoretical ones of an equivalent completely stirred tank reactor and of a plug flow reactor, some comparisons could be

made. In particular, the 1950s' configuration resembles that of a plug flow reactor as they both create a more channeled path for the inflow waters towards the outlet. The PFR is widely known for being the most efficient reactor, as it guarantees a minimum contact time for the pollutant to be removed, avoids short-circuiting and creates accumulations of pollutant which ultimately increase the removal rate. Given the filtering role of Torbiere towards lake Iseo, its removal efficiency is important, and the collapse of the banks has compromised it: the present configuration is now similar to a completely stirred tank reactor. The reactor analogy allowed to conclude that the division in ponds of the 1950s is preferable in terms of pollutant removal efficiency and suggests the direction to follow for a possible remediation strategy. Moreover, and possibly even more important, the subdivision into separate ponds protected the more isolated ponds from the negative influence of the strong pollutant load and of the invasive species that now spread all over the area of Lame.

A back-of-the-envelope design was proposed of Torbiere, starting from the analysis of the residence time distribution. If one reproduces a PFR geometry within Torbiere, a much smaller volume would be necessary to reach the removal that is now exerted by the wetland, due to the greater efficiency of this reactor's geometry. Following this idea, a constructed wetland could be made within the volume of Torbiere, to convey the waters of the two polluted inflows and, after a channeled path where cattails have been planted with an active role on the reduction of nutrients by exploiting the natural bioaccumulation abilities of plants, delivers them to the receiving body of Lake Iseo. Given the PFR geometry, a much smaller area is needed, and the remaining ponds can be isolated from the inflows. The unique characteristics of this basin ensure that these ponds would not dry out and, once prevented the incoming pollutant loading from the affluents, other remediation strategies could be implemented to recover them. This project would guarantee the same pollutant removal exerted nowadays but would allow 2/3 of Lame's ponds to be protected by the negative influence of the tributaries. This idea follows the rules of a Nature Based Solutions and does not change the landscape, it follows what was a pristine condition of the banks of Torbiere and requires limited maintenance costs.

Limits of this research and recommendations for future works

In a situation of fundamental lack of systematic studies on the physics and chemistry of Torbiere, the attempt of understanding such a complex system is only at the beginning and, despite the previously explained findings, there are still many unresolved questions. Furthermore, the observations and the analyses carried out, arose new questions and need for new specific studies that could not be done within the period of this Thesis due to lack of time and of specific expertise.

We try here to list, without claiming to be exhaustive, a few ideas that could be followed in the future.

- A more precise quantification of the exosystemic service exerted by Torbiere is needed to put emphasis on its role and to design a constructed wetland. Lame receives the waters of Ri's and CSO and delivers them to Lake Iseo but the actual removal efficiency is difficult to estimate. This work assumed a 90% removal for Nitrates, considering the concentrations of the inflows and the one of the lake itself, but a systematic sampling campaign is recommended, where the inflows' and the outflow's qualities are monitored over time. A study on the best parameter to be used as reference should be done, considering also Phosphorus' species and the overall trophic chain.
- The temperature modelling of Lame could be improved, as it now leads to an underestimation of water temperatures during the winter. The installation of a water temperature sensor at depth could help in this direction, to validate the model during periods of diurnal thermal stratification.
- The clay tanks located in the South show a clear salinity gradient in the warmest months, that is disrupted with colder temperatures. Such a steep gradient needs to be taken into account when trying to model the water temperatures of these ponds, as it acts as a barrier to the warming of the bottom layers. As it is variable over time, a fixed salinity gradient cannot be applied to the water column and a 1D water quality model for these ponds is recommended.
- Torbiere are a phytoplankton-dominated wetland. The environmental engineering expertise needs to be complemented with a biological expertise, in order to deeply understand the mechanisms of primary production, the oxygen dynamics and to

characterize the phytoplankton species present in this system. In this direction, the installation of a fixed dissolved oxygen probe is recommended.

Appendix A: historical maps and satellite images

This appendix collects all the historical maps of Torbiere that were found, together with the satellite images obtained from Geoportal of Lombardy Region and from Google Earth service. Please note that sometimes the source of some images is absent because it was not possible to trace it back.

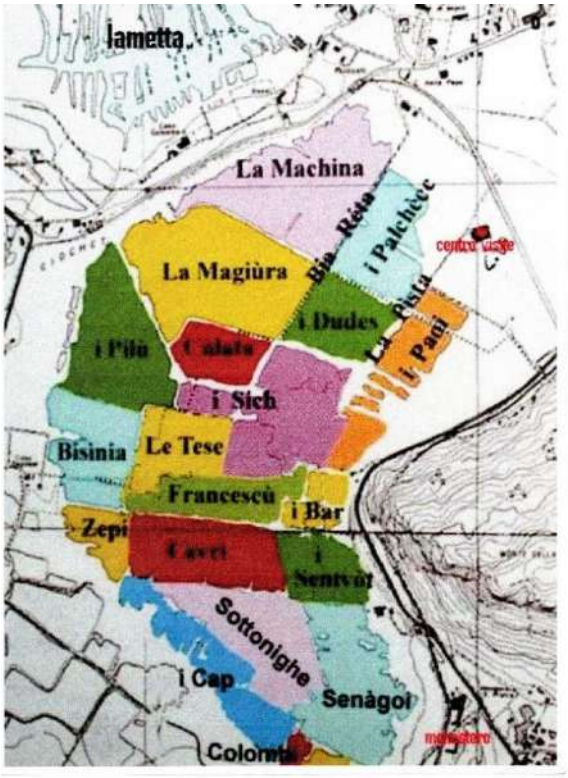

Fig. A.1 Toponyms of the different areas of Lame. *Sich* in the dialect of Brescia is "five" indicates the deepest area of Torbiere, (arguably) at 5 m depth. *La Machina*, literally "the machine" refers to the presence of the pump. *I Palchècc* means "the shelves" and indicates the presence of some stilt-like wood construction inside the waters. *I Pilù* refers to the presence of wooden poles inside this tank. *Francescù*, *Zepi* and others are family names of the surrounding municipalities, who owned those tanks.

A.1 Maps and aerial pictures of IGM (Military Geographical institute)

IGM 1885

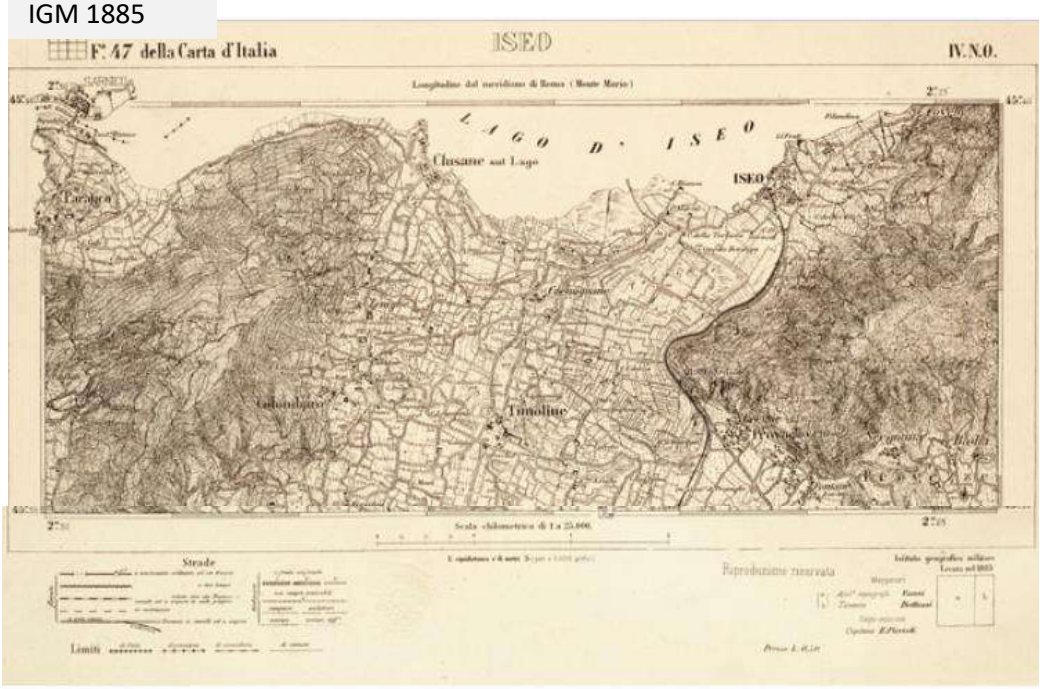

IGM 1913

IGM 1931

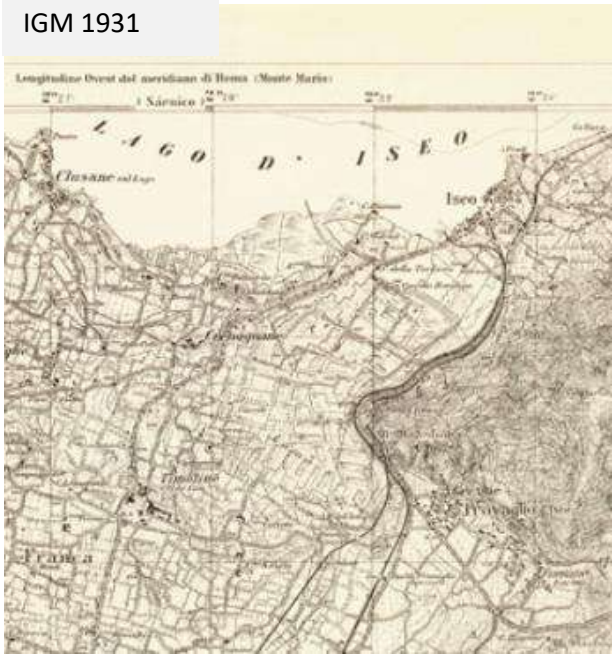

IGM 1958 area

IGM map 1959

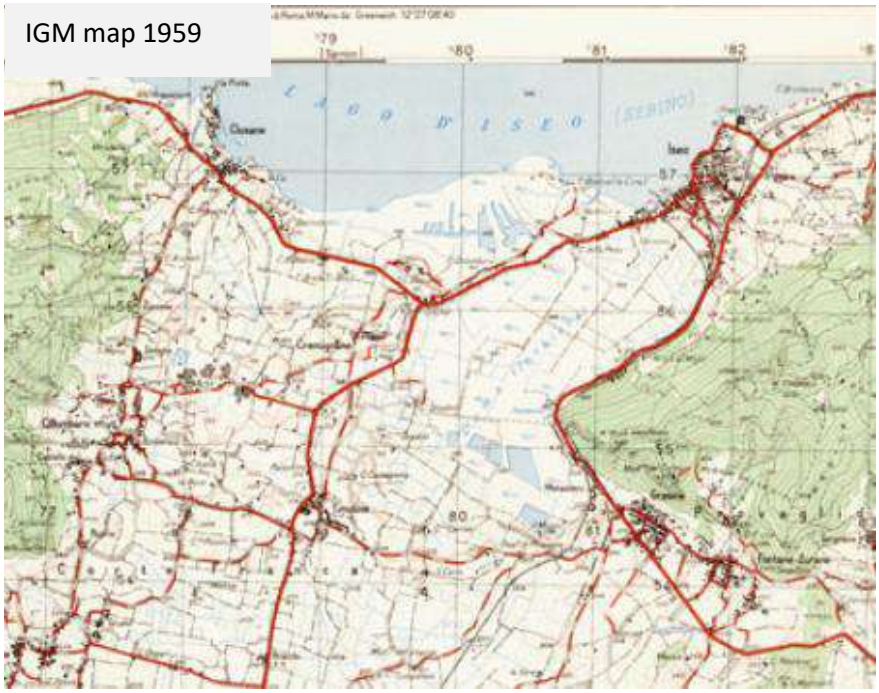

IGM map 1963

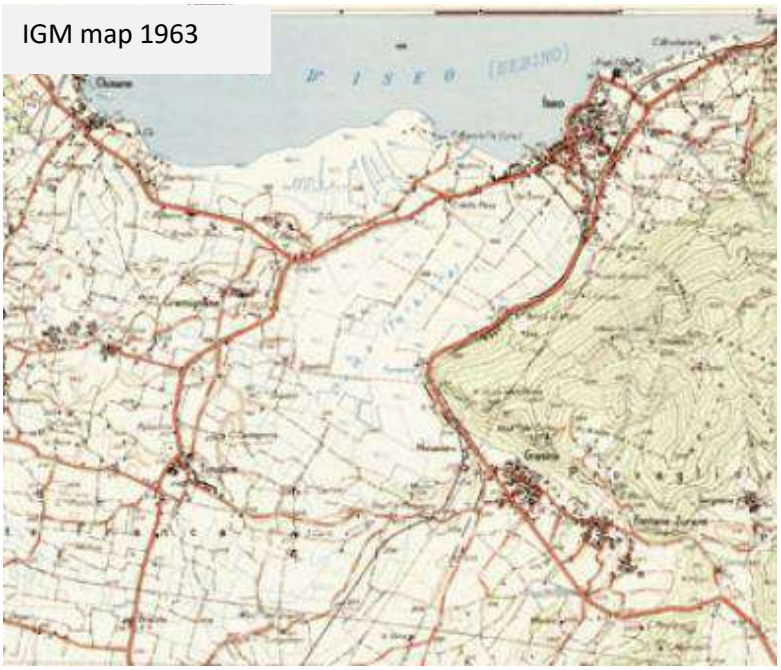

IGM 1970

IGM map 1971

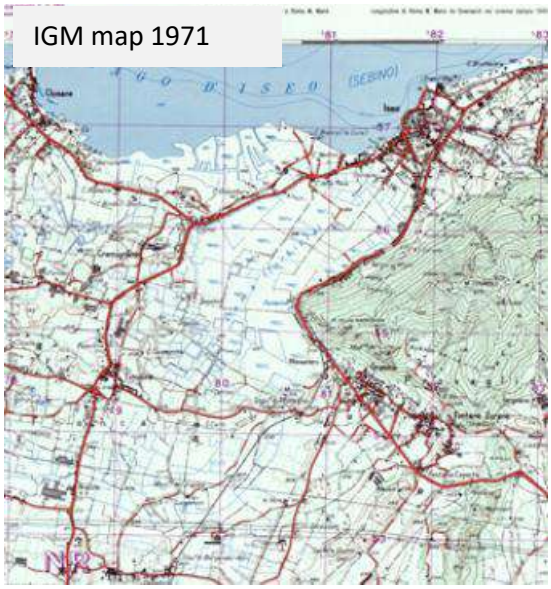

IGM map 1977

IGM 1986

IGM 1992

IGM 1992

IGM 2003

A.2 AGEA (Agenzia per le Erogazioni in Agricoltura)

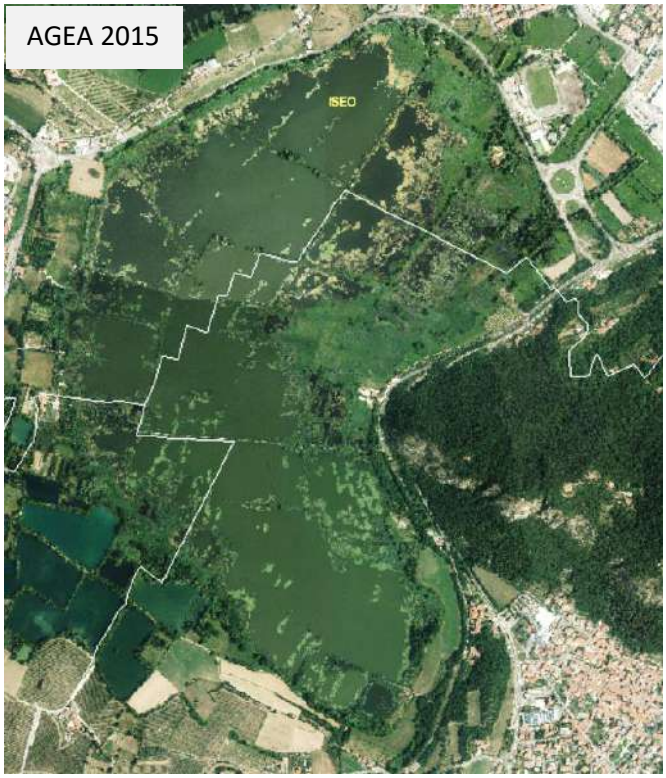

A.3 Geoportal of Lombardy Region

1975 Ortofoto Geoportale

Ortofoto geoportale 1998

Ortofoto geoportale 2003

Ortofoto geoportale 2007

A.3 GAI flight

1954 Volo GAI (Geoportale)


1980 volo

A.5 Google Earth

Google earth 2017 (July)

2017 (august)

Google earth 2018 (April)

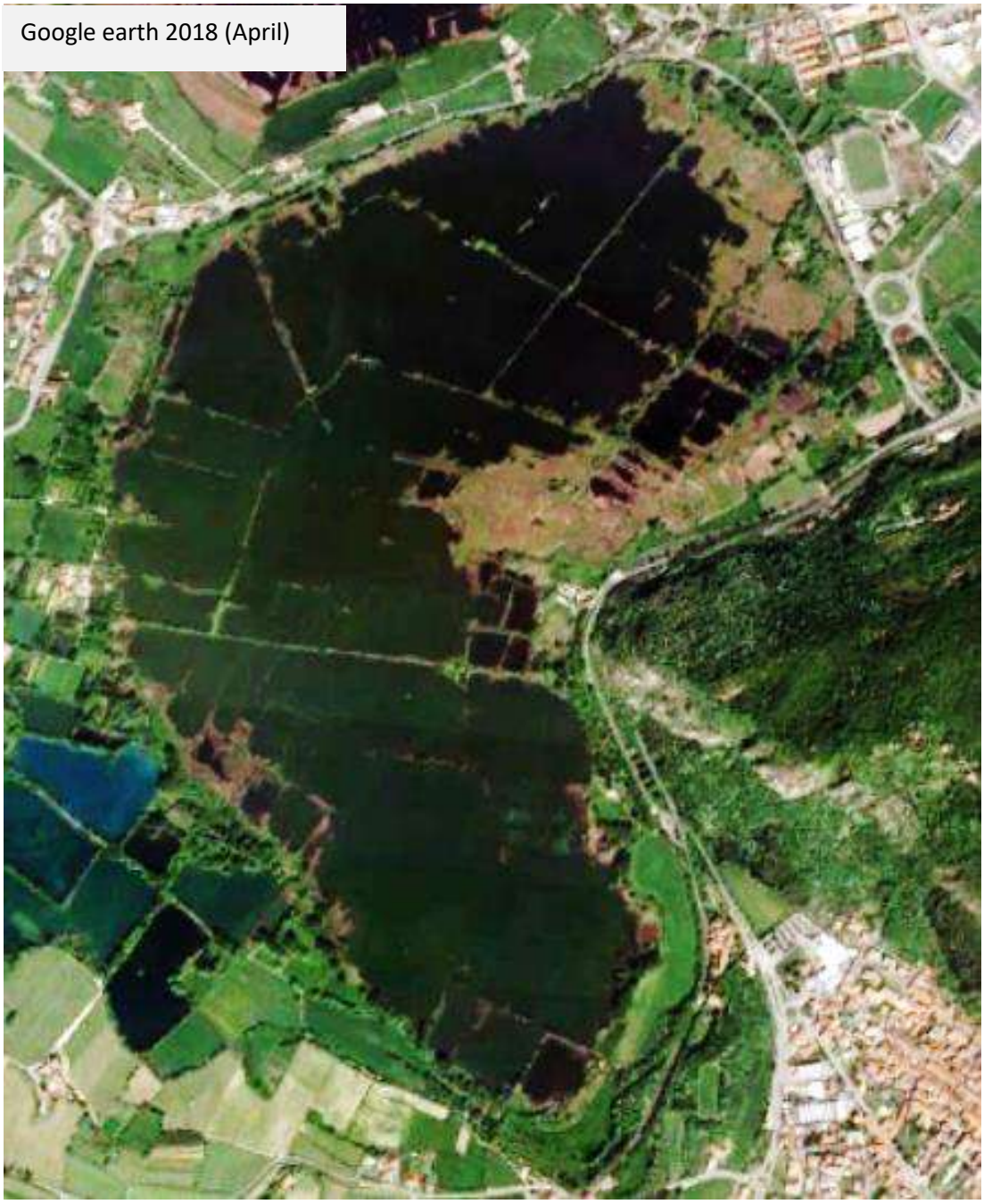

Google earth 2020 (march)

Appendix B: interviews

This appendix contains all the information gathered during the interviews with people that have lived / worked in or have experienced the territory of the Reserve of Torbiere.

B.1 Life in Torbiere

Until the 1950s some families lived inside the actual borders of the Reserve. They were mostly fishermen, and they were involved in the excavation of peat.

During the 1960s and 1970s, the area of Torbiere was still an important center for the economic lives of people of the surrounding municipalities, especially Provaglio d'Iseo. It was a hunting ground, fishing area, people collected ant nests as feed for their farm animals and collected marsh grass to rush chairs.

Before the institution of the Natural Reserve of Torbiere, visiting the area was not allowed: only hunters and fishermen could enter this territory.

B.2 Observations about the ecosystem

When asked about any changes in the biodiversity and in the conditions of the waters of Torbiere, all the interviewees agreed on:

- There used to be more water lilies in Torbiere, while now their proliferation is limited to two areas: the Fontanì tank and the arrival of the combined sewer overflow.
- There was more marsh grass around the ditches and more types of cattails. Nowadays the *amorpha fruticosa* has become the dominant, invasive species.
- Lame used to freeze completely every winter, sometimes the ice lasted until March.
- During winter, when Torbiere froze, they used to cut all the marshes and in February, the owners of each tank used to burn any left grass in a controlled manner. In this way, every spring the vegetation was renewed.
- The sediment levels have increased, waters are shallower and heat more easily.

- The sheat-fish was absent, while sunfish was extremely abundant in some shallow areas. Catfish was introduced but disappeared in 2010 due to sheat-fish. Nowadays, only large-sized fish are present, as small-sized ones are preyed by sheat-fish and cormorants.
- The water of Lame was clearer before 1970s and 1980s. There are much more cyanobacteria on the surface while in the past there used to be macrophytes. Before 1960, people used to drink the water of Torbiere.
- There were folagas, swans and ducks, while now the bird dominant species are cormorants, seagulls and herons.
- Frogs, snakes and bats were much more present.
- Overall, the biodiversity has diminished.

B.3 Observations about banks and pedestrian routes

This paragraph includes some observations about the geometry of Lame. Questions were asked about the separating banks and the connection between tanks in order to understand if there was any change in the inner circulation of water. The information that was collected are listed below.

- There once were much more banks separating the different tanks of Lame.
- There was a higher number of visiting paths that were closed to allow the nidification of certain species.
- The sole passage of waters between the southern and the northern tanks of Lame was *el tai*, a cut in the central bank that divides the two portions of Torbiere. Some passages between smaller tanks were excavated by fishermen to create zones of current to catch fish. However, more recently, additional cuts were done in between tanks, to enhance the circulation of the waters.

B.4 Other information and observations

The tanks located in the North-eastern part of Torbiere never freeze, probably due to the presence of some source of groundwater.

The groundwater fountain located in the location *fontanì* feeds the first tank located immediately westward. There's an abandoned building that used to be the aqueduct used by the families living in Torbiere and by the

population of Provaglio d'Iseo, as the other wells were not reliable because of the typhus.

Along the East-South coast of Lame there are several groundwater fountains.

Appendix C: Other drogue deployments

Chapter 6 contains the description of the drifter construction together with one example of deployment. As a total number of ten surveys was done, in this annex we show the other ones for completeness.

C.1 March 16th, 2022

The drifter was left at 03:20 pm from the main wooden pier in the central portion of Torbiere. Here the average depth is 2 m. The drifter was left floating for 42 hours and 25 minutes, during which it moved Northward and Eastward. The drifter trajectory follows the Iseo wind pattern. In the first hours, the "Ora" wind was present, that blew from South-West, resulting in the drifter going North-East. Then, the drifter remained stuck for several hours during the evening, due to the presence of reefs, it was able to move again in the night, under the action of "Vet". Overall, it has travelled a distance of 400 m, with an average speed of 0.1 cm/s.

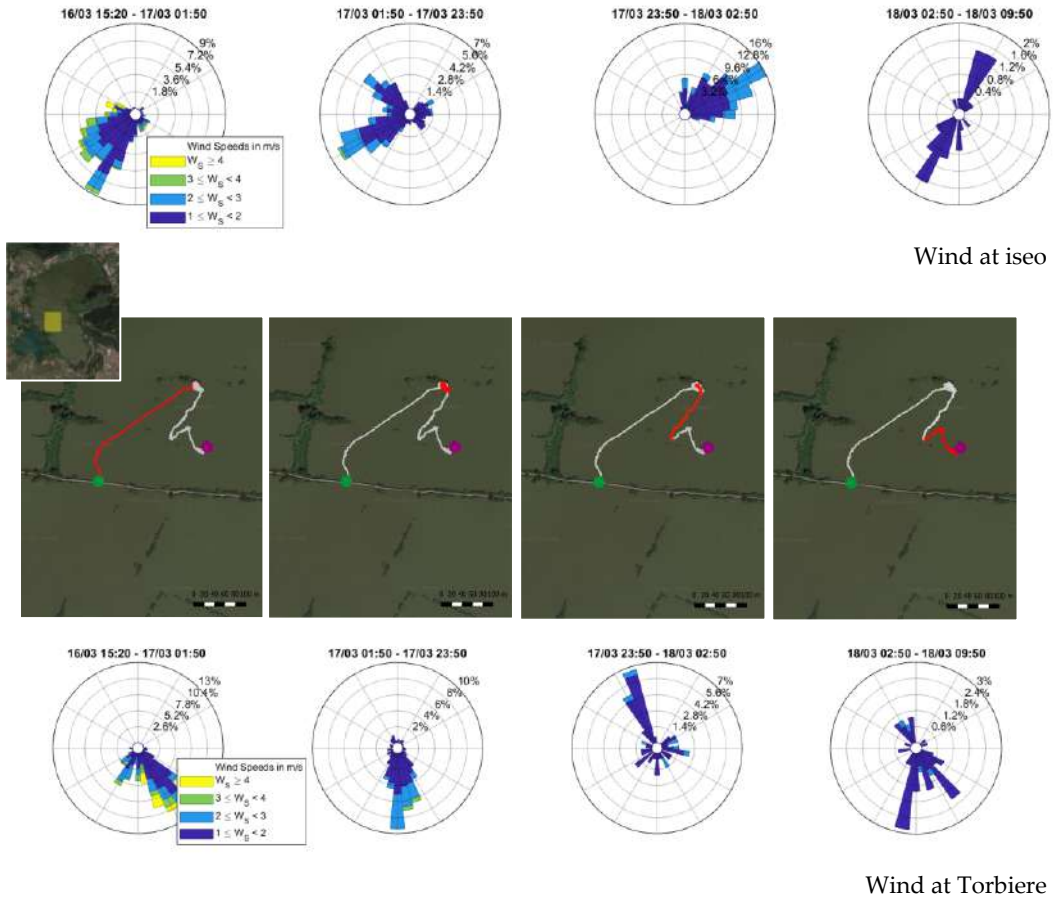

Figure C.1: Wind roses of Iseo (top row) and Torbiere (bottom row) and maps

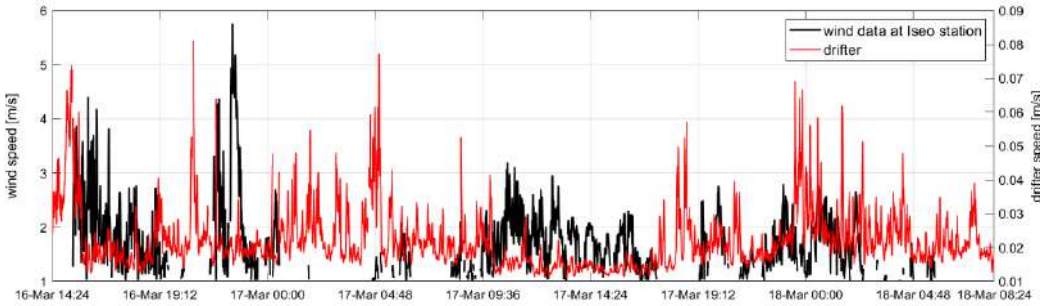

Figure C.2: Time series of wind intensities at iseo and drifter speeds.

C.2 May 13th, 2022 (#1)

The drifter was left at 10:50 am in one of the northern tanks. Here the average depth is 2.5 m. The drifter was left floating for 40 minutes during which it moved Northward. It has travelled a distance of 140 m, with an average speed of 6.2 cm/s.

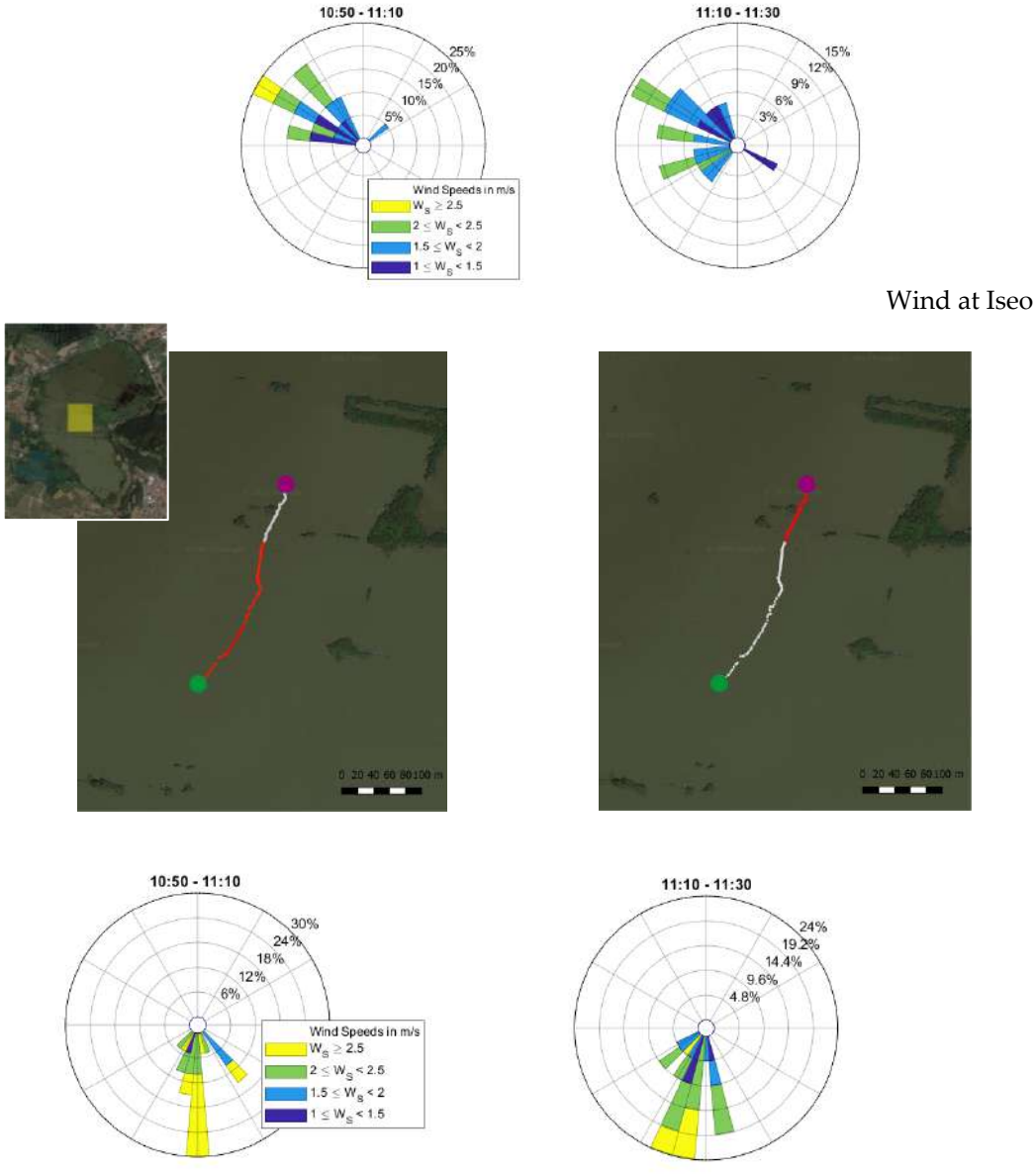

Figure C.3: Wind roses of Iseo (top row) and Torbiere (bottom row) and maps of the deployment of 13th May 2022. The campaign is subdivided into two subsections in order to visualize the wind intensity and direction acting during each sub-period.

C.3 May 13th, 2022 (#2)

The drifter was left at 10:50 am in one of the northern tanks. Here the average depth is 2.5 m and is one of the deepest areas. The drifter was left floating for one hour and fifteen minutes, during which it moved Northward and Eastward. It has travelled a distance of 102 m, with an average speed of 4.3 cm/s.

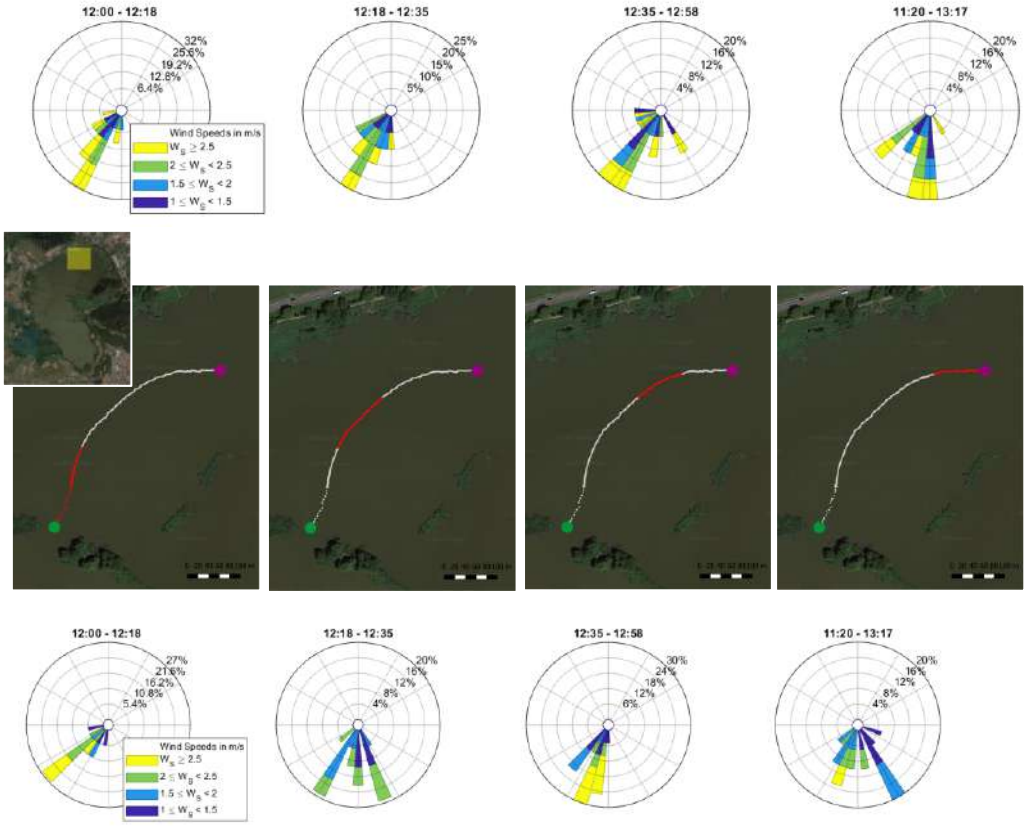

Figure C.4: Wind roses of Iseo (top row) and Torbiere (bottom row) and maps of the deployment of 13th May 2022. The campaign is subdivided into four subsections in order to visualize the wind intensity and direction acting during each sub-period.

C.4 June 10th, 2022 (#1)

The drifter was left at 09:50 am in one of the southern tanks. Here the average depth is 2.2 m. The drifter was left floating for one hour during which it moved towards South-West. It has travelled a distance of 130 m, with an average speed of 2.9 cm/s.

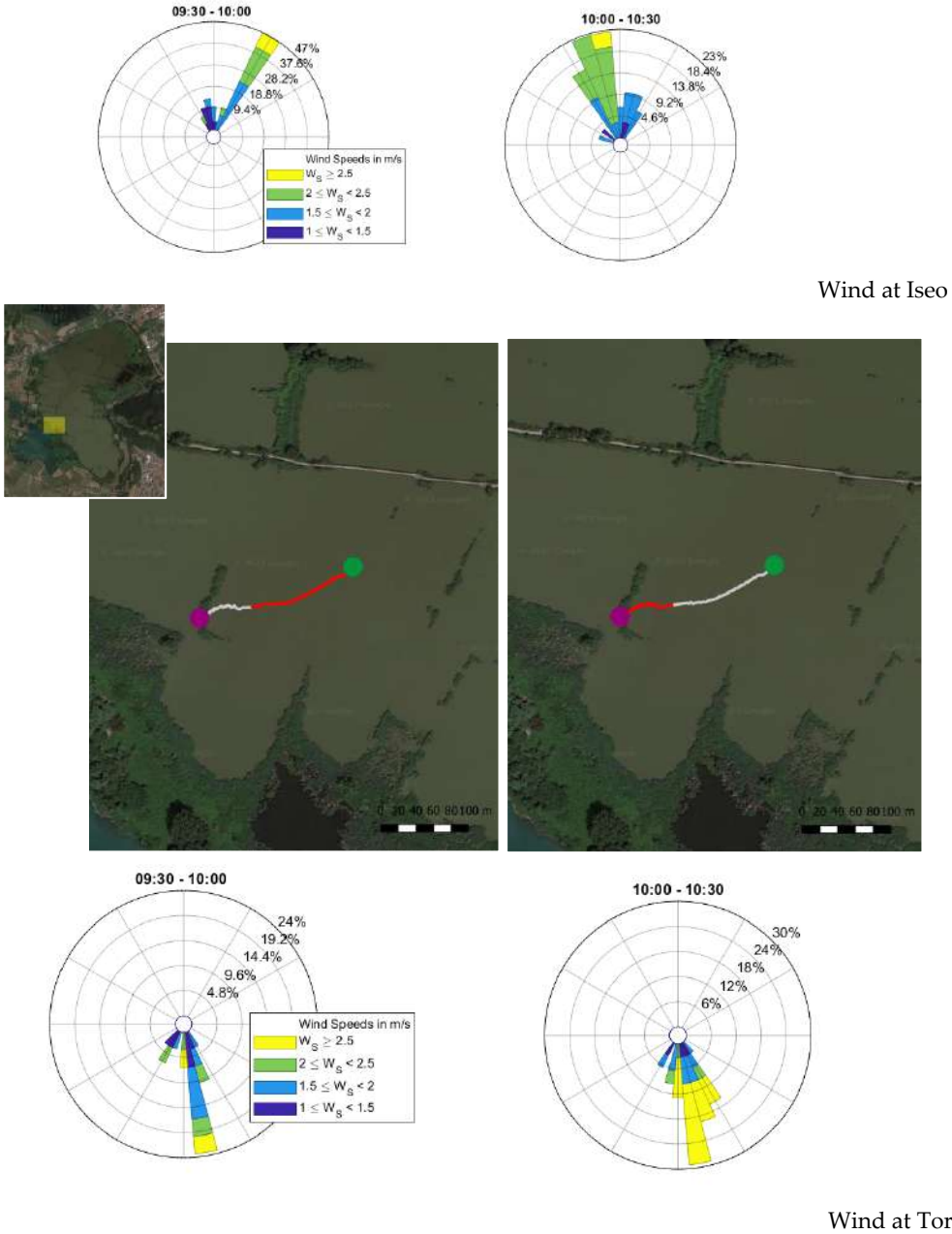

Figure C.5 Wind roses of Iseo (top row) and Torbiere (bottom row) and maps of the deployment of 10th June 2022. The campaign is subdivided into two subsections in order to visualize the wind intensity and direction acting during each sub-period.

C.5 June 10th, 2022 (#2)

The drifter was left at 10:35 am in one of the central tanks. Here the average depth is 2.2 m. The drifter was left floating for four hours and 55 minutes during which it moved towards North. It has travelled a distance of 486 m, with an average speed of 2.03 cm/s.

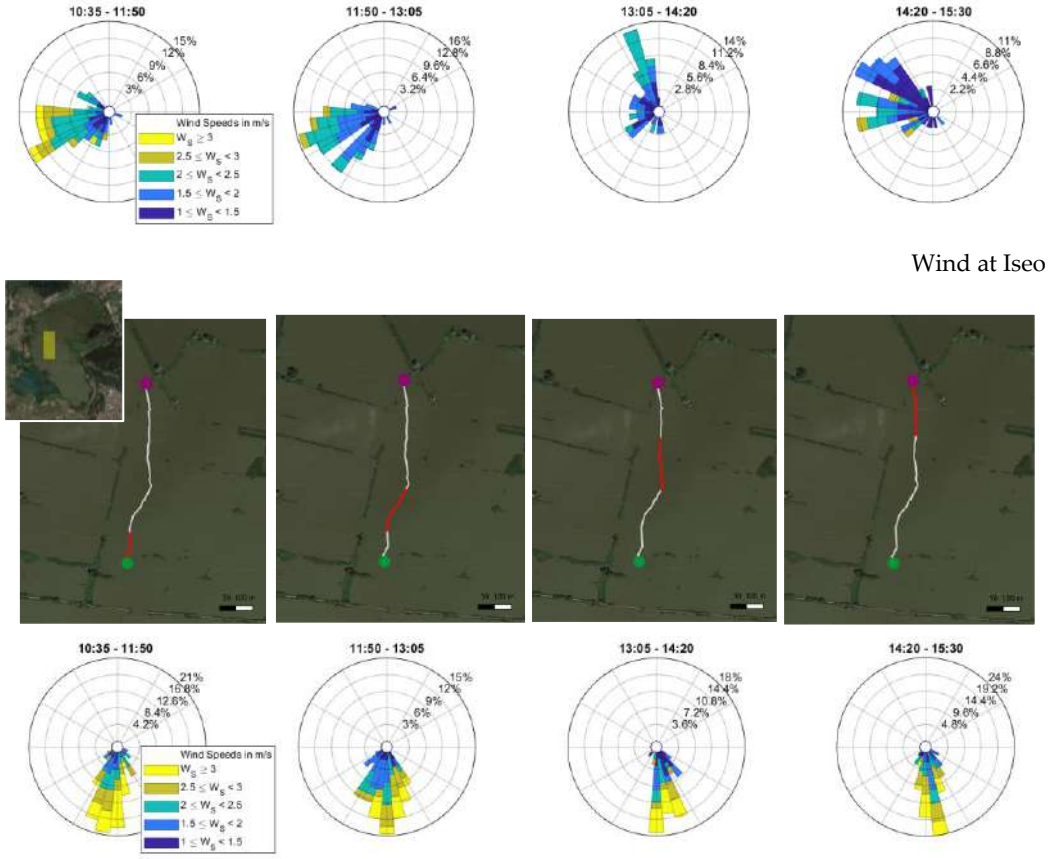

Figure C.6: Wind roses of Iseo (top row) and Torbiere (bottom row) and maps of the deployment of 10th June 2022. The campaign is subdivided into four subsections in order to visualize the wind intensity and direction acting during each sub-period.

C.6 June 10th, 2022 (#3)

The drifter was left at 03:40 pm in one of the central tanks. Here the average depth is 2 m. The drifter was left floating for one hour and 45 minutes during which it moved towards North. It has travelled a distance of 178 m, with an average speed of 1.7 cm/s.

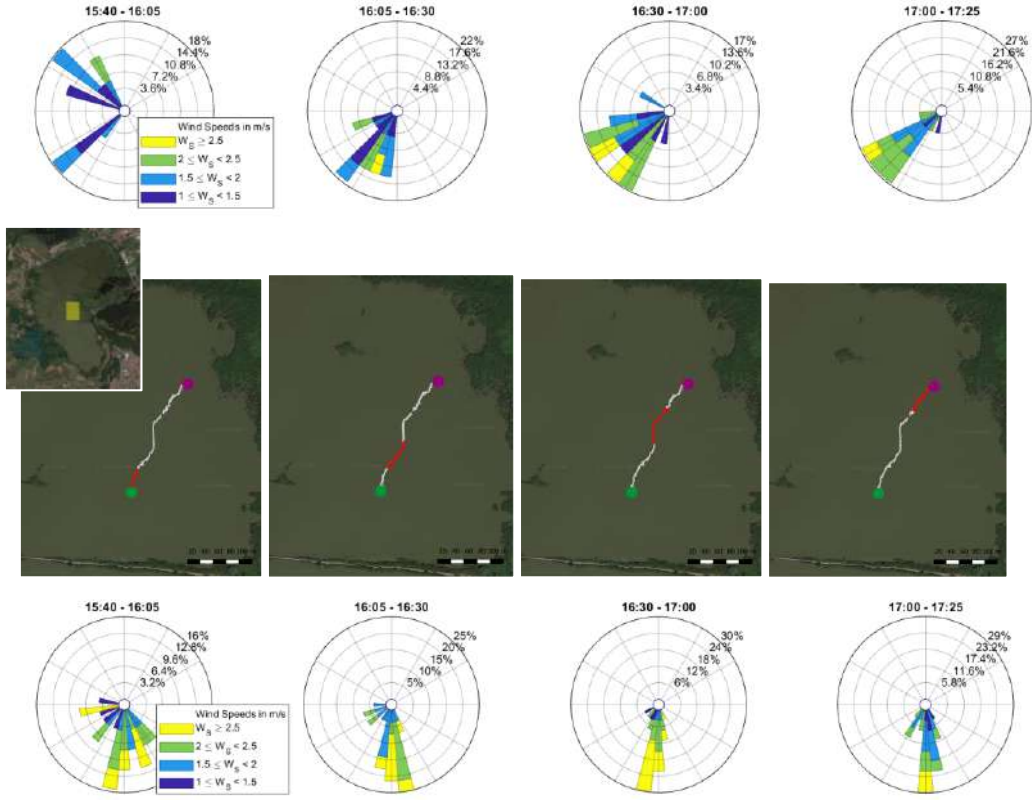

Figure C.7: Wind roses of Iseo (top row) and Torbiere (bottom row) and maps of the deployment of 10th June 2022. The campaign is subdivided into four subsections in order to visualize the wind intensity and direction acting during each sub-period.

C.7 August 8th, 2022 (#1)

The drifter was left at 09:30 am in one of the southern tanks. Here the average depth is 1.6 m. The drifter was left floating for 2 hours until it got stuck against some reefs. Overall, it has travelled a distance of 250 m towards South -South/West, with an average speed of 2.5 cm/s. Given the location of the release, both winds measured at Iseo station and at Torbiere station were considered. Even if the drifter is closer to the Torbiere station, the wind at Iseo is much more compatible with the trajectory of the drifter.

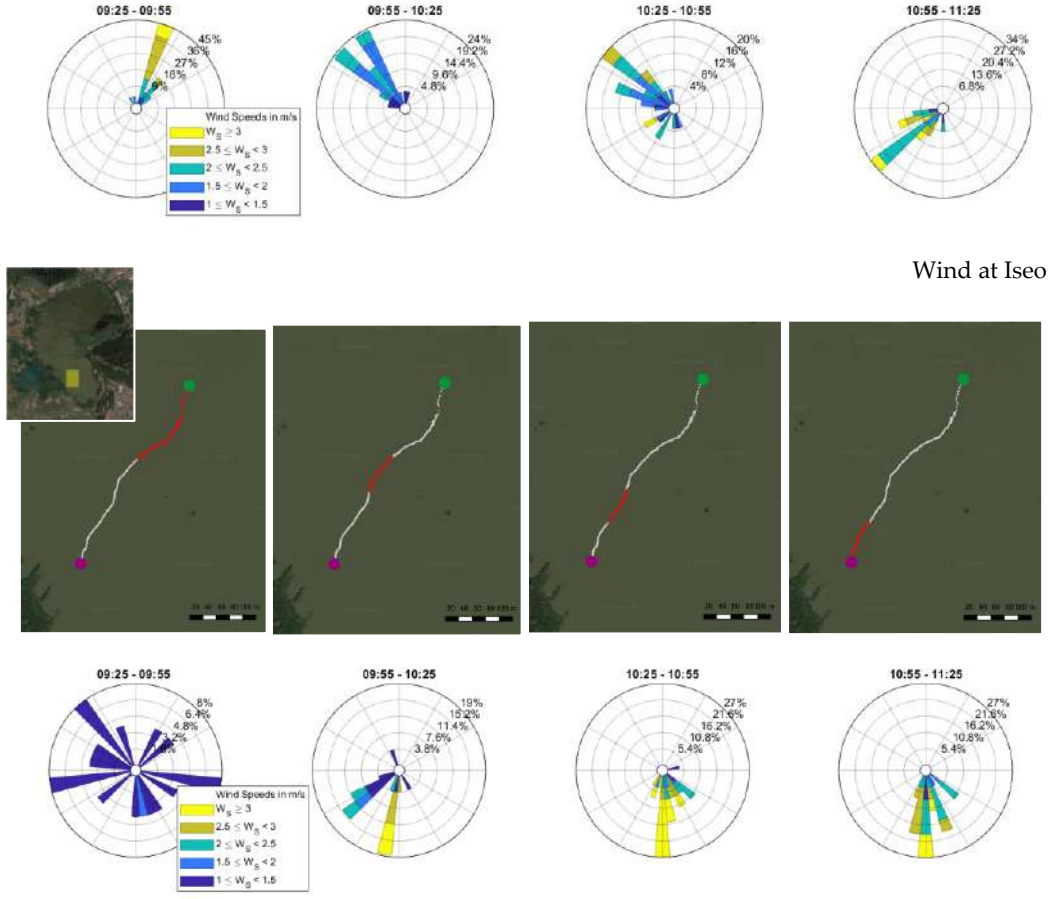

Figure C.8: Wind roses of Iseo (top row) and Torbiere (bottom row) and maps of the deployment of 08th August 2022. The campaign is subdivided into four subsections in order to visualize the wind intensity and direction acting during each sub-period.

C.8 August 8th, 2022 (#2)

The drifter was left at 11:30 am in the southern tank just outside the inlet of Rì. Here the average depth is 1.2 m, it is one of the shallowest areas. The drifter was left floating for 1 hour and 10 minutes until it got stuck in a very shallow area. Overall, it has travelled a distance of 140 m, with an average speed of 0.4 cm/s. Given the location of the release, both winds measured at Iseo station and at Torbiere station were considered. Even if the drifter is closer to the Torbiere station, the wind at Iseo is much more compatible with the trajectory of the drifter. This might be due to the fact that most of the body of Torbiere is subjected to Iseo's wind, and currents are mainly caused by that; a local change in the local wind is not enough to establish a new set of currents. Also, wind intensity at Torbiere's station is lower than the one measured in Iseo.

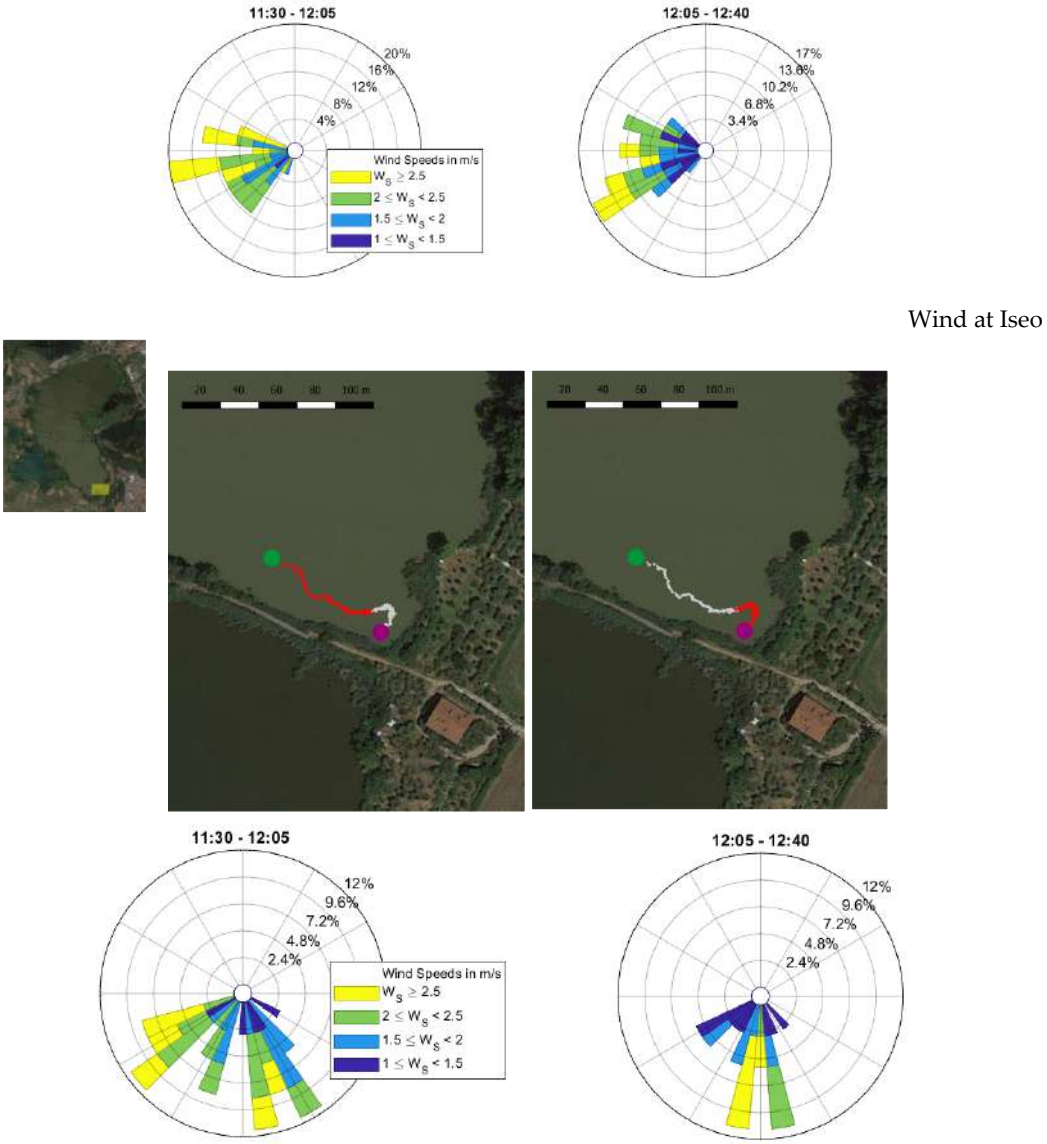

Figure C.9: Wind roses of Iseo (top row) and Torbiere (bottom row) and maps of the deployment of 08th August 2022. The campaign is subdivided into two subsections in order to visualize the wind intensity and direction acting during each sub-period.

C.8 August 8th, 2022 (#3)

The drifter was left at 2:00 pm in one of the southern tanks where the average depth is 1.4 m. The drifter was left floating for 2 hours and 30 minutes until it got stuck in a very shallow area. Overall, it has travelled a distance of 190 m, with an average speed of 0.9 cm/s. The trajectory of this deployment is unusual, and the drifter seems to follow the wind measured at Torbiere's station.

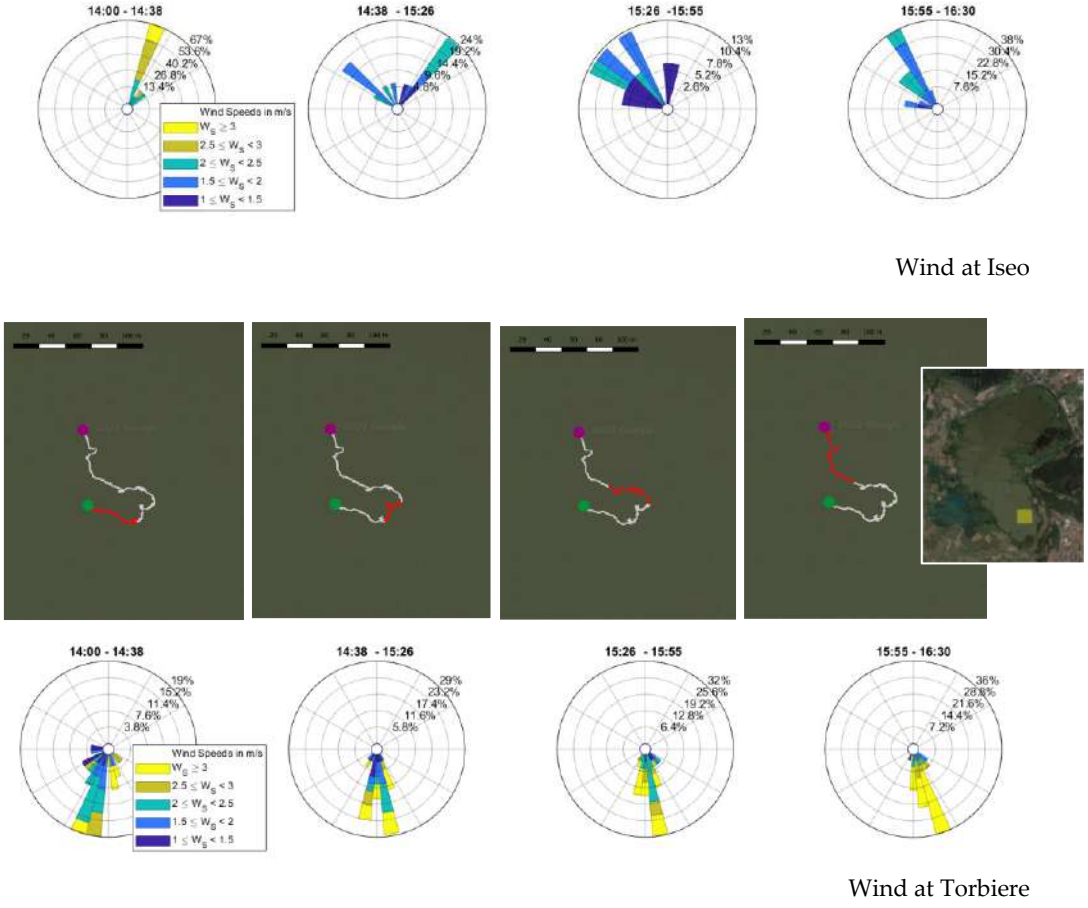

Figure C.10: Wind roses of Iseo (top row) and Torbiere (bottom row) and maps of the deployment of 08th August 2022. The campaign is subdivided into four subsections in order to visualize the wind intensity and direction acting during each sub-period.

Appendix D: additional materials

D.1 Measurements by Istituto di Entomologia Agraria – University of Milan, 1990

In 1990 some measurements were carried out in two of the clay tanks of Torbiere. All the available data is shown in Figure D.1. "Lake 1" refers to a pond in the province of Monza.

TABLE 1: Main physico-chemical characteristics of the three experimental lakes measured during the preliminar annual cicle.

	LAKE 1 (Monza)			LAKE 2 'Mantovani'			LAKE 3 LAGHETTO		
	max	min	mean	max	min	mean	max	min	mean
Secchi depth m	-	-	-	3.0	1.3	-	1.8	1	-
pH	7.9	7.4	7.5	8.2	7.2	8.1	8.5	7.6	7.9
Conductivity µS/cm	673	552	618	493	326	350	424	276	365
Alcalinity meq/l	-	-	5.5	-	-	2.9	-	-	2.8
DUREZZA Hardness mg $CaCO_3$/l	-	-	300	-	-	170	-	-	135
Dissolved oxygen mg/l	18.9	10.7	13.4	13.8	0	8.1	14.6	0	6.5
Dissolved oxygen % sat.	197	93	136	147	0	76	188	0	62
FOSFORO P-PO_4 µg/l	25	1	5	27	2	5	38	3	4
P tot µg/l	65	20	30	134	21	82	137	30	77
NITRATI N-NO_3 µg/l	5710	4350	5060	1070	32	260	1250	44	450
NITRITI N-NO_2 µg/l	11.5	7.4	9.0	10.7	2.8	5.7	15.2	2.6	10.4
AMMONIACA N-NH_3 µg/l	43	5	18	1490	15	187	1010	18	340

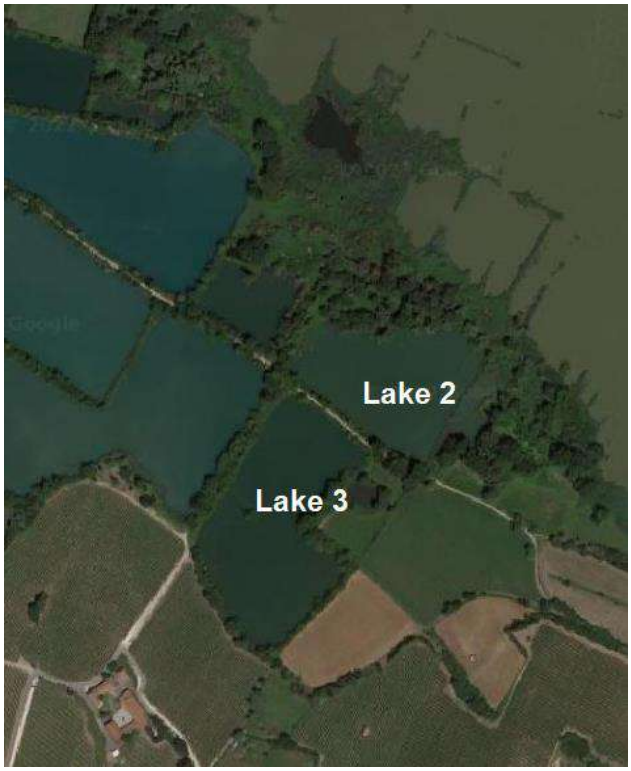

Figure D.1 measurements of physical-chemical characteristics (left panel) and map of the two tanks of Torbiere involved in the study (right panel)

D.2 CTD probe surveys

Chapter 3.3.1 presented the 2D interpolated maps of the parameters acquired with the multiparametric probe across 10 campaigns. Here the interpolated spatial distribution of the data measured during the surveys are presented, together with the recorded forcings of temperature, discharge and wind, in the ten days before the survey. The red vertical line plotted on the time series corresponds to the time the campaigns were done.

18/06/2020 (09:20 am – 12:55 pm)

points: 48

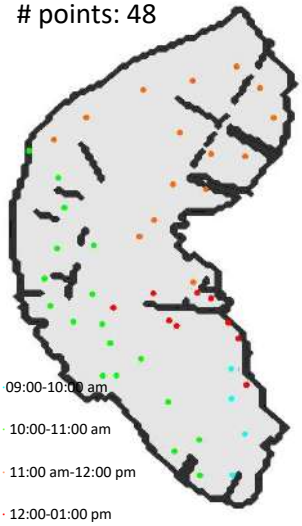

Temperature

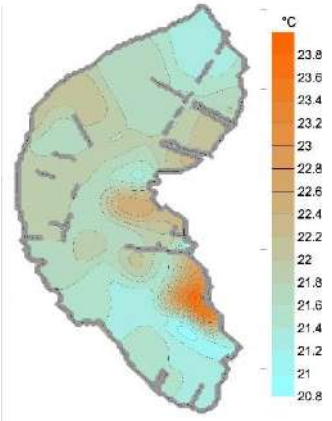

Discharge Rì [m³/s]

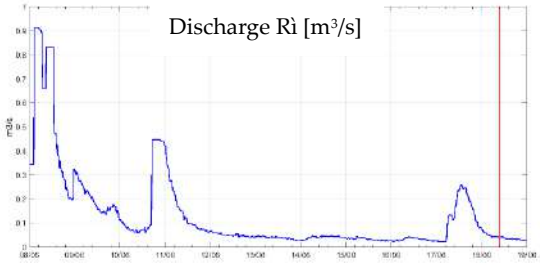

Precipitation in Provaglio [mm/h]

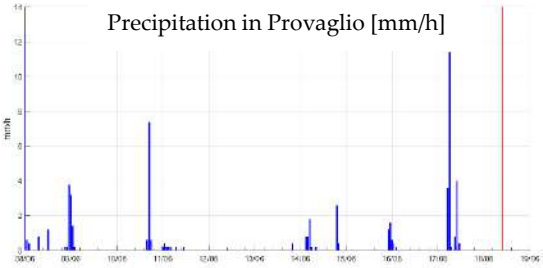

Specific conductivity

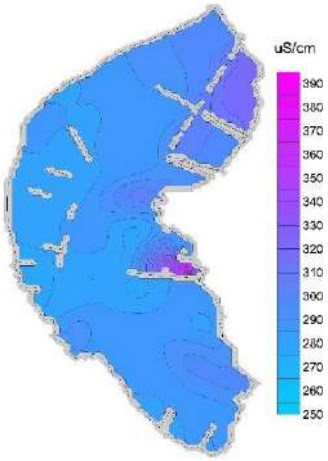

Turbidity

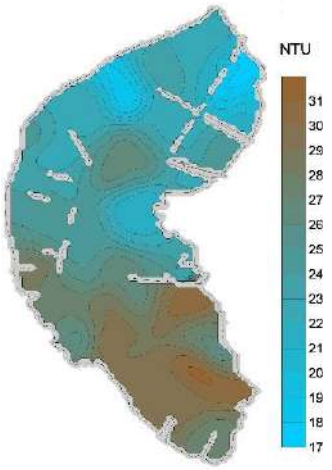

Air temperature in Iseo [°C]

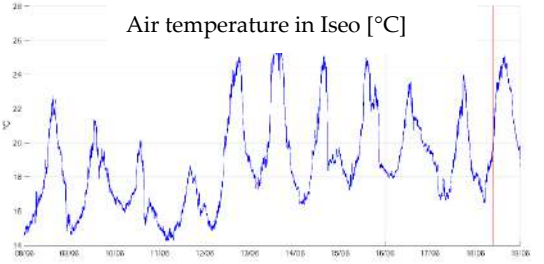

Wind speed [m/s] and direction [°] in Iseo

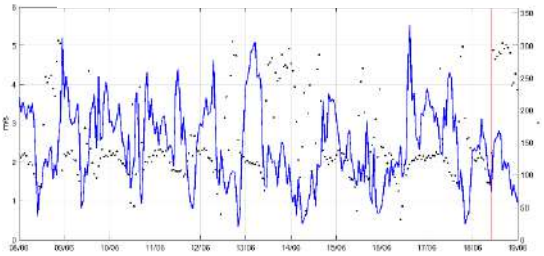

Proxy of Chlorophyll-a

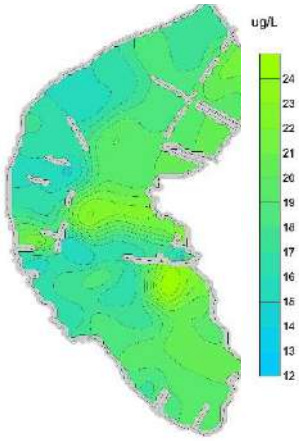

Dissolved Oxygen Saturation

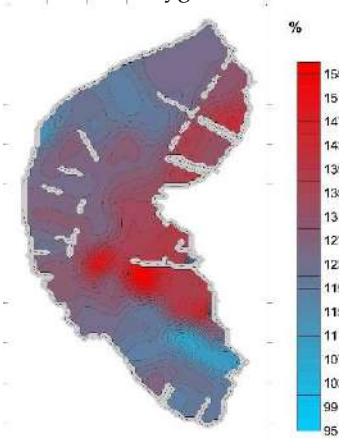

27/07/2020 (08:50 am – 11:30 am)

points: 47

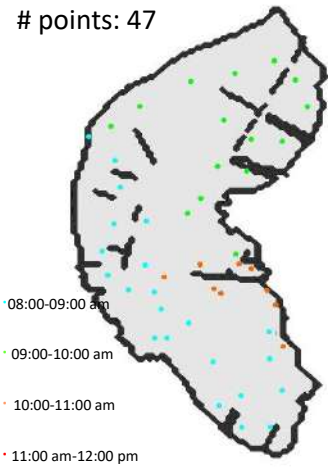

Temperature

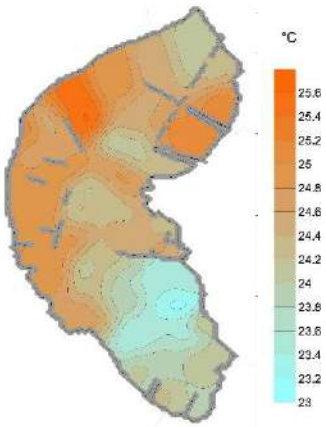

Discharge Rì [m³/s]

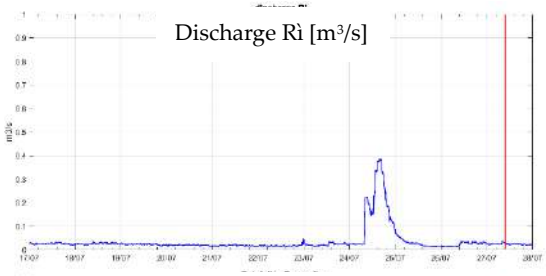

Precipitation in Provaglio [mm/h]

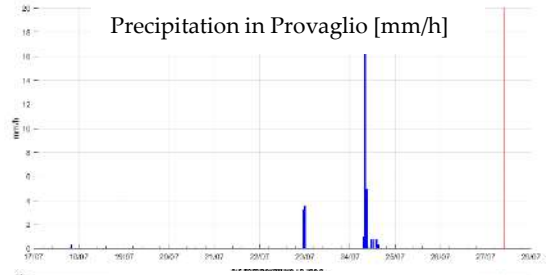

Specific conductivity

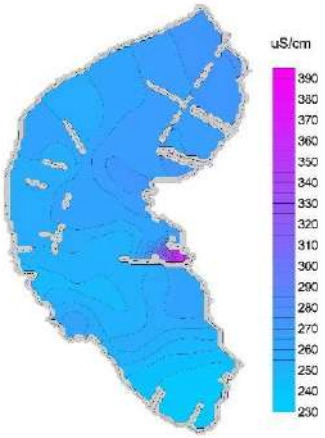

Turbidity

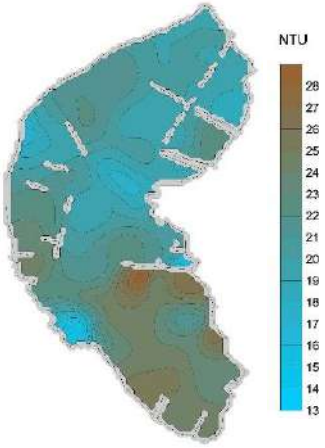

Air temperature in Iseo [°C]

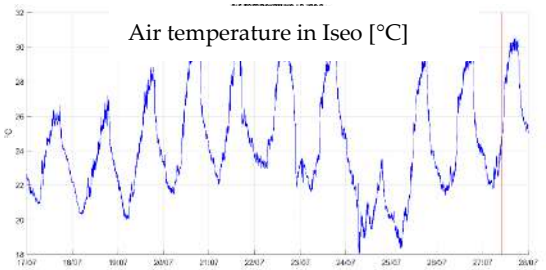

Wind speed [m/s] and direction [°] in Iseo

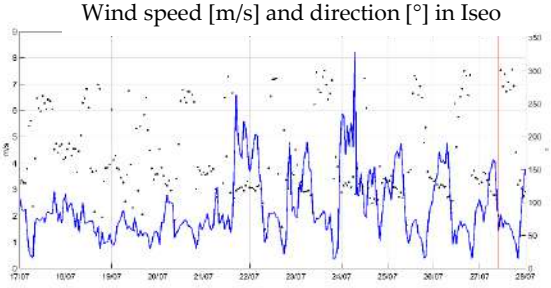

Proxy of Chlorophyll-a

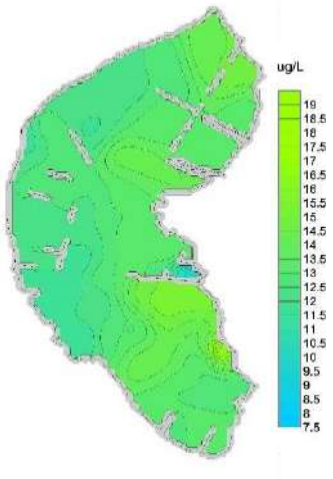

Dissolved Oxygen Saturation

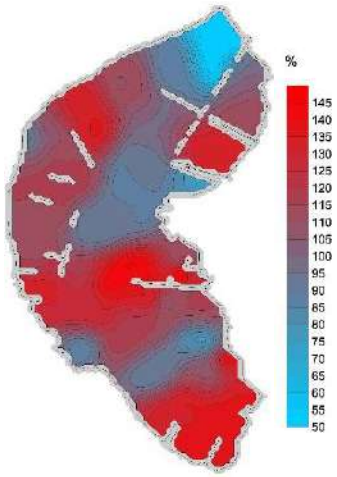

07/10/2020 (10:50 am – 11:55 am)

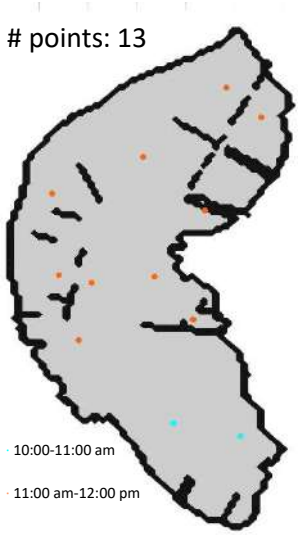

Temperature

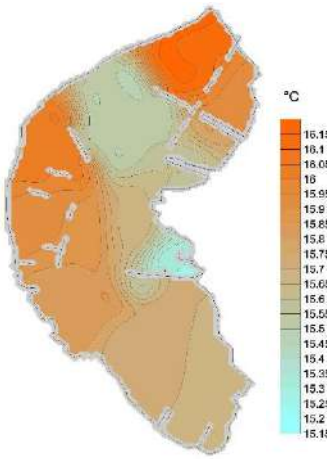

Discharge Rì [m³/s]

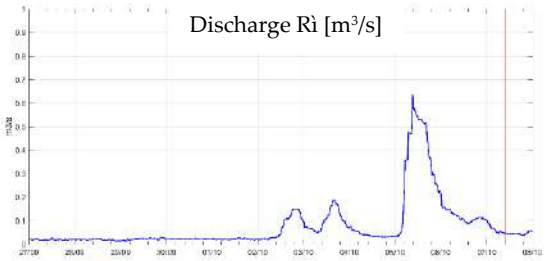

Precipitation in Provaglio [mm/h]

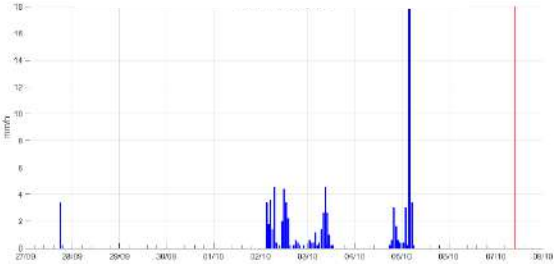

Specific conductivity

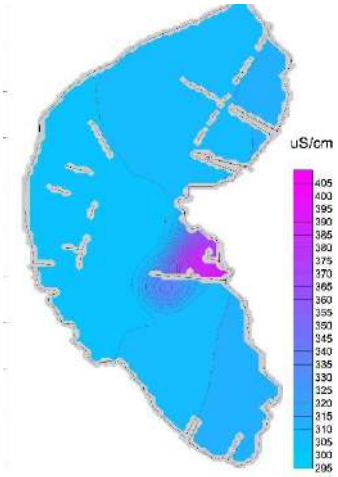

Turbidity

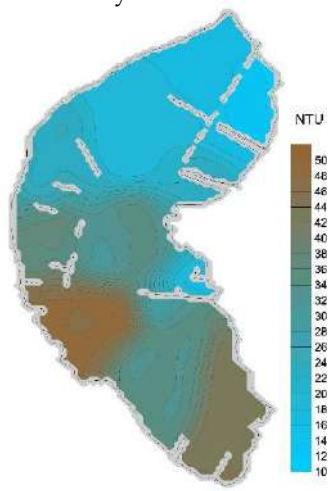

Air temperature in Iseo [°C]

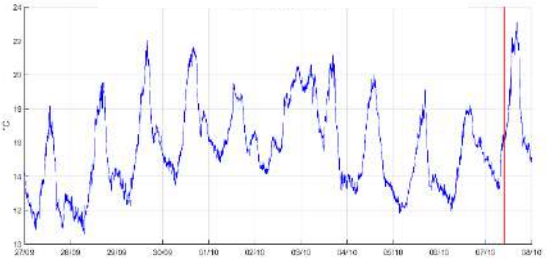

Wind speed [m/s] and direction [°] in Iseo

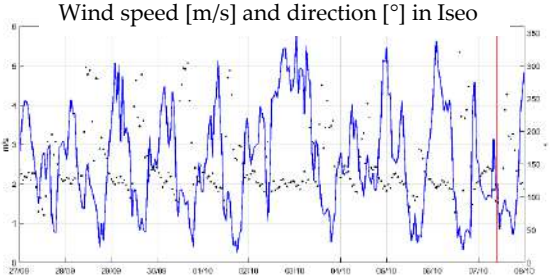

Proxy of Chlorophyll-a

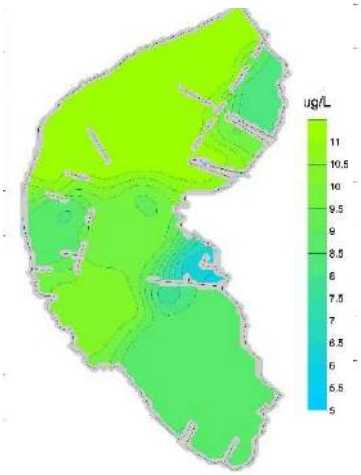

Dissolved Oxygen Saturation

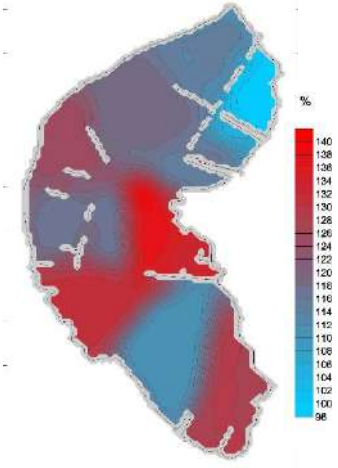

15/06/2021 (09:20 am – 11:55 am)

points: 49

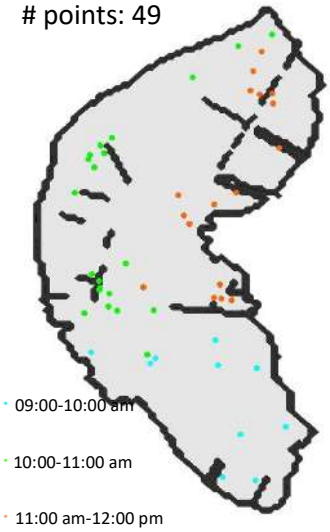

- 09:00-10:00 am
- 10:00-11:00 am
- 11:00 am-12:00 pm

Temperature

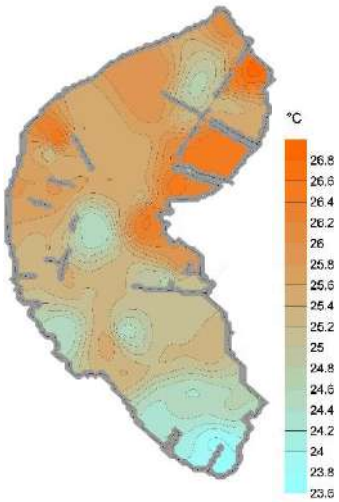

Discharge Rì [m³/s]

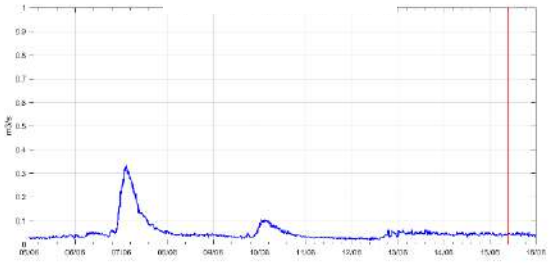

Precipitation in Provaglio [mm/h]

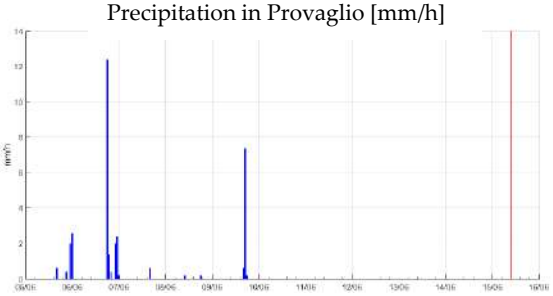

Specific conductivity

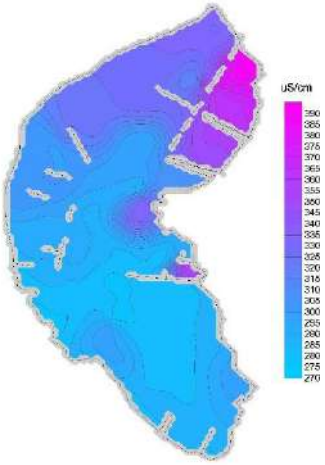

Turbidity

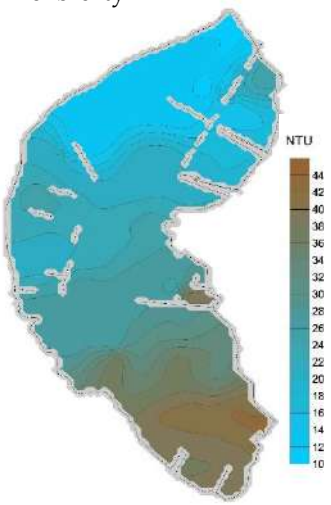

Air temperature in Iseo [°C]

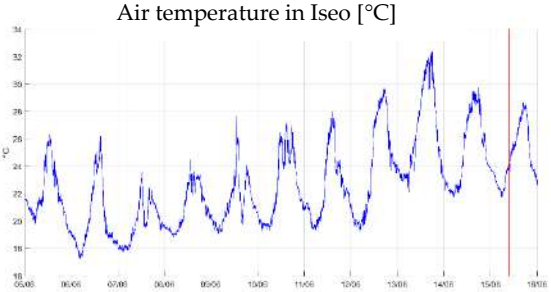

Wind speed [m/s] and direction [°] in Iseo

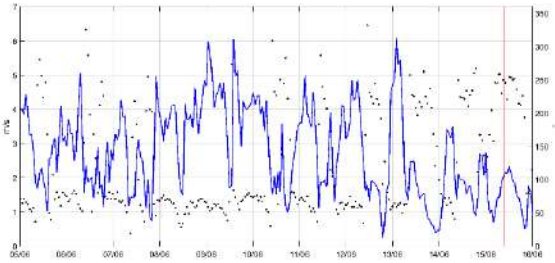

Proxy of Chlorophyll-a

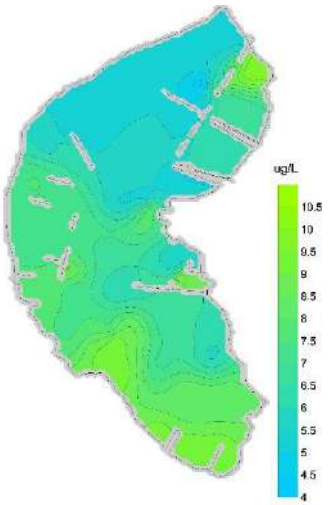

Dissolved Oxygen Saturation

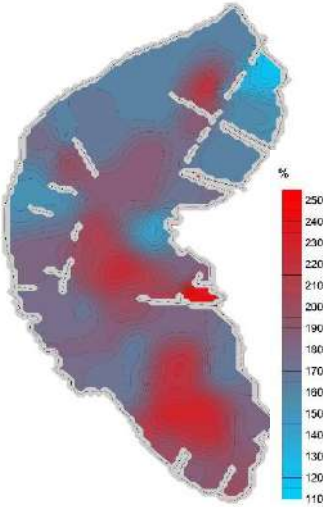

Water Level Torbiere [m]

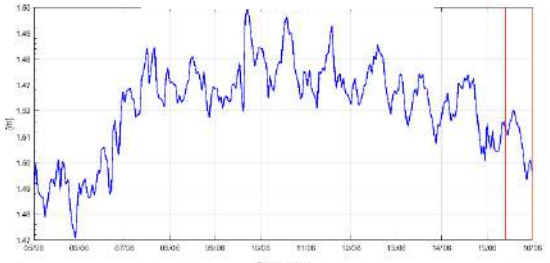

Temperature Torbiere [°C]

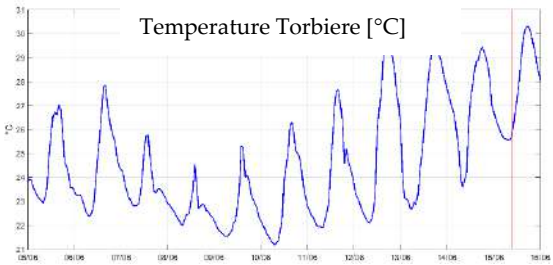

30/07/2021 (09:30 am – 11:50 am)

points: 56

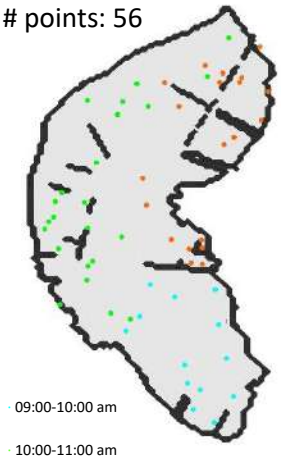

09:00-10:00 am

10:00-11:00 am

11:00 am-12:00 pm

Temperature

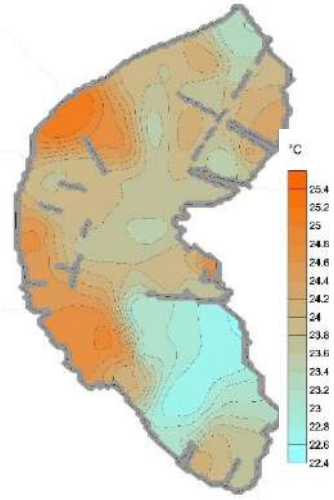

Discharge Rì [m³/s]

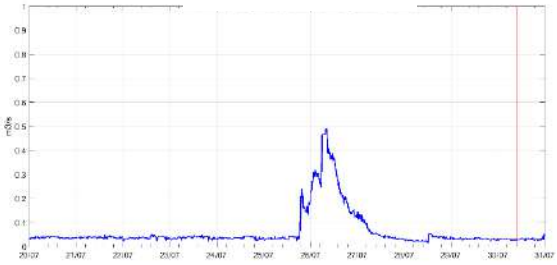

Precipitation in Provaglio [mm/h]

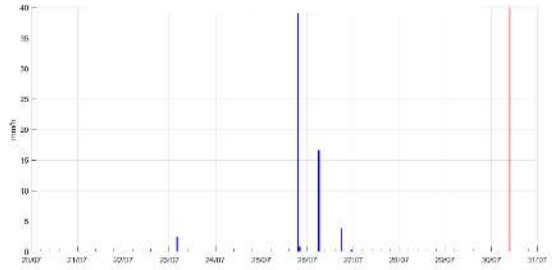

Specific conductivity

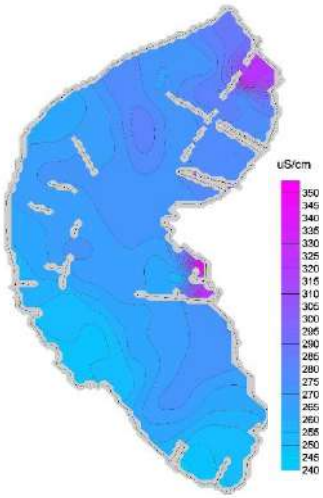

Turbidity

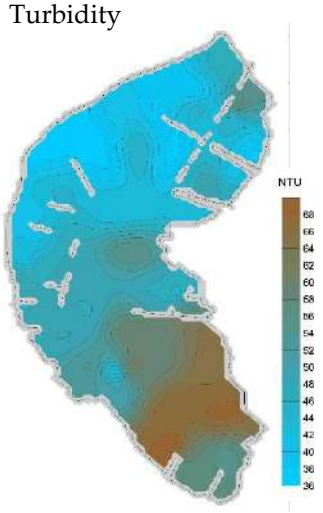

Air temperature in Iseo [°C]

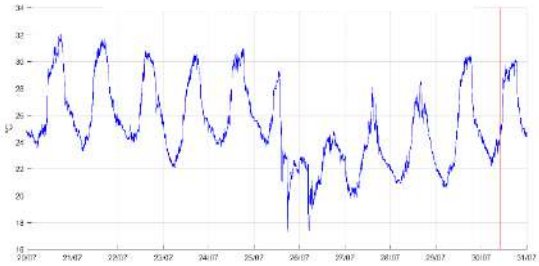

Wind speed [m/s] and direction [°] in Iseo

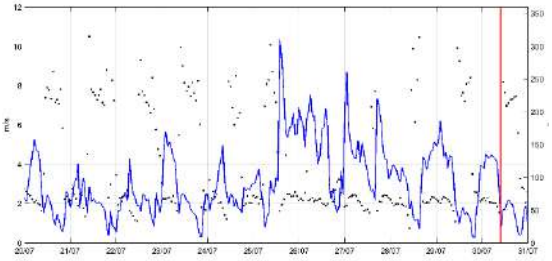

Proxy of Chlorophyll-a

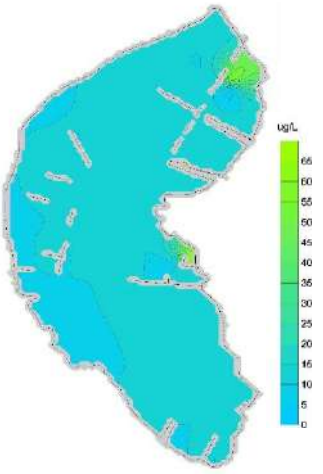

Dissolved Oxygen Saturation

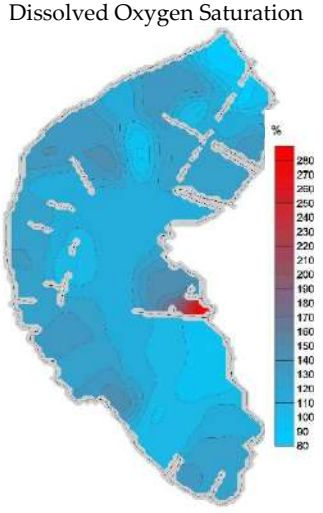

Water Level Torbiere [m]

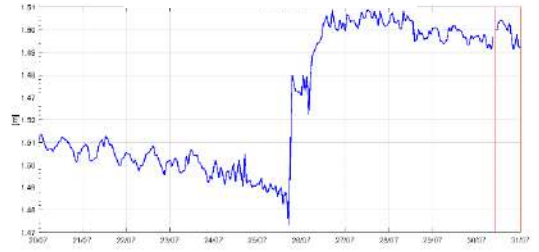

Temperature Torbiere [°C]

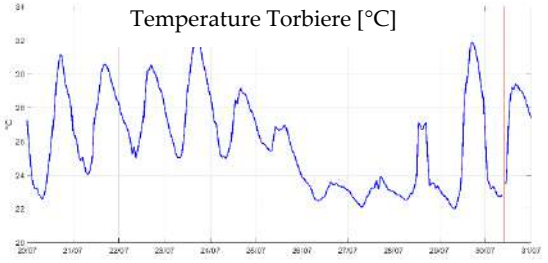

15/09/2021 (09:30 am – 12:05 pm)

points: 48

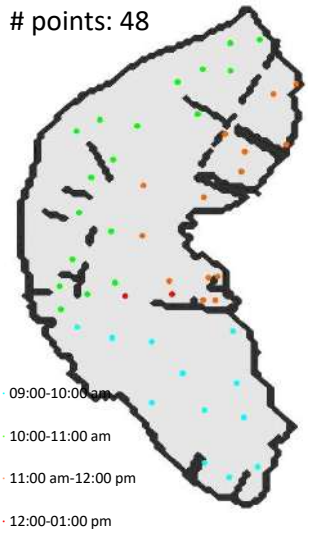

Temperature

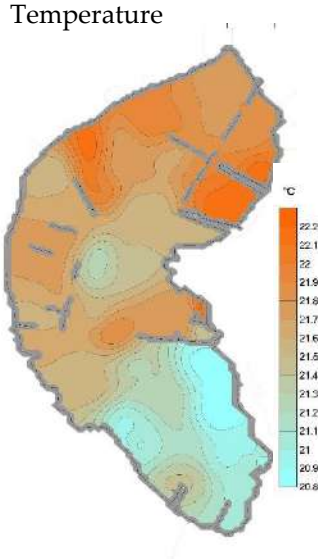

Discharge Rì [m³/s]

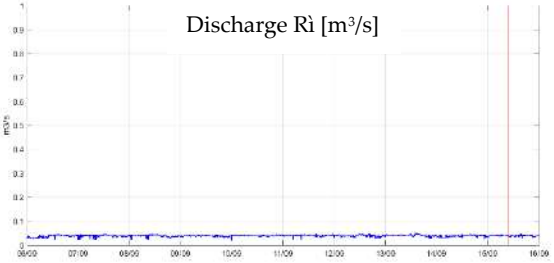

Precipitation in Provaglio [mm/h]

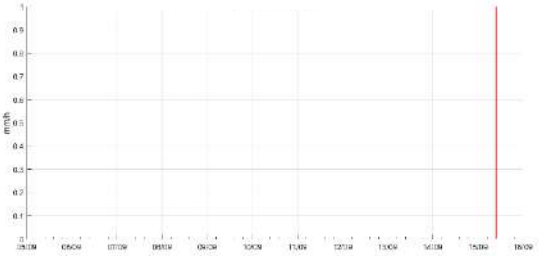

Specific conductivity

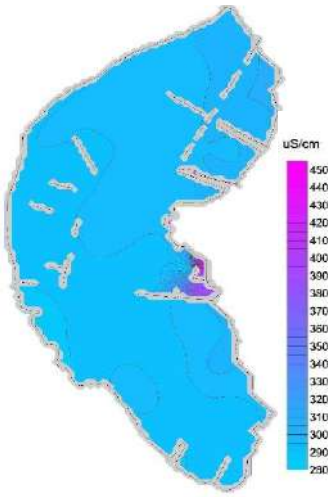

Turbidity

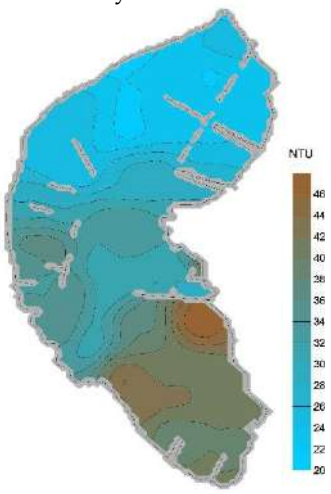

Air temperature in Iseo [°C]

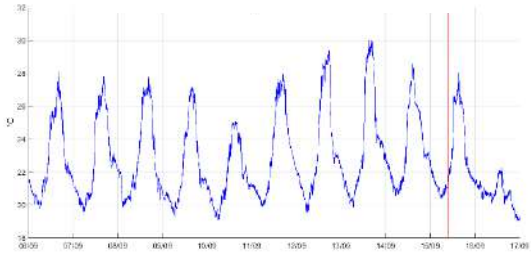

Wind speed [m/s] and direction [°] in Iseo

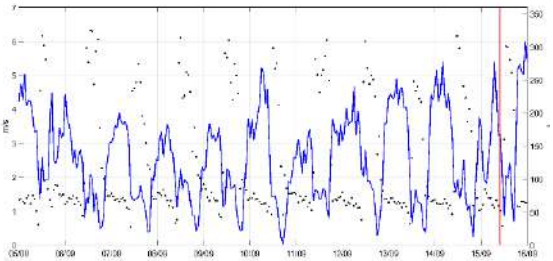

Proxy of Chlorophyll-a

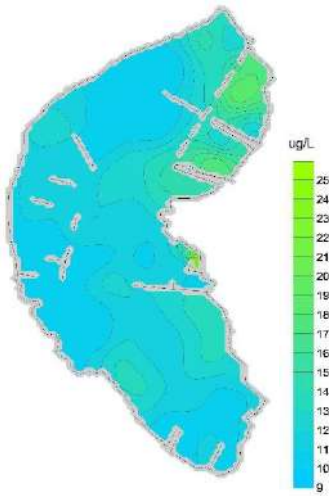

Dissolved Oxygen Saturation

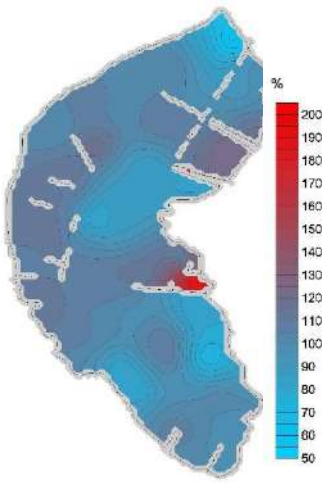

Water Level Torbiere [m]

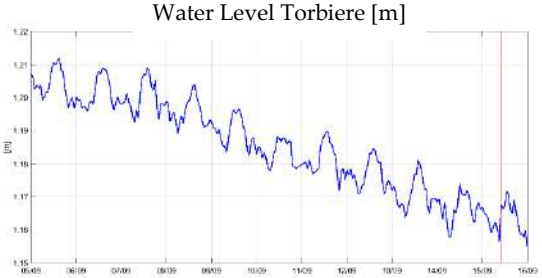

Temperature Torbiere [°C]

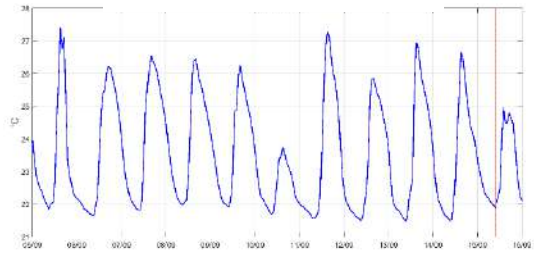

28/10/2021 (09:30 am – 12:00 pm)

points: 40

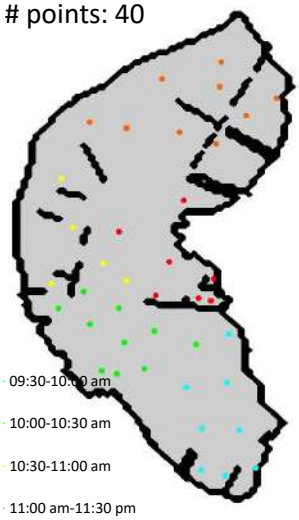

- 09:30-10:00 am
- 10:00-10:30 am
- 10:30-11:00 am
- 11:00 am-11:30 pm
- 11:30 am-12:00 pm

Temperature

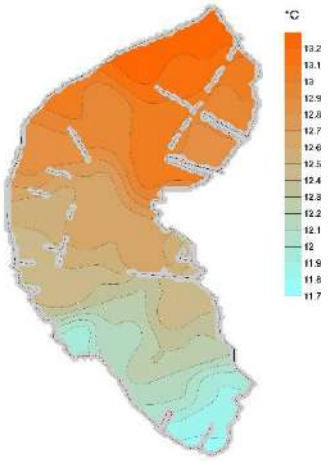

Discharge Rì [m³/s]

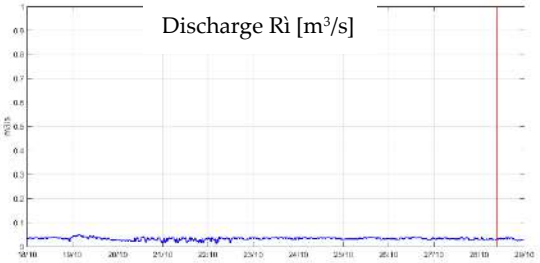

Precipitation in Provaglio [mm/h]

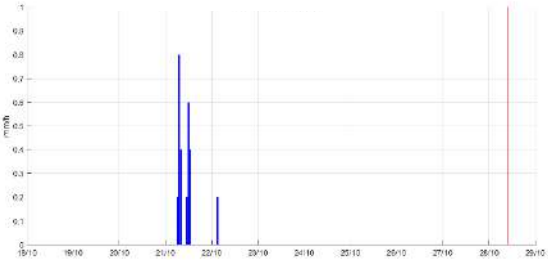

Specific conductivity

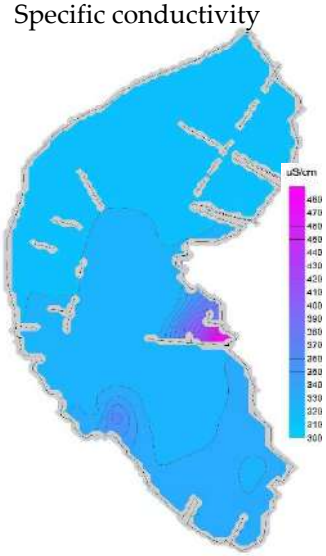

Turbidity

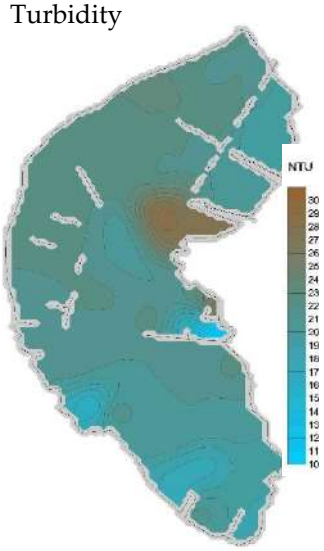

Air temperature in Iseo [°C]

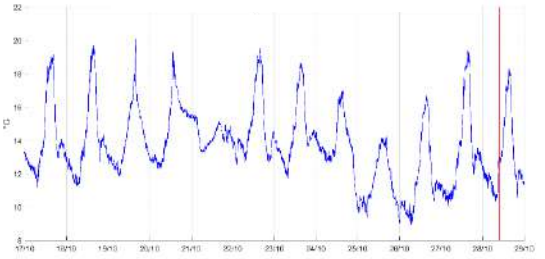

Wind speed [m/s] and direction [°] in Iseo

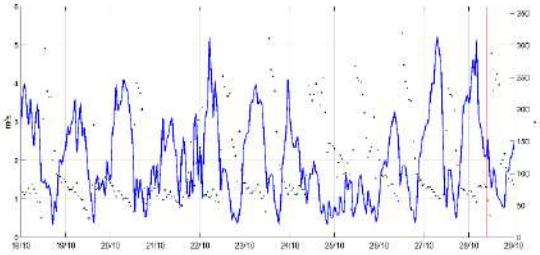

Proxy of Chlorophyll-a

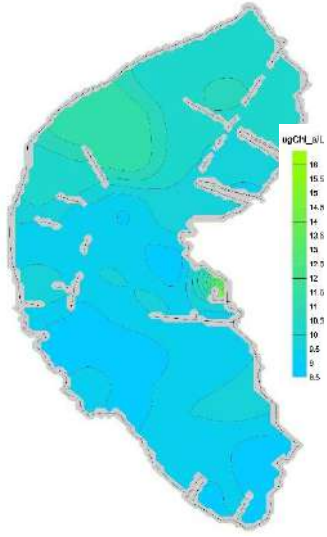

Dissolved Oxygen Saturation

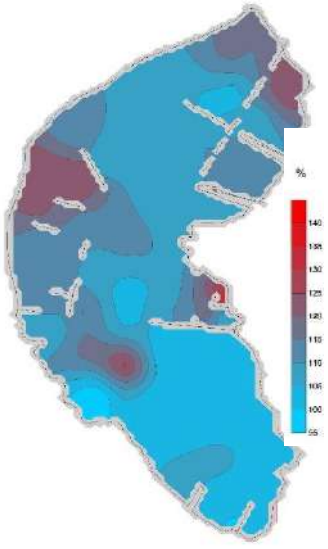

Water Level Torbiere [m]

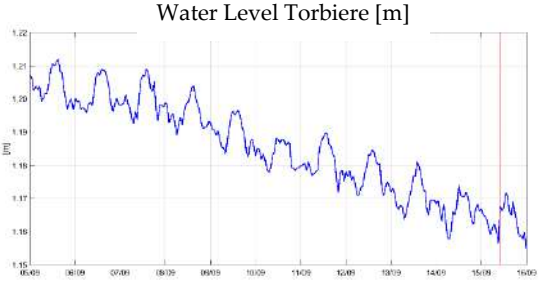

Temperature Torbiere [°C]

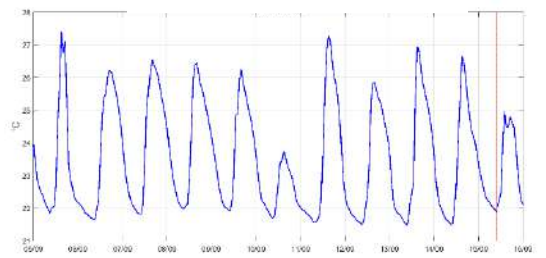

13/12/2021 (14:00 pm – 17:00 pm)

points: 40

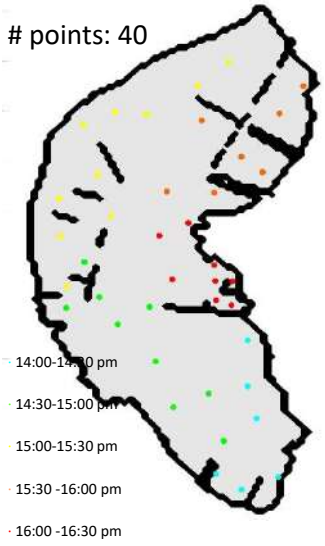

Temperature

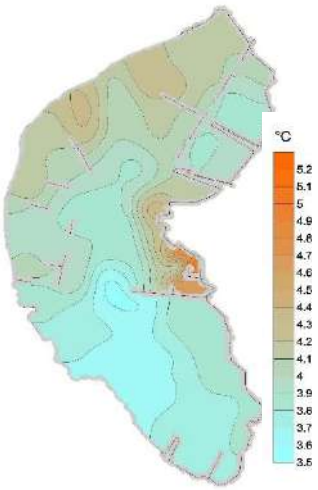

Discharge Rì [m³/s]

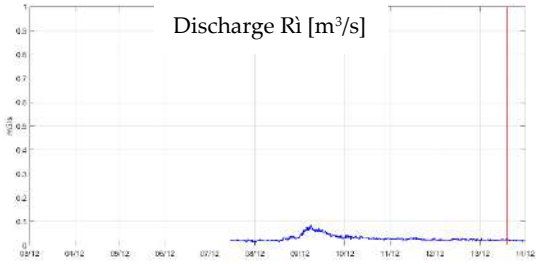

Precipitation in Provaglio [mm/h]

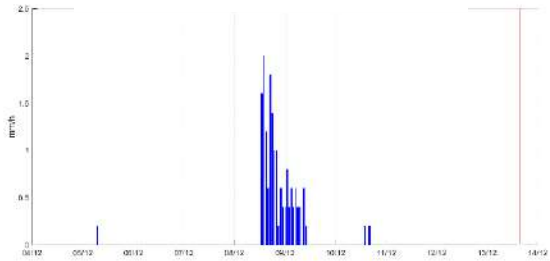

Specific conductivity

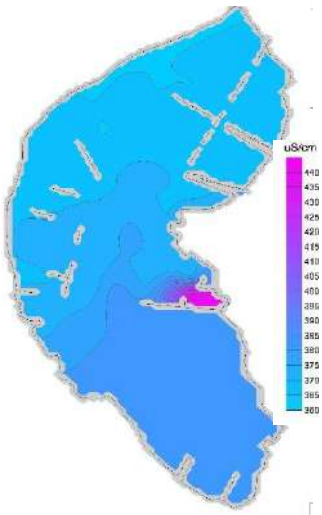

Turbidity

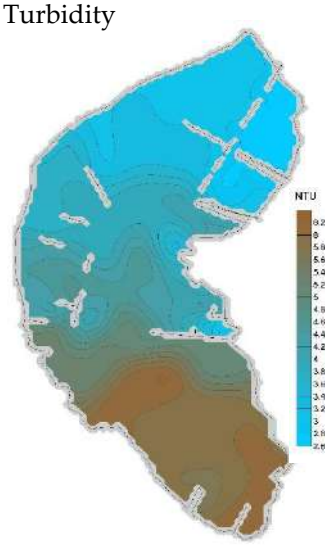

Air temperature in Torbiere [°C]

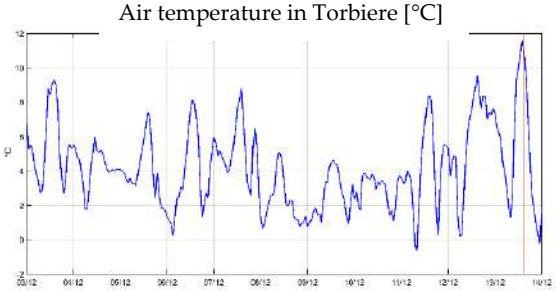

Wind speed [m/s] and direction [°] in Torbiere

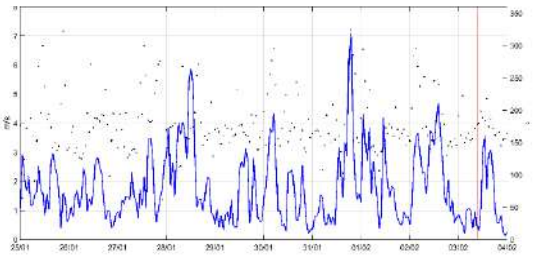

Proxy of Chlorophyll-a

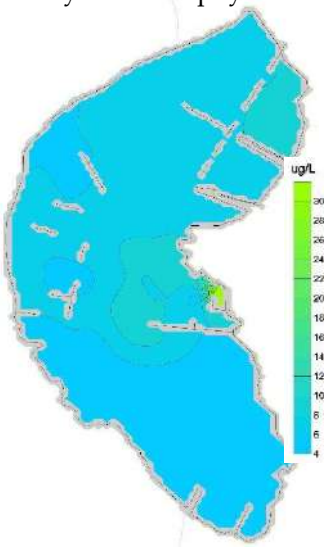

Dissolved Oxygen Saturation

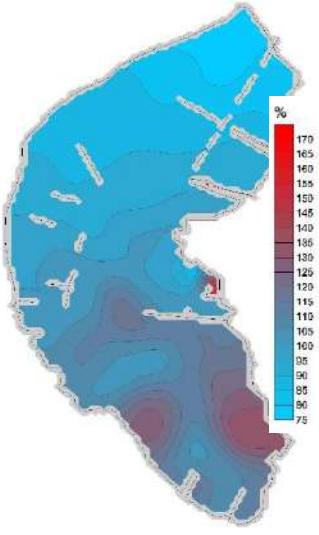

Water Level Torbiere [m]

Temperature Torbiere [°C]

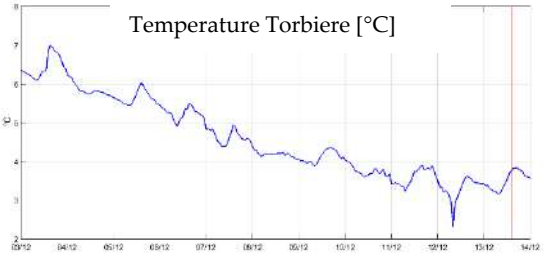

03/02/2022 (09:45 am – 11:45 am)

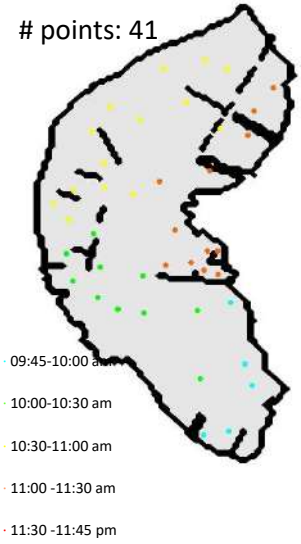

Temperature

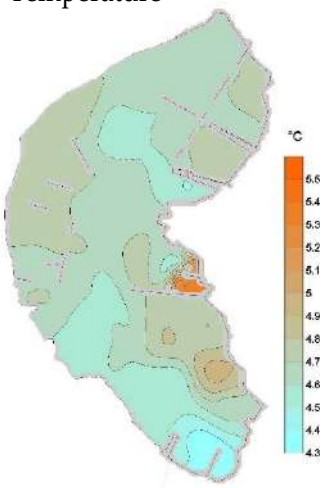

Precipitation in Provaglio [mm/h]

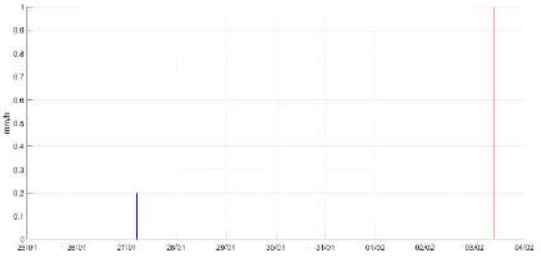

Specific conductivity

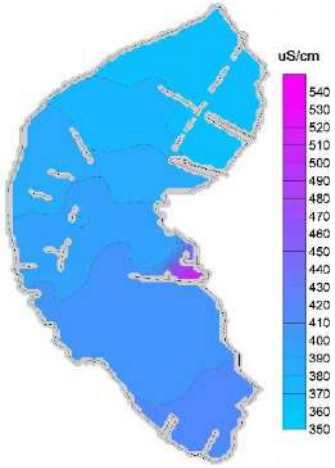

Turbidity

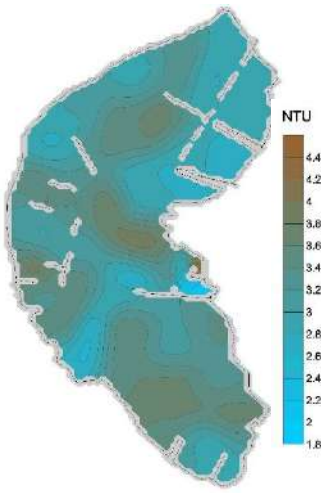

Air temperature in Torbiere [°C]

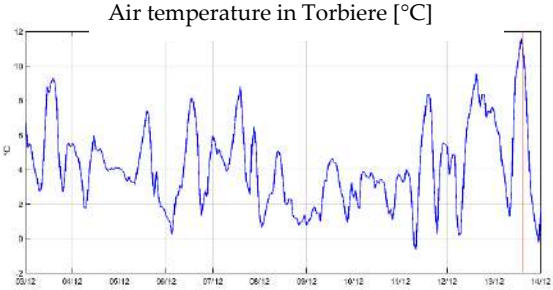

Wind speed [m/s] and direction [°] in Torbiere

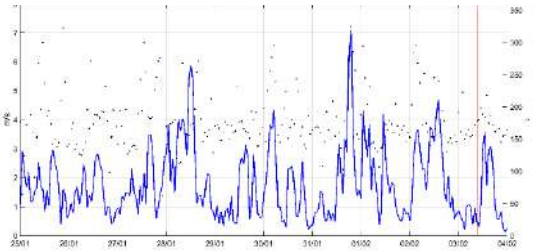

Proxy of Chlorophyll-a

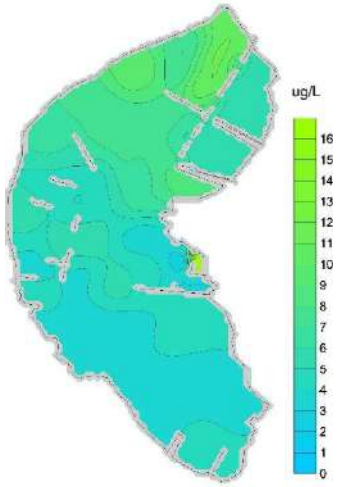

Dissolved Oxygen Saturation

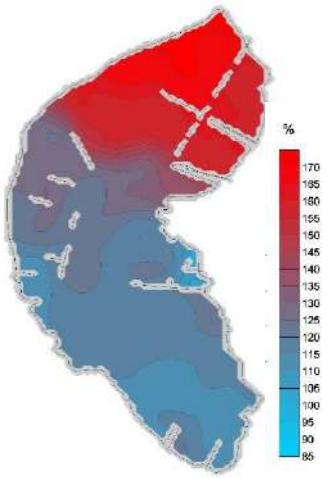

Water Level Torbiere [m]

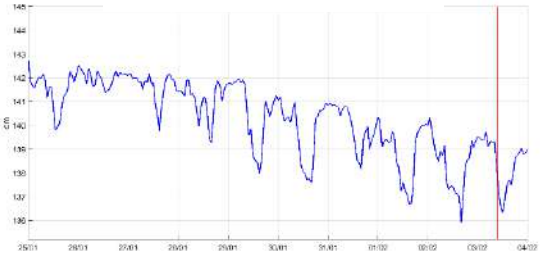

Temperature Torbiere [°C]

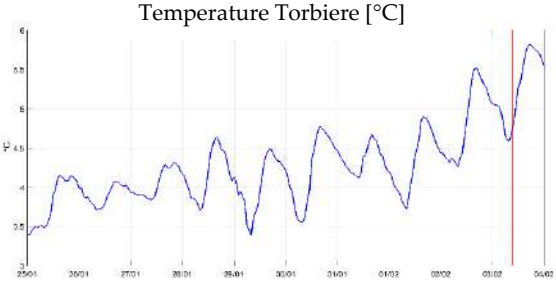

13/04/2022 (10:15 am – 12:15 am)

points: 38

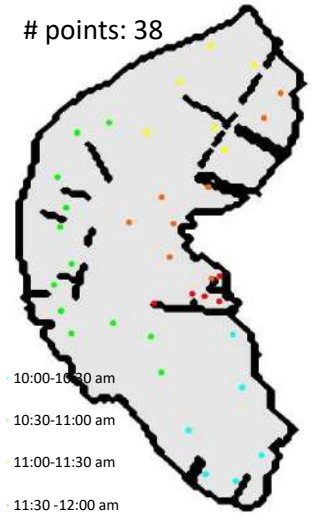

Temperature

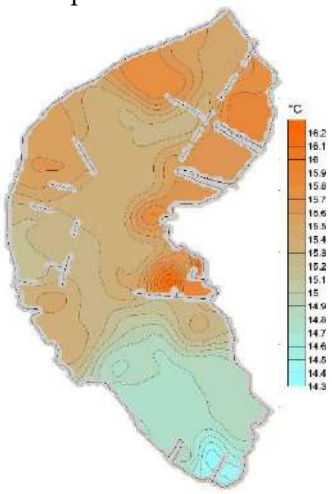

Precipitation in Provaglio [mm/h]

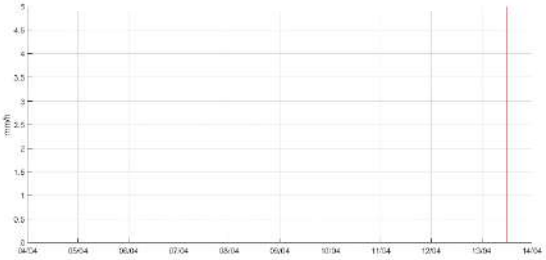

Specific conductivity

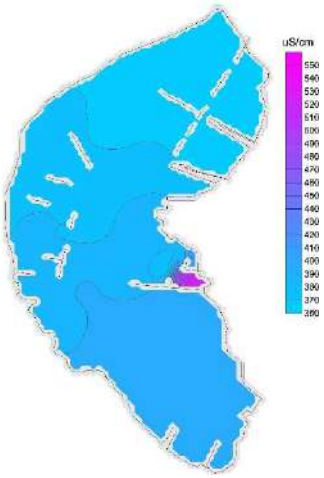

Turbidity

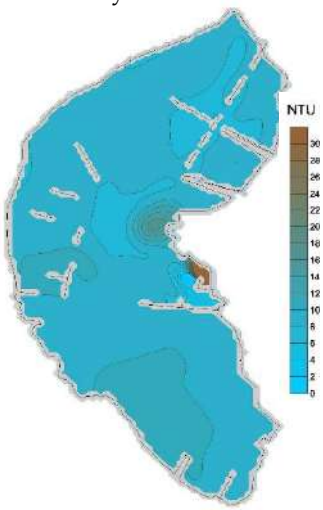

Air temperature in Torbiere [°C]

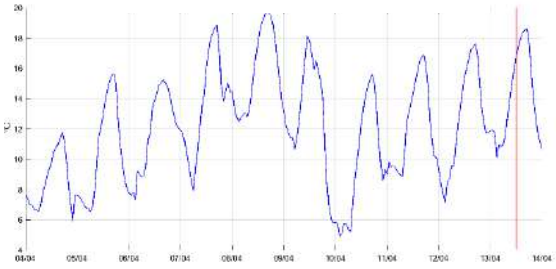

Wind speed [m/s] and direction [°] in Torbiere

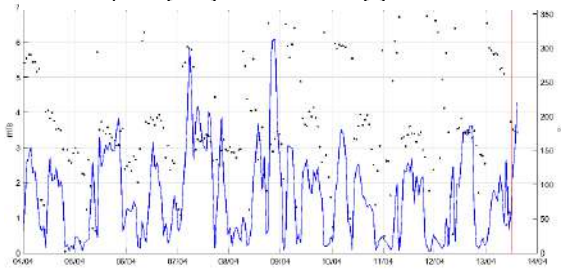

Proxy of Chlorophyll-a

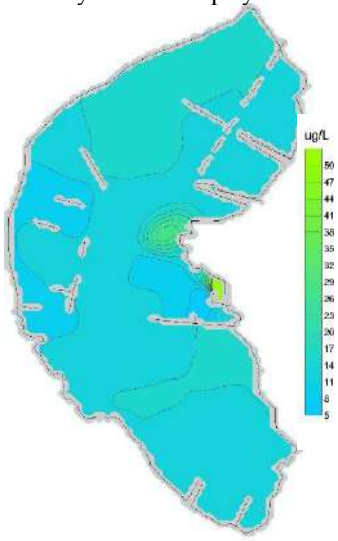

Dissolved Oxygen Saturation

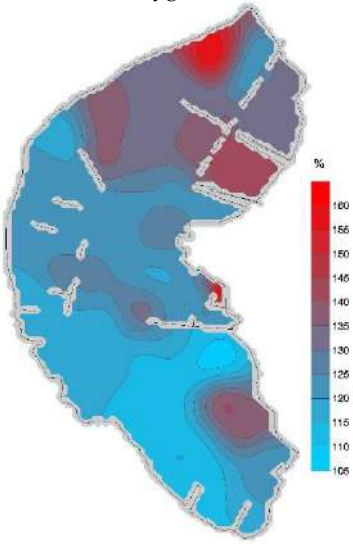

Water Level Torbiere [m]

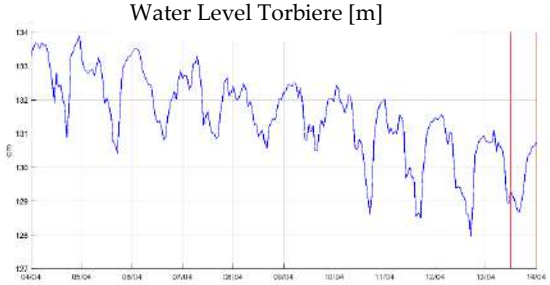

Temperature Torbiere [°C]

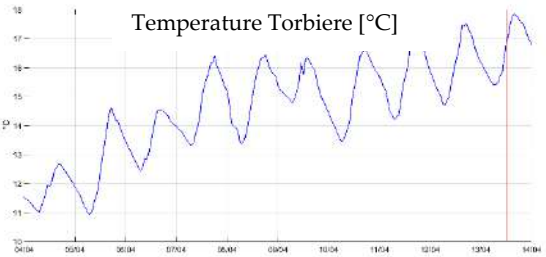

D.3 Habitat of Torbiere

Regione Lombardia published in 2016 a map of the habitat of Torbiere, that was reviewed in the Relazione Botanica 2019 of Torbiere del Sebino by Patera G. (2019).

Here, the map of the habitats is shown, together with a brief description.

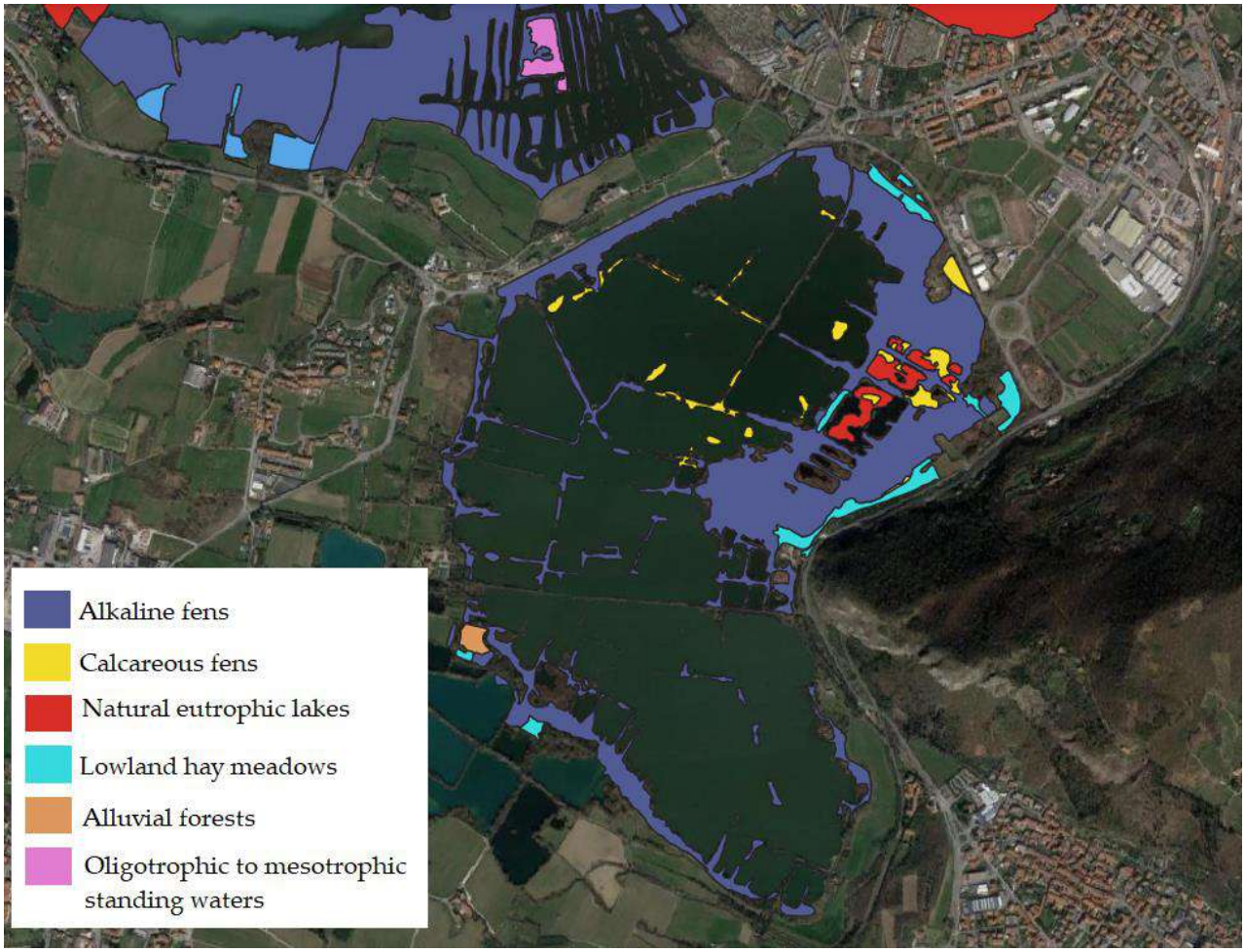

Figure D.2 Map of the habitats of Torbiere

"Alkaline fens" is the most abundant habitat and refers to wetlands that are mostly or largely occupied by peat or tufa. Soil is permanently waterlogged, and the water supply is often calcareous. The typical vegetation of this habitat consists of *Schoenus nigricans*, *S. ferrugineus*, *Carex spp.*, *Eriophorum latifolium*, *Cinclidium stygium* and *Tomentypnum nitens*.

"Calcareous fens" refers to a zone where *Cladium mariscus* beds are in contact with the vegetation of the *Caricion davallianae* or other *Phragmition* species.

"Natural eutrophic lakes" are lakes and ponds with mostly dirty grey to blue-green, turbid waters. Waters are particularly rich in dissolved bases and the most common plants are: *Hydrocharition - Lemna spp.*, *Spirodela spp.*, *Wolffia spp.*, *Hydrocharis morsus-ranae*, *Stratiotes aloides*, *Utricularia australis* and *U. vulgaris*.

"Lowland hay meadows" are species-rich due to the moderately fertilised soils. The predominant plants are: *Arrhenatherum elatius*, *Trisetum flavescens ssp. flavescens*, *Pimpinella major*, *Centaurea jacea*, *Crepis biennis*, *Knautia arvensis*, *Tragopogon pratensis*, *Daucus carota*, *Leucanthemum vulgare*, *Alopecurus pratensis*, *Sanguisorba officinalis*, *Campanula patula*, *Leontodon hispidus*, *L. nudicaulis*, *Linum bienne*, *Oenanthe pimpinelloides*, *Rhinanthus lanceolatus*, *Malva moschata* and *Serapias cordigera*.

"Alluvial forests" consist of riparian forests of *Fraxinus excelsior* and *Alnus glutinosa*.

"Oligotrophic to mesotrophic standing waters" include aquatic to amphibious short perennial vegetation such as *Littorella uniflora*, *Luronium natans*, *Potamogeton polygonifolius*, *Pilularia globulifera*, *Juncus bulbosus ssp. bulbosus*, *Eleocharis acicularis* and Sparganium minimum. Please note that this type of habitat appears in Lamette but not in Lame, which are never oligotrophic.